



<https://theses.gla.ac.uk/>

Theses Digitisation:

<https://www.gla.ac.uk/myglasgow/research/enlighten/theses/digitisation/>

This is a digitised version of the original print thesis.

Copyright and moral rights for this work are retained by the author

A copy can be downloaded for personal non-commercial research or study,  
without prior permission or charge

This work cannot be reproduced or quoted extensively from without first  
obtaining permission in writing from the author

The content must not be changed in any way or sold commercially in any  
format or medium without the formal permission of the author

When referring to this work, full bibliographic details including the author,  
title, awarding institution and date of the thesis must be given

Enlighten: Theses

<https://theses.gla.ac.uk/>  
[research-enlighten@glasgow.ac.uk](mailto:research-enlighten@glasgow.ac.uk)

GENERATION AND MEASUREMENT OF MICROWAVES

A thesis submitted for  
the degree of Doctor of Philosophy

by

Michael Henry Nachemia Potok  
B.Sc., A.R.T.C., A.M.I.E.E.

Based on research carried out by the author in  
the Department of Electrical Engineering,  
The Royal Technical College, Glasgow,  
in the years 1950/1955.

ProQuest Number: 10646774

All rights reserved

INFORMATION TO ALL USERS

The quality of this reproduction is dependent upon the quality of the copy submitted.

In the unlikely event that the author did not send a complete manuscript and there are missing pages, these will be noted. Also, if material had to be removed, a note will indicate the deletion.



ProQuest 10646774

Published by ProQuest LLC (2017). Copyright of the Dissertation is held by the Author.

All rights reserved.

This work is protected against unauthorized copying under Title 17, United States Code  
Microform Edition © ProQuest LLC.

ProQuest LLC.  
789 East Eisenhower Parkway  
P.O. Box 1346  
Ann Arbor, MI 48106 – 1346

# GENERATION AND MEASUREMENT OF MICROWAVES

## Synopsis

Part I reviews methods of generating microwaves in the shorter cm and mm region examining their possibilities, technical problems and limitations. It concludes that the spark microwave generator has its part to play in this field. A historical survey of past work on microwave spark generators which has been published by the author in Brit.I.R.E. Journal 13. 1953. p.490 is attached as Appendix I.

Part II analyses the theory and evidence in support of the characteristic radiation from a dipole type spark generator. It also examines in detail methods of frequency analysis and spectrum filtering by a large variety of semi-optical and waveguide devices. The Boltzmann interferometer is dealt with exhaustively. Some discussion of available power is also included.

Part III describes some technical problems of spark generation and methods of solving them.

Experiments are described to test waveguide devices which permit the control of radiated frequency band and result in a source tunable over a 2 to 1 range of frequencies. The established principles can be used to test waveguide components for matching characteristics and filters - in particular wide band filters - for their response and any spurious

effects. The range covered extends from 8 mm to 5 cm.

Appendix II contains a paper on the theory of a quarter wave transformer filter which is due to appear in "Wireless Engineer".

Appendix III dealing with the diffraction of non-monochromatic e.m. waves by a slit and a grating is a reprint from Proc. Phys. Soc. 68B. 1955. p.171.

## ACKNOWLEDGEMENTS

The author wishes to thank Professor F.M. Bruce for guidance and encouragement throughout the work.

Thanks are also due to several colleagues, in particular Mr. Z. Jelonek and Mr. A.S. Husbands (now with Messrs. Metropolitan-Vickers) for helpful discussion of many aspects of the work and Mr. J. Brown and C. Hammond for help with building the equipment.

# I N D E X

## PART I. SURVEY

	<u>Page No.</u>
1. Introduction	1
2. Coherent sources of mm waves	2
2.1. Coherent, monochromatic sources of mm waves	4
2.2. Harmonic generators of mm waves	7
2.2.1. Magnetron harmonics	8
2.2.2. Crystal generated harmonics	9
2.3. The Cerenkov generator	13
2.4. The "Doppler" generator	15
3. Incoherent sources of mm waves	17
3.1. Microwave noise generator	17
3.2. The microwave spark generator	22
3.2.1. The dipole system	23
3.2.2. The fixed array system	26
3.2.3. The mass radiator	27
3.2.4. Other systems	30
3.2.5. The question of coherence of spark generated waves	31

INDEX (Continued)

	<u>Page No.</u>
4. Detection of mm waves	32
4.1. The Bolometer	32
4.2. The Golay cell	33
4.3. The crystal detector	34
5. Conclusions	36

PART II. ANALYSIS

1. Introduction	38
1.1. The scope	38
1.2. The source	39
2. The self-oscillation of a dipole radiator	41
2.1. Some experimental evidence	49
3. Frequency analysis of radiation from a spark excited dipole	54
3.1. The frequency spectrum	54
3.2. Detector response	55
3.3. The determination of the spectrum of a radiating dipole	58

## INDEX (Continued)

	<u>Page No.</u>
3.3.1. The characteristics of dipole detectors	58
3.3.2. Measurement of dipole spectrum	59
3.4. The Boltzmann interferometer	61
3.4.1. Limitations of the Boltzmann interferometer method of measuring radiated waveform	66
3.4.2. The effect of "tuned circuit" filter on the Boltzmann interferogram	68
3.5. The standing wave method	72
3.6. Decaying waves in waveguides	75
4. Dispersion of spectrum of radiating dipole	79
4.1. Dispersion by a slit	79
4.1.1. Limits of solution	79
4.1.2. Spectral characteristics of a slit	82
4.2. Dispersion by a finite slit grating	85
4.3. Dispersion by an echellette grating	91

## INDEX (Continued)

	<u>Page No.</u>
4.3.1. Radiation normal to individual reflectors	91
4.3.2. Radiation normal to the plane of the echellette	96
4.4. General comments on the diffraction methods	101
4.4.1. Wire gratings used as high pass filters	103
5. The Fabry Perot interferometer	105
5.1. Fabry Perot interferometer using a dielectric slab	107
5.2. A metal film interferometer	108
5.3. The wire grating interferometer	110
6. Cavity and waveguide filters	111
6.1. The iris type filters	113
6.2. The inductive post type filters	114
6.3. The quarter wave transformer type filter	114
6.4. Conclusions on filters for spark generated waves	116

## INDEX (Continued)

	<u>Page No.</u>
7. Power output from a simple radiator	117
 PART III. EXPERIMENTAL  	
1. Introduction	122
2. Measurement technique	124
3. Equipment	126
3.1. Pulse generator	126
3.2. Radiating elements	127
3.3. Detected signal amplifiers	129
3.4. Wavelength measuring equipment	129
3.4.1. The Boltzmann interferometer	131
3.4.2. The echellette grating	132
3.5. Other equipment	134
4. Experiments with mark I dipole radiator	134
4.1. Output fluctuations	134
4.2. Auxiliary gaps	136
4.3. Spectrum analysis by Boltzmann interferometer	137

## INDEX (Continued)

	<u>Page No.</u>
5. The mark II radiator	140
6. Experiments with filters in the 1 to 3 cm region	142
6.1. The post type filter	142
6.1.1. Measurements at 3.1 cm	142
6.1.2. Measurements with spark generated waves	145
6.2. Experiments with iris filter	148
7. Filtering by wave guide cut-off changes	150
8. Experiments with wire netting	151
9. Experiments with reflection and diffraction gratings	152
10. Output power	153
10.1 Output power fluctuations at the upper frequency range	155
11. Conclusions	157
11.1. Performance	157
11.2. Filtering	158

## INDEX (Continued)

	<u>Page No.</u>
11.3. Measurement technique	159
11.4. Further developments	160
12. References	161
<p><u>Note:</u> References are given in alphabetical order and, where possible, are cited in text by author's name only. When this is not given, reference index number is quoted in superscript.</p>	
13. Appendices	

## PART I. A SURVEY

### 1. Introduction

Recent years have seen a rapid development in the techniques of generating electromagnetic waves occupying the portion of spectrum between radio frequencies and infra-red frequencies. <sup>(18,38,40)</sup> This development has been towards shorter and shorter waves reaching eventually the region described by the term microwaves and extending roughly between 10 cm. and a millimetre or less. This region is further sub-divided into "cm. waves" and "mm. waves", the latter extending to waves less than 3 cm. long.

There is nothing hard and fast about this subdivision, nor in fact about the limits of the larger group, the limits having been the outcome of war and post-war developments which concentrated in the 5 main bands "S" around 10 cm. "X" just above 3cm., "K" around 12.5 mm., "Q" around 8-9 mm., and "O" around 3 mm.

Historically, the work on what is now called microwaves preceded the development at the much lower radio frequencies. That was due to the fact that the original generators were of the spark oscillator type, and - as will be described later - after Hertz's original experiments it soon became apparent that mm. and cm. waves can be generated

by the same process. It was only when the thermionic valve oscillator was invented by Armstrong and was found to be limited to audio and radio frequencies that the emphasis shifted to long waves. The return to microwaves took place largely via radar and thanks to the development of the reflex klystron and the cavity magnetron. Both these devices rely for their operation on fairly high voltage, a dense electron beam and a resonator cavity, all of which tend to set a limit as to how small the valve can be made and hence it appears that the upper frequency limit is being reached at around 60,000 Mc/s (5 mm.).

Several methods of filling the remaining gap between 0.5 cm. and 0.1 mm. have been tried at various times. These will be described in some detail. Finally this thesis will concern itself with work on microwaval spark generators, both theoretical and experimental, using the waveguide as well as optical and semi-optical techniques.

## 2. Coherent sources of mm. waves

In discussing the various types of mm. wave generators, it is often necessary to consider their coherence. A source can be called coherent if the phase of the generated wave is at all times related to some reference phase by a fixed law. If, on the other hand, arbitrary shifts in phase take place, the wave becomes incoherent. These terms become

3

fully significant when one considers the effect of mixing the wave with a fixed frequency continuous oscillator and of detecting the intermediate frequency. With a coherent wave the detector will reproduce all the "information" about relative amplitudes and frequency and no more, while with an incoherent wave the detector output will contain random variations due to phase changes, which will constitute noise.

If waves are generated in short pulses with small duty ratio (ratio of pulse width to pulse period) it is clear that when the pulse of oscillation is appreciably longer than the period of intermediate frequency, there need be no common reference phase between the individual pulses unless the detector itself is phase sensitive.

The effect of random displacement of phase of a pulse of oscillation with respect to a continuous local oscillation on i.f. output, and the resultant noise in a peak detector has been studied by Jelonek. Fig. 1. taken from his paper shows the resulting shift in envelope which is given by the

$$\text{expression } \tau' = \frac{T_0}{4} \cos 2\theta'$$

where  $\tau'$  is time shift of the leading edge

$T_0$  is the i.f. period

$\theta'$  is the phase at the onset of the pulse

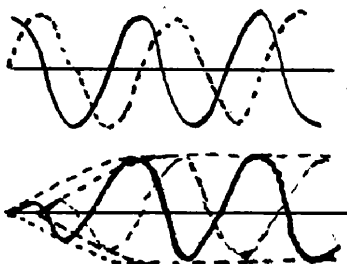


Fig. 1.

An identical expression gives the phase shift of the trailing edge, except for  $\phi''$  the phase at the end of pulse - in place of  $\phi'$ . This paper gives also the maximum amplitude of noise voltage caused by these phase differences when the pulses of oscillation are rectangular and of equal length:

$$V_n = A l f_a \sqrt{\frac{f_r f_a}{2\sqrt{3} f_0}}$$

where A = amplitude of pulse at the demodulating filter

l = pulse length

f<sub>a</sub> = audio frequency bandwidth

f<sub>r</sub> = pulse repetition frequency

f<sub>0</sub> = carrier frequency

Thus, as an example, if f<sub>a</sub> = 10 kc/s, f<sub>r</sub> = 1000 pps., f<sub>0</sub> = 3.10<sup>10</sup> c/s and l = 0.1 μ sec., then the minimum signal to noise ratio = 10 log  $\frac{A}{V_n} = 10 \log \frac{1}{l f_a} \sqrt{\frac{2\sqrt{3} f_0}{f_r f_a}} = 50$

The pulse contains 3,000 cycles and if the intermediate frequency of 45 Mc/s is chosen, there will be some 4 to 5 cycles of the intermediate frequency in the output pulse.

It is of interest to note also, that the noise is maximum when the i.f. pulse envelope is rectangular and is less for pulses with sloping edges.

### 2.1. Coherent, Monochromatic sources of mm. waves

The most important monochromatic sources are the magnetron and the klystron. These devices have been so

fully investigated and described that having become - as it were - classical generators they merit no further discussion here beyond stressing again that with present technique they do not appear to work successfully below 5 mm. although 3 mm. magnetrons have been made, but even at twice that wavelength the difficulties of construction are very great, the stability of operation in particular avoidance of mode jumping and requisite power output is difficult to achieve and the life is short. Spangenberg gives the relation between flux density  $B_2/B_1$ , voltage  $V_2/V_1$ , and current  $I_2/I_1$ , and the wavelength ratio of two magnetrons  $W = \lambda_2/\lambda_1$  and dimensional ratio  $D = r_2/r_1$  as:

$$\frac{B_2}{B_1} = \frac{1}{W} \quad ; \quad \frac{V_2}{V_1} = \frac{D^2}{W^2} \quad ; \quad \frac{I_2}{I_1} = \frac{D^2}{W^3}$$

Figure 2 plots the output power against wavelength for a number of modern British and American reflex klystrons.

(14)  
 Recently it has been reported from France that klystrons working in the 8 mm. region have been developed to give up to 40 mw. power output, while around 4 cm. power output of 5 watts (continuous) has been measured on another tube. These tubes are still in development. A 3 cm. water cooled klystron producing 500 watt output has been exhibited recently in this country.

Even more striking results have been obtained with the backward travelling wave tube (or "O" type carcinotron). This tube works on the same principle as a travelling wave

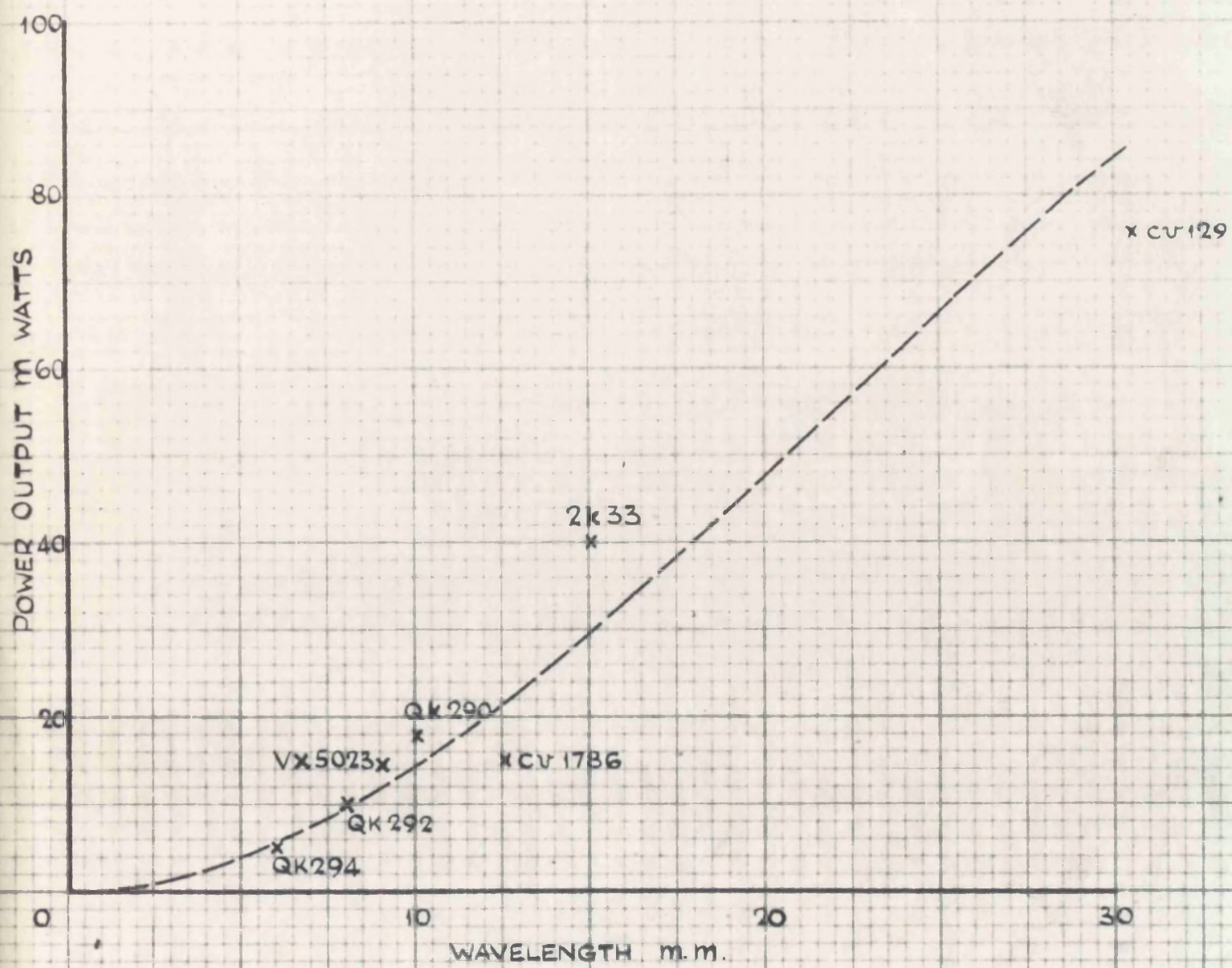


FIG. 2.

OUTPUT AND WAVELENGTH OF SOME MODERN BRITISH AND AMERICAN REFLEX KLYSTRONS.

amplifier, except that the travelling wave moves in the opposite direction to the electron beam. If the electron beam is made to interact with the travelling wave at regular intervals, it is quite possible to arrange the two velocities so that the electron always sees the wave in the same phase and is thus suitably accelerated by short equidistant pulses. This bunches the electrons and the bunches in turn induce and amplify the travelling wave. As long as certain basic conditions are satisfied and the structure carrying the travelling wave is matched at both ends to prevent reflections and forward travelling waves, the system will oscillate and can be tuned over very wide range of frequencies by changing the beam voltage. Great strides have been made in America in developing these valves and individual tubes tuning between 4.9 and 5.3 mm. and also between 4.8 and 6.7 mm. have been reported giving an output of the order of 1 mw. The lower limit appears to lie at present around 2.5 mm. This tuning is obtained by varying the beam potential, wavelength being somewhat inversely proportional to voltage, and from the published figures it appears that the rate of changes of frequency with voltage is of the order of  $20 \text{ Mc/V}$  around 1,000 V (7 mm.) and  $6 \text{ Mc/V}$  around 2,000 V (5 mm.). The main difficulty in reaching the very wide frequency range is the absolute necessity for matching over the whole band which has not been possible to achieve as yet with the result that blind spots occur in

7

the range.

It is as yet difficult to foresee the use for these valves but it seems clear that as sources of monochromatic waves they would call for supply stability of the order of .005% to keep the frequency within 1 Mc of desired value. The solution will probably be found on the lines of the Pound stabiliser used with klystrons.

It would appear that the backward travelling wave oscillator will offer a good, working solution to the problem of generation of millimetric waves.

Of other methods of producing monochromatic waves in the mm. region the most important to-day are various forms of harmonic generators using the klystron or the magnetron as the source of the fundamental oscillation at lower frequency.

## 2.2. Harmonic generators of mm. waves

Both the klystron and the magnetron generate waves which are not strictly sinusoidal, such effects as non uniform bunching in a klystron or magnetic field distribution in a magnetron may be the cause of this. Since both valves employ cavities of high Q the harmonics are of necessity very weak, hence klystron harmonics are negligible. In pulsed magnetrons the peak powers can be very large hence harmonics become appreciable. This then is one method of obtaining mm. waves from larger valves.

Another method is to use the non-linear characteristic of a silicon or germanium crystal. When microwave energy impinges on a crystal, rectification takes place resulting in the crystal reradiating waves rich in harmonics.

### 2.2.1. Magnetron harmonics

The theory behind magnetron harmonics appears to be too complex to lead to any numerical predictions. Klein and others who obtained some experimental evidence for these found that even minor unaccountable changes in manufacturing techniques, such as occur between the manufacture of successive batches of one type of magnetron lead to considerable changes in harmonic content.

By filtering out fundamental and lower order harmonics by the use of tapered waveguides and then dispersing the remaining harmonics by an echellette grating they observed the following maximum peak powers in the fourth to tenth harmonic of 5J31 magnetrons (1.25 cm. fundamental; peak power of the order of 20 Kw in 0.5 microsec. pulse) 300,000, 36,000; 7,200; 2,200; 2,800; 70; 120 respectively. The observed average signal to noise ratios from third to eighth were 400,000; 18,000; 9,000; 1,100; 1,000, 300 respectively,  $\frac{S}{N} = 1$  corresponding to 0.6  $\mu$ W peak power.

The main troubles with this sort of mm. wave generator are difficulties in varying the frequency and the need to test a large batch before one can be sure of obtaining

enough power in the desired harmonic. For example, the peak powers for the 3rd harmonic (just over 3 mm. wave) have been found to vary from valve to valve between 1 mw. and 50 mw.

Since all magnetrons tested have been made to work in the fundamental mode, it is possible that suitable distortion could result in magnetrons rich in harmonics although not very good in fundamental mode. No such work has been reported to date.

### 2.2.2. Crystal generated harmonics

The current through and voltage across a semi conductor such as a silicon or germanium crystal are related within certain limits by the law

$$i = A(e^{bE} - 1)$$

which leads to the well known graph. (Fig. 3.) Typical values are  $A = 7 \mu A$ ,  $b = 18 \text{ volts}^{-1}$

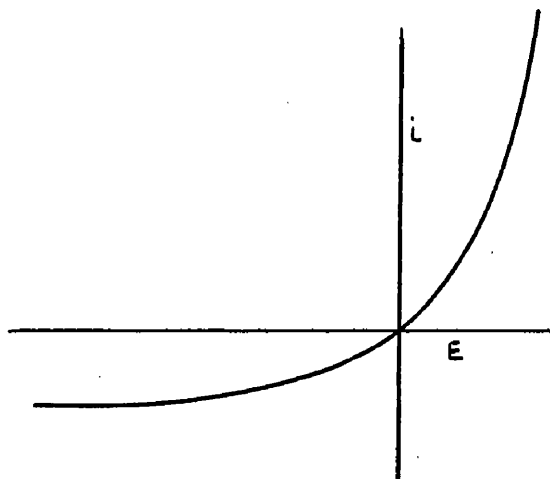


Fig. 3.

### Crystal Characteristics

When a low frequency signal is applied to such a device, the resultant distortion in current wave form will be rich in harmonics. At high frequencies it is not possible to take this simple view because of crystal capacity as well as spreading resistance.

When this is considered, the expressions for generated harmonics become very involved. Christensen attempted to calculate this by neglecting C. He arrived at an expression for power in harmonics in the form

$$P_{n\max} = \left(\frac{L}{2}\right)^2 \cdot \frac{k}{2b} \cdot \frac{1}{1+rbk} \text{ Watts}$$

where k is a constant approximately equal to the crystal current,

L is a figure characteristic of each harmonic,

r is the spreading resistance (about  $15\Omega$ )

Thus for 7th harmonic

$$k = 2.74 \text{ mA}$$

$$L = .12$$

$$P_{7\max} = .16 \mu\text{w}$$

Where input power at fundamental frequency was .69 mW corresponding to maximum input Voltage of 0.5 V and current of 2.75 mA. Thus the 7th harmonic is 36.4 db below fundamental power. A similar calculation shows that the 9th harmonic should be 48 db below fundamental power. These results have been compared by Christensen with those obtained from an experiment conducted at comparatively low

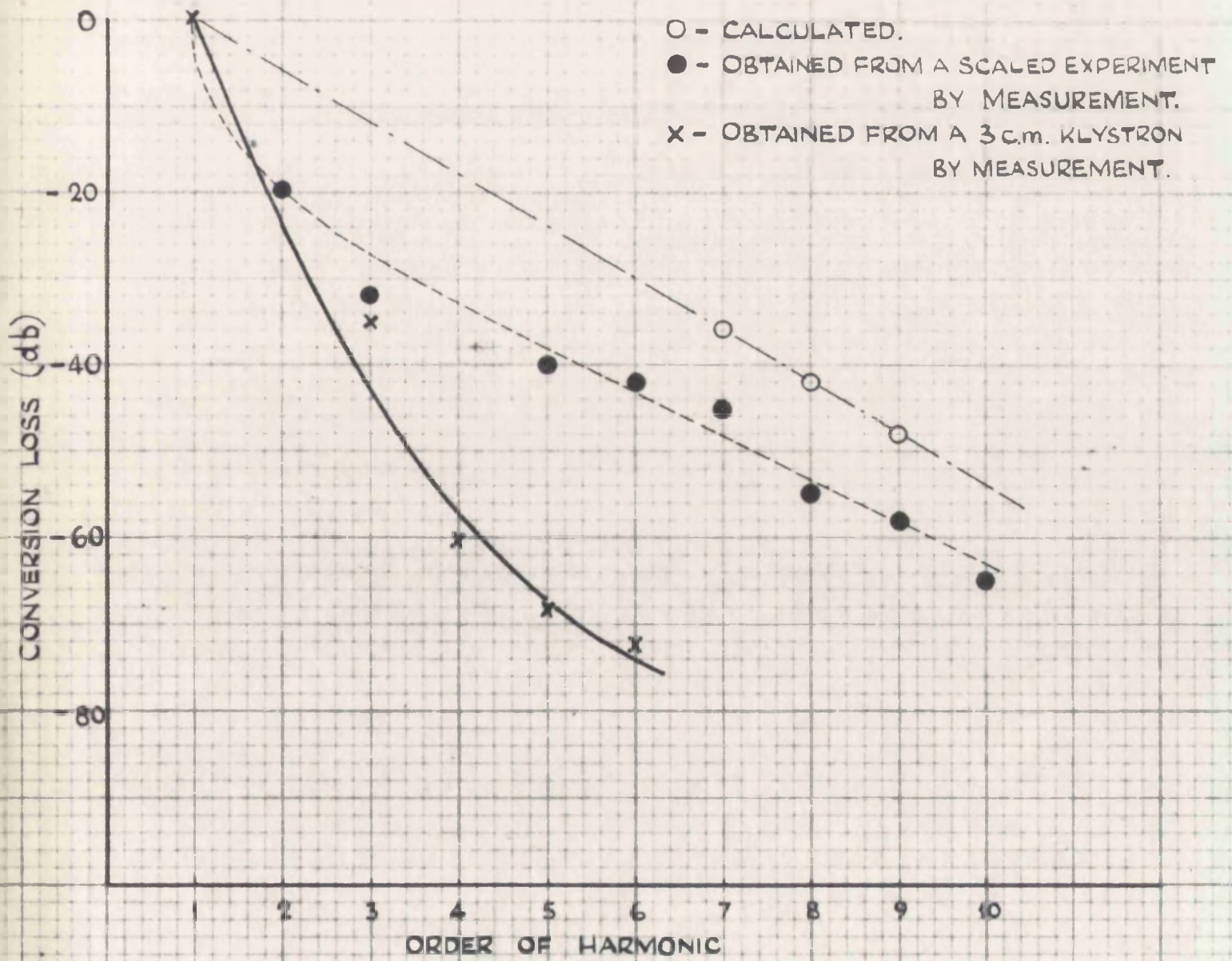


FIG. 4.

CONVERSION LOSS IN CRYSTAL GENERATED HARMONICS (AFTER CHRISTENSEN)

frequencies which gave the conversion loss as in Fig. 4, which contains also the calculated values and the results of experiment conducted with 3 cm. klystron supplying the fundamental power.

Tests conducted by Johnson, Slager & King using klystrons working at higher frequencies led to results which are illustrated in Fig.5. The same authors examined the effects of varying the fundamental power and found that harmonic power increases at a greater than linear rate within the limits of the experiment in which maximum fundamental power was 50 mW. Since no selection of even as against odd harmonics appears, the crystal current must be a power series of voltage in spite of the apparent linearity of modern crystals at powers in excess of 0.1 mW.

Considerable work has also been done by Gordy and collaborators in connection with mm. wave spectroscopy. They have reported success down to .77 mm. waves.

Attempts to improve harmonic power by biasing the crystal have led to inconclusive results in so far as an improvement has been observed in a few cases, but not as a rule.

The signal to noise ratio depends very much on the amplifier used and, in particular, great improvement can be obtained with very narrow band or with phase sensitive detectors, but even without these elaborations a signal to

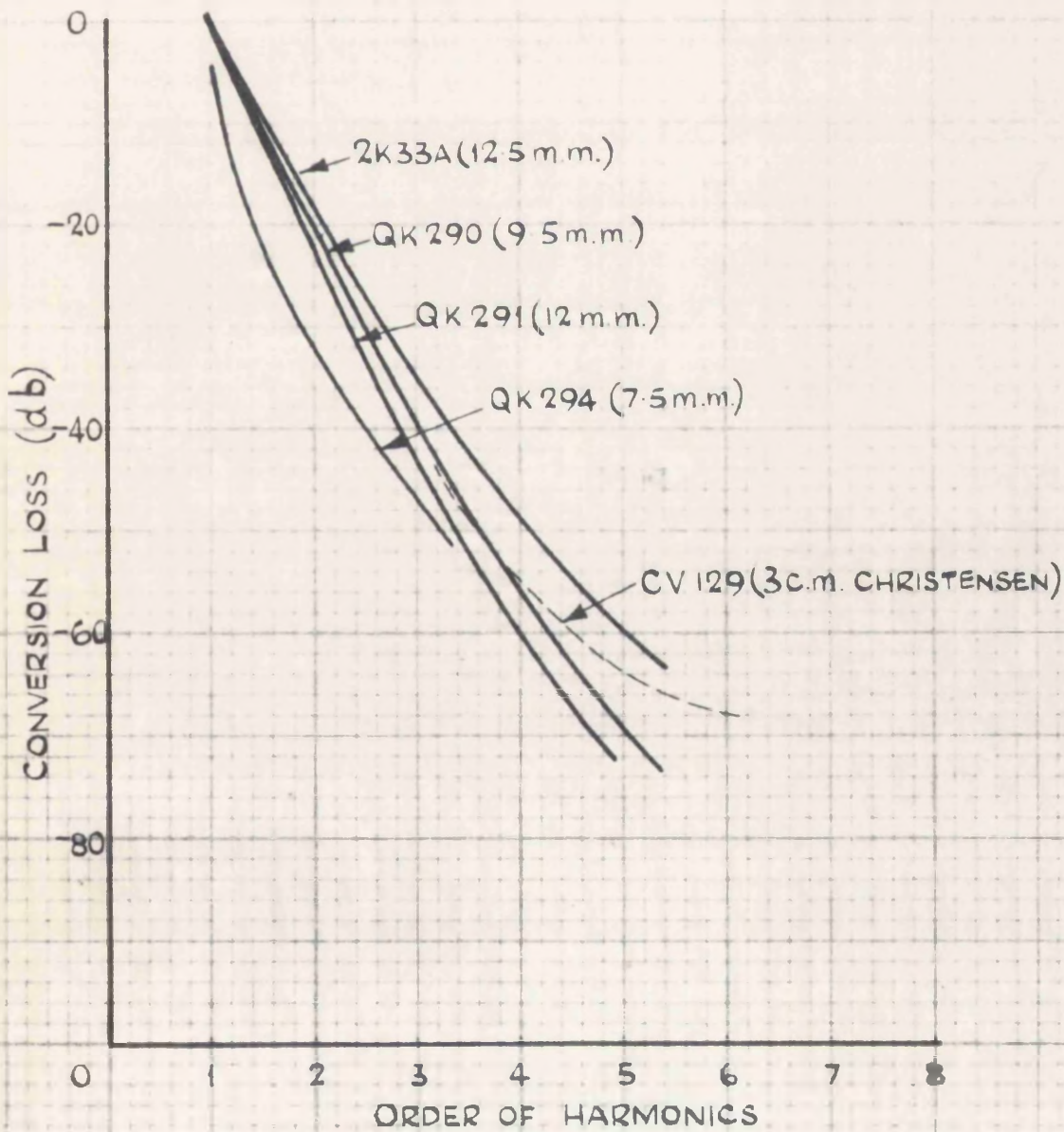


FIG. 5.

CONVERSION LOSS IN CRYSTAL GENERATED HARMONICS.  
(AFTER JOHNSON, SLAYER AND KING. DASHED LINE SUPERIMPOSES  
RESULTS OBTAINED BY CHRISTENSEN.)

noise ratio of well over 60 db can be expected up to the 6th harmonic. Silicon crystals have been commonly used although investigation on welded germanium crystals proved them superior to silicon ones.

The harmonic generator has the great advantage of being a source of monochromatic radiation and fairly stable at that, since the klystron or magnetron generating the fundamental can be made in the band where stability and good life can be achieved. On the other hand the limited tuning permissible on the fundamental source does not allow for continuous variation of frequency. Usually a coverage of 5% around the centre frequency is all that can be expected.

It is true that 10% of 30,000 Mc/s is quite a wide band, nevertheless it is only a small portion of the spectrum. On the other hand the driving klystron must be very closely stabilised since the harmonics accentuate any instability.

Fig. 6. below gives a typical set-up for harmonic generation using a coax or a wave guide feed. Other ingenious systems have been described recently by Wilshaw, Lamont and Hickin.

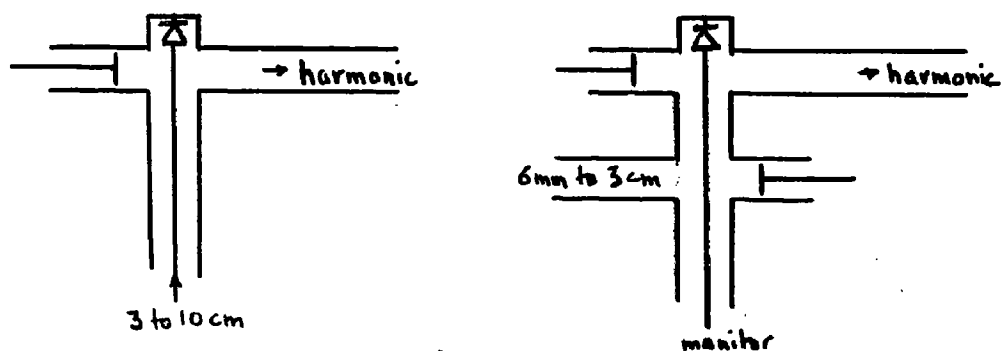


Fig 6.

Details of arrangements and suitable circuits have been discussed at length by Gordy, Smith and Trambarulo.

### 2.3. The Cerenkov Generator

Following the discovery by Cerenkov that visible radiation is emitted when fast electron beam passes through matter, it has been proved theoretically by Frank and Tamm that <sup>when</sup> the electrons traverse a medium with a velocity greater than that of light through the same medium then light will be radiated. (23, 24, 31, 32, 36) This theory has been extended to show that all waves will be radiated whose velocities of propagation through a given medium are lower than that of a beam of electrons crossing the medium. If the electron velocity is  $u$  and the dielectric constant of the medium at a given frequency  $f$  is  $k$  then the velocity of propagation of a wave at that frequency =  $\frac{c}{\sqrt{k}}$  hence the wave will be radiated if  $u > \frac{c}{\sqrt{k}}$  or  $\frac{u\sqrt{k}}{c} > 1$ , the direction of radiation making an angle  $\alpha$ . with direction of the beam such that  $u \cos \alpha = \frac{c}{\sqrt{k}}$  Since the electrons cannot be made to cross the medium undisturbed one either has to let the beam go through a hole in the medium or very close to its surface, which has been shown to be as good.

The latter case is the most promising to achieve. In that case it has been shown that the power radiated by a beam of  $I$  amps in the frequency band  $df$  around the frequency  $f$  is

$$P(f)df = \frac{I\pi e^2 L}{2k_0 c^2} \left(1 - \frac{c^2}{u^2 k}\right) e^{-\frac{4\pi L f \sqrt{c^2 - u^2}}{uc}} f df$$

where  $L$  = length of beam in medium

$l$  = distance of beam above medium surface

$k_0$  = dielectric constant of air (MKS units)

Twiss shows that the frequency around which maximum energy is radiated is given by

$$f_{max} = \frac{uc}{4\pi l \sqrt{c^2 - u^2}}$$

which means that for any desired wavelength  $\lambda$  to correspond to condition of maximum energy  $l = \lambda/24$  for 50 kev electrons and  $l = \lambda/6$  for 500 kev. Thus for mm. waves practical difficulties will demand ultra high electron velocities.

It can be shown that if the beam, instead of being continuous, were bunched so, that each bunch would be less than  $1/2$  space charge wavelength long, the radiated wave would consist only of harmonics of the frequency of bunches as long as these satisfy the basic considerations of the Cerenkov effect. In that case the power radiated at a wavelength  $\lambda$  would be

$$P = \frac{I l}{\lambda} \left(1 - \frac{c^2}{u^2 k}\right) e^{-\frac{4\pi l \sqrt{c^2 - u^2}}{\lambda u}} \cdot 10^{-2} \text{ watts}$$

where  $I$  = the average current in the bunched beam

$L$  = length of dielectric

Under practical conditions this gives a power output at 5 mm. of the order of 100 microwatt, which has to be multiplied by a further factor  $< 1$  depending on the efficiency of concentrating the energy on a receiver.

The difficulties of radiating shorter waves appear at present very great indeed.

## 2.4. The "Doppler" Generator

When an electron, moving at velocities where relativistic effects take place, accelerates, it radiates energy. This led several writers to discuss the possibility of producing mm. waves by this means. Some success was achieved by Motz and collaborators by making these fast electrons cross a succession of magnetic fields of opposite polarities (an undulator) so that the electrons describe a sinusoidal path. This is equivalent to a steady axial motion with transverse oscillation superimposed, or an oscillator travelling at very high speed. For a stationary observer, by virtue of the relativistic Doppler effect, the frequency of radiation varies from maximum if the oscillator approaches him to a minimum if it recedes. At any angle  $\theta$  the observed frequency will be

$$f = \frac{u}{\ell_0} \left( \frac{1}{1 - \frac{u}{c} \cos \theta} \right)$$

where  $\ell_0$  is the distance between alternate poles, i.e. half wavelength of the sinewave described by the beam.

The term in brackets is the effect of relativistic contraction within the Doppler effect. This expression assumes an infinitely long undulator. Since the observer is stationary he receives a whole spectrum of frequencies incoherently. This can be overcome theoretically by bunching the electrons to such an extent that the observer facing the oncoming beam receives a series of pulses which add up to a coherent, fairly narrow band radiation, provided

the bunches are less than half wavelength of radiation long, i.e., for 1 mm. waves the bunches have to be less than .5 mm. long and occur every 1 mm. along the beam.

In practice the beam is sent through a waveguide across the undulator which can be shown to lead to a number of modes

$$f_{mn} = \left( f' + \frac{u \beta'_{mn}}{2\pi} \right) \cdot \frac{1}{\sqrt{1 - (u/c)^2}}$$

where

$$f' = \frac{u}{L_0 \sqrt{1 - (u/c)^2}}$$

$$\beta'_{mn} = \sqrt{\left( \frac{2\pi f'}{c} \right)^2 - \left( \frac{\pi m}{a'} \right)^2 - \left( \frac{\pi n}{b'} \right)^2}$$

$a'$  and  $b'$  are the waveguide dimensions contracted according to Lorentz law.

Theoretically, large powers can be expected at mm. range. In the experiments carried out the undulator consisted of 14 pairs of poles, 4 cm. apart. The electrons came from a 3-5 Mev accelerator and were bunched at 2856 Mc/s to within  $30^\circ$  of the travelling wave. Waves were detected in a band around 1.9 mm. at an estimated peak power of over 10 watts. This power could probably be increased with a better design of the equipment, but it is doubtful if one could make this generator into a strictly monochromatic one.

The very large voltages required and the very exacting demands on bunching tend to limit this method at present to a laboratory.

### 3. Incoherent sources of mm. waves

Two such sources will be described here: the microwave noise generator and the microwave spark generator. In the case of the latter source it will be shown that under suitable circumstances it need not be incoherent (within the earlier definition of that term).

#### 3.1. Microwave noise generator

A black body whose temperature exceeds absolute zero radiates energy in the form of incoherent noise. The available noise power =  $kTB$

where  $k$  is Boltzmann's constant

$T$  is absolute temperature

$B$  is bandwidth over which radiation takes place or is measured.

Any source of noise can thus be described in terms of an equivalent black body temperature.

The temperatures to which ordinary bodies can be raised for the purpose of generating noise are too small for effective output power, at least on the laboratory level (very high temperatures and therefore powerful sources of noise do exist in the universe outside our planet).

It is known, however, that the electrons in the positive column of a gas discharge have energies corresponding to a very high temperature. Cobine gives the following graph (Fig. 7.) representing the relation between

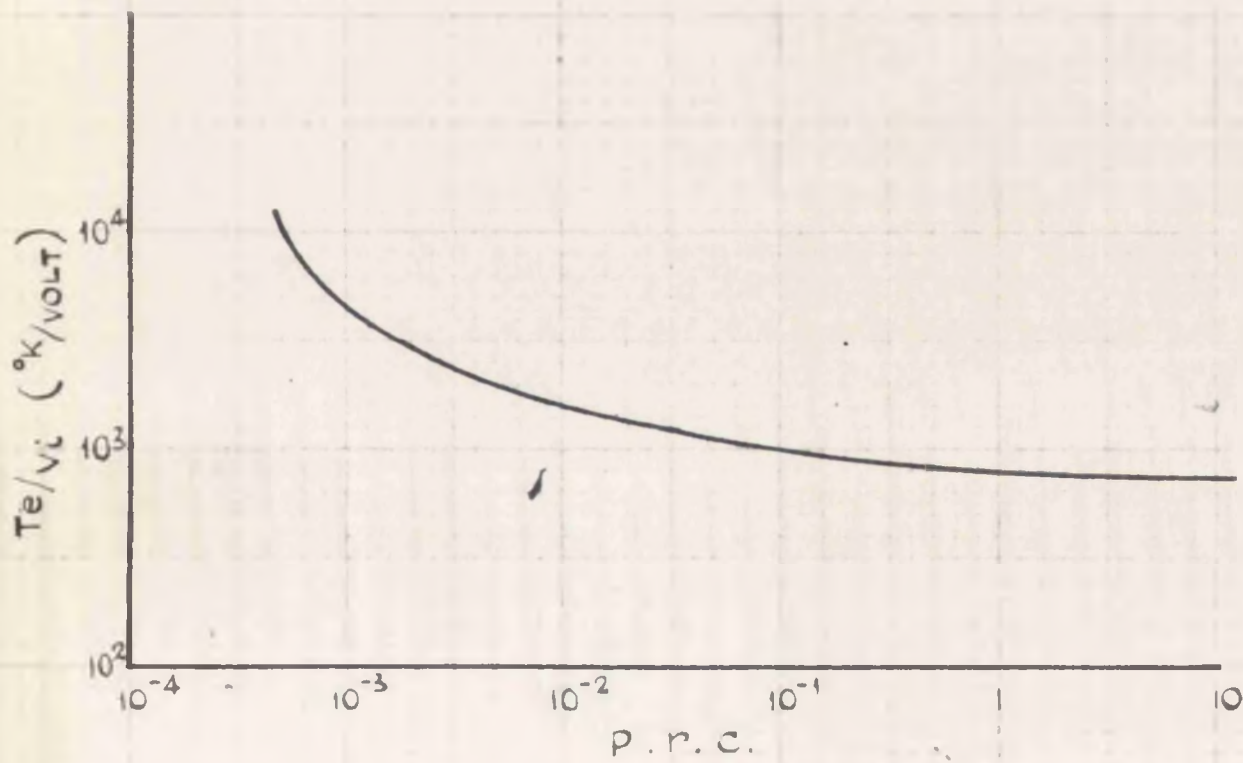


FIG. 7.

ELECTRON TEMPERATURE AS RELATED TO IONISATION POTENTIAL, PRESSURE AND DISCHARGE COLUMN RADIUS. (AFTER COBINE)

the ratio of electron temperature and ionisation potential ( $T_e/V_i$ ) and the product of pressure, radius of discharge column and a constant characteristic of the gas (p.R.C.)

The values of C and  $V_i$  are as follows:-

	C	$V_i$
Helium (He)	$3.9 \times 10^{-3}$	24.5
Neon (Ne)	$5.9 \times 10^{-3}$	21.5
Argon (A)	$5.3 \times 10^{-2}$	15.7
Mercury Vapour (Hg)	$1.1 \times 10^{-1}$	10.4

Thus it will be seen that by suitable choice of gas, tube radius and pressure, temperatures of the order of  $10^4$ K can be obtained. One is not quite free to choose the values of p and r arbitrarily, because other conditions, such as current density  $\alpha$  (pressure)<sup>2</sup>, make it advisable to keep the product p.r constant, i.e. reduction of radius calls for increase in pressure.

As an example a tube  $3/8$ " diameter filled with argon at 30 mm. Hg pressure should give electron temperature of  $11,000^\circ\text{K}$  or noise power of 15.8 db above  $290^\circ\text{K}$  ambient. A  $3/16$ " diameter tube filled with argon at 20 mm. pressure should give electron temperature of  $12,600^\circ\text{K}$  or noise power 16.4 db above  $290^\circ\text{K}$ . Johnson and Dermer using such tubes found noise powers in excess of  $290^\circ\text{K}$  of 15.5 db and 17.4 db respectively showing good agreement with theory. The first tube worked in the X band, the second in the Q band.

Similar experiments carried out in the Q band by Bridges gave the following results:

Tube No.	1 (Ne)	2 (A)
Gas pressure mm. Hg.	30	20
Insertion loss	.7 db	.3 db
VSWR	1.1	1.1
Tube current mA	45	35
Measured noise temp. °K.	19,300	11,500
Noise figure db	18.2	15.9
Calculated noise temp. °K.	21,000	10,000

For best results the correct tube diameters, gas pressure and discharge current have to be found empirically. Reducing the diameter and increasing pressure in direct proportion with wavelength reduction the equivalent temperature remains constant, hence tubes can be designed for appropriate bandwidths. The tube can be placed across the long dimension (X axis) of the guide or along its length (Z axis) with the guide bent to keep the electrodes outside the waveguide and the positive column within it, as in Fig. 8.

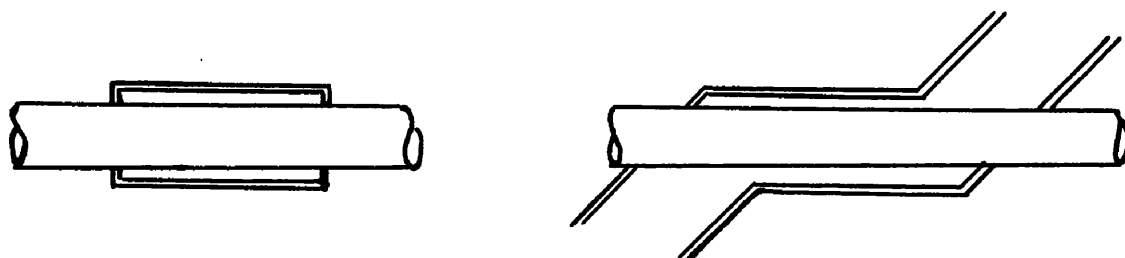


Fig. 8.

The total power depends, of course, on the bandwidth (kTB) i.e. at an equivalent black body temperature of  $10^4$  the available energy per cycle is of the order of  $10^{-19}$  watts.

Mumford in his investigations of noise generated by discharge tubes obtained a very interesting confirmation of Wien's displacement law which appears to apply down to frequencies in the mm. region.

The Wien's law is a direct outcome of Planck's law which states that the energy density per unit wavelength range radiated by a black body at absolute temperature T around wavelength  $\lambda$  is given by the expression

$$E_{\lambda\nu} = \frac{8\pi ch}{\lambda^3 (e^{ch/\lambda kT} - 1)} \text{ watts/cm}^3$$

where c is velocity of light

h is Planck's constant

k is Boltzmann's constant

If plotted this gives a series of curves shown in graph, Fig. 9.

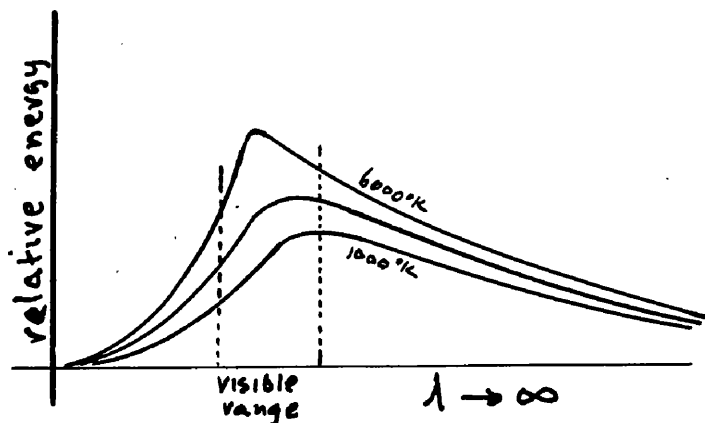


Fig. 9.

Energy distribution of radiation  
of a black body.

When the maximum energy is found it is seen that the product of wavelength at which maximum energy is radiated ( $\lambda_m$ ) and the corresponding absolute temperature (T) is constant and equal to 0.288 cm. degree. This is the Wien's displacement law. For bodies other than black, the value of  $\lambda_m T$  is still constant, but less than 0.288.

Mumford found that a mercury discharge tube (containing also Argon for starting purposes) produced noise power in the band between 4200 and 7300 Mc/s of 15.8 db above 290 K, i.e. equivalent to a temperature of 11,400K. The measured  $\lambda_m$  for the discharge is  $2536.5 \times 10^{-8}$  cm., which by Wien's law gives  $T = 11550$  K which is in very close agreement with observation.

The Planck's law expressed in terms of energy density per unit bandwidth around a frequency  $f$  is given by

$$E_{fv} = \frac{8\pi h f^3}{c^3 (e^{hf/kT} - 1)}$$

At the frequencies corresponding to mm. waves (i.e. well to the right of  $\lambda_m$  in the Fig. 9 above),  $e^{hf/kT} \doteq 1 + \frac{hf}{kT}$

$$\text{hence } E_{fv} = \frac{8\pi kT}{c\lambda^2}$$

which means that energy density is inversely proportional to the square of wavelength. If the energy is fed through a suitable wave guide whose cross section is proportional to  $\lambda^2$ , the total energy per cycle will be constant and depend only on temperature.

While the discharge tube offers a very simple source of uniform noise power at any desired range, the energies obtainable are too small for any purposes other than developing and testing mm. wave components, especially where wide band matching problems are involved.

Work has also been carried out on radiation from high pressure mercury arcs which are used for infra-red work. Radiation within .3 - .5 mm. was isolated by Daunt et al. The measured power was  $1.2 \times 10^{-5}$  watts per square cm. The authors estimated that at 1 mm. the power would be reduced by a factor of 16. Experiments were also conducted with thallos bromide, which, as a highly polar compound, should give rise to long infra-red radiation when subjected to a discharge. The thallos bromide was introduced into a discharge tube containing Helium at a few mm. pressure. Only slight increase in power around .5 mm., as compared with the mercury discharge tube, was observed.

3.2. The microwave spark generator

This generator is a development of the original work by Hertz in which he caused a circuit to oscillate at its resonant frequency by producing first an electric discharge across a gap in the circuit.

It can be proved theoretically, as will be discussed in part II, that when field is made to change rapidly around a conductor, the conductor will generate a damped sinusoidal

oscillation characteristic of its shape and medium surrounding it. Righi is credited with being first to make a reasonably efficient radiator of microwaves in the form shown in Fig. 10.

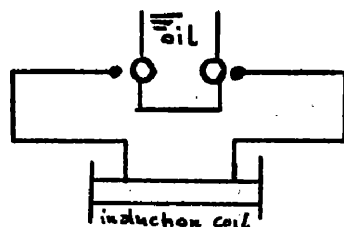


Fig. 10.

The Righi generator

The two balls were half immersed in oil so that the high voltage had to be established across the entire gap before it would break down. Thus Righi achieved a sudden and large change in field across the balls, which resulted in radiation

Lebedev achieved the same results by substituting rods of platinum for balls, radiating waves down to 3 mm. Since this pioneer work a great deal of experimental evidence has been gathered using various systems which will now be discussed. A review of work done by various researchers has been published by the present author recently. Appendix I.

3.2.1. The dipole system

This is the system used by Righi and Lebedev. As will be discussed later, the spherical dipoles should radiate at

wavelength of the order of 7 times the radius while the cylindrical dipole should radiate at wavelength of the order of 2 to 4 times the overall length, depending on the ratio of length to diameter of the cylinders. A further increase in wavelength in the ratio of relative dielectric constants of surrounding media to air has to be made as necessary.

The following table gives some of the results obtained:-

Spherical dipoles:

Sphere dia.	$\lambda$ mm.	$\lambda$ /radius	Experimentors
8 mm.	26	6.5	Righi (1895)
7.9 mm.	40	10.1	Hull (1897)
9.5 to 38.1		9.9	Webb and Woodman (1909)

Cylindrical dipoles:

Length mm.	dia. mm.	$l/d$	$\lambda$ mm.	$\lambda/l$	
40	2	20	101	2.52	Melloh (1940)
30	.9	33.3	64.5	2.15	Hasselbeck (1932)
22	1	22	55.6	2.52	Melloh
20	.9	22.2	52	2.60	Hasselbeck
12	1	12	45.9	3.82	Melloh
10	.9	11.1	31.3	3.13	Hasselbeck

Continued overleaf/

Cylindrical dipoles (Continued)

Length mm.	dia. mm.	$l/d$	$\lambda_{mm.}$	$\lambda/l$	Experimenters
10	.5	20	27	2.7	Nichols & Tear(1923)
6.6	.5	13.2	21.6	3.3	Nichols & Tear
6	.9	6.7	23.3	4.7	Hasselbeck
4.5	.5	9	16.2	3.6	Mobius (1920)
4	.5	8	11	2.8	Nichols & Tear
4	.9	4.45	21.3	5.3	Hasselbeck
2.6			6	2.3	Lebedev (1895)
.85	.25	3.4	4.2	4.9	Nichols & Tear
.4	.25	1.6	1.9	4.8	Nichols & Tear

(For detailed references see appended paper by the author: Appendix I.)

Plotting  $\lambda/l$  against  $l/d$  one obtains the graph below, Fig. 11., showing that as  $l/d$  tends to infinity  $\lambda/l$  tends to 2. The considerable differences obtained by various experimenters are possibly due to different lengths of the dipoles being sealed in glass and immersed in oil or paraffin, thus increasing the effective length of the dipole. Apart from that it is seen that as one goes to shorter and shorter waves, the combined effect of increased ratio of length to diameter and of larger portion of dipole scaled

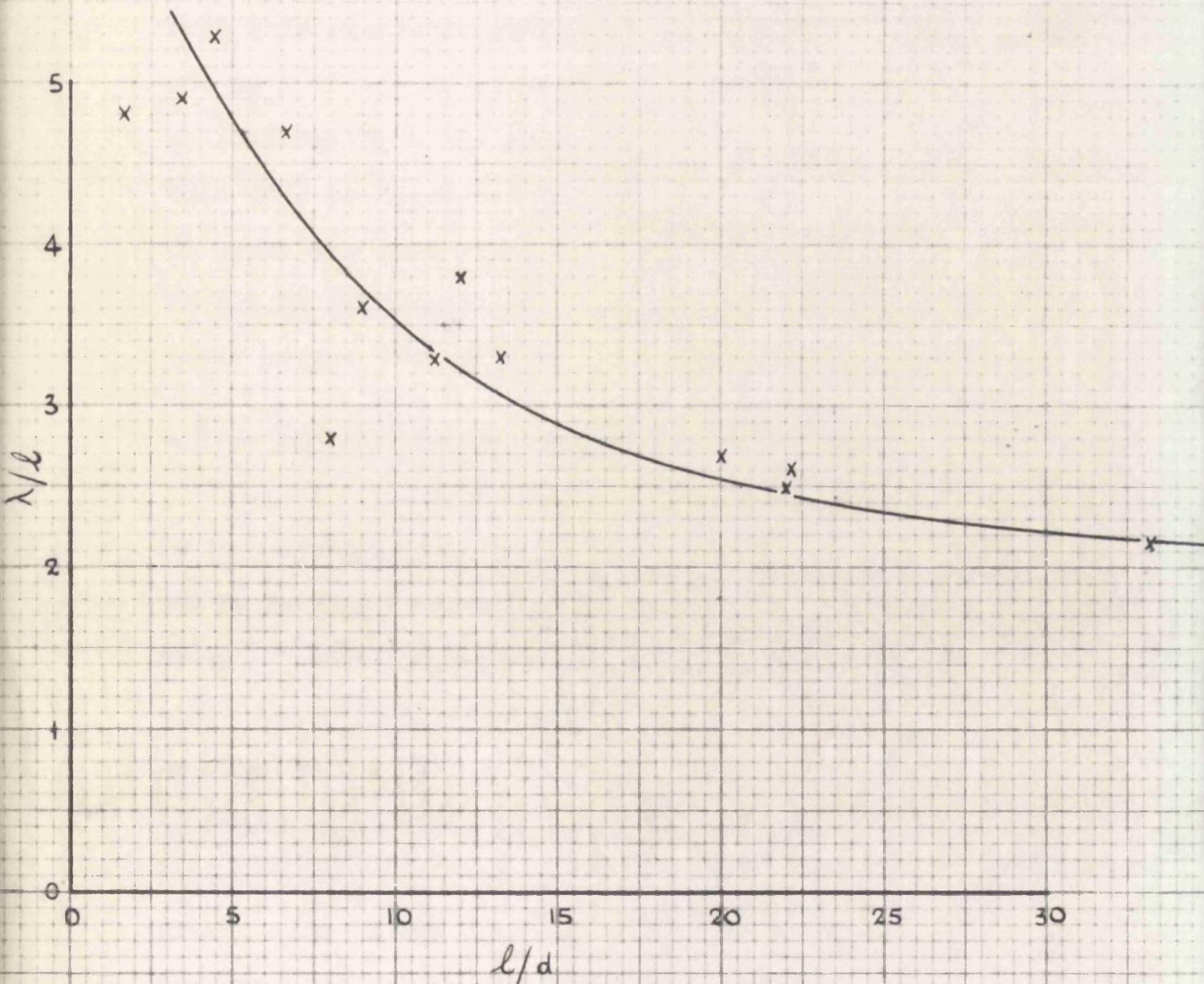


FIG. 11.

RELATION BETWEEN  $\lambda/l$  AND  $l/d$  FOR CYLINDRICAL DIPOLES.

in a dielectric such as glass (dielectric constant of the order of 6) is to increase the ratio  $\lambda/\epsilon$  to over 5. In view of the necessity to make the dipoles substantial enough to withstand repeated sparking and to mount them securely, it would appear doubtful if one could reach wavelengths much below 2 mm. This, however, neglects the fact that this generator radiates over a wide band of frequencies, and so a dipole of reasonable dimensions can be - by suitable filtering - the source of waves down to 1 mm. or less. This will be discussed at length in part II. No estimate of power has been given by the experimenters, but it appears to lay in the microwatt region. A fuller discussion of power output will also be given in part II.

3.2.2. The fixed array system

In this arrangement a large number of dipoles spherical or cylindrical, are assembled end-on in several parallel lines and high voltage pulses are applied across the whole array. Levitzky built up such an array using 8 mm. lead balls fixed to a glass plate with canada balsam but gives no results. She also built up an array using tiny pieces of molybdenum wire 2 mm. in diameter and varying in length from 1 to 4 mm. These were again fixed to a glass plate with canada balsam in rows, the rows being kept 1 mm. apart. She measured the wavelength of radiation with the help of various plane and concave gratings and found many maxima corresponding to wavelength between .03 and .51 millimetres.

Some of the wavelength and corresponding intensities are given in table below:

<u><math>\lambda</math> microns</u>	<u>32</u>	<u>75</u>	<u>92</u>	<u>136</u>	<u>187</u>	<u>270</u>	<u>305</u>	<u>330</u>	<u>432</u>	<u>470</u>
relative intensity	1	2	1.5	4	3	3.5	3	3.5	2	2

Later, however, she suggested that the shortest of these waves were possibly due to some other causes. Most of the energy appeared to be radiated from the outermost elements of each row.

Similar experiments using 12 mm. balls have been conducted by Montani who claims to have generated an appreciable amount of energy spread over a very wide spectrum. This system suffers from the serious disability of adjusting the individual gaps so that as time goes on the arcing becomes irregular and fewer elements radiate.

### 3.2.3. The mass radiator

The difficulties of adjusting an array have been overcome by Glagoleva Arkadieva by suspending the elements in oil. The suspension is then drawn between two electrodes to which the high voltage pulse is applied, causing violent sparking. Several modifications of this idea have been tried such as: stirring the suspension to keep it uniform by air blast and then taking it up to the electrodes by a rotating wheel; allowing the suspension to drop past one

electrode on to another below; allowing the suspension to fall slowly as in an hour glass between the electrodes placed in the neck of the glass; forcing the suspension through a horizontal tube past the electrodes, etc.

All of these methods appear to work fairly satisfactorily but very irregularly due to the random variations of number of elements in each sample sparked when the pulse is applied.

In the experiments performed by Glagoleva Arkadieva and by Cooley & Rohrbaugh, the particles were iron or aluminium fillings of sizes varying from .5 to 3.2 mm.; accordingly, radiation extends over very wide spectrum from 100 microns to several millimetres.

Daunt and others repeated those experiments using lead shot of diameters between 1.1 and 1.35 mm. suspended in oil (castrol R). The resultant output examined with the help of an echelette grating gave the relation between intensity and wavelength reproduced in Fig. 12.

This shows a maximum at 5.7 mm. with a half power spread from 4 mm. to 8 mm. The figure of 5.7 mm. compares well with the theoretical one 4.5 mm. when one corrects for the dielectric effect of oil. (It is interesting to note that an estimated 90% of energy radiated was at wavelength shorter than 3 cm.). The estimated output power at the spark repetition frequency

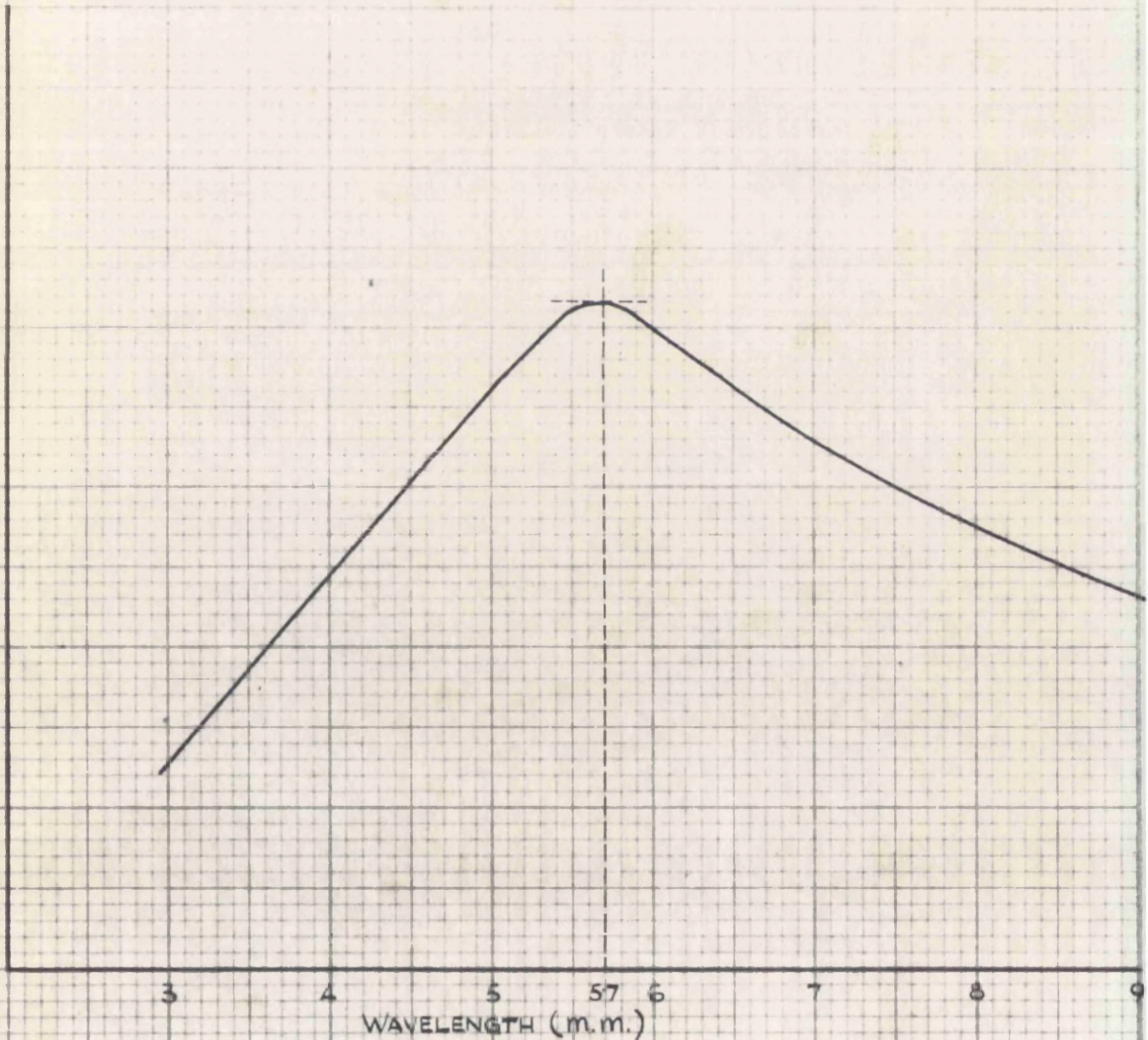


FIG. 12.

EHELLETE SPECTRUM OF A SPARK GENERATOR CONSISTING OF  
.1 TO 1.35 m.m. DIA. BALLS.  
(AFTER DAUNT, JACKSON, HULL AND HURST)

of 80 per second is estimated by the authors as 30 mW, although only 6 mW could actually be beamed out.

Glagoleva Arkadieva attempted to calculate the maximum power obtainable under optimum conditions:

Let  $D$  = diameter of spheres in suspension

$d$  = distance between centres of spheres

$k$  = ratio of volume of spheres to vol. of mixture

$k_0$  = maximum possible value of  $k$ ,

then  $d = D \left( \sqrt[3]{k_0/k} - 1 \right)$

and energy stored per cm.<sup>3</sup> =  $\frac{N}{2} \cdot \frac{CV^2}{2} = \frac{5.31 KCV^2}{D^3} \cdot 10^{-7}$  Joules/cm.<sup>3</sup>

where

$C$  = capacity between a pair of spheres

$V$  = breakdown voltage between a pair

$N$  = number of spheres per cm.<sup>3</sup> = density of suspension

A plot of energy against  $k$  shows that maximum energy corresponds to  $k = 12\%$  of  $k_0$ , which for 1 mm. spheres gives maximum energy of about  $3 \times 10^{-3}$  joules/cm.<sup>3</sup>, i.e. with 80 sparks per second, maximum power = 240 mW. Daunt et al. worked with a random density of suspension, which fell by gravity between two spherical electrodes  $3/4$ " and  $1/2$ " dia. respectively, and separated by 1 cm. so that the volume sparked is approximately equal to 1 cm.<sup>3</sup>. Average number of balls in the discharge was 20, making  $k = 2\%$  which leads

to output power of about 45 mW as against the estimated 30mW. The difference between actual and calculated output power may well be due to the likelihood that not all spheres radiate because some gaps may not break down and also these sparks which do occur may not be simultaneous, in which case reduction in power can be expected. Nevertheless, there is a satisfactory agreement between theory and experiment here.

#### 3.2.4. Other systems

Several other systems have been tried. Some success was achieved with vibrating spheres, but the most interesting case is that studied by Dickey. He produced mercury droplets by allowing a column of mercury to emerge at a controlled rate out of a tube. The column was kept at a high potential so that the droplets on emerging carried with them a charge. The droplets fell towards a pool at the bottom held at a low potential. Thus, just before reaching the pool surface a breakdown occurred in the gap between the droplet and the pool and this caused radiation. Both the number of droplets per second and their size could be studied for various sizes of these almost spherical droplets. Dickey found that the maximum of radiated power corresponded with  $\lambda = 7 \times$  diameter, which is about twice as large as would be expected. The system appears to work well and efficiently, but by its very nature it is somewhat

immobile. Also the rate of pulsing is limited by the rate of producing mercury droplets, which is not high.

### 3.2.5. The question of coherence of spark generated waves

It is clear that the mass radiator is an incoherent radiator, so will probably be the fixed array because of the possible time lags between the breakdown of the many gaps. The dipole system will also radiate incoherently within the definition of the term given earlier, unless some filtering is achieved. The very heavy damping of the radiation from a mm. wave spark generator will cause the individual pulses of radiation to last for only a few cycles, which at - say -  $3 \cdot 10^{10}$  c/s means pulse length of the order of  $10^{-10}$  sec.; hence for the signal to remain coherent through the intermediate stage the i.f. frequency would have to be greater than  $10^{10}$  c/s, which is impracticable on account of the very low conversion efficiency of mixers and absence of amplifiers at that order of frequencies. If, on the other hand, the spark generated wave were first sent through a band pass filter, there would be a considerable loss of power but also a lengthening of the pulse (the narrowing of the spectrum of the signal is equivalent to the reduction in damping). Thus, if the pulse were made some 100 cycles long, each cycle  $\frac{1}{3 \cdot 10^{10}}$  seconds, the i.f. could be reduced to some 300 Mc/s, which being feasible, the generator could now be made coherent. In order to achieve this, the filter would have to have a Q of about 300, which is easily obtained

at microwave frequencies by waveguide filters.

The inherent variations of power from pulse to pulse due to differences in voltage at breakdown and changes in composition of liquid and gas in the gap will result in additional noise and add to incoherence, and this defect must be reduced as far as possible by special attention to the spark mechanism.

#### 4. Detection of mm. waves

The very small powers radiated in the mm. wave region virtually limit the detectors available to three: the bolometer, the Golay cell and the crystal.

##### 4.1. The bolometer

The usual type of bolometers used at cm. waves for larger powers are not suitable, nor are the infra-red bolometers efficient enough at these wavelengths. Daunt et al. used bolometers based on work done by Walterdorff. These are made in the form of a silver film a few Angstrom thick deposited on very clean mica strips, with a narrow strip of thicker silver layer deposited over the thin film to act as conductor of the heat energy absorbed by the thin film. The back of the mica strip is also coated with silver to reduce radiation loss. Two such units are used in a bridge, one exposed to radiation and the other acting as compensating unit to balance out any environmental changes. A radiation sensitivity of  $10^{-8}$  watts was achieved. The

time constant was of the order of 3 seconds. This has the disadvantage when working with pulsed sources such as spark generators of giving the mean power which is very small on account of the very small duty ratio (pulse width to pulse period). On the other hand the detector tends to average out the power generated by individual pulses which is very useful when there are large random variations from pulse to pulse as in all types of spark generators.

#### 4.2. The Golay cell

This device has been described by Golay in a series of papers. It has been developed to detect infra and far infra-red radiation. The principle of this device is the expansion of a gas when it absorbs heat energy. The radiation falls on an aluminium layer a few Angstrom thick deposited on collodion 100 Angstrom thick, which absorbs the energy and transmits it to a small gas cell behind. The gas expands flexing a mirror made of antimony at the rear of the cell. The mirror has a surface tension of 120 dynes/cm. A narrow beam of light falls on the mirror and is reflected back to a photocell. The flexing of the mirror causes deflection of the beam and, in consequence, loss of photocell illumination. The photocell output is amplified. In order to avoid d.c. amplification the light beam can be interrupted at a suitable rate by a rotating disc with an aperture. This device has a time constant of 3 m.sec.,

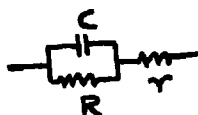
which is much shorter than the previously described bolometer. The estimated noise of the cell, which is also the minimum energy that can be detected, is of the order of  $5 \times 10^{-11}$  watts.

Since the Golay cell measures average energy it can best be used for continuous sources such as harmonic generators and is not very efficient when spark generators are used. The small cavity containing the gas tends to resonate at around 2 mm., hence the cell cannot be used reliably above 2 mm. wavelengths, but it appears to be the most sensitive receiver of continuous energy around 1 mm. wavelength.

#### 4.3. The crystal detector

The last years have seen considerable advances in the development of crystal detectors from the original "cat's whiskers". Much information is available about the characteristics of silicon crystal detectors in the cm. wavelength region, and less in mm. region. At the power levels obtainable the crystal operated as a square law device. The voltage/power and resistance/power characteristics of a Sylvania crystal type 1N 23 are given in the graph, Fig. 13. These are typical of most silicon crystals, and show the linear relation between voltage and power.

Torrey and Whitmer discuss the operation of a crystal rectifier which they represent as shown:



where  $r \ll R$ . They derive the current sensitivity of the crystal as

$$\beta = \frac{i}{P} = \frac{\alpha}{2} \cdot \frac{1}{1+(f/f_0)^2} \cdot \frac{1}{(1+r/R)^2}$$

where  $i$  = short circuit rectified current

$P$  = rf power absorbed in crystal when matched

$f$  = operating frequency

$$f_0 = \frac{1}{2\pi C\sqrt{Rr}} \quad (\text{usually about } 5000 \text{ Mc/s})$$

$\alpha$  is a constant varying from 2 to 13 volts<sup>-1</sup>. Denoting the current sensitivity at low frequencies by  $\beta_0 = \frac{\alpha}{2(1+r/R)^2}$

one can write  $\beta = \beta_0 \cdot \frac{1}{1+(f/f_0)^2}$

Dickey derives voltage sensitivity by assuming the load across the crystal to be  $R_L$  in the form

$$\gamma = \frac{e}{P} - \frac{\alpha}{2} = \frac{RR_L}{R+R_L} \cdot \frac{1}{1+(f/f_0)^2}$$

where  $e$  is the voltage change across the load resistance  $R_L$ .

Taking the value of  $R$  as 500 ohms and  $R_L$  as 70 ohms (coaxial line), one obtains as typical values

$$\gamma = 7.9 \text{ volts/watt at } 5.6 \times 10^{10} \text{ c/s}$$

$$\gamma = 4.3 \text{ " " at } 5.6 \times 10^{10} \text{ c/s}$$

Compared with the values given in Fig. 13, the figures obtained by Dickey appear to refer to somewhat higher rf. powers. When the power is radiated over a wide band the output is reduced by the bandwidth limitation of the receiver. Dickey estimated also that for a spark generator

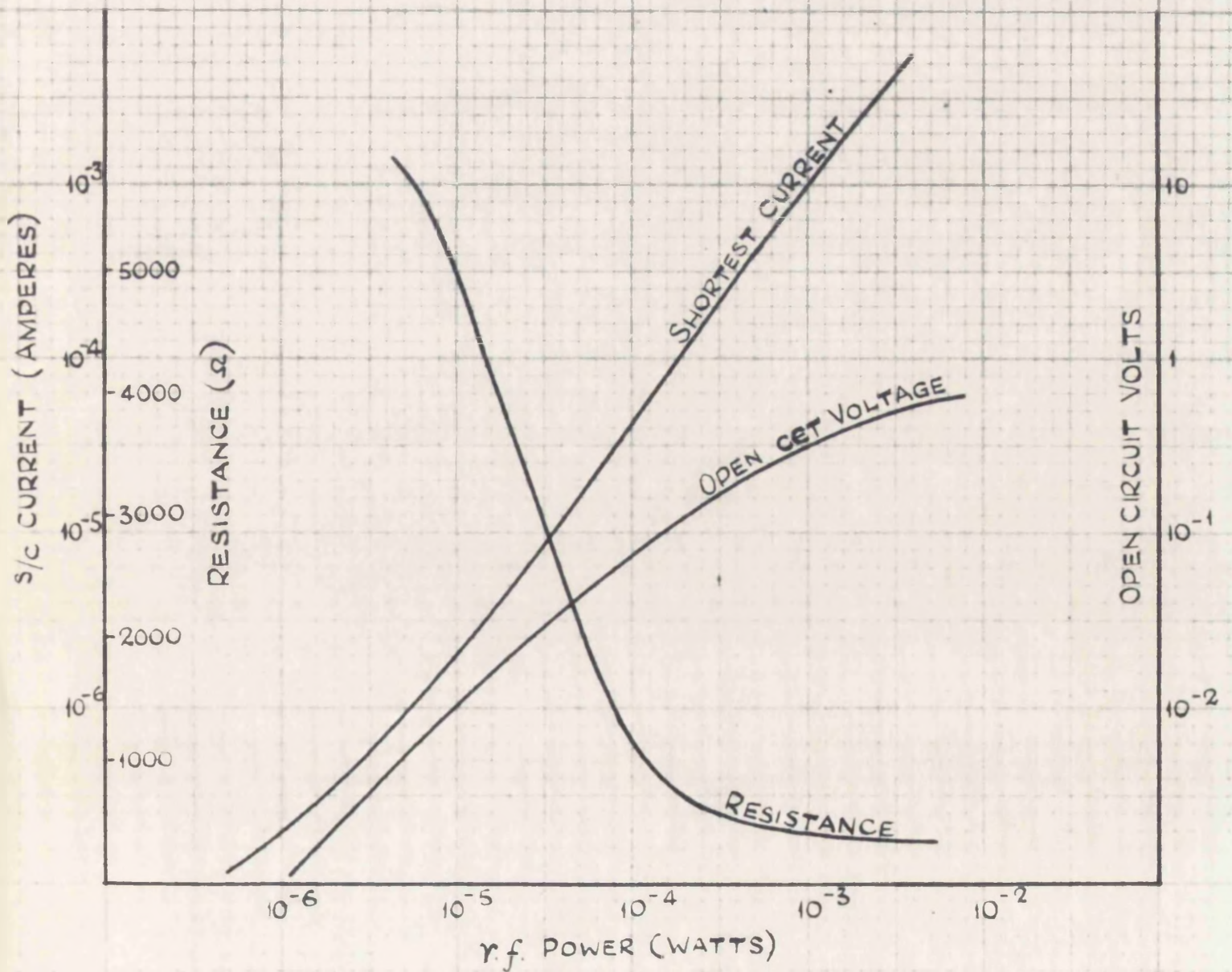


FIG. 13

THE RELATION BETWEEN RESISTANCE, OPEN CCT VOLTAGE AND SHORT CIRCUIT CURRENT OF A TYPICAL SILICON CRYSTAL.  
(SYLVANIA INFORMATION.)

working at  $N$  pulses/sec. and a receiver of bandwidth  $B$ , the output voltage produced by radiated power  $P$  is given by

$$\frac{3}{2} \times \frac{B}{N} \times P \times \gamma \text{ volts}$$

which results in the minimum detectable energy of  $.95 \times 10^{-10}$  watts at 36,000 Mc/s and of  $1.7 \times 10^{-10}$  watts at 56,000 Mc/s for  $N = 1,000$  pps., which compares well with Golay cell. It is doubtful, however, if these figures of minimum signal power could be obtained on account of crystal noise and a figure of  $0.6 \mu\text{W}$  has been quoted as minimum. This, however, can be improved considerably by using very narrow band amplifiers or gating circuits (Klein et al.).

The most serious drawback of crystals is that their sensitivity falls off so rapidly as frequency increases. Fig. 14. gives the current sensitivity  $\beta$  as found by the above quoted expression as well as by experiments, in terms of  $\beta$ .

## 5. Conclusions

The survey indicates the relative merits of the various methods of generating mm. waves. Further research would appear to be indicated on magnetron harmonics and on improving the conversion efficiency of crystals.

Of the wide band sources the spark generator appears most promising both on account of its comparative simplicity and power output well in excess of the gas discharge source at mm. waves.

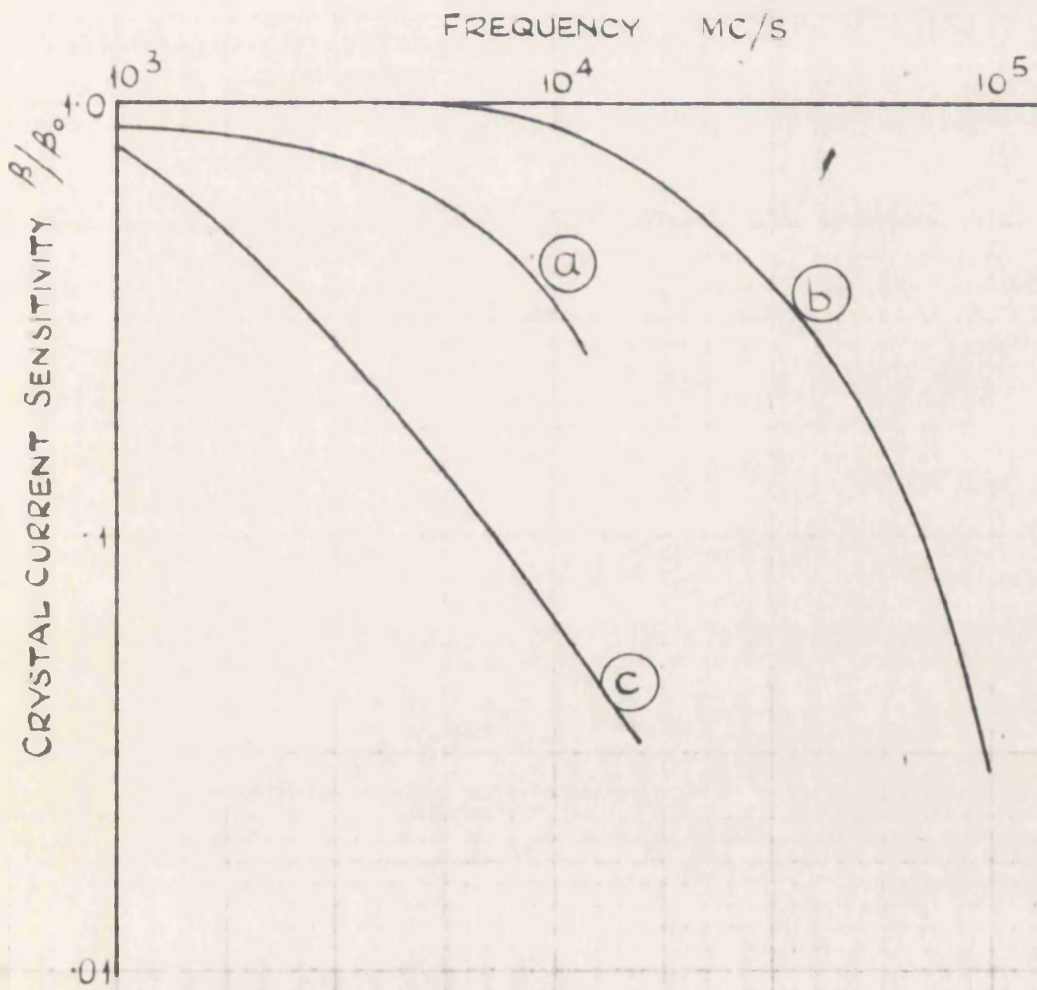


FIG. 14.

RELATIVE CURRENT SENSITIVITY OF A CRYSTAL RECTIFIER

- (a) AS DEDUCED EXPERIMENTALLY (TORREY AND WHITMER)
- (b) AS OBTAINED BY SCALED MEASUREMENTS (CHRISTENSEN)
- (c) AS CALCULATED (BERINGER)

The wide band generated by the microwave spark generator has been held in the past as a serious handicap. It may be that too much stress was laid on this point and instead some attention should have been directed to possible advantages of the wide band.

To mention but a few, the wide band allows a desired narrower band to be filtered out and modulated in the waveguide so that a common generator might be split into many channels. The whole band could be sent through a narrow band filter whose centre frequency could be varied by a modulating signal so that a fixed frequency narrow band receiver would receive a modulated signal. In the field of measurements, a narrow band variable frequency receiver could be used to study dielectric effects, absorption etc. over a wide range of microwave frequencies, etc.

The inherent variations in power output of a spark generator from pulse to pulse would make high precision of measurement difficult, but with suitably designed integrating receivers or recorders the error could be reduced considerably.

A further study of the spark generator as a source of mm. waves is called for and results of work in that direction are reported in parts II (theoretical) and III (experimental).

## PART II. THE ANALYSIS

### 1. Introduction

#### 1.1. The Scope

The discussion in Part I led to the conclusion that the possibilities of a spark microwave generator should be considered further. In this part, the emphasis will be laid on the frequency spectrum of radiation from a simple spark generator of the Righi-Lebedev type, and on various consequences of the spectrum; its dispersion and filtering will be followed up in detail. This will be followed by a discussion of power output.

The emphasis will be laid throughout on a comprehensive analysis of the aspects dealt with, although often the results of the analysis will not be followed up by experimental work, which for obvious reasons was much more selective and concerned with the ultimate result of obtaining millimetre waves. These remarks apply particularly to the chapters dealing with dispersion and filtering, the object there being to bring out their full significance when applied to a wide band source of radiation. Some of the results quoted later can be found in standard textbooks, but it is believed that they have been here arrived at by a novel method and the emphasis is laid at all times on the frequency or wavelength spectral characteristics of the

devices analysed rather than on the radiation intensity and resolving power which is of importance with discrete frequency sources.

## 1.2. The Source

The simple dipole system has been chosen so as to reduce to the minimum the number of parameters - which in the author's opinion based on the results obtained by various workers is essential if the output is to be kept reasonably stable.

The expression for the wave radiated by the dipole will be discussed in the next chapter. It is based on the assumption of an instantaneous change of field around the dipole. Such a rapid change cannot, of course, be obtained in practice. The collapse of the field depends on the build up of discharge current and that depends again on the magnitude and time rise of the overvoltage applied to the gap. It has been stated that current across the gap will be of the form

$$I = \frac{eu}{d} \varepsilon^{\alpha d}$$

where  $e$  = charge of electron

$d$  = gap length

$u$  = drift velocity of electrons

$\alpha$  = Townsend ionisation coefficient

Dickey uses the following argument to show the dependence of frequency of radiated wave on  $\alpha$  and  $u$ :

Since the time concerned is very short, he assumes  $\alpha$  and  $u$  to be constant, hence  $I = \frac{eu}{d} \epsilon^{\alpha u t}$  i.e. current increases exponentially. When the rate of change of this current equals the rate of change of the would be oscillatory current across the gap, oscillations commence. Thus, if the oscillatory current across the gap is  $i' = I' \sin \omega t$  then  $\frac{dI}{dt} = \left| \frac{di'}{dt} \right|_{t=0}$  or  $\frac{eu}{d} \alpha u \epsilon^{\alpha u t} = \omega I'$  i.e.  $\alpha u I = \omega I'$

Hence, if  $I'$  is to be appreciably large,  $(\alpha u)$  must be larger than  $(\omega)$ ,

The relation between  $(\alpha u)$  and voltage across the gap has been given by Dickey and is reproduced here in Fig. 15. This shows the order of voltages across the gap that are required; e.g. for 5 mm. radiation,  $\alpha u \doteq 4 \times 10^{11}$  hence required voltage is 650 kV/cm. For 1 mm. radiation  $\alpha u \doteq 2 \times 10^{12}$  calling for a voltage of 4,000 kV/cm. Thus with a gap of the order of .05 mm. long a voltage of the order of 20 kV would be required with a time rise of the order of 1 millimicrosecond to produce 1 mm. waves of appreciable power.

Such overvoltages with such short rise times are not easily obtained and it appears that the function of the paraffin oil which has very high breakdown strength is to allow that to happen. The auxiliary gaps also help in the achievement of these overvoltages, but they are not essential (see part III).

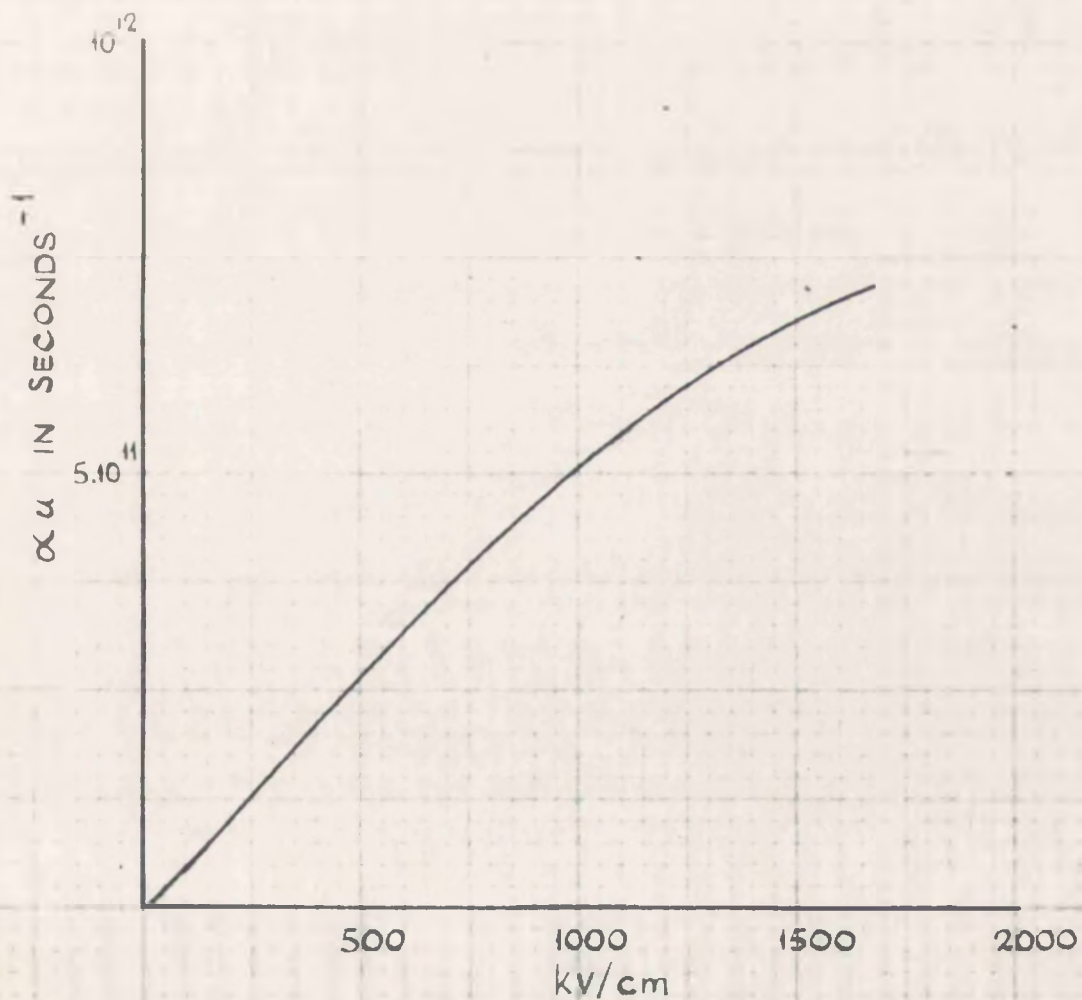


FIG. 15.

THE RELATION BETWEEN THE PRODUCT OF TOWNSEND  
IONISATION POTENTIAL ( $\alpha$ ) BY DRIFT VELOCITY OF  
ELECTRONS ( $u$ ) AND VOLTAGE ACROSS THE GAP (KV/cm)

A rapidly changing field can be analysed by Fourier transform, to find that its spectrum is very wide. If this spectrum contains the natural frequency of oscillation of the dipole, then the dipole will be excited and reradiate the energy at that frequency. This gives another way of looking at the problem. In either case, assuming a rapidly changing voltage, it is necessary to examine now the natural frequency of oscillation and the damping characteristic of dipoles.

## 2. The self-oscillation of a dipole radiator

The theory behind the working of the spark microwave generator is the self-oscillation of a rod or a sphere when subjected to a sudden change of electric field such as may result from an electric discharge.

The problem has exercised the human mind for a long time, because it is also the basis of the solution to the behaviour of an aerial of arbitrary shape. Basically the solution of Maxwell's equations with a zero field at the aerial boundary would give the answer.

In the simplest case, that of a sphere, a solution has been obtained first by Thomson, and later by Stratton and others. Schellkunoff gives a very simple solution which is reproduced here (Advanced Antenna Theory, pp.152-154).

The electric field due to a freely oscillating elementary

infinitesimally small dipole perpendicular to its radius is known to be

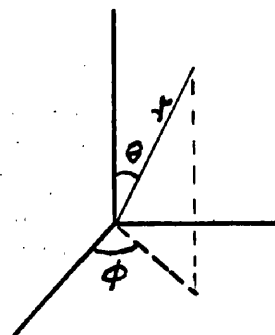
$$E_{\theta} = \frac{\mu A}{4\pi r} \left(1 + \frac{c}{pr} + \frac{c^2}{p^2 r^2}\right) e^{p(t-r/c)} \sin \theta \quad (1)$$

where  $p = \alpha + j\omega$

$c =$  velocity of em wave

$r =$  distance from dipole

$\mu =$  permeability



Consider a sphere of radius  $a$  and let a field  $E_0$  be impressed across its vertical diameter at time  $t = 0$ , then  $E_{\theta} = -E_0 \sin \theta$ ; hence, by using Laplace transform

$$E_{\theta}(a, \theta, t) = \frac{E_0 \sin \theta}{2\pi j} \int_c \frac{e^{pt}}{p} dp \quad (2)$$

where  $\int_c$  denotes integration round a closed contour  $c$ .

Transforming from  $E(a, \theta)$  to  $E(r, \theta)$  with the help of earlier expression (1) we get

$$E_{\theta}(r, \theta, t) = \frac{E_0 a \sin \theta}{2\pi j r} \int_c \frac{\left(\frac{pa}{c}\right)^2 + \frac{pa^2}{rc} + \frac{a^2}{r^2}}{p \left[\left(\frac{pa}{c}\right)^2 + \frac{pa^2}{rc} + 1\right]} e^{\frac{p}{c}(ct-r+a)} dp$$

the poles are  $p = 0$

and  $\left(\frac{pa}{c}\right)^2 + \frac{pa^2}{rc} + 1 = 0$  giving  $p_1 = \frac{c\gamma}{a}$ ,  $p_2 = \frac{c\gamma^*}{a}$  where  $\gamma = -\frac{1}{2} + \frac{1}{2}j\sqrt{3}$

$$\begin{aligned} \text{Hence } E_{\theta}(r, \theta, t) &= \frac{E_0 a}{r} \left[ \frac{a^2}{r^2} + \frac{\gamma^2 + \gamma \frac{a}{r} + \frac{a^2}{r^2}}{\gamma(\gamma - \gamma^*)} e^{\gamma/a (ct-r+a)} \right. \\ &\quad \left. + \frac{\gamma^2 + \gamma \frac{a}{r} + \frac{a^2}{r^2}}{\gamma^*(\gamma^* - \gamma)} e^{\gamma^*/a (ct-r+a)} \right] \sin \theta \\ &= \frac{E_0 a^3 \sin \theta}{r^3} + \frac{2E_0 a}{\sqrt{3} r} \left(1 + \frac{a}{r} + \frac{a^2}{r^2}\right) e^{\frac{\gamma-a-ct}{2a}} \cos \left[ \frac{\sqrt{3}(r-a-ct)}{2a} - \psi \right] \sin \theta \end{aligned}$$

$$\text{where } \cos \psi = \frac{\sqrt{3}}{2} \left(1 + \frac{a}{r}\right) \left(1 + \frac{a}{r} + \frac{a^2}{r^2}\right)^{-1/2}$$

$$\sin \psi = \frac{1}{2} \left(1 - \frac{a}{r}\right) \left(1 + \frac{a}{r} + \frac{a^2}{r^2}\right)^{-1/2}$$

Hence, it will be seen that the damping constant is  $\alpha = \frac{c}{2a}$

and angular frequency  $\omega = \frac{c\sqrt{3}}{2a}$  i.e.  $\lambda = \frac{4\pi a}{\sqrt{3}}$  and log. dec.  $\delta = \frac{2\pi}{\sqrt{3}}$

In 1898, Abraham obtained a solution for an ellipsoid of revolution. The problem has also been solved and extended to the case of forced oscillations by Brillouin (1904), Page and Adams (1938), Stratton and Chu (1941) and Ryder (1942).

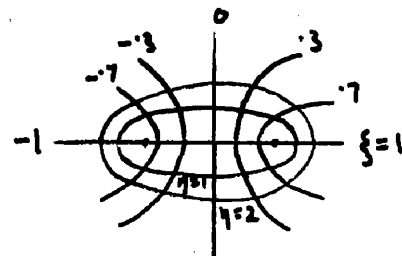
Briefly, the method used is to assume an ellipsoid whose axis of revolution is  $2a$ , and the axis perpendicular to it is  $2b$ , with  $2a > 2b$  (prolate spheroid).

Maxwell's equations are then transformed to spheroidal co-ordinates based on a system of confocal ellipses and hyperbolae with focal distance  $= 2f$ .

The conversion from Cartesian system is obtained by

$$x = f\xi\eta$$

$$y^2 = f^2(1-\xi^2)(\eta^2-1)$$



and the boundary conditions are set by identifying one of the ellipses with the metallic surface of the aerial and making  $E = 0$  along it.

By separating the variables it is possible to obtain expressions from which solutions could be derived. These

are, however, very involved, and approximations have to be introduced. Abraham postulated a quantity  $\varepsilon = \frac{1}{4 \ln 2a/b}$ .

In the light of later work by Hallen, the now generally accepted factor  $\Omega = 2 \ln \frac{2a}{b}$  is preferred, so that  $\varepsilon = \frac{1}{2\Omega}$ .

By neglecting terms or orders higher than  $\frac{1}{\Omega^2}$ , Abraham

arrived at the solution for  $\lambda = 4a(1 + \frac{14}{\Omega^2})$  for the funda-

mental and generally for higher modes  $\lambda_n = \frac{4a}{n} (1 + \frac{2.4 + \ln n}{2n\Omega^2})$

with a fundamental mode decrement of  $\frac{4.87}{\Omega} + \frac{10.4}{\Omega^2}$  and higher

mode decrements

$$\delta_n = \frac{4.83 + 2 \ln n}{n\Omega}$$

Page and Adams attempted to solve the problem by numerical computations of expansions. These expansions fall into two groups: when  $0.6 < \frac{b}{a} \leq 1$ , i.e. a sphere or nearly a sphere and when  $\frac{b}{a}$  is very small, i.e. a very elongated ellipsoid.

For the first case they obtained the following results:

$\frac{1}{\eta} = \sqrt{\frac{a^2 - b^2}{a^2}}$	$\lambda/4a$	$\delta$
0	1.814	3.628 (sphere)
.1	1.809	3.618
.2	1.794	3.588
.3	1.770	3.557
.4	1.734	3.461
.5	1.686	3.356
.6	1.625	3.214
.7	1.549	3.024
.8	1.455	2.772

In the second case, the results are as follows (including in brackets Abraham's results for comparison)

$b/a$	0	$1.02 \times 10^{-11}$	$3.34 \times 10^{-5}$	$1.42 \times 10^{-3}$	$4.96 \times 10^{-3}$	$1.35 \times 10^{-2}$
$\lambda/4a$	1(1)	1.001(1.005)	1.004(1.0029)	1.009(1.0066)	1.015(1.0097)	1.023(1.014)
$\delta$	0(0)	.098(.0968)	.247(.2433)	.396(.3889)	.444(.437)	.613(.607)

These results leave a gap as yet unsolved between  $b/a = .6$  and  $b/a = .155$ . By extrapolating the two sets of results L. Brillouin obtained the following graphs: Figs. 16A and B.

Since the results for eccentricity around 1 are congested, this has been replotted to a " $\log b/a$ " scale, which allows for corrections to be made to each graph in turn.

Stratton & Chu, dealing with the ellipsoid as a transmitting aerial calculated and plotted the impedance from which one can estimate the following values

$b/a$	$1.41 \times 10^{-4}$	$1.41 \times 10^{-3}$	$1.41 \times 10^{-2}$	.142
$\lambda/4a$	1.02	1.03	1.05	1.11
$Q$	16.7	10.9	5.4	2.25
$\delta = \frac{1}{Q}$	.188	.288	.582	1.4

Only rough estimates were possible because actual figures are not available, but since the range overlaps that obtained by Page & Adams, one can estimate the possible error

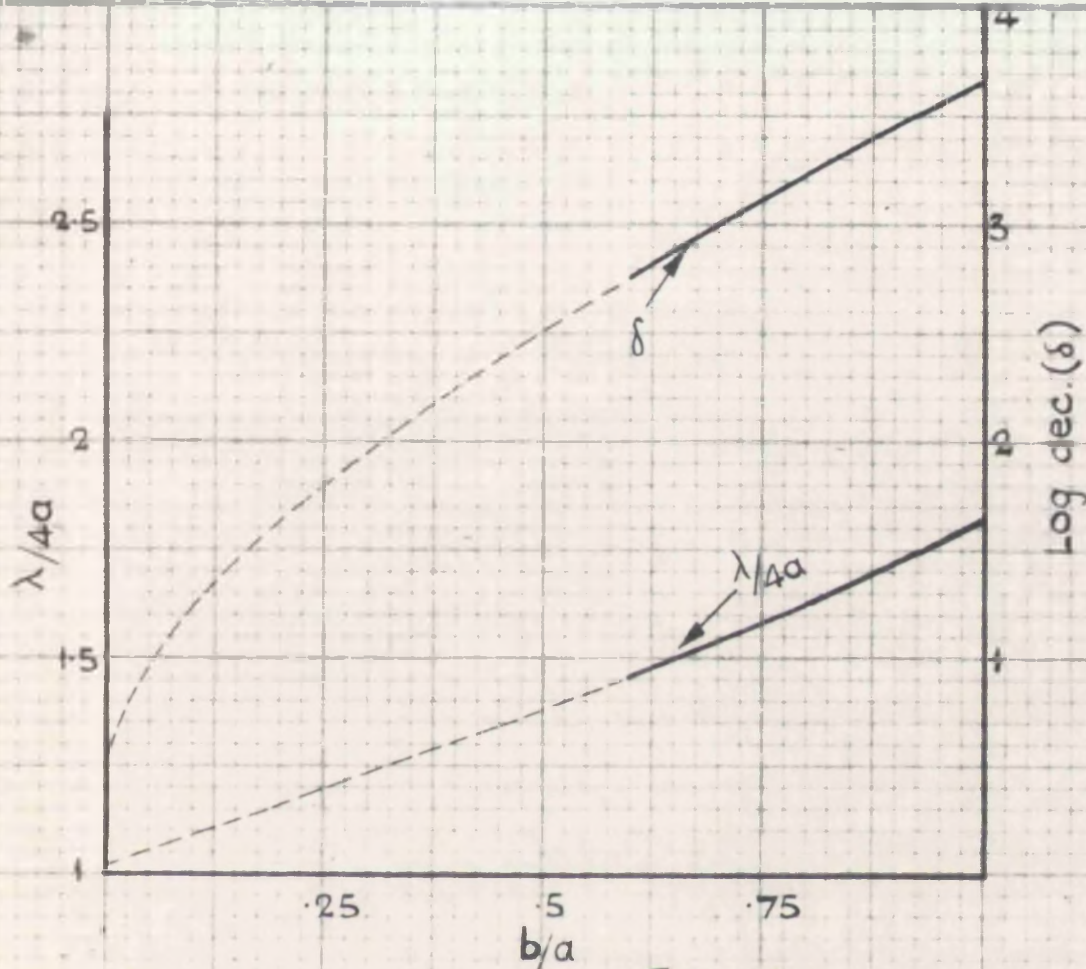


FIG. 16A.

LINEAR SCALE

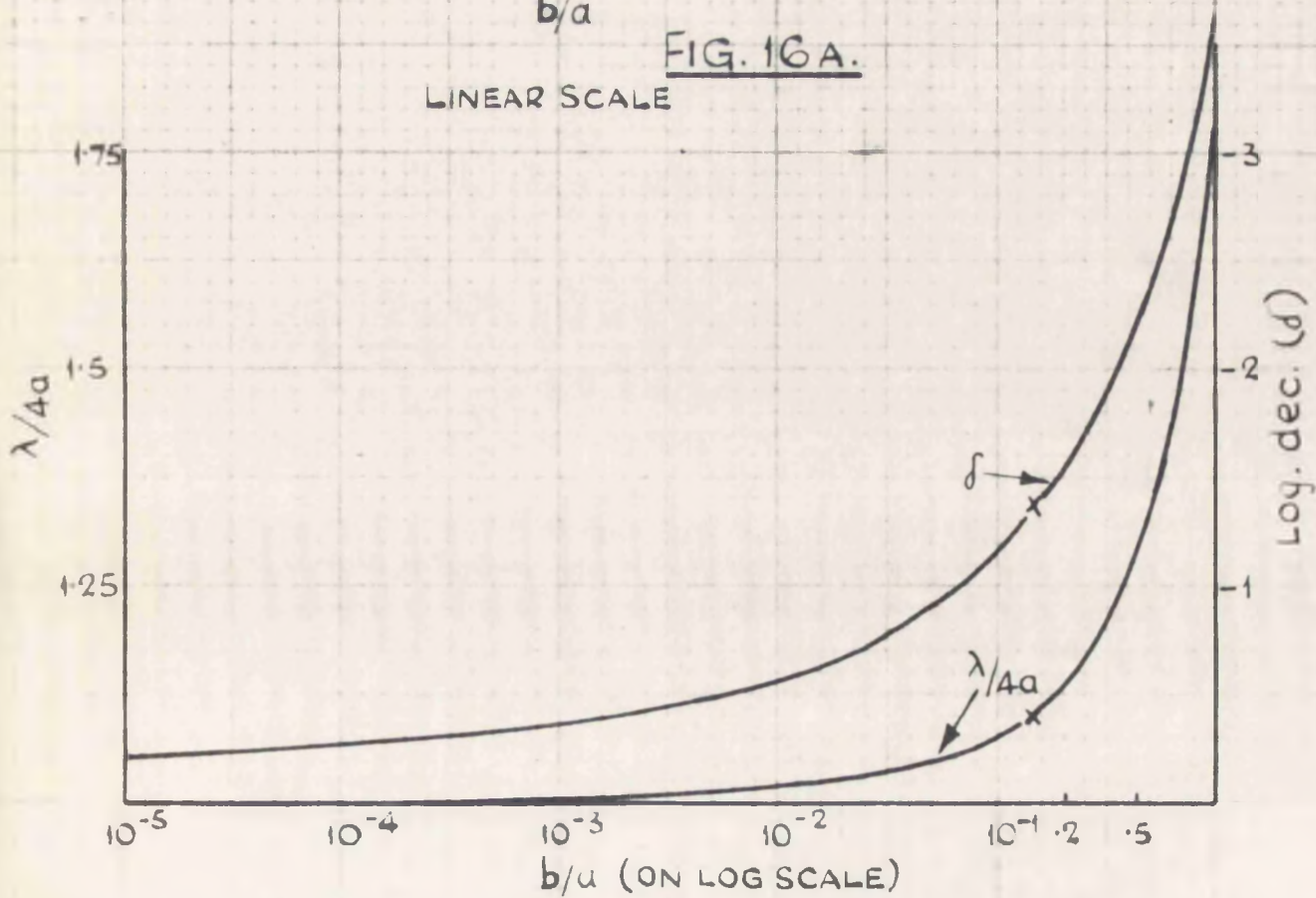


FIG. 16 B.

RELATION BETWEEN THE RATIO OF RADIUS/HALFLENGTH OF A SPHEROIDAL DIPOLE AND RADIATED NATURAL WAVELENGTH  $\lambda$  AND LOG DECREMENT  $\delta$ . (AFTER PAGE AND ADAMS.)

and fill in the point corresponding to  $b/a = .142$  with fair accuracy. This point is indicated on the graphs by a cross.

One other point is of some importance: The solutions show that the natural frequency is inversely proportional to the square root of the dielectric constant of the surrounding medium, i.e. if the ellipsoid is embedded in paraffin (dielectric constant = 2.25) then an infinitely thin ellipsoid will oscillate at a frequency 1.5 times less than if in air, but the log decrement is not affected by the medium.

This leads to the following conclusion; if we assume that the natural oscillation is of the form

$$e^{-\alpha t} \sin \omega_0 t = e^{-\delta_1 f_0 t} \sin 2\pi f_0 t$$

in air, then in a dielectric of constant  $\epsilon$  it will become

$$e^{-\delta_1 f_0' t} \sin 2\pi f_0' t \quad \text{where} \quad f_0' = \frac{f_0}{\sqrt{\epsilon}}$$

The same natural frequency could be obtained with an ellipsoid in air, but approximately  $\sqrt{\epsilon}$  x longer which would in turn reduce the log decrement to  $\delta_2$  hence, of two aerials embedded in different dielectrics and oscillating at the same natural frequency, the lower the dielectric constant, the less will the oscillation be damped.

The importance of the solution for ellipsoid lies in the fact that a very thin ellipsoid can be taken as a good approximation for a cylinder - the aerials being more

commonly cylindrical than ellipsoidal in shape. On the other hand, the solution of Maxwell's equations for any but infinitely thin cylinders is so difficult that no exact answer is known. There are, however, several good approximate methods which give satisfactory answers as long as  $\Omega$  is not too small. The most appropriate are based on the Hallen method. Instead of Maxwell's equations, Hallen starts from magnetic and electric vector potentials (which, of course, are themselves derived from Maxwell's equations),

$$A = \int_V \frac{J e^{-j\beta r}}{4\pi r} dv$$

$$V = \int_V \frac{q e^{-j\beta r}}{4\pi r} dv$$

where  $J$  = electric current density

$q$  = electric charge volume density

then it can be shown that if current is parallel to the

$$z \text{ axis then } E_z = -j\omega\mu A_z = \frac{\partial V}{\partial z} = \frac{1}{j\omega\epsilon} \left( \frac{\partial^2 A_z}{\partial z^2} + \beta^2 A_z \right)$$

$$= \frac{1}{4\pi j\omega\epsilon} \int_V \left( \frac{\partial^2 \psi}{\partial z^2} + \beta^2 \psi \right) J dv$$

where

$$\psi = \frac{e^{-j\beta r}}{r}$$

Since one has to consider an actual aerial at high frequency, which to all intents and purposes is a cylinder of infinitely thin walls, the potentials have to take into account the rather complex interaction between current element on the surface.

With the notation of the figure one can introduce a function

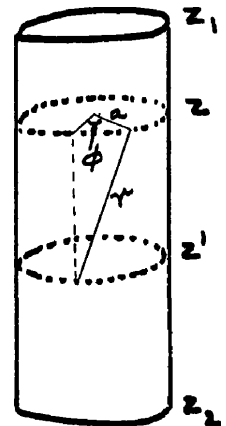
$$G(z'-z, a) = \frac{1}{2\pi} \int_0^{2\pi} \frac{e^{-j\beta r}}{r} d\phi$$

$$\text{where } r^2 = (z'-z)^2 + 2a^2(1-\cos\phi)$$

$$\text{then } A_2 = \frac{1}{4\pi} \int_{z_1}^{z_2} G(z'-z, a) I(z') dz'$$

$$E_2 = \frac{1}{4\pi j \epsilon \omega} \int_{z_1}^{z_2} \left( \frac{\partial^2 G}{\partial z^2} + \beta^2 G \right) I(z') dz' \dots (4)$$

$$\text{where } J dv = \frac{I(z') dz' d\phi}{2\pi}$$



Equation (3) is the integro-differential equation solved by Hallen by a method of iteration. The solution which contains the factor  $\Omega$  mentioned earlier, is very complex, and it has been extended only to terms  $\frac{1}{\Omega^2}$ , thus its accuracy is limited to aerials for which  $\frac{1}{\Omega^3}$  is negligible.

The greatest draw-back to this theory appears to be the effect of end surfaces. The assumption that current is 0 at the end surfaces which is made in the theory cannot be accepted, and leads to a possible error, unless the aerial is made in the form of a cylindrical tube with infinitely thin walls.

Hallen calculated the natural frequencies of several of the modes existing on cylindrical aerials to be:

$$\lambda_1 = 2l \left( 1 + \frac{4574}{\Omega} + \frac{3.31}{\Omega^2} + \dots \right)$$

$$\lambda_2 = \frac{2l}{2} \left( 1 + \frac{2375}{\Omega} + \frac{2.10}{\Omega^2} + \dots \right)$$

$$\lambda_3 = \frac{2l}{3} \left( 1 + \frac{1611}{\Omega} + \frac{1.58}{\Omega^2} + \dots \right)$$

$$\lambda_n = \frac{2l}{n} \left[ 1 + \frac{1}{\Omega} \left( \frac{1}{2n} - \frac{1}{24n^2} \right) + \frac{1}{n\Omega^2} (1.5 \ln n + 2.93) \right]$$

$$\delta_1 = \frac{4875}{\Omega} + \frac{11.71}{\Omega^2} + \dots$$

$$\delta_2 = \frac{3.114}{\Omega} + \frac{10.38}{\Omega^2} + \dots$$

$$\delta_n = \frac{2 \ln n + 4.83}{\Omega} + \frac{3(\ln n)^2 + 11.72 \ln n + 9.98}{n \Omega^2}$$

The plot of  $\lambda/2l$  and  $\delta_1$  against  $d/l$  corresponding to  $b/a$  used earlier is given in Fig. 17. which contains for comparison the values found by Page & Adams and by Stratton.

Several advances have been made to Hallen's theory, notably by King and Middleton, but these are mainly concerned with the solution of receiving and transmitting aerials and the effects of feeds, etc. and are not of direct interest here.

### 2.1. Some experimental evidence

Looking back at Fig. 17., it will be seen that as far as length of aerial is concerned the two solutions, i.e. one based on ellipsoid and the other on cylinder, approach one another for very thin aerials but differ increasingly for short ones. The experimental evidence collected over the years has been concerned mainly with receiving and transmitting aerials which require a serious adaptation of the theories to allow for feed, capacity between centre falls or face and earth. The only extensive investigation of self-oscillating aerials appears to have been carried out by

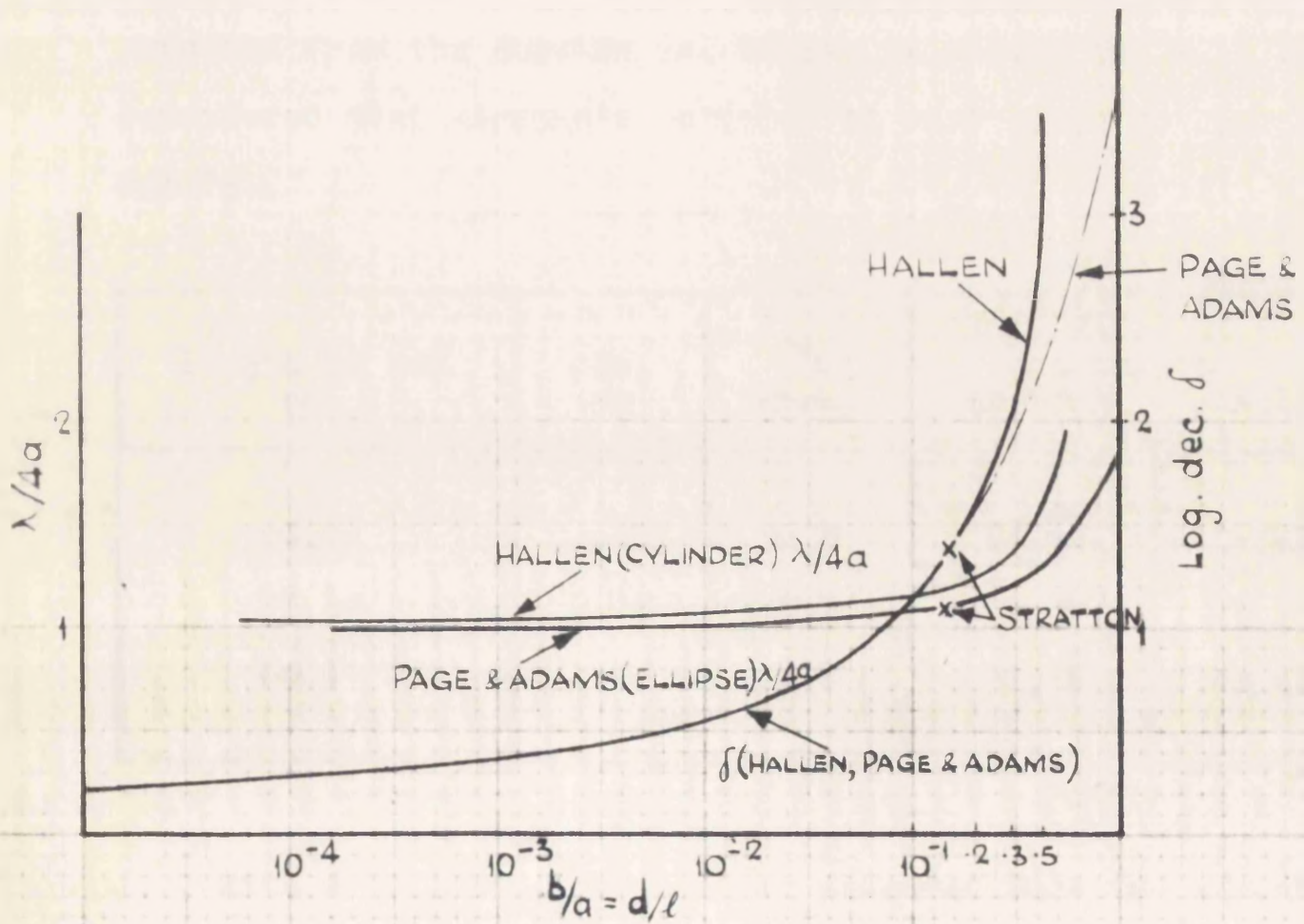


FIG. 17.

COMPARISON OF RESULTS OBTAINED BY HALLEN, PAGE AND ADAMS AND STRATTON.

Lindman (1932). Webb & Woodman and Nichols & Tear also carried out some systematic measurements, but their dipoles were partly embedded in glass or wood and partly in oil, thus complicating the issue.

The details of Lindman's method will be discussed later. It will suffice to say here that he measured the wavelength of oscillation produced by a continuous rod resonator suspended on silk threads when shocked into oscillation by a primary, spark excited and very heavily damped radiator. The following table gives his results as well as results expected from the Abraham and Hallen solutions (it will be remembered that Abraham's solution is very close to Page & Adam's).

Length of rod cm	dia. cm	$\lambda/2$ meas.	$\lambda/2$ calculated	
			Abraham	Hallen
24.2	.13	24.5	24.44	25.45
73.15	.13	73.4	73.67	76.73
30.7	1.5	31.7	31.48	34.41

With a 23.1 long rod Lindman measured also the effect of shaping the ends:

dia.	end shape	$\lambda/2$ observed	$\lambda/2$ Abraham	$\lambda/2$ Hallen
.8		23.6	23.59	-
.8		23.9	-	25.55
.8		23.7	-	-
.8		24.2	-	-
1.6		24.6	24.55	-
1.6		24.8	-	28.73
1.6		24.9	-	-

These tables show that up to  $\frac{d}{2l} \leq 0.07$  ( $\Omega \geq 7$ ) the ellipsoid approximation is, if anything, better than the Hallen's solution for a cylinder.

Lindman extended his work to cover thicker aerials (down to  $\Omega = 2$ ,  $\frac{d}{2l} \doteq .55$ ). Figures 18. & 19. are based on those given in his paper. They show the order of agreement between measurements and theories.

Since in the present investigation the dimensions of the oscillator are likely to be within the range  $.05 < \frac{d}{2l} < 1.5$  i.e.  $2 < \Omega < 8$ , with a tendency towards 2 the solution given by Hallen should be the more applicable.

It should be explained here that all the results obtained with spark microwave generators of the Lebedev or

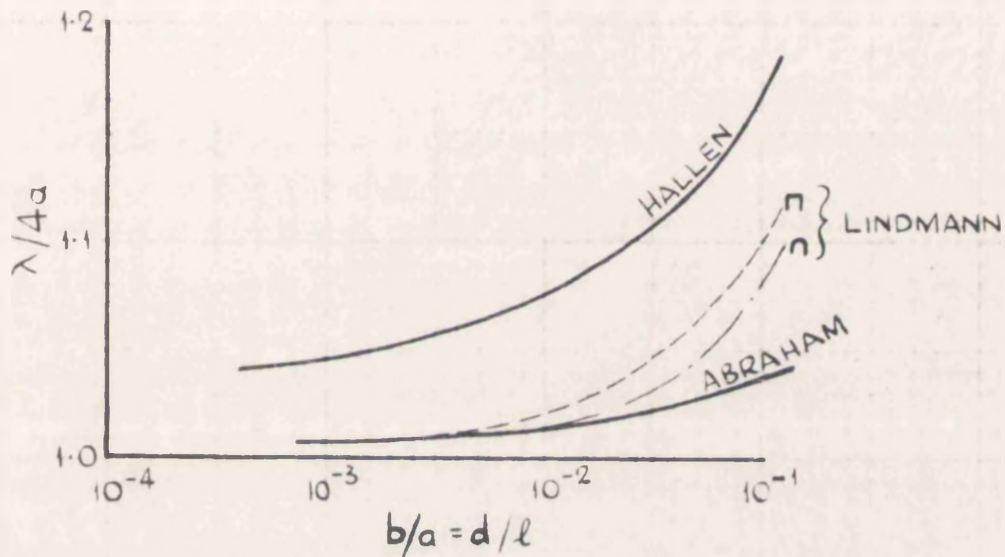


FIG. 18.

COMPARISON BETWEEN VALUES OF  $\lambda/4a$  OBTAINED THEORETICALLY BY LINDMANN FOR TWO END SHAPES: SQUARE  $\square$  AND SEMISPHERICAL  $\cap$

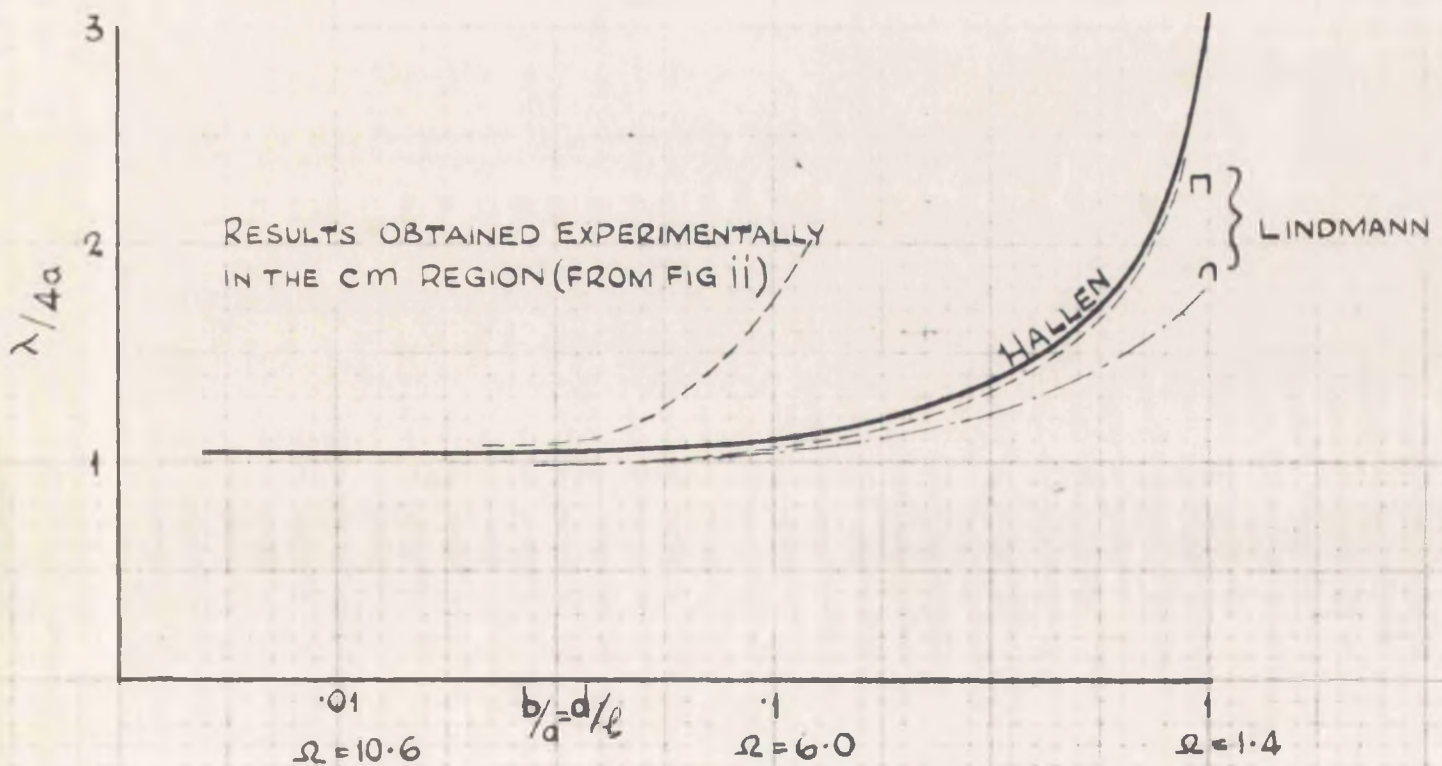


FIG. 19.

COMPARISON BETWEEN RESULTS EXPECTED BY HALLEN AND OBTAINED BY LINDMANN FOR TWO END SHAPES: SQUARE  $\square$  AND SEMISPHERICAL  $\cap$  IN THE REGION OF LARGE  $b/a$  RATIO, WHEN  $a > 5$  c.m.

Right type could be used in evidence for or against the theory. Unfortunately, the fact mentioned earlier that the dipoles are partly embedded in various dielectrics complicates the issue considerably. Results of Fig. 11, part I, have been included in Fig. 19. for comparison. Taking into account the difficulties of solving the problem when the aerial is in a homogeneous dielectric no attempt has been made so far to consider the effects of sudden changes in dielectric along the aerial surface. It is usually assumed that length of the radiated wave is that obtained in air multiplied by a factor

$$K = \frac{1}{2\ell} (\ell_1 \sqrt{\epsilon_1} + \ell_2 \sqrt{\epsilon_2} + \dots)$$

where  $\ell_1 + \ell_2 + \dots = 2\ell =$  overall length

$\epsilon_1, \epsilon_2$  etc. are the constants of dielectrics in which the respective portions of the total length  $\ell_1, \ell_2 \dots$  etc. are embedded. A confirmation for this can be found in experiments of Möbius, Lindman and others. In particular, Lindman examined also the effect of dielectric thickness arriving at Fig. 20. for rubber as dielectric. The rubber sleeve was a cylinder 32 mm long fitting a 1 mm rod. Lindman showed by experiment that the curve can be used for other dielectrics and other dimensions by taking the right proportions. This experiment has been carried out at around 1000 Mc/s and may not hold at much higher frequencies. Thus a serious approximation is involved whose magnitude is

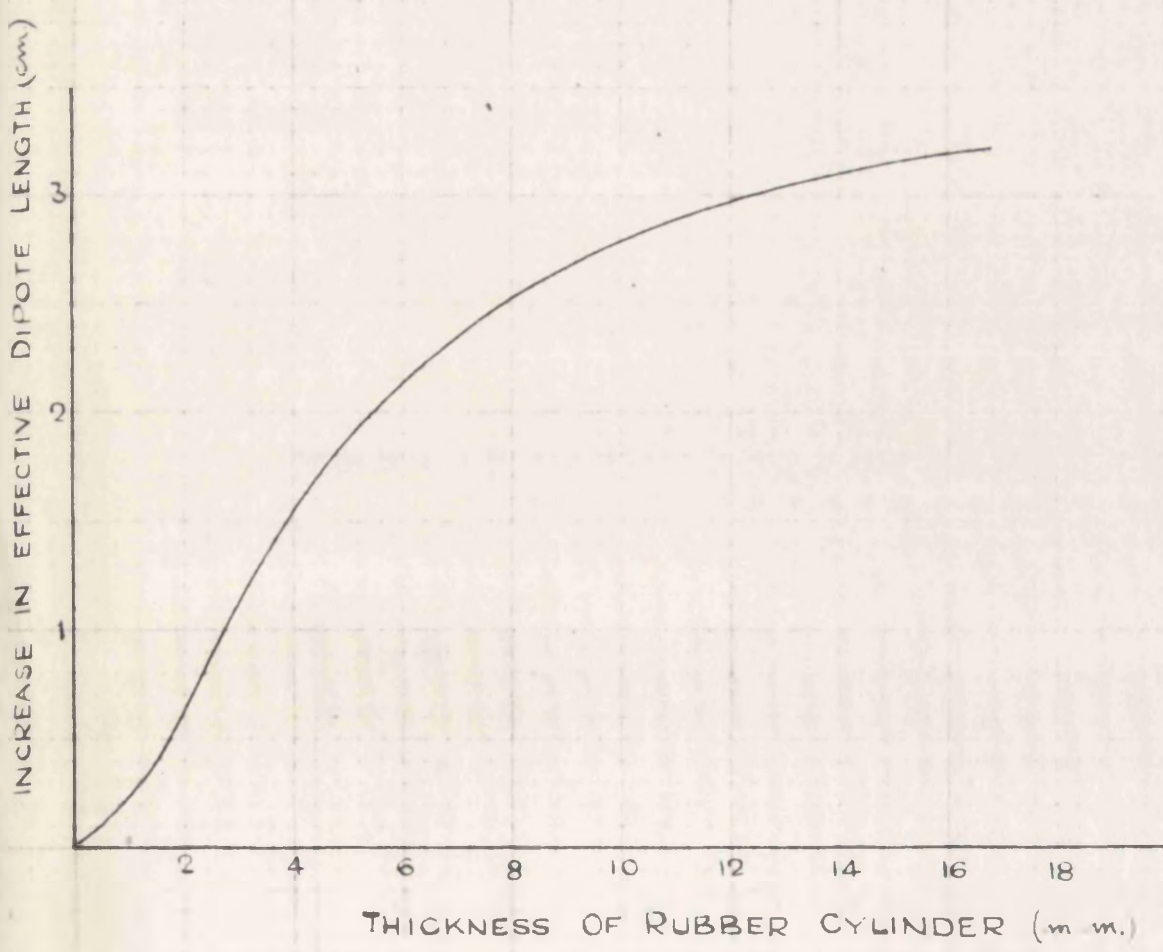


FIG 20.

RELATION BETWEEN THICKNESS OF RUBBER DIELECTRIC  
AND INCREASE IN EFFECTIVE DIPOLE LENGTH.  
(AFTER LINDMANN)

totally unknown. It is possible that a more exact solution might be obtained by very lengthy numerical solution of the Maxwell or the integro-differential equations with pre-determined boundaries and changes of dielectric. The high speed electronic computers might make this feasible. On the other hand, the approximate solution appears to be good enough for practical purposes.

The higher modes of oscillations, which are foreseen by the theories are primarily characteristic by the smaller damping effect. The graph, Fig. 21., contains the relation between  $\lambda_1, \lambda_2, \delta_1, \delta_2$  and  $\frac{d}{\ell}$ . In view of the rapid fall in energy in higher modes, these are not dealt with.

For comparison, the values obtained by Hallen and by Abraham are plotted ( $\lambda_i$  and  $\delta_i$  are indicated by dotted lines).

Lindman measured the modes radiated by a 42.7 cm long 1.5 mm dia rod. He gives the following table:

mode	Observed	Abraham Calculated	Hallen
$\lambda_{1/2}$	-	43.06	45.14
$\lambda_{2/2}$	21.4	21.45	21.99
$\lambda_{3/2}$	14.2	14.27	14.53
$\lambda_{4/2}$	10.65	10.70	10.85
$\lambda_{5/2}$	8.55	8.56	8.65
$\lambda_{6/2}$	7.1	7.13	7.20
$\lambda_{7/2}$	6.1	6.11	6.16
$\lambda_{8/2}$	5.35	5.35	5.38

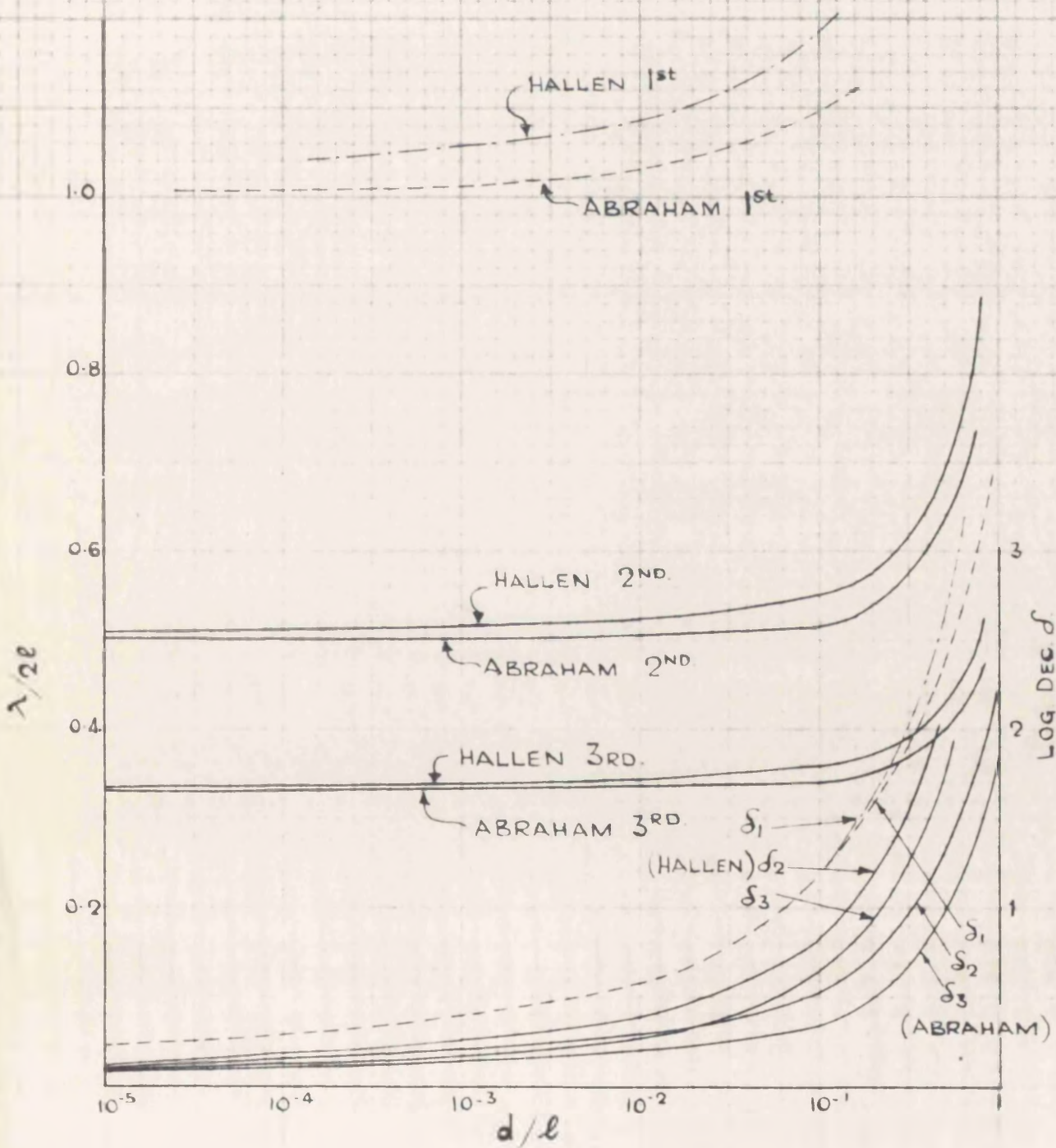


FIG 21.

RELATION BETWEEN FUNDAMENTAL, SECOND AND THIRD HARMONIC WAVELENGTH AND DIPOLE DIMENSIONS AND ALSO BETWEEN LOG DECREMENT AND DIPOLE DIMENSIONS. DOTTED AND DASHED LINES REFER TO FUNDAMENTAL.

showing a good agreement between theory and observation at least when  $\frac{d}{l}$  is small.

### 3. Frequency analysis of radiation from a spark excited dipole

#### 3.1. The frequency spectrum

Although the relation between  $\alpha$ ,  $\omega$  and dimensions is known only approximately, nevertheless the expression for the radiated wave is of the form

$$f(t) = e^{\alpha t} \sin \omega_0 t \quad \text{where } \alpha = \delta f_0$$

and  $\delta$  is the log decrement of the wave. The Fourier transform of  $f(t)$  is

$$g(\omega) = \frac{1}{2\pi} \int_{-\infty}^{\infty} f(t) e^{-j\omega t} dt = \frac{\omega_0}{2\pi(\omega - \omega_0 - j\alpha)(\omega + \omega_0 - j\alpha)}$$

Since the detectors used give output proportional to power rather than voltage, it is more useful to work with power spectrum. The power radiated between  $\omega - \frac{d\omega}{2}$  and  $\omega + \frac{d\omega}{2}$  is given by

$$g(\omega) \cdot g(\omega)^* \cdot d\omega = P(\omega) d\omega = \frac{\omega_0^2 d\omega}{4\pi^2(\omega - \omega_0 - j\alpha)(\omega - \omega_0 + j\alpha)(\omega + \omega_0 - j\alpha)(\omega + \omega_0 + j\alpha)}$$

$P(\omega)$  is a distribution type function, i.e. at any frequency  $\omega$  the power is 0 but in any frequency band  $\Delta\omega$  the power is equal to the area enclosed by the function  $P(\omega)$  and the corresponding ordinates.

The function  $P(\omega)$  has a maximum when  $\frac{dP(\omega)}{d\omega} = 0$  which occurs when  $\omega = \sqrt{\omega_0^2 - \alpha^2} = \omega_0 \sqrt{1 - \delta^2/4\pi^2}$

The corresponding value of  $P(\omega)_m = \frac{1}{4\omega_0^2\delta^2} = \frac{1}{16\pi^2\alpha^2}$

hence one can normalise the power spectrum function in the form

$$\frac{P(\omega)}{P(\omega)_m} = \frac{\delta^2}{\pi^2 \left[ \left(1 - \frac{\omega}{\omega_0}\right)^2 + \frac{\delta^2}{4\pi^2} \right] \left[ \left(1 + \frac{\omega}{\omega_0}\right)^2 + \frac{\delta^2}{4\pi^2} \right]}$$

Fig. 22. gives the normalised power spectrum for various values of  $\delta$ .

It will be seen that the shift of the maximum to the lower frequency becomes appreciable when  $\delta > 1$  and reaches almost 20% at  $\delta = 5.62$  i.e. for spherical dipole.

The power does not fall to 0 at low frequencies, in fact at  $\omega = 0$

$$\left| \frac{P(\omega)}{P(\omega)_m} \right|_0 = \frac{\delta^2}{\pi^2 \left(1 + \frac{\delta^2}{4\pi^2}\right)^2} \doteq \frac{\delta^2}{\pi^2} \left(1 - \frac{\delta^2}{2\pi^2}\right)$$

### 3.2. Detector response

The spectrum of detected power will depend also on the detector response  $R(\omega)$ .

In early work on spark generators the detector was usually a thin dipole of variable length. Under those circumstances, assuming the receiving dipole to be much thinner than the radiator, it acts as a very narrow band receiver. If one assumes that within that band the radiator has uniform spectrum (which is near enough to fact with thick or spherical radiators) then the detected power

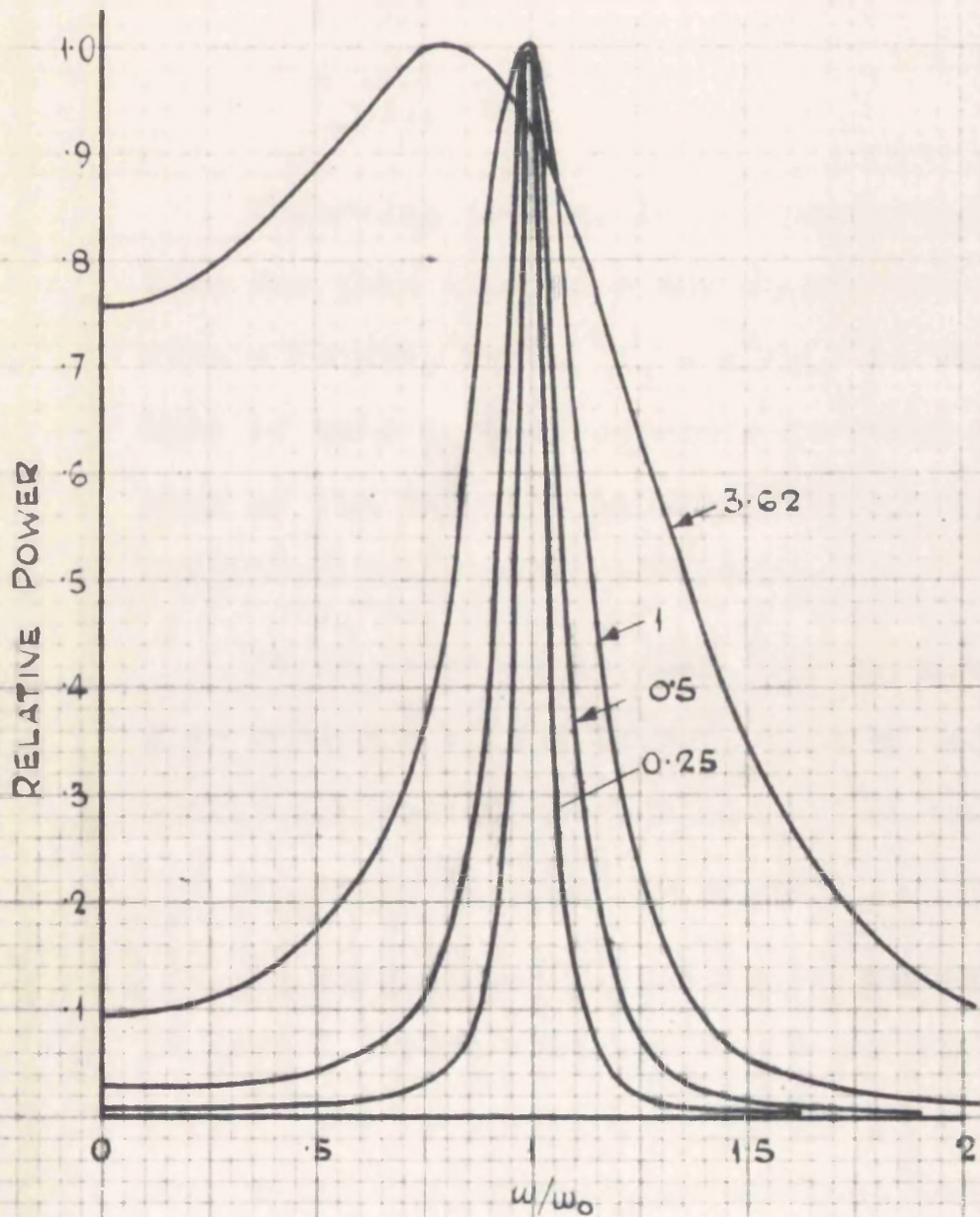


FIG. 22.

SPECTRUM OF RADIATING, SELFOSCILLATING DIPOLE  
OF VARIOUS LOG DECREMENTS.

$$\begin{aligned}
\int_{-\infty}^{\infty} F(f)^2 df &= \int_{-\infty}^{\infty} 4\pi |g(\omega)|^2 d\omega = \\
&= \int_0^{\infty} \frac{4\pi \omega_0^2 d\omega}{4\pi^2 (\omega - \omega_0 - j\alpha)(\omega - \omega_0 + j\alpha)(\omega + \omega_0 - j\alpha)(\omega + \omega_0 + j\alpha)} = \int_{-\infty}^{\infty} \frac{\omega_0^2 d\omega}{2\pi (\omega - \omega_0 - j\alpha) \dots} \\
&= j\omega_0^2 \left[ \frac{1}{8\omega_0 \alpha j (\omega_0 + j\alpha)} + \frac{1}{8(\omega_0 \alpha j)(\omega_0 - j\alpha)} \right] \\
&= \frac{\omega_0^2}{4\alpha (\omega_0^2 + \alpha^2)} = \frac{1}{4\alpha (1 + \frac{\alpha^2}{\omega_0^2})} \\
&\doteq \frac{1}{4\alpha} \\
&\doteq \frac{1}{4\delta f_0}
\end{aligned}$$

Referring to Fig. 16. of paragraph 2 it will be seen that for thin dipoles  $\delta$  and  $\lambda_0$  are both proportional to dipole length, hence  $\delta f_0 = c\delta/\lambda_0$  is virtually constant, so that if this type of detector is tuned over the frequency band of the radiator it will closely reproduce the frequency distribution of radiated power.

It is possible to make this type of receiver into a wide band one by the introduction of large amount of additional resistance but it is then necessary to disperse the radiation in order to measure its spectrum.

In view of the discussion of means of detection given in part I, it is proposed to use crystals in the experimental work. The response of a crystal is given in Fig. 14. part I from which the crystal law has been computed to be in the form

$$\frac{1}{1 + 5.10^{22} \omega^2} \doteq \frac{1}{1 + 2 \left(\frac{f}{10^{10}}\right)^2}$$

Since the power is to be propagated at least part of

the way through a rectangular wave guide to fit in with standard modern practice one should also consider the waveguide attenuation, but in view of short paths expected it seems justified to look on the waveguide as causing a sharp cutoff at its appropriate frequency and no attenuation above that, acting - as it were - as a perfect high pass filter. Thus if the cutoff frequency of the waveguide is  $f_c$  then the combined response of waveguide and crystal detector will be

$$R(\omega) = \left| \frac{1}{1 + 2(f/f_c)^2} \right|_{f_c}^{\infty}$$

Thus the response of a standard X-band waveguide and crystal, relative to output at 1000 Mc/s, will be as shown in Fig. 23., neglecting all effects of mismatch.

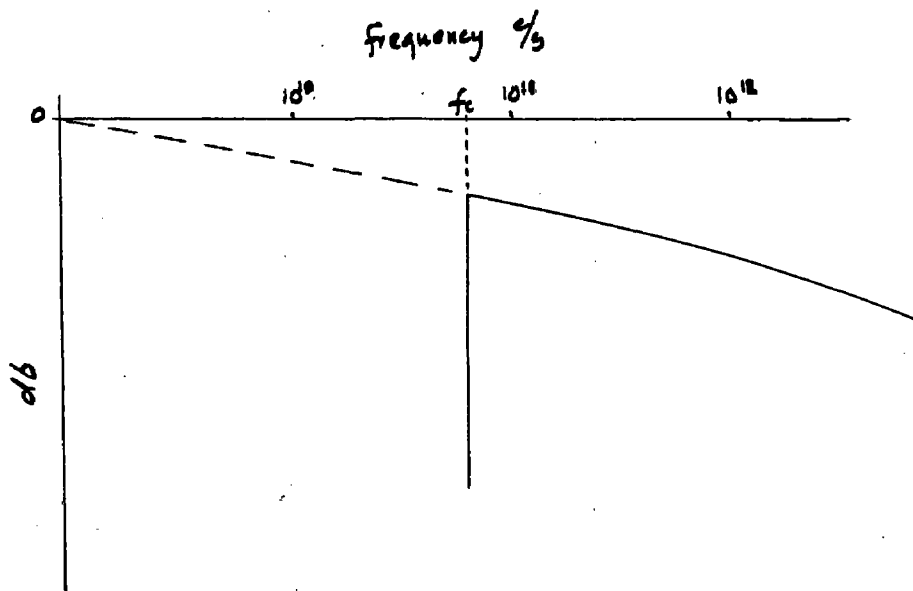


Fig. 23.

With this method of detection a dispersive medium will be necessary to obtain the detected power frequency response.

Recently Farrands & Brown suggested a method of deriving the radiated power spectrum by the use of a Boltzmann interferometer. This method and its limitations will be examined later.

### 3.3. The determination of the spectrum of a radiating dipole

#### 3.3.1. The characteristics of dipole detectors

The method of determining power spectrum by using a dipole detector has been analysed in paragraph 3.2. It has been used frequently in earlier researches into the spark radiators. Glagoleva Arkadieva and Sokolov examined several types of such detectors consisting of a dipole with a thermocouple at the centre, to detect the received power.

They developed two types of detectors with thermocouple in vacuum for shorter waves and in air for longer ones.

The detector dipoles consisted of aerials .145 cm in diameter. For the air detector the thermojunction consisted of 15  $\mu$  diameter Manganin and Constantan wires. The dipoles varied in length from 1.7 to 12.3 cm. The vacuum detector used Nichrome-Constantan 20  $\mu$  wires and dipole lengths between .008 and 3 cm. These detectors were very frequency selective giving a Boltzmann interferogram of almost pure sine wave.

Arkadieva and Sokolov do not give any results of measurements of spectrum of a dipole; for these results one has to go to Lindman.

### 3.3.2. Measurement of dipole spectrum

Lindman carried out a vast amount of research into the spectrum of dipoles of various lengths, diameters and materials, using a narrow band (thin) detector dipole at wave lengths of the order of 10 to 100 cm. The technique adopted by Lindman is to produce primary oscillation by a thick radiator. These in turn cause a secondary oscillator, inclined at  $45^{\circ}$  to the primary, to absorb and reradiate energy spectrum characteristic of its dimensions. Finally, these secondary radiations are received by the detector dipole inclined at  $45^{\circ}$  to the secondary and  $90^{\circ}$  to primary (so that it is unaffected by the primary radiation). In this way the secondary radiator whose spectrum is measured can be suspended by silk threads in air, avoiding any effects of dielectric constant of mounting and of oil required for primary radiation. (This method is not very suitable for mm waves because of the small dimensions of dipoles and of minute powers).

Fig. 24. is a reproduction of results obtained by Lindman using a 1.2 mm diameter detector of variable length and secondary sources of various materials and thicknesses. The level of output power is of consequence only when comparing resonators of equal dimensions. In that it will be noted that the resistivity of the material has some effect, power falling as resistivity increases.

RELATIVE POWER OUTPUT

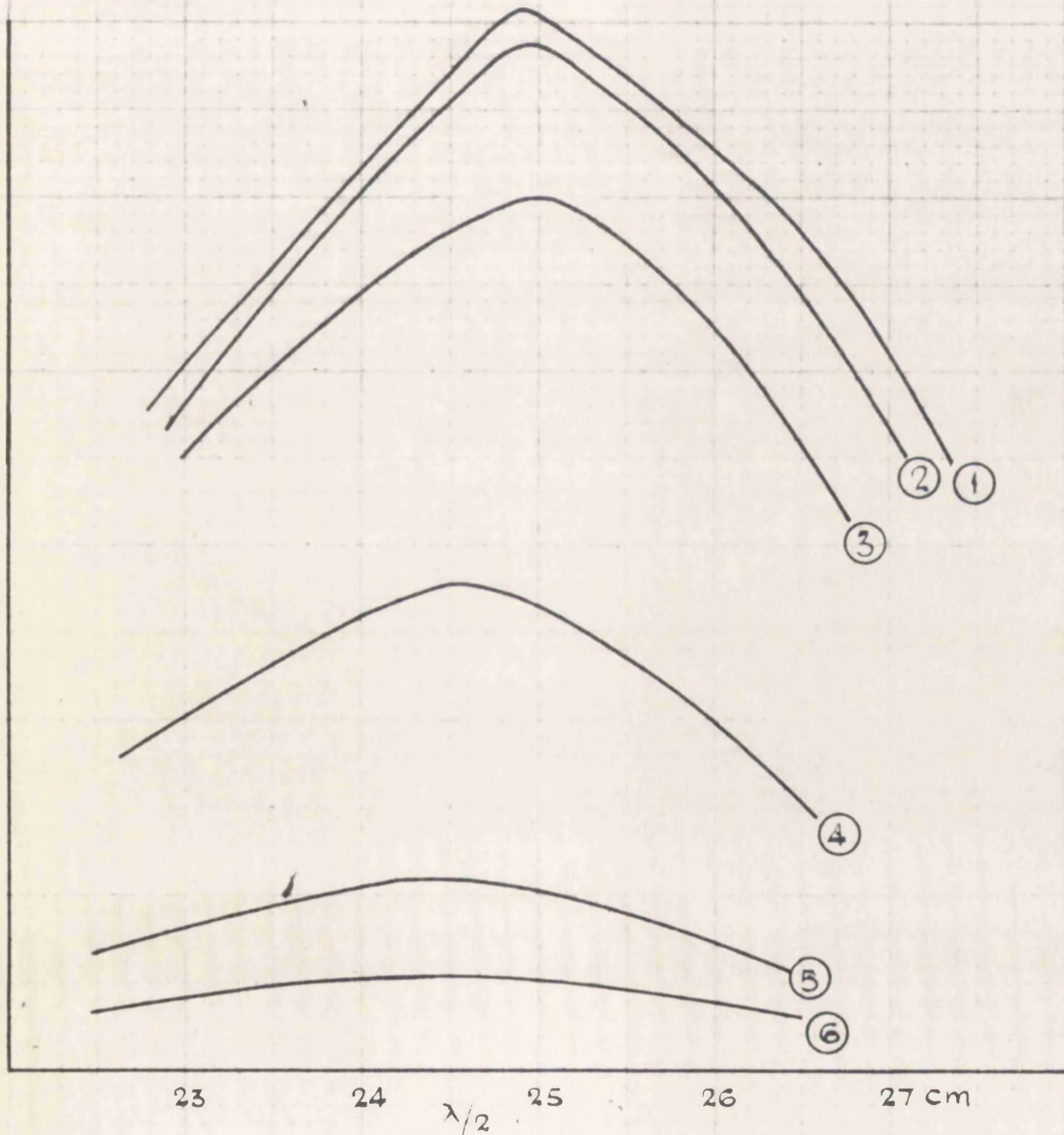


FIG. 24.

FREQUENCY SPECTRUM OF CYLINDRICAL OSCILLATORS.

- ① 24 cm x 1.2 mm. DIAMETER COPPER
- ② 24 cm x .7 mm " "
- ③ 24 cm x .7 mm " IRON
- ④ 24 cm x .02 mm " PLATINUM

- ⑤ 24 cm x .02 mm DIAMETER CONSTANTAN
- ⑥ 24 cm x .02 mm " IRON

The shift of maximum power towards lower frequencies for thicker resonators agrees with the results expected from the analysis of the spectrum (para. 3.1.). When the curves are rationalised by dividing the points by the maximum value for each one separately there is practically no difference between them showing virtually the same value of log dec.

Fig. 25. gives the spectrum of an oscillator 59.8 cm long, 1.5 cm diameter obtained by varying the length of a 1.3 mm diameter detector. For comparison this Fig. 25. gives also the calculated spectrum of this oscillator. It appears that the calculated log.dec. is rather low.

Lindman measured the log.dec. obtained with various lengths of the oscillator arriving at the results obtained from spectrum analyses and tabulated below:

Osc. length cm	diameter cm	log. dec. meas.	log. dec. calc.
5.4	1.5	4.42	1.23
10.4		2.02	.93
19.8		.78	.75
35.5		.85	.63
59.8		.93	.53

These experimental results, while not coinciding with the calculated values, are of the right order, the differences

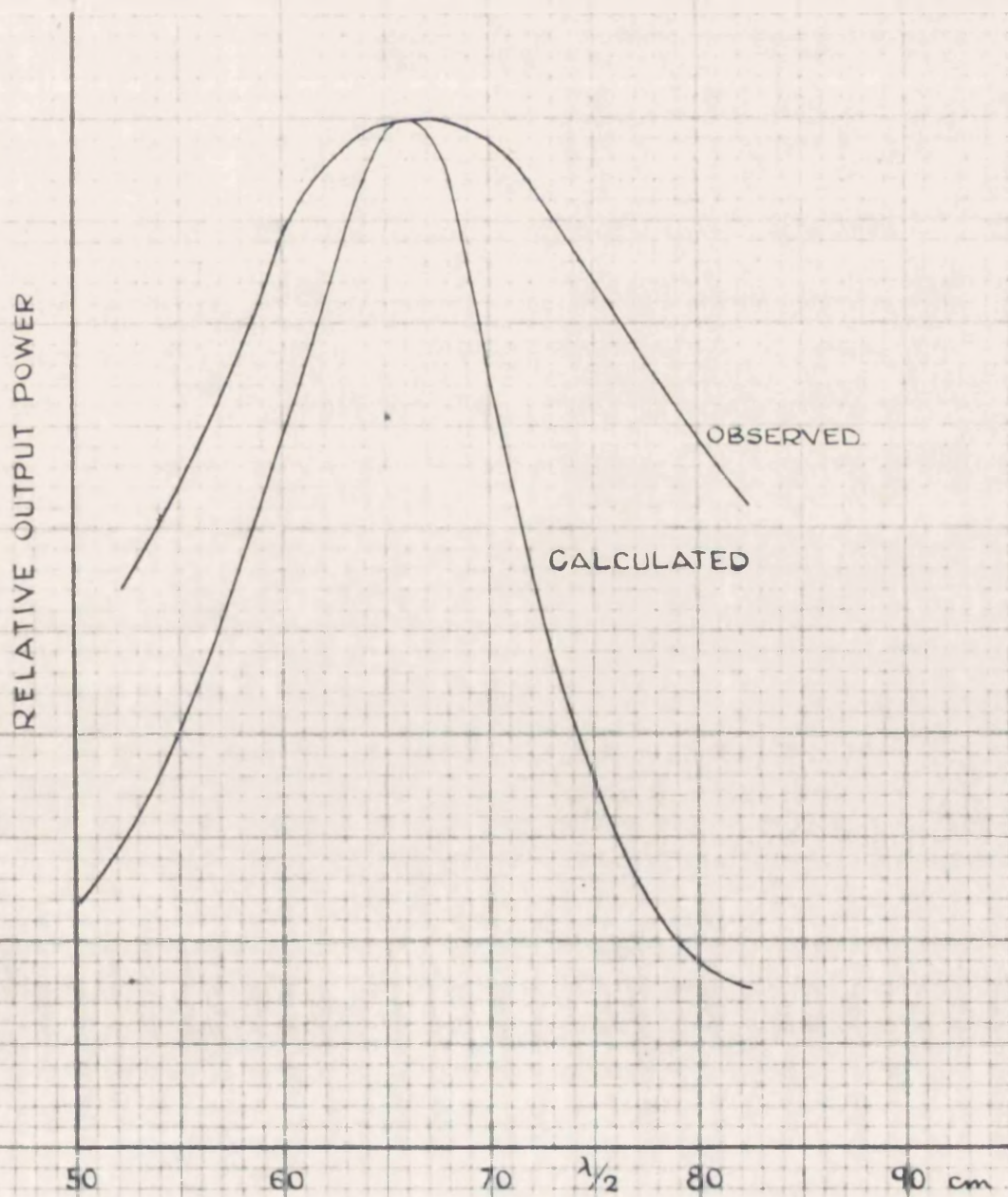


FIG 25

FREQUENCY SPECTRUM OF A CYLINDRICAL DIPOLE 59.8 cm LONG  
1.5 cm DIAMETER AS MEASURED BY LINDMANN AND AS  
CALCULATED ON THE BASIS OF ESTIMATED NATURAL  
WAVELENGTH OF  $66 \times 2$  cm AND LOG DEC OF 0.52  
(CALCULATED WITH THE HELP OF HALLEN'S FORMULA)

being accountable possibly by resistivity of materials, spectrum of the receiver and last but not least by reflection and diffraction difficulties in the laboratory. On account of finite thickness of receivers and difficulty in manipulating with very short dipoles, the method used by Lindman is unsuitable for mm waves, where, as has been shown by Arkadieva and Sokolov, the damping of the receiver becomes appreciable, affecting the detected spectrum. Thus, while Lindman's results can be read as confirmation of the existing theories, they do not add to the technique of measurement at mm waves.

#### 3.4. The Boltzmann interferometer

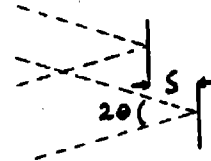
In a Boltzmann interferometer the incident wave falls on two parallel mirrors separated by a distance  $s$  as shown in Fig below, so that the reflected wave consists of two components  $f(t)$  and  $f(t - \tau)$  where  $\tau = \frac{2s \cos \theta}{c}$ . Usually  $\theta \doteq 0$  so that  $\tau = \frac{2s}{c}$  ( $c$  being the velocity of light).

Hence, if 
$$g(\omega) = \frac{1}{2\pi} \int_{-\infty}^{\infty} f(t) e^{-j\omega t} dt$$

then 
$$g'(\omega) = \frac{1}{2\pi} \int_{-\infty}^{\infty} f(t - \tau) e^{-j\omega t} dt = e^{-j\omega\tau} g(\omega)$$

so that the reflected wave has a spectrum  $G(\omega) = g(\omega)(1 + e^{-j\omega\tau})$  and the power spectrum becomes

$$P(\omega) = |G(\omega)|^2 = |g(\omega)|^2 2(1 + \cos \omega\tau)$$



The total reflected power is given by

$$\begin{aligned} P &= \int_{-\infty}^{\infty} |F(t)|^2 dt = 4\pi \int_0^{\infty} |G(\omega)|^2 d\omega \\ &= 4\pi \int_0^{\infty} P(\omega) d\omega = 8\pi \int_0^{\infty} |g(\omega)|^2 (1 + \cos \omega \tau) d\omega \\ &= 8\pi \int_0^{\infty} |g(\omega)|^2 d\omega + 8\pi \int_0^{\infty} |g(\omega)|^2 \cos \omega \tau d\omega \end{aligned}$$

Now the second of the two terms is a cosine Fourier transform of  $|g(\omega)|^2$ , hence one can find  $|g(\omega)|^2$  by taking the corresponding transform of the second term, i.e.

$$|g(\omega)|^2 = \int_0^{\infty} \left[ \int_0^{\infty} |g(\omega)|^2 \cos \omega \tau d\omega \right] \cos \omega \tau d\tau$$

The two terms can be separated because the first one is constant and the second one must become 0 when  $\tau$  is infinitely large. In fact, all that is necessary is to increase  $\tau$  until the output power remains constant and then to subtract that value from the output power at the intermediate values of  $\tau$ ,  $|g(\omega)|^2$  can then be computed by numerical integration for various values of  $\omega$ .

If one assumes the radiation to be of the form  $e^{-\alpha t} \sin \omega_0 t$  which - as has been shown - gives

$$|g(\omega)|^2 = \frac{\omega_0^2}{4\pi^2 (\omega - \omega_0 - j\alpha)(\omega - \omega_0 + j\alpha)(\omega + \omega_0 - j\alpha)(\omega + \omega_0 + j\alpha)}$$

then

$$\begin{aligned} P &= 4\pi \int_0^{\infty} P(\omega) d\omega = \int_0^{\infty} \frac{2\omega_0^2 d\omega}{\pi(-)(-+)(+-)(++)} + \int_0^{\infty} \frac{2\omega_0^2 \cos \omega \tau d\omega}{\pi(-)(-+)(+-)(++)} \\ &= \frac{\omega_0^2}{2\alpha(\omega_0^2 + \alpha^2)} + \int_{-\infty}^{\infty} \frac{\omega_0^2 e^{j\omega \tau} d\omega}{\pi(-)(-+)(+-)(++)} \\ &= \frac{\omega_0^2}{2\alpha(\omega_0^2 + \alpha^2)} + \frac{\omega_0^2}{4\alpha} \left[ \frac{e^{j(\omega_0 + j\alpha)\tau}}{\omega_0 + j\alpha} + \frac{e^{-j(\omega_0 - j\alpha)\tau}}{\omega_0 - j\alpha} \right] \end{aligned}$$

$$\begin{aligned}
&= \frac{\omega_0^2}{2\alpha(\omega_0^2 + \alpha^2)} \left[ 1 + \frac{e^{-\alpha\tau}}{\omega_0} (\omega_0 \cos \omega_0 \tau + \alpha \sin \omega_0 \tau) \right] \\
&= \frac{\omega_0^2}{2\alpha(\omega_0^2 + \alpha^2)} \left[ 1 + \frac{\sqrt{\omega_0^2 + \alpha^2}}{\omega_0} e^{-\alpha\tau} \cos(\omega_0 \tau - \phi) \right] \quad \text{where } \phi = \tan^{-1} \frac{\alpha}{\omega_0} = \tan^{-1} \frac{\delta}{2\bar{r}} \\
&= \frac{1}{\omega_0 \delta (1 + \delta^2/4\bar{r}^2)} \left[ 1 + \sqrt{1 + \delta^2/4\bar{r}^2} e^{-\alpha\tau} \cos(\omega_0 \tau - \phi) \right]
\end{aligned}$$

This shows that as  $\tau$  (i.e. mirror separation  $s$ ) is increased the output describes a decaying oscillatory variation as in Fig. 26. below:

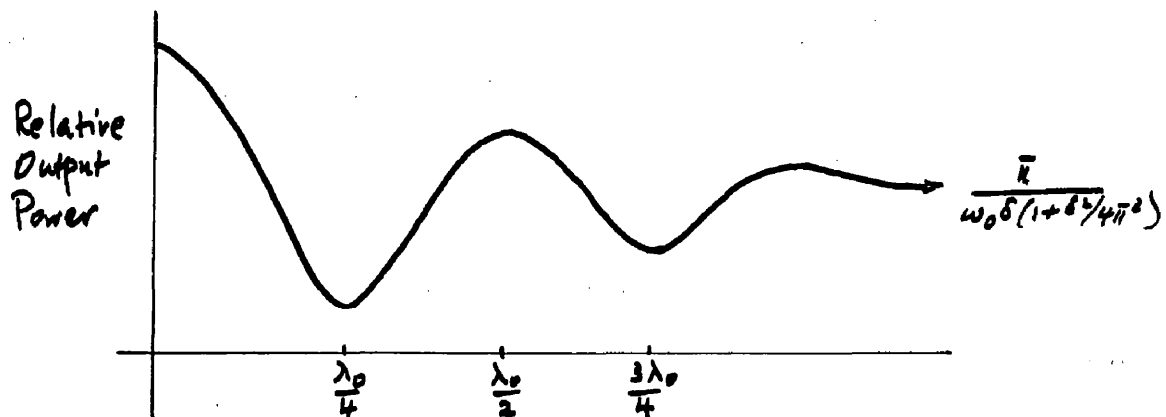
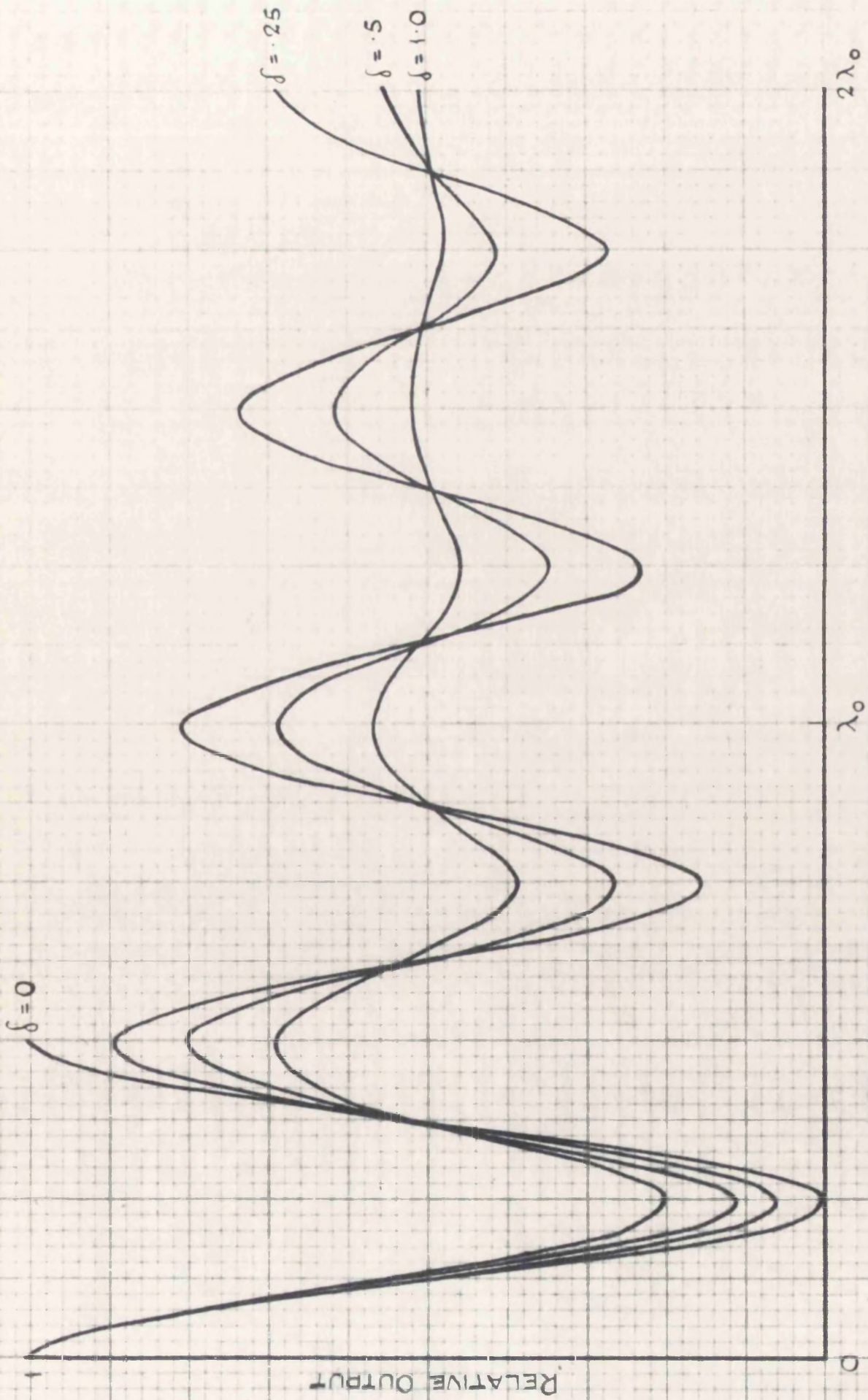


Fig. 26.

Fig. 27. gives an accurately computed form of output power for various values of  $\delta$ .

It follows from the above results that if the assumption of radiated waveform could be accepted and if the detector had uniform response one could find  $\lambda_0$  &  $\delta$  from the interferogram. Since

$$\begin{aligned}
\frac{dP}{d\tau} &= \sqrt{1 + \frac{\delta^2}{4\bar{r}^2}} \left[ -\alpha e^{-\alpha\tau} \cos(\omega_0 \tau - \phi) - \omega_0 e^{-\alpha\tau} \sin(\omega_0 \tau - \phi) \right] \\
&= \sqrt{1 + \frac{\delta^2}{4\bar{r}^2}} \left( \sqrt{\omega_0^2 + \alpha^2} \right) \sin \omega_0 \tau \\
&= \omega_0 \left( 1 + \frac{\delta^2}{4\bar{r}^2} \right) \sin \omega_0 \tau
\end{aligned}$$



MIRROR SEPARATION AS FUNCTION OF NATURAL WAVELENGTH

FIG. 27.

OUTPUT FROM A BOLTZMAN INTERFEROMETER FOR ANY GIVEN MIRROR SEPARATIO

Maxima and minima occur when this = 0, i.e. when  $\omega_0 \tau = m\pi$   
where m is any integer

$$\therefore \frac{2\pi f_0 s}{c} = m\pi$$

$$s = \frac{m\lambda_0}{4}$$

$$\text{hence } \lambda_0 = \frac{4s}{m}$$

At first maximum when  $m=0, s=0$

$$P_{1m} = \frac{1}{4\omega_0 \delta (1 + \delta^2/4\pi^2)} \left( 1 + \sqrt{1 + \frac{\delta^2}{4\pi^2}} \cos \phi \right)$$

at second maximum  $m=2, s = \frac{\lambda_0}{2}, \tau = \frac{\lambda_0}{c} = \frac{1}{f_0}$

$$P_{2m} = \frac{1}{4\omega_0 \delta (1 + \delta^2/4\pi^2)} \left[ 1 + \sqrt{1 + \frac{\delta^2}{4\pi^2}} e^{-\delta} \cos (2\pi - \phi) \right]$$

when s is large  $P_{\infty} = \frac{1}{4\omega_0 \delta (1 + \delta^2/4\pi^2)}$

$$\text{hence } \frac{P_{1m} - P_{\infty}}{P_{2m} - P_{\infty}} = e^{\delta} \quad \text{or} \quad \delta = 2.3 \log \frac{P_{1m} - P_{\infty}}{P_{2m} - P_{\infty}}$$

Before closing one should consider the following point:-

The first assumption made in deriving the form of the interferogram was that the system is so balanced that the wave at the receiver end due to the two mirrors when in the same plane is exactly twice that due to either mirror when the other is removed to infinity. This condition is not, in fact, obtainable. Consider then the effect of one mirror reflecting more power to the receiver than the other. In that case the wave after reflection will be

$$F(t) = f(t) + (1+a)f(t-\tau)$$

where (a) represents the unbalance fraction.

Hence the Fourier transform of  $F(t)$  will be

$$G(\omega) = g(\omega) + (1+a)g(\omega)e^{-j\omega\tau} = g(\omega)[(1+e^{-j\omega\tau}) + ae^{-j\omega\tau}]$$

and therefore the power spectrum

$$\begin{aligned} P(\omega) &= |G(\omega)|^2 = |g(\omega)|^2 \left\{ [1 + \cos \omega\tau(1+a)]^2 + [j\sin \omega\tau(1+a)]^2 \right\} \\ &= |g(\omega)|^2 [2(1+a)(1 + \cos \omega\tau) + a^2] \end{aligned}$$

Thus the total reflected power is

$$\begin{aligned} P &= 4\pi \int_0^{\infty} |G(\omega)|^2 d\omega = \\ &= 4\pi \int_0^{\infty} |g(\omega)|^2 [2(1+a) + a^2] d\omega + 4\pi \int_0^{\infty} |g(\omega)|^2 2(1+a) \cos \omega\tau d\omega \end{aligned}$$

which, when compared with the solutions given in previous paragraph is seen to differ from it by a scale factor  $(1+a)$  and an increase in the constant term. If  $(a)$  is small, i.e. if the mirrors are nearly balanced, then  $(a^2)$  will be much smaller than  $(1+a)$  hence only the amplitude scale of the interferogram will be affected and, since the scale is in any case relative, no error will be introduced. Even an appreciable error in  $(a)$  will only mean that in the computation of  $g(\omega)^2$  from the interferogram an error would be introduced in the choice of the constant term. The effect of such an error on the computed spectrum is, however, small as will be seen from the results of computations given in Fig. 60 . part III. Thus the balancing of the system is not critical.

### 3.4.1. Limitation of the Boltzmann interferometer method of measuring radiated waveform

It has been assumed in the previous paragraph that the detector response is uniform. In fact, this is not likely to be the case and with a crystal and waveguide system the response will be as shown in Fig. 23. and  $P = \int_0^{\infty} R(\omega) |G(\omega)|^2 d\omega$ . This puts a severe condition on the method described because not only is the solution too complex to be derived analytically, but crystal response is not known accurately over the whole band, having been measured at a few frequencies only. Also the waveguide system will produce severe mismatch at all frequencies removed from the one for which the various chokes, couplings and heads have been designed.

Figure 28. shows the computed results of interferograms expected when the natural wavelength of the source is 3 cm but the waveguide dimensions produce a cutoff at 6, 8, 10 and  $12 \times 10^3$  Mc/s using a crystal whose law is given by

$$\frac{1}{1 + 2(f/10^{10})^2} \quad \text{and assuming no mismatch.}$$

As it would be expected the interferograms retain the general shape, but the estimation both of  $\lambda_0$  and of  $\delta$  would be in error.

From an earlier consideration it follows that the detected power

$$P_d = 2 \int_0^{\infty} R(\omega) |G(\omega)|^2 d\omega + 2 \int_0^{\infty} R(\omega) |G(\omega)|^2 \cos \omega \tau d\omega$$

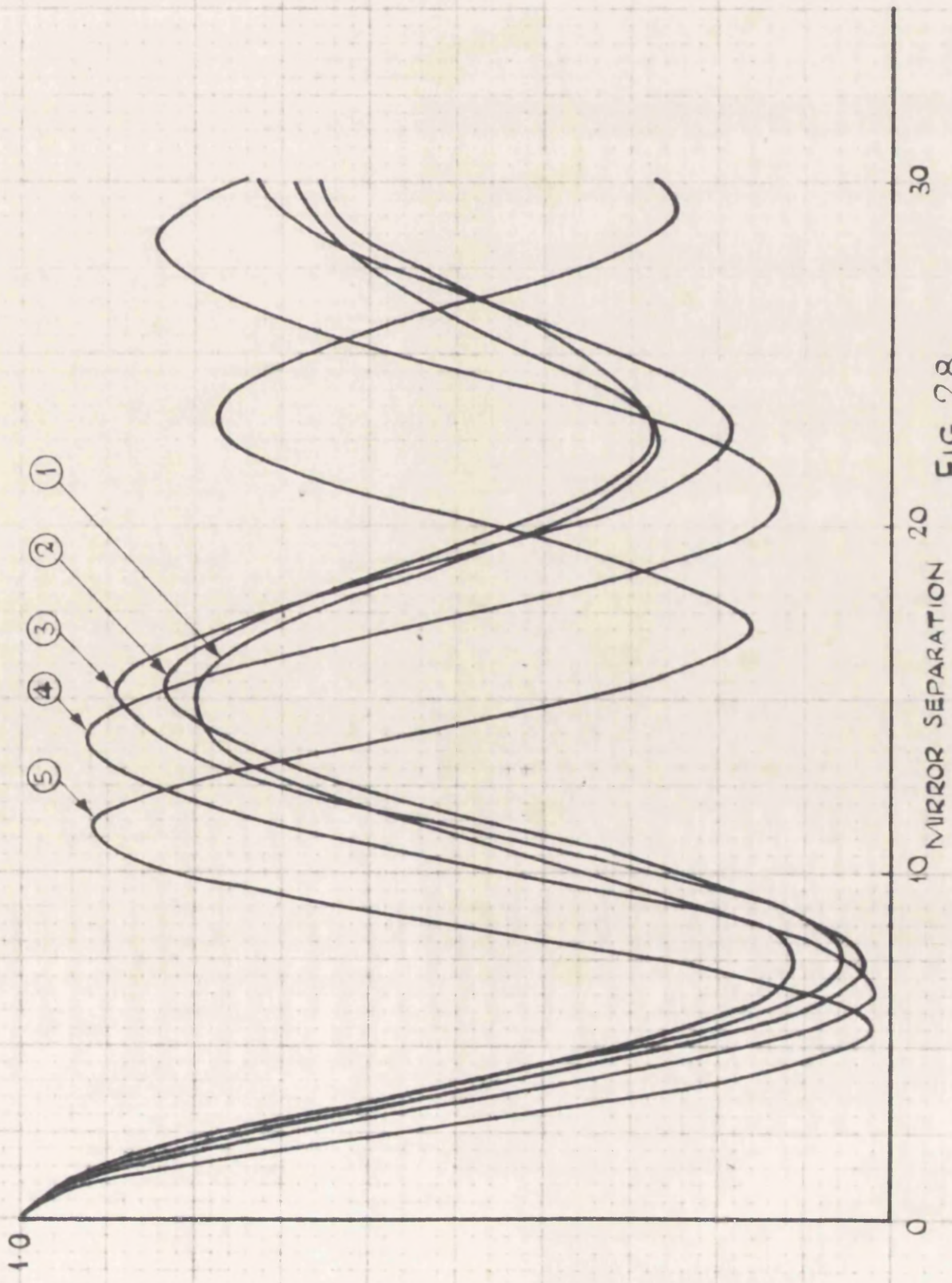


**FIG. 28.**

BOLTZMAN INTERFEROGRAM OBTAINED WITH A CRYSTAL AND A WAVEGUIDE SYSTEM CAUSING CUT OFF A

① ZERO FREQUENCY, ② 6 MC/S, ③ 8 MC/S, ④ 10 MC/S, ⑤ 12 MC/S, WHEN LOG. DEC. OF RADIATION IS 0.5.

$$\begin{aligned} \text{hence } R(\omega) |g(\omega)|^2 &= \int_0^{\infty} \left[ \int_0^{\infty} R(\omega) |g(\omega)|^2 \cos \omega \tau d\omega \right] \cos \omega \tau d\tau \\ &= \int_0^{\infty} P_{\tau} \cos \omega \tau d\tau \end{aligned}$$

and  $P_{\tau}$  could be obtained from the interferogram as described earlier.

A typical series of interferograms as obtained by a method to be described later is shown in Fig. 31. It will be seen that in spite of the expected high value of  $\delta$  the interferogram would appear to be very long, extending over several wavelengths. With such large separation between mirrors the accuracy of interferograms cannot be very large and if one limits it to but one or two wavelengths, the transform may not be accurate enough. To illustrate this point, the transform has been calculated assuming the original wave to be of the form  $e^{-\alpha t} \sin \omega_0 t$  when the interferogram is one, two, three or four wavelengths long. Typical result for  $\delta = 0.25$  appears in Figure 29. Fig. 30. gives the  $Q$  (or  $\delta$ ) found on the basis of  $s = 1, 2, 3$  or  $\infty$  number of wavelengths showing the order of correction which has to be applied to find the true incident spectrum if only a part of the interferogram is analysed.

It will be seen that when  $\delta \leq 1$  the interferogram has to be taken at least up to a mirror separation of  $2\lambda_0$ ; when  $\delta < 0.1$  the correction even with  $2\lambda_0$  would be excessive.

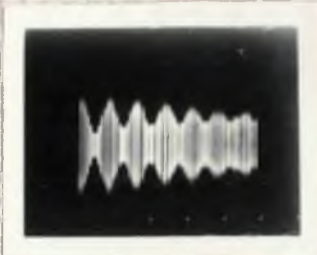
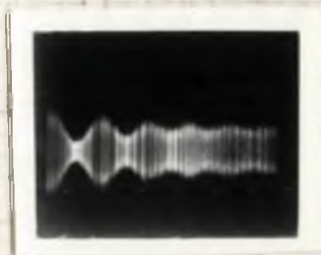


Fig 31.  
Typical interferograms.

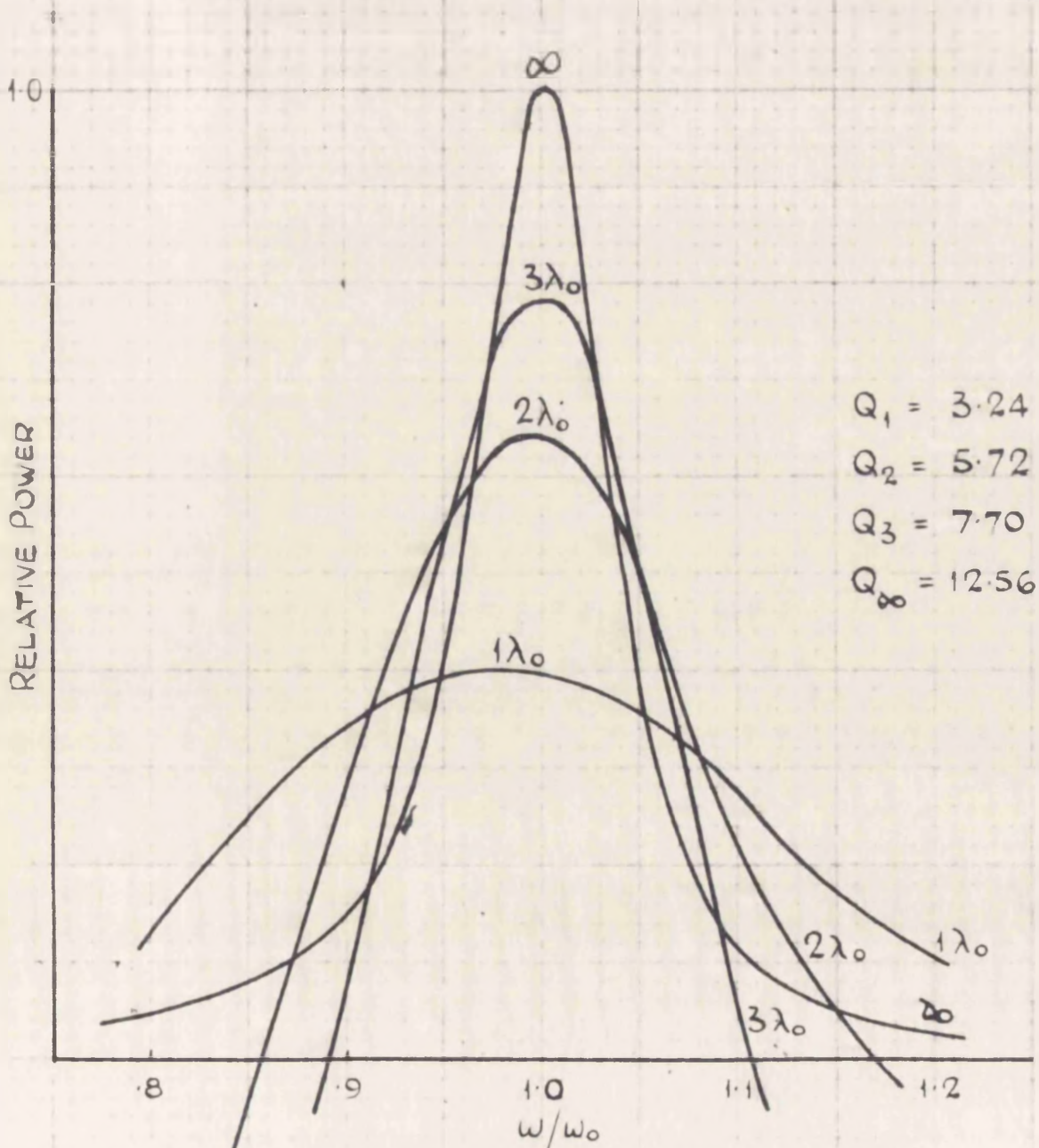


FIG. 29.

SPECTRUM OF POWER COMPUTED FROM THE BOLTZMAN INTERFERROGRAM TAKING INTO ACCOUNT A LENGTH =  $1\lambda_0, 2\lambda_0, 3\lambda_0$  AND  $\infty$  WHEN THE LOG DECREMENT OF THE ANALYSED WAVE  $e^{-\delta f_0 t} \sin 2\pi f_0 \lambda$  IS .25.

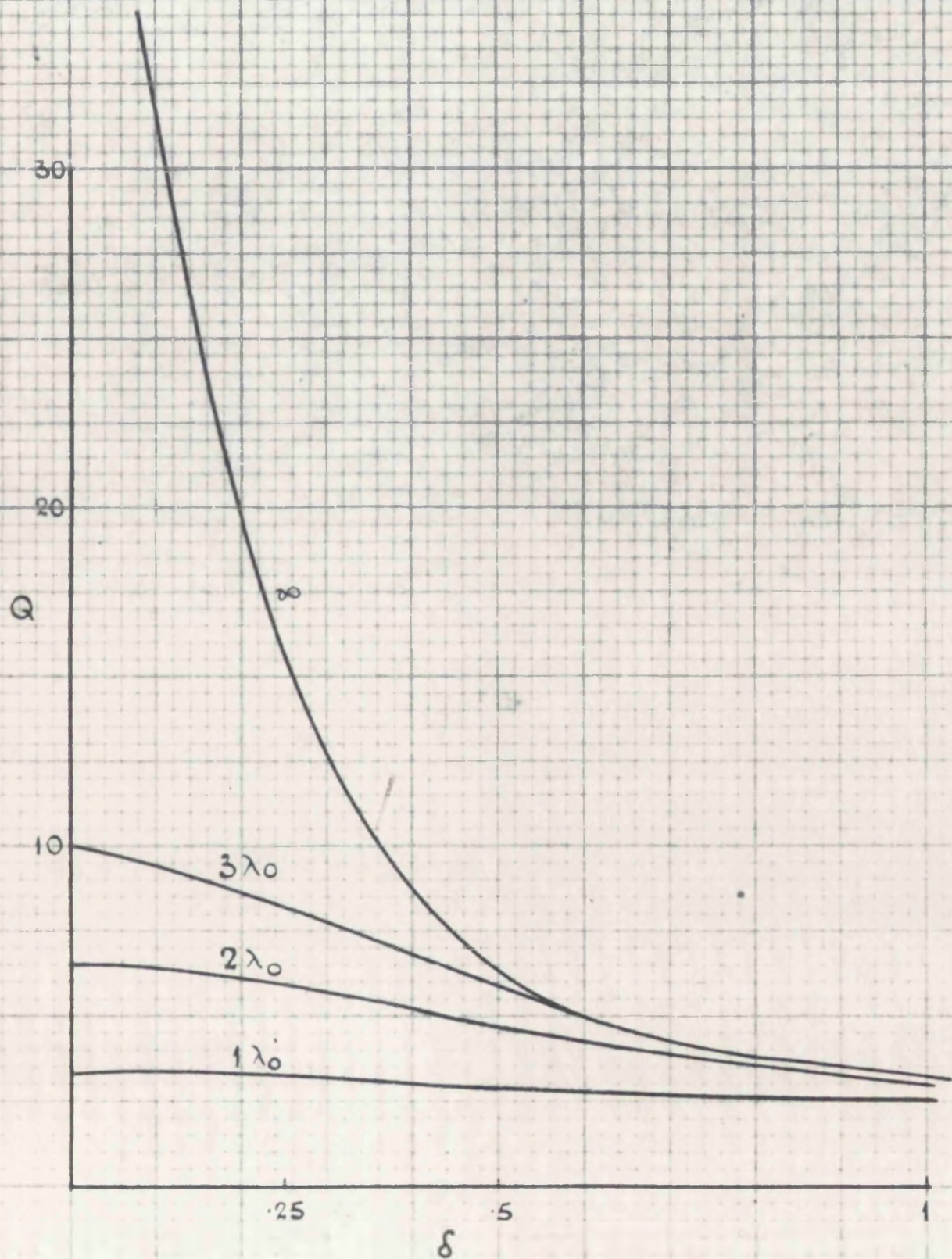


FIG. 30.

THE  $Q$  OF THE SPECTRUM OF A WAVE  $e^{-\delta f_0 t} \sin 2\pi f_0 t$   
FOUND FROM THE ANALYSIS OF A BOLTZMAN INTERFERROGRAM  
OF THE WAVE WHEN THE LENGTH OF THE INTERFERROGRAM  
IS  $= \lambda_0, 2\lambda_0, 3\lambda_0$  AND  $\infty$ .

From the above discussion it can be concluded that the Boltzmann interferometer method can only be used at present to arrive at the approximate form of the spectrum of detected power, i.e.  $R(\omega) |G(\omega)|^2$ . Neither the spectrum of radiated power  $|g(\omega)|^2$  nor the original wave form of radiation can be found until  $R(\omega)$  is known.

In view of the mismatch that occurs in the waveguide and crystal at frequencies other than those for which the components and chokes have been designed and consequent difficulties in calculating power output over a wide frequency band, the solution of this problem will have to be obtained experimentally and so await the availability of a source of microwaves variable over a wide frequency range such as may become possible with a backward travelling wave valve.

If, however, one neglects the effects of mismatch and accepts  $R(\omega)$  as given in Fig. 23. then one can arrive at  $|g(\omega)|^2$  and hence of  $|g(\omega)|$ . The actual results of experiments and computation will be given in part III.

#### 3.4.2. The effect of "tuned circuit" filter on the Boltzmann interferogram

The effect of waveguide and crystal response on the interferogram has been discussed above. It is of interest to examine the effect of a narrow band pass filter, which has been used extensively in the experimental part of this

work. For the sake of simplicity it will be assumed that the filter has the response characteristic of a tuned circuit with a spectrum similar to that of the radiating dipole. Thus the resultant spectrum can be taken as a product of the two spectra of source and filter.

If one denotes the natural angular frequency of the source by  $\omega_1$ , and its rate of decay by  $\alpha_1$ , while the corresponding values for filter are  $\omega_2$  and  $\alpha_2$ , then the power spectrum  $|G(\omega)|^2$  will be

$$|G(\omega)|^2 = \frac{\omega_1^2}{4\pi^2(\omega - \omega_1 - j\alpha_1)(\omega - \omega_1 + j\alpha_1)(\omega + \omega_1 - j\alpha_1)(\omega + \omega_1 + j\alpha_1)} \cdot \frac{\omega_2^2}{4\pi^2(\omega - \omega_2 - j\alpha_2)(\omega - \omega_2 + j\alpha_2)(\omega + \omega_2 - j\alpha_2)(\omega + \omega_2 + j\alpha_2)}$$

The resultant power output from a Boltzmann interferometer, when the mirror separation is  $s$ , is

$$P(s) = \int_0^\infty 4\pi |G(\omega)|^2 d\omega + \int_0^\infty 4\pi |G(\omega)|^2 c\tau \omega \tau d\omega$$

where  $\tau = \frac{2s}{c}$

$$\text{Now } \int_0^\infty 4\pi |G(\omega)|^2 \omega \tau d\omega = \frac{\omega_1^2 \omega_2^2}{64c} \left\{ \frac{e^{-\alpha_1 \tau}}{\alpha_1 \omega_1} \left[ \frac{(\omega_1 - j\alpha_1)(A^2 - B - j4\alpha_1 \omega_1 A e^{j\omega_1 \tau})}{\omega_1^2 + \alpha_1^2} + \frac{(\omega_1 + j\alpha_1)(A^2 - B + j4\alpha_1 \omega_1 A e^{-j\omega_1 \tau})}{\omega_1^2 + \alpha_1^2} \right] + \frac{e^{-\alpha_2 \tau}}{\alpha_2 \omega_2} \left[ \frac{(\omega_2 - j\alpha_2)(A^2 + B + j4\alpha_2 \omega_2 e^{j\omega_2 \tau})}{\omega_2^2 + \alpha_2^2} + \frac{(\omega_2 + j\alpha_2)(A^2 + B - j4\alpha_2 \omega_2 e^{-j\omega_2 \tau})}{\omega_2^2 + \alpha_2^2} \right] \right\}$$

where

$$A = \omega_1^2 - \omega_2^2 - \alpha_1^2 + \alpha_2^2$$

$$B = 4(\omega_1^2 \alpha_1^2 - \omega_2^2 \alpha_2^2)$$

$$C = A^2 + 4(\omega_1^2 \alpha_1^2 + \omega_2^2 \alpha_2^2) - 64\omega_1^2 \alpha_1^2 \omega_2^2 \alpha_2^2$$

$$\text{hence } 4\pi \int_0^{\infty} |G(\omega)|^2 \cos \omega \tau d\omega = \frac{\omega_1^2 \omega_2^2}{32c} \left\{ \frac{e^{-\alpha_1 \tau}}{\alpha_1 \omega_1 \sqrt{\omega_1^2 + \alpha_1^2}} \cos(\omega_1 \tau - \phi_1) + \frac{e^{-\alpha_2 \tau}}{\alpha_2 \omega_2 \sqrt{\omega_2^2 + \alpha_2^2}} \cos(\omega_2 \tau - \phi_2) \right\}$$

$$\text{where } \tan \phi_1 = \frac{\alpha_1}{\omega_1} \cdot \frac{(A^2 - B + 4\omega_1^2 A)}{(A^2 - B - 4\alpha_1^2 A)}$$

$$\tan \phi_2 = \frac{\alpha_2}{\omega_2} \cdot \frac{(A^2 + B - 4\omega_2^2 A)}{(A^2 + B + 4\alpha_2^2 A)}$$

$$\begin{aligned} \text{also } 4\pi \int_0^{\infty} |G(\omega)|^2 d\omega &= \frac{\omega_1^2 \omega_2^2}{32c} \left\{ \frac{\omega_1 (A^2 - B - 4\alpha_1^2 A)}{\omega_1 \alpha_1 (\omega_1^2 + \alpha_1^2)} + \frac{\omega_2 (A^2 + B + 4\alpha_2^2 A)}{\omega_2 \alpha_2 (\omega_2^2 + \alpha_2^2)} \right\} \\ &= \frac{\omega_1^2 \omega_2^2}{32c} \left\{ \frac{1}{\omega_1 \alpha_1 \sqrt{\omega_1^2 + \alpha_1^2} \sec \phi_1} + \frac{1}{\omega_2 \alpha_2 \sqrt{\omega_2^2 + \alpha_2^2} \sec \phi_2} \right\} \end{aligned}$$

$$\begin{aligned} \text{hence } P(s) &= \frac{\omega_1^2 \omega_2^2}{32c} \left\{ \frac{1}{\sqrt{\omega_1^2 + \alpha_1^2} \omega_1 \alpha_1 \sec \phi_1} [1 + e^{-\alpha_1 \tau} \sec \phi_1 \cos(\omega_1 \tau - \phi_1)] + \right. \\ &\quad \left. + \frac{1}{\sqrt{\omega_2^2 + \alpha_2^2} \omega_2 \alpha_2 \sec \phi_2} [1 + e^{-\alpha_2 \tau} \sec \phi_2 \cos(\omega_2 \tau - \phi_2)] \right\} \\ &= \frac{\omega_1^2 \omega_2^2}{32c} \left\{ \frac{A^2 - B - 4\alpha_1^2 A}{\alpha_1 (\omega_1^2 + \alpha_1^2)} [1 + e^{-\alpha_1 \tau} \sec \phi_1 \cos(\omega_1 \tau - \phi_1)] + \right. \\ &\quad \left. + \frac{A^2 + B + 4\alpha_2^2 A}{\alpha_2 (\omega_2^2 + \alpha_2^2)} [1 + e^{-\alpha_2 \tau} \sec \phi_2 \cos(\omega_2 \tau - \phi_2)] \right\} \end{aligned}$$

This is seen to consist of two terms each of the same form as that obtained in paragraph 3.4 for the case of uniform frequency response of receiver. The individual terms, however, depend both on the source and filter characteristics. This expression is too involved to allow a full interpretation of the resultant plot of  $P(s)$  against  $s$  and only a few special cases can be considered.

It can be shown that if  $\omega_2 = k\omega_1$  and  $\alpha_1 = \alpha_2$  then the

relative power output from the interferometer will be of the form

$$\left\{ k^2 + 1 + e^{-\alpha_1 \tau} \left[ k^2 \omega_2 (\omega_1 \tau - \phi_1) + \omega_2 (k \omega_1 \tau - \phi_2) \right] \right\}$$

When  $k$  is close to 1 this results in a decaying cosine waveform whose frequency is  $\frac{\omega_1 + \omega_2}{4\pi}$  and which also displays

a beat effect of frequency  $\frac{\omega_2 - \omega_1}{2\pi}$ .

A frequent case will be one in which  $\alpha_1^2 \ll \omega_1^2$  and  $\alpha_2^2 \ll \omega_2^2$ . In this case, if  $\omega_1 \neq \omega_2$  the term  $P(s)$  reduces to

$$P(s) = \frac{\omega_1^2 \omega_2^2}{32(\omega_1^2 - \omega_2^2)^2} \left\{ \frac{1}{\alpha_1^2 \omega_1^2} \left[ 1 + e^{-\alpha_1 \tau} \cos(\omega_1 \tau - \phi_1) \right] + \frac{1}{\alpha_2^2 \omega_2^2} \left[ 1 + e^{-\alpha_2 \tau} \cos(\omega_2 \tau - \phi_2) \right] \right\}$$

where

$$\phi_1 = \tan^{-1} \frac{\alpha_1}{\omega_1} \cdot \frac{5\omega_1^2 - \omega_2^2}{\omega_1^2 - \omega_2^2}$$

$$\phi_2 = \tan^{-1} \frac{\alpha_2}{\omega_2} \cdot \frac{\omega_1^2 - 5\omega_2^2}{\omega_1^2 - \omega_2^2}$$

It will be observed here that the resultant interferogram will be a sum of two interferograms resembling closely but not wholly the interferograms obtained from the individual spectra. The difference is in the position of the individual maxima and minima which will not correspond to multiples of  $s = \frac{\lambda_1}{4}$  and  $s = \frac{\lambda_2}{4}$  respectively.

In general, the above expression allows one to draw the following conclusions: if  $\omega_2$  (the centre frequency of

the filter) is not very much greater than  $\omega_1$  (the natural frequency of source) while  $\delta_2 = \frac{\alpha_2}{F_2}$  (i.e. the log. dec. of filter response) is much less than  $\delta_1 (= \frac{\alpha_1}{F_1}$  i.e. the log. dec. of source) then the interferogram displays the pattern characteristic of the filter response (there is a slight shift in the position of maxima since as  $\omega_2 \rightarrow \omega_1, \phi_2 \rightarrow \tan^{-1} \frac{2\omega_1}{\omega_2}$  but since  $\alpha_2 \ll \omega_2$  the shift is insignificant).

As, however,  $\omega_2$  is increased for a given  $\delta_2$  the pattern becomes more and more a fusion of the two individual patterns and loses any value for measurement purposes. Similarly for given values of  $\omega_1$  and  $\omega_2$  if  $\delta_2$  is reduced the filter pattern will appear. Finally, for any given  $\omega_2$  and  $\delta_2$  it is possible to accentuate the filter pattern by forcing  $\omega_1$  up towards  $\omega_2$  (by reducing the guide width for example and thus shifting the maximum of the source spectrum towards higher frequencies).

It should be understood, of course, that the clearer the filter pattern the better will the radiated spectrum approach the filter response

### 3.5. The standing wave method

A similar method of obtaining the spectrum to that using a Boltzmann interferometer is to produce a standing wave by letting the radiated wave be reflected from a highly conducting surface at right angles to the direction of

propagation. The standing wave can then be plotted by using some sort of a probe and the plot can be analysed.

The only difference between the approach to the solution of this problem and that of Boltzmann interferometer is that here the wave on reflection undergoes a phase reversal so that the resultant wave is the difference between the oncoming and the reflected wave and its Fourier transform

$$G(\omega) = g(\omega) \left(1 - e^{-j\frac{\omega x}{c}}\right)$$

where  $x$  is distance of probe from screen and  $c$  is the velocity of light; which leads to

$$|G(\omega)|^2 = 2 |g(\omega)|^2 \left(1 - \cos \frac{2\omega x}{c}\right)$$

and by applying Parseval's theorem the total power measured at the point distant  $x$  from the screen is

$$\begin{aligned} P(x) &= \int_{-\infty}^{\infty} |F(t)|^2 dt = 4\pi \int_0^{\infty} |G(\omega)|^2 d\omega = \\ &= 8\pi \int_0^{\infty} |g(\omega)|^2 d\omega + 8\pi \int_0^{\infty} |g(\omega)|^2 \cos \frac{2\omega x}{c} d\omega \end{aligned}$$

As in the case of Boltzmann interferometer this can be used to find the value of  $|g(\omega)|$  since the first term being independent of  $x$  must be the value to which  $P(x)$  will tend, and the second term is a cosine transform of  $|g(\omega)|^2$  from which one can compute  $|g(\omega)|$  as explained earlier.

If, as an example, one assumes the radiated wave to be  $f(t) = e^{-\alpha t} \sin \omega_0 t$ , then by analogy with previous cases

$$P(x) = \frac{\omega_0^2}{2\alpha(\omega_0^2 + \alpha^2)} \left[ 1 - e^{-\frac{2\alpha x}{c}} \frac{\omega_0 \cos \frac{2\omega_0 x}{c} + \alpha \sin \frac{2\omega_0 x}{c}}{\omega_0} \right]$$

$$= \frac{1}{\omega_0 \delta (1 + \delta^2/4\pi^2)} \left[ 1 - \sqrt{1 + \delta^2/4\pi^2} e^{-\frac{2\alpha x}{c}} \cos(2\frac{\omega_0 x}{c} - \phi) \right]$$

where  $\phi = \tan^{-1} \frac{\alpha}{\omega_0} = \tan^{-1} \frac{\delta}{2\pi}$

and  $\delta = \frac{\alpha}{f_0}$

Thus  $P(x)$  becomes as shown in Fig. 31. below:

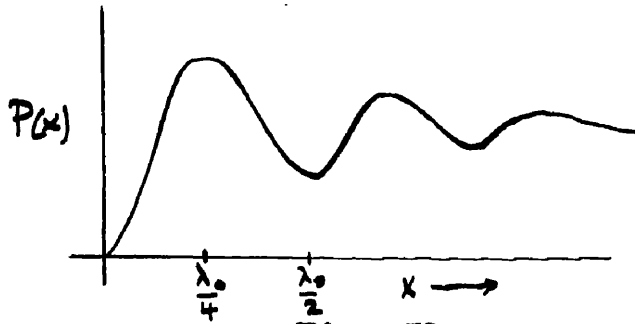


Fig. 31.

Kawano has calculated also  $P(x)$  for other forms of radiated wave, the most important of which is, that, if the wave consists of two components

$$f(t) = e^{-\alpha t} (\sin \omega_1 t + \sin \omega_2 t)$$

then the interferogram  $P(x)$  displays a beat effect whose wavelength  $\lambda_b = \frac{c}{\Delta f}$  where  $\Delta f = \frac{\omega_2 - \omega_1}{2\pi}$ . This again is similar to the effect obtained with a Boltzmann interferometer.

On the face of it the standing wave method of spectrum analysis would appear the simpler of the two, requiring no moving mirrors which are bound to introduce some error and - a very important point when the available power is very small as in spark generators - there is less power loss due to dispersion and shorter air distances can be adopted.

However, when one goes into details of probe mounting etc., it will become clear that in fact the Boltzmann interferometer has the advantage of allowing the use of receiving horn which is more efficient and causes less disturbance to the field than any probe direct in the beam. On the balance, the Boltzmann interferometer appears the more suitable and more adaptable a method than the standing wave measurement.

### 3.6. Decaying waves in waveguides

It has been said earlier that the effect of crystal mounts, connecting chokes etc, will be to cause a mismatch at all but one frequency, thus distorting the resultant spectrum. The question arises, whether, should one be able to overcome the mismatch difficulties, could an all-waveguide system be used to obtain the spectrum since a hybrid T can be used as a Boltzmann interferometer while a moving shorting plunger behind a crystal would produce standing waves. Consider the latter case first: If  $f(t)$  is the incident wave then at a distance  $x$  from the short-circuiting plunger the reflected wave is given by

$f(t - \frac{x}{u_g} - \frac{2x}{u_g})$  where  $u_g$  is the guide velocity of propagation (phase velocity) and  $u_g = \frac{\omega}{\beta_g} = \frac{u_c}{\sqrt{\omega^2 - \omega_c^2}}$

where  $\beta_g$  is propagation constant

$\omega_c$  is cutoff radial frequency

Thus the Fourier transform of the incident and reflected wave at the point  $x$  becomes

$$G(\omega) = g(\omega) (1 - e^{-j\omega \frac{2x}{u_g}}) = g(\omega) (1 - e^{-j \frac{2x \sqrt{\omega^2 - \omega_c^2}}{c}})$$

$$\text{and } |G(\omega)|^2 = 2|g(\omega)|^2 \left(1 - \cos \frac{2x}{c} \sqrt{\omega^2 - \omega_c^2}\right)$$

$$\text{hence } P(x) = 8\bar{u} \int_0^{\infty} |g(\omega)|^2 \left(1 - \cos \frac{2x}{c} \sqrt{\omega^2 - \omega_c^2}\right) d\omega$$

If  $f(t) = e^{-\alpha t} \sin \omega_0 t$ ; where  $\omega_0 > \omega_c$ , this condition being necessary in order that the integration can be carried out by residue methods,

$$\text{then } P(x) = \frac{\omega_0^2}{2\alpha(\omega_0^2 + \alpha^2)} - \frac{\omega_0}{4\alpha} \left[ \frac{e^{j\frac{2x}{c}\sqrt{(\omega_0 + j\alpha)^2 - \omega_c^2}}}{\omega_0 + j\alpha} + \frac{e^{j\frac{2x}{c}\sqrt{(\omega_0 - j\alpha)^2 - \omega_c^2}}}{\omega_0 - j\alpha} \right]$$

Let

$$\sqrt{(\omega_0 + j\alpha)^2 - \omega_c^2} = p_1 + jq_1$$

$$\sqrt{(\omega_0 - j\alpha)^2 - \omega_c^2} = -(p_2 + jq_2)$$

Note that the RHS can be either positive or negative, but setting  $\omega_c = 0$  and comparing with the results obtained in paragraph 5.5. to which the above should then correspond leads to the correct choice of signs.

It follows that

$$p_1 = p_2 = p = \sqrt{\frac{1}{2} \left[ \sqrt{(\omega_0^2 - \alpha^2 - \omega_c^2)^2 + 4\alpha^2\omega_0^2} + (\omega_0^2 - \alpha^2 - \omega_c^2) \right]}$$

$$= \frac{\omega_0}{\sqrt{2}} \sqrt{\left( \frac{\lambda_0^2}{\lambda_g^2} - \frac{\delta^2}{4\pi^2} \right)^2 + \frac{\delta^2}{\pi^2} + \left( \frac{\lambda_0^2}{\lambda_g^2} - \frac{\delta^2}{4\pi^2} \right)}$$

$$q_1 = q_2 = q = \frac{\omega_0}{\sqrt{2}} \sqrt{\left( \frac{\lambda_0^2}{\lambda_g^2} - \frac{\delta^2}{4\pi^2} \right)^2 + \frac{\delta^2}{\pi^2} - \left( \frac{\lambda_0^2}{\lambda_g^2} - \frac{\delta^2}{4\pi^2} \right)}$$

$$\text{Thus } P(x) = \frac{\omega_0^2}{2\alpha(\omega_0^2 + \alpha^2)} - \frac{\omega_0}{4\alpha} \left[ \frac{e^{j\frac{2x}{c}(p+jq)}}{\omega_0 + j\alpha} + \frac{e^{-j\frac{2x}{c}(p-jq)}}{\omega_0 - j\alpha} \right]$$

$$= \frac{\omega_0^2}{2\alpha(\omega_0^2 + \alpha^2)} - \frac{\omega_0}{2\alpha} \cdot \frac{e^{-\frac{2xq}{c}}}{\sqrt{\omega_0^2 + \alpha^2}} \cdot \cos\left(\frac{2xp}{c} - \phi\right)$$

$$= \frac{1}{\omega_0\delta(1 + \delta^2/4\pi^2)} \left[ 1 - \sqrt{1 - \delta^2/4\pi^2} e^{-\frac{2xq}{c}} \cos\left(\frac{2xp}{c} - \phi\right) \right]$$

$$\text{where } \phi = \tan^{-1} \frac{\alpha}{\omega_0} = \tan^{-1} \frac{\delta}{2\pi}$$

and by analogy the corresponding output from a hybrid T in which the two plungers in the side arms are unequally displaced from the centre of symmetry, the difference being  $s$  is

$$P(s) = \frac{1}{\omega_0 \delta (1 + \delta^2/4\pi^2)} \left[ 1 + \sqrt{1 + \delta^2/4\pi^2} e^{-\frac{2sq}{c}} \cos(2\frac{sq}{c} - \phi) \right]$$

Since for any given guide and wave  $p$  &  $q$  are constant, it is seen that the resultant interferograms are of the same shape as those obtained with the Boltzmann interferometer and a reflecting screen in air.

To find the position of maxima and minima one has to find the condition when  $\frac{dP}{dx} = 0$ .

$$\text{This leads to the relation } \tan\left(\frac{2sq}{c} - \phi\right) = -\frac{q}{p}$$

which is seen to be rather involved and the several variables contained in it make the determination of  $\alpha$  and  $\omega_0$  very difficult.

In order to have a better conception of the standing wave that would result one can simplify the above condition for maxima by assuming that

$$\frac{\delta^2}{4\pi^2} \ll \frac{\lambda_0^2}{\lambda_g^2}$$

$$\text{and } \frac{\delta^2}{\pi^2} \ll \frac{\lambda_0^4}{\lambda_g^4}$$

the first of which, in fact, is a reasonable assumption because the above solution holds only when  $\omega_0$  is appreciably

greater than  $\omega_c$ , in which case  $(\lambda_0/\lambda_g)^2$  will be  $> 0.5$  while  $\frac{\delta^2}{4\pi^2}$  is likely to be of the order of .025. But the second assumption will hold only if  $\omega_0 \ll \omega_c$  i.e.  $\frac{\lambda_0}{\lambda_g} \rightarrow 1$

Under those circumstances

$$p = \omega_0 \lambda_0 / \lambda_g \text{ and } q = 0$$

hence

$$X_{1\max} = \frac{(\pi + \phi)c}{2p} = \frac{(\pi + \phi)\lambda_g}{4\pi}$$

and since  $\phi \ll \pi$ ,  $X_{1\max} \doteq \lambda_g/4$  as expected.

The consecutive maxima will be seen to show no decrease since  $q = 0$ .

At the other end of the scale let  $\frac{\delta^2}{4\pi^2} \ll \frac{\lambda_0^2}{\lambda_g^2}$

$$\text{but } \frac{\delta^2}{\pi^2} \gg \frac{\lambda_0^4}{\lambda_g^4}$$

In this case  $p = \omega_0 \sqrt{\delta/2\pi}$

$$q = \omega_0 \sqrt{\delta/2\pi}$$

$$\text{hence } X_{1\max} = \frac{(\frac{3\pi}{4} + \phi)c}{2p} \doteq \frac{3\pi c}{8\omega_0} \sqrt{\frac{2\pi}{\delta}} = .47 \frac{\lambda_0}{\delta}$$

and the consecutive maxima decrease according to the law

$$e^{-\frac{2\pi\omega_0}{c} \sqrt{\delta/2\pi}}$$

This analysis shows that this method of spectrum analysis is unsuitable because of the difficulty of interpreting the resultant output.

It can be used, however, to measure  $\lambda_0$  fairly accurately provided  $\omega_0 \ll \omega_c$  and  $\delta$  is small - a condition,

which, as will be seen later, is met when filters are used to select an upper portion of the radiated spectrum resulting in very small log decrement ( $\delta = \pi/Q$ ) and

#### 4. Dispersion of spectrum of radiating dipole

Several methods of dispersion of the radiated spectrum are available such as various forms of gratings or dielectric lenses in which the dielectric constant varies with wavelength as in water or in artificial dielectrics.

In view of the vastness of the field covered by artificial dielectrics this analysis will not concern itself with them beyond noting their great possibilities in this application in view of the very wide band of radiation from spark generators.

##### 4.1. Dispersion by a slit

##### 4.1.1. Limits of solution

Considerable amount of work has been done on the general solution of diffraction of monochromatic electromagnetic waves by holes and obstacles. A comprehensive review of the work in the last 15 years has been published by Bouvkamp. The solutions are mostly very involved. In the case of a narrow slit it has been possible to arrive at a rigorous solution by using elliptic coordinates. These solutions, however, require lengthy computations. Some results have been quoted and are given in Fig. 32.

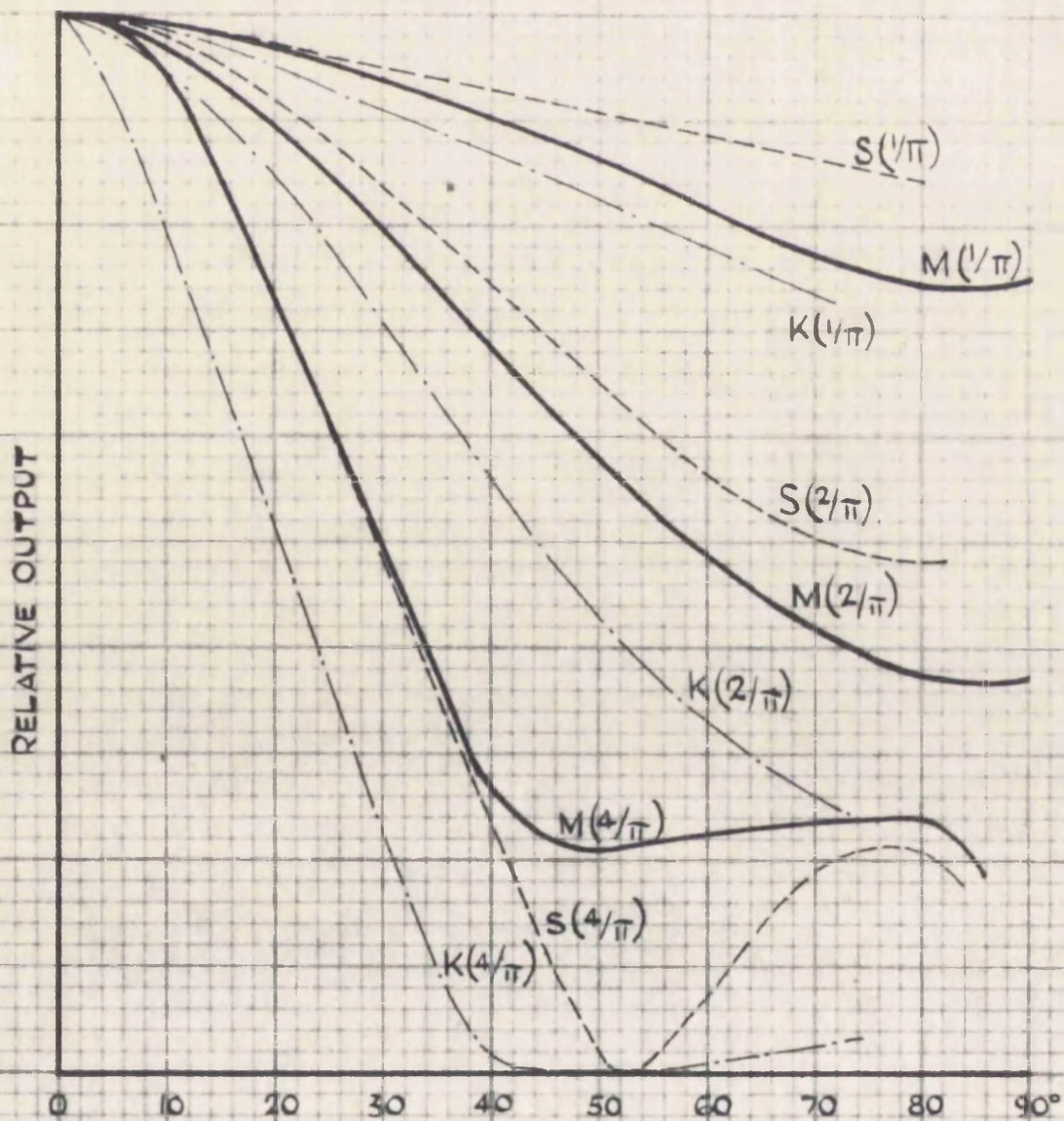


FIG. 32.

DIFFRACTION OF ELECTROMAGNETIC WAVE WHOSE ELECTRIC VECTOR IS PARALLEL TO A SLIT, BY THE SLIT WHEN THE RATIO OF SLIT WIDTH TO WAVELENGTH IS  $1/\pi$ ,  $2/\pi$  AND  $4/\pi$  ACCORDING TO MORSE'S RIGOROUS SOLUTION (M), STRATTON AND CHU (S) AND KIRCHHOFF'S (K).

Approximate solutions have been arrived at by Schwarzschild and by a different approach by Stratton and Chu.

Schwarzschild's solution for the intensity of radiation diffracted at an angle  $\theta$  to normal to an infinitely long slit of width "a" illuminated by a monochromatic radiation of wavelength  $\lambda$  at right angles to the plane of the slit when the electric vector is parallel to the sides of the slit is given by the expression

$$J = \frac{\sin^2\left(\frac{\pi a}{\lambda} \sin \theta\right)}{\left(\frac{2\pi a}{\lambda} \sin \theta/2\right)^2} + \frac{\cos^2\left(\frac{\pi a}{\lambda} \sin \theta\right)}{\left(\frac{2\pi a}{\lambda} \cos \theta/2\right)^2} + J'$$

where it can be shown that

$$J' < \frac{4\lambda}{\pi a (\pi \sqrt{a/\lambda} - 1)} \cdot \frac{\cos \theta/2}{\cos \theta}$$

Now Kirchoff advanced a simple solution of diffraction by slits according to which each element of the slit acts as a source whose magnitude and phase is that due to the original source at that point in the absence of any obstacles. A well-known formula for the total power diffracted by a slit at an angle  $\theta$  derived from Kirchoff's analysis is

$$P_k = \frac{\sin^2\left(\frac{\pi a}{\lambda} \sin \theta\right)}{\left(\frac{\pi a}{\lambda} \sin \theta\right)^2}$$

Since the width of the diffracted beam at an angle  $\theta$  is narrower than the incident in the ratio  $\cos \theta$  to 1, the intensity of diffracted radiation  $J_k = P_k / \cos \theta$ , hence it

can be shown that  $J = J_k \cos^2 \theta + \frac{\lambda^2}{(2\pi a \cos^2 \theta/2)^2}$  with an error less than  $|J^1|$  given earlier. This shows that when  $\theta < 45^\circ$  and  $\lambda < a/2$  the total error introduced by accepting the Kirchhoff's solution - which is preferable on account of its simplicity - is not very large.

Stratton and Chu arrived at a different approximation, assuming a finite slit of width "a" and length "b", which for normal incidence with vector E parallel to the length "b" leads to intensity of dispersed radiation at an angle  $\theta$  to xZ plane (horizontal pattern)

$$J_{sh} = \frac{b^2}{\pi^2} \cos^2 \theta \frac{\sin^2(\frac{\pi a}{\lambda} \sin \theta)}{\sin^2 \theta}$$

$$= \frac{b^2 a^2}{\lambda^2} \cos^2 \theta = J_k$$

which, except for the constant coefficient, is similar to the solution of Schwarzschild and again shows that for small values of  $\theta$  the Kirchhoff solution is close enough.

The expression derived by Stratton and Chu allows for the evaluation of the vertical pattern as well, i.e. when  $\theta = 0$  the intensity of dispersed radiation at an angle to YZ plane is

$$J_{sv} = \frac{a^2 \sin^2(\frac{\pi b}{\lambda} \sin \psi)}{\pi^2 \sin^2 \psi}$$

showing that if "b" is small the vertical pattern is virtually uniform. Figs. 32 and 33. show the horizontal and vertical patterns obtained by Stratton and Chu when the

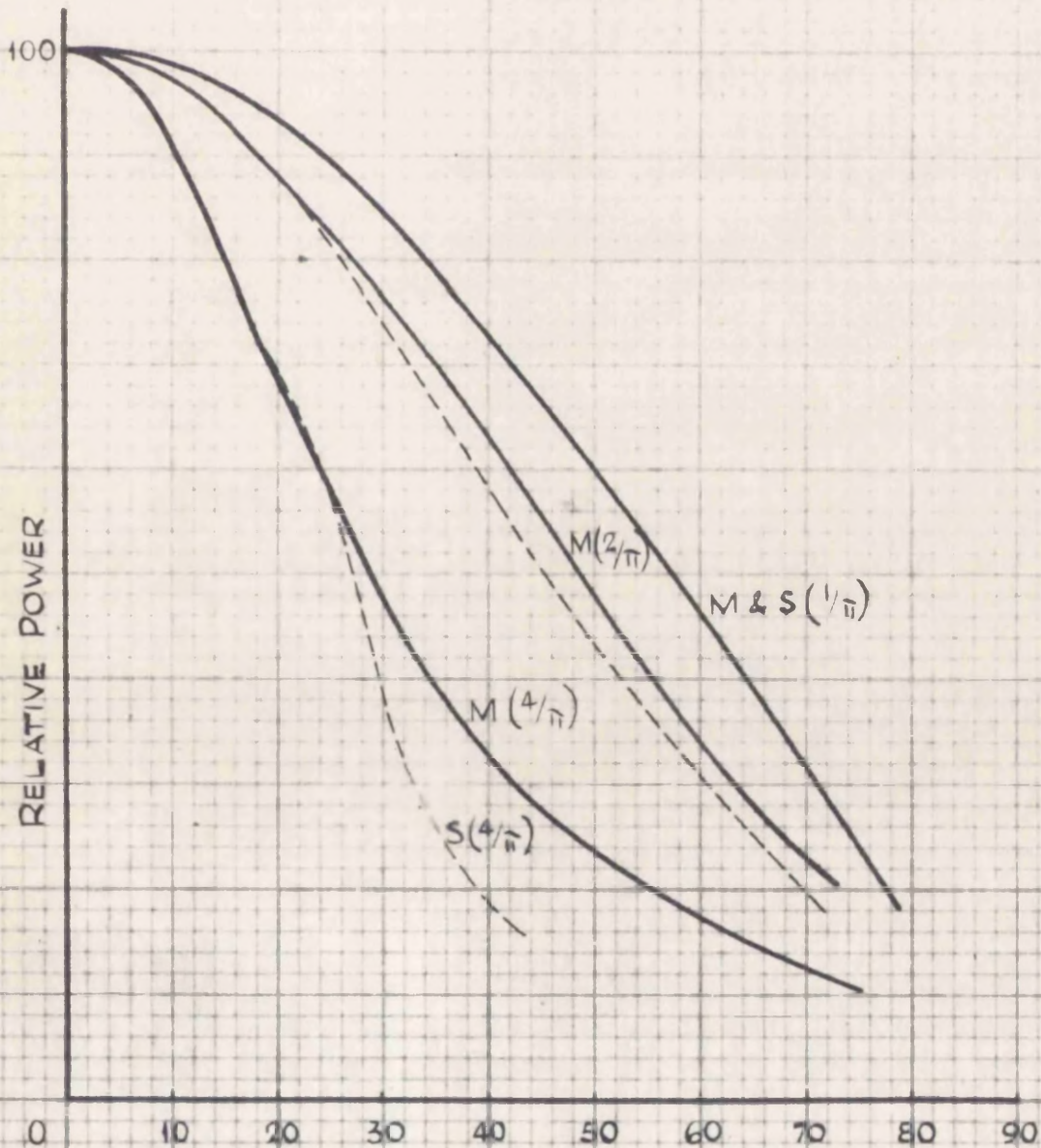


FIG. 33.

THE VERTICAL PATTERN OF THE DIFFRACTION OF ELECTROMAGNETIC WAVE BY A SLIT OF LENGTH 'b' WHOSE RATIO TO WAVELENGTH IS  $1/\pi$ ,  $2/\pi$  AND  $4/\pi$  ACCORDING TO MORSE (RIGOROUS SOLUTION) AND STRATTON & CHU.

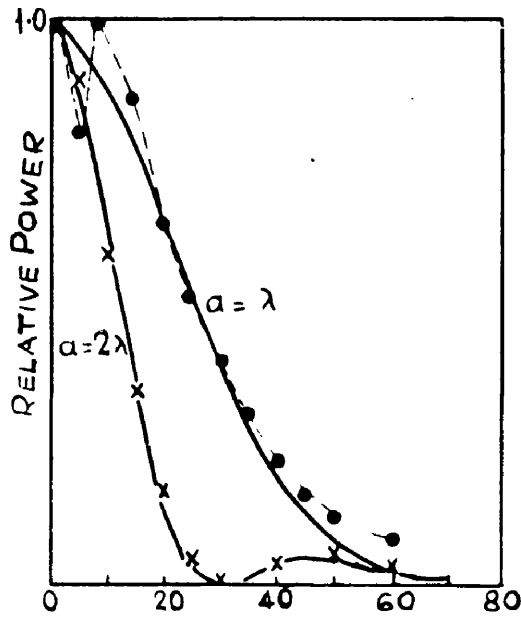
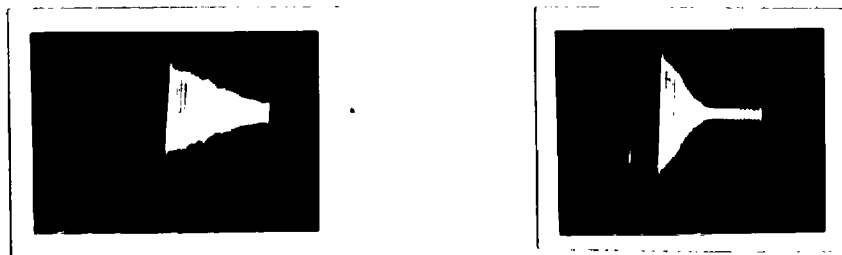


FIG. 34.

DIFFRACTION OF ELECTROMAGNETIC WAVE BY A SLIT OF WIDTH  $a$ .

● } MEASURED VALUES  
 x } AT  $\lambda = 3.1\text{cm}$



ratio of slit dimensions to wavelength is  $\frac{1}{\pi}$ ,  $\frac{2}{\pi}$  and  $\frac{4}{\pi}$  showing by comparison with exact solution that the above expressions are accurate enough in this range hence it follows that Kirchhoff's solution is satisfactory for  $a \gg \lambda$  as long as  $\theta \leq 45^\circ$ . Fig. 34. gives the results obtained with e.m. waves generated by a klystron,  $\lambda = 3.1$  cm, when  $a = \lambda$  and when  $a = 2\lambda$ , as well as those calculated from Kirchhoff's formula. A close agreement is seen confirming the previous conclusions as to applicability of Kirchhoff's solution when  $a \gg \lambda$ .

#### 4.1.2. Spectral characteristics of a slit

After this preliminary discussion one can now proceed to calculate the spectrum of power dispersed by a slit when the incident wave is non-monochromatic, on the basis of Kirchhoff's solution, it being assumed that slit width is not less than the longest wave length of those present in the spectrum of the source.

Referring to Fig. 35. the detector at an angle  $\theta$  to normal receives radiation from the element  $x$  delayed with respect to that originating at 0 by time  $\frac{x \sin \theta}{c}$  where  $c$  is velocity of e.m. wave.

$$\text{Hence } F_{\theta}(t) = \int_0^a f\left(t - \frac{x \sin \theta}{c}\right) dx$$

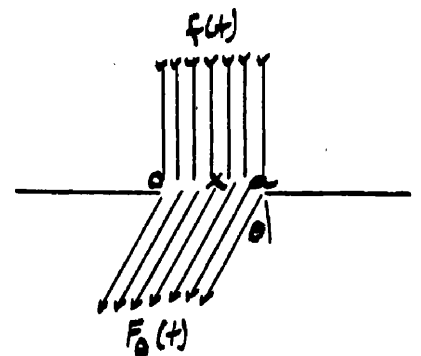


Fig. 35.

If spectrum of  $f(t)$  is  $g(\omega) = \frac{1}{2\pi} \int_{-\infty}^{\infty} f(t) e^{-j\omega t} dt$

then spectrum of  $F_{\theta}(t)$  is

$$\begin{aligned} G_{\theta}(\omega) &= \frac{1}{2\pi} \int_{-\infty}^{\infty} \int_0^a f\left(t - \frac{x \sin \theta}{c}\right) e^{-j\omega t} dx dt \\ &= \frac{1}{2\pi} \int_{-\infty}^{\infty} \int_0^a f(t) e^{-j\omega x \frac{\sin \theta}{c}} e^{-j\omega t} dx dt \\ &= \frac{1}{2\pi} \int_{-\infty}^{\infty} \frac{c}{j\omega \sin \theta} \left( e^{-j\omega a \frac{\sin \theta}{c}} - 1 \right) f(t) e^{-j\omega t} dt \\ &= g(\omega) \frac{c}{j\omega \sin \theta} (1 - e^{-j\omega \eta}) \quad \text{where } \eta = \frac{a \sin \theta}{c} \end{aligned}$$

The power spectrum becomes

$$P_{\theta}(\omega) = |G_{\theta}(\omega)|^2 = |g(\omega)|^2 \frac{2c^2}{\omega^2 \sin^2 \theta} (1 - \cos \omega \eta)$$

and power dispersed at angle  $\theta$  is  $P_{\theta} = 4\pi \int_0^{\infty} |G_{\theta}(\omega)|^2 d\omega$

Since the power spectrum of radiation is  $4\pi |g(\omega)|^2$  the spectral characteristic function of the slit is

$$S(\omega) = \frac{2c^2}{\omega^2 \sin^2 \theta} (1 - \cos \omega \eta) = \frac{4c^2 \sin^2 \omega \eta / 2}{\omega^2 \sin^2 \theta}$$

and rationalised by dividing into  $S(\omega)_{\theta=0}$

$$S(\omega) = \frac{\sin^2 \omega \eta / 2}{(\omega \eta / 2)^2}$$

which, of course, is the well-known expression for the dispersion of a slit.

When differentiated with respect to  $\theta$  it is found that the function is at a maximum when  $\frac{\omega \eta}{2} = \tan \frac{\omega \eta}{2}$  and at a minimum when  $\omega \eta = 2\pi n$  where  $n = 1, 2, 3, \text{ etc.}$

hence

$$\frac{S(\omega)_{\theta \text{ max}}}{S(\omega)_{\theta=0}} = \cos^2 \frac{\omega \eta}{2}$$

and, of course,  $S(\omega)_{\theta_{min}} = 0$

The magnitudes of the successive maxima occurring at  $\omega\eta = 0, 8.98, 15.4, 21.6, \text{ etc.}$  are respectively 1, .047, .017, .008, etc. showing a rapid and pronounced fall beyond the zero order. Fig. 36. illustrates the power spectral characteristic of a slit in terms of  $a/\lambda$  for  $\theta = 10^\circ$ . For any other angle  $\theta$ , the scale  $a/\lambda$  has to be multiplied by a factor  $\sin 10^\circ / \sin \theta$ .

The spectral characteristic function  $S(\omega)$  such as is illustrated in Fig. 36. is a distribution function, representing the relative amplitude of a wave of a given frequency  $f \propto \frac{a}{\lambda}$  at an angle  $\theta$  to the normal to the diffracting medium. If the spectrum of radiated power is given by  $|G(\omega)|^2$  and the detector spectral characteristic by  $R(\omega)$  then the detected power spectrum will be

$$P(\omega) = |G(\omega)|^2 R(\omega) S(\omega)$$

If this spectrum is to be narrower than that of  $|G(\omega)|^2$  itself then  $R(\omega) S(\omega)$  must act as a filter. Now  $R(\omega)$  using a waveguide and a crystal will act as a high pass filter hence  $S(\omega)$  must provide the narrow band pass effect. This is provided by the first principal peak, the  $Q$  of which can be seen to be 2.75. This small value of  $Q$  implies that the method is unsuitable for the spectrum analysis since the  $Q$  of the spectrum of the spark radiator is of the same order. On the other hand, it is possible to use the slit

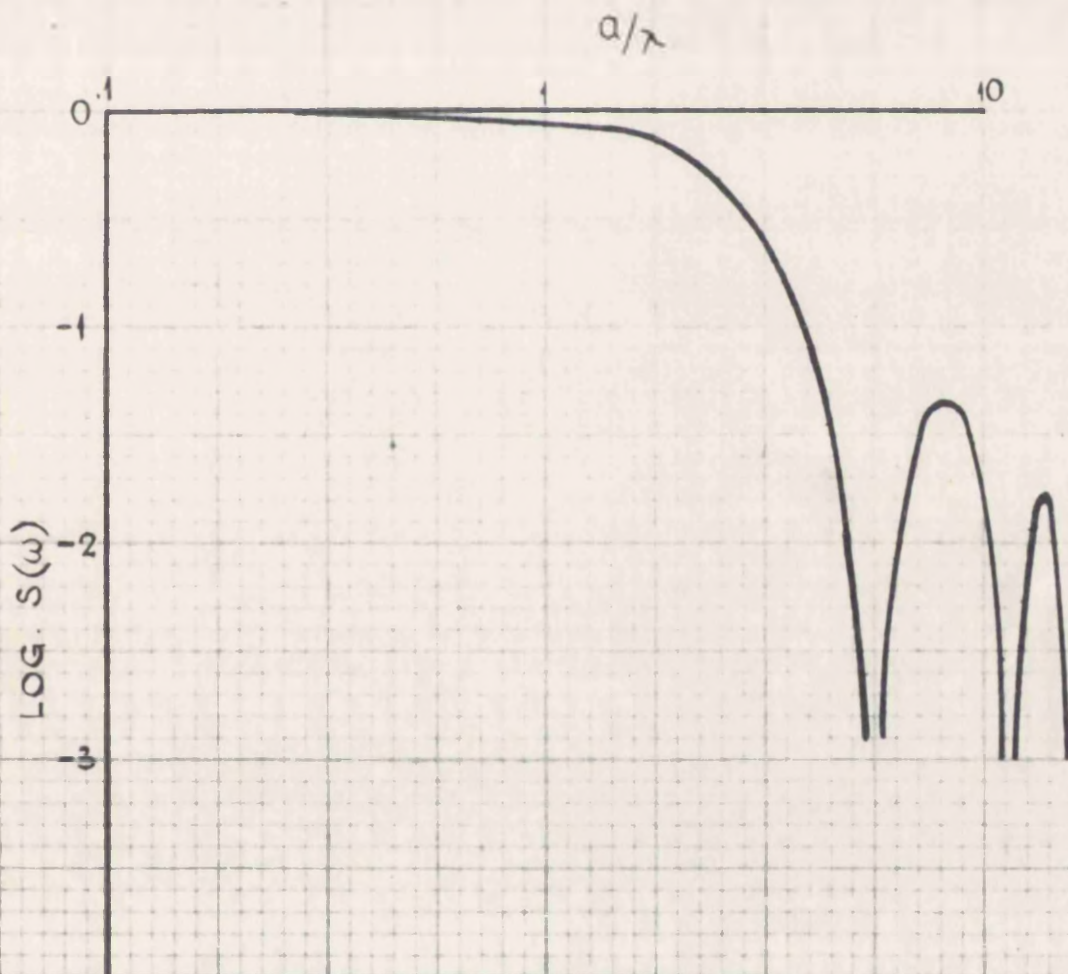


FIG. 36.

SPECTRAL CHARACTERISTICS OF A SIMPLE SLIT  
OF WIDTH "a" AT AN ANGLE OF 10° TO NORMAL.

to select a desired portion of the radiated band. In order to do so, it is necessary first of all to remove almost the whole of the zero order but since the first zero occurs at  $\omega\eta = 6.28$  and the first maximum at  $\omega\eta = 8.98$ , the ratio of cut-off  $\lambda_c$  to desired  $\lambda_m$  must be  $\lambda_c/\lambda_m = 8.98/6.28 = 1.43$ . Since the cut-off wavelength of an  $H_{10}$  wave in a rectangular waveguide of width  $x$  is  $\lambda_c = 2x$ , the required high pass filter will be given by a guide whose width is  $.72 \lambda_m$ . For any given ratio of slit width "a" to wavelength of desired radiation  $\lambda_m$  the angle of diffraction  $\theta$  will have to be chosen so that

$$\sin \theta = \frac{8.98 \lambda_m}{2\pi a} = 1.43 \frac{\lambda_m}{a}$$

The disadvantage of this method is the need for varying the waveguide width when a different band is desired, also the band is still quite wide.

#### 4.2. Dispersion by a finite slit grating

Little work has been published on the exact solution of a slit grating with finite number of slits comparable in width to the wavelength. This is not surprising when one considers the difficulties of solving the simple, one slit, problem.

In view of the preceding discussion, however, and results obtained by the author with 3 cm waves (Appendix III) one would appear to be justified in accepting once again Kirchhoff's simple solution when the grating constant is not

less than one wavelength. In fact, the following discussion will concern itself only with symmetrical gratings having slits of width  $a$  and grating constant (distance between centres of two consecutive slits) of  $2a$ .

Consider normal incident radiation and a wave diffracted at angle  $\theta$  to normal as in Fig. 37.

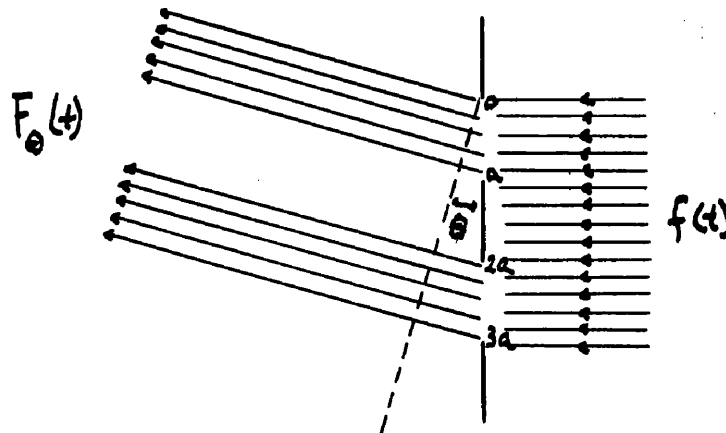


Fig. 37.

Let incident wave be  $f(t)$  then diffracted wave

$$F_{\theta}(t) = \int_0^a f\left(t - \frac{x \sin \theta}{c}\right) dx + \int_{2a}^{3a} f\left(t - \frac{x \sin \theta}{c}\right) dx + \dots$$

If spectrum of  $f(t)$  is  $g(\omega)$

and spectrum of  $F(t)$  is  $G(\omega)$

$$\text{then } G(\omega) = \frac{c}{j\omega \sin \theta} g(\omega) \left[ 1 - e^{-\frac{j\omega a \sin \theta}{c}} + e^{-\frac{2j\omega a \sin \theta}{c}} - e^{-\frac{3j\omega a \sin \theta}{c}} + \dots \right]$$

$$= \frac{a g(\omega)}{j\omega \eta} \left[ 1 - e^{-j\omega \eta} + e^{-2j\omega \eta} - e^{-3j\omega \eta} + \dots + e^{-(2k-1)j\omega \eta} \right]$$

where  $k$  = number of slits

$$\text{hence } G(\omega) = \frac{a \cdot g(\omega)}{j\omega\eta} \cdot \frac{1 - e^{-j\omega\eta 2k}}{1 + e^{-j\omega\eta}}$$

$$\text{and } |G(\omega)|^2 = \frac{a^2 |g(\omega)|^2}{\omega^2 \eta^2} \cdot \frac{1 - \cos 2k\omega\eta}{1 + \cos \omega\eta}$$

which gives the spectrum of diffracted power.

$$\text{At } \theta = 0, |G(\omega)|_0^2 = \frac{a^2 |g(\omega)|^2}{\omega^2 \eta^2} \cdot \frac{\sin^2 k\omega\eta}{\cos^2 \omega\eta/2} = a^2 k^2 |g(\omega)|^2$$

hence the rationalised spectral characteristic of the grating becomes

$$\frac{S(\omega)_\theta}{S(\omega)_0} = \frac{1 - \cos 2k\omega\eta}{k^2 \omega^2 \eta^2 (1 + \cos \omega\eta)} = \frac{\sin^2 k\omega\eta}{k^2 \omega^2 \eta^2 \cos^2 \omega\eta/2} = \frac{\sin^2 \omega\eta/2}{(\omega\eta/2)^2} \cdot \frac{\sin^2 k\omega\eta}{k^2 \sin^2 \omega\eta}$$

Fig. 38. gives the plot of the above to the base of  $a/\lambda$  when  $k = 3$ , and  $\theta = 10^\circ$  on a log scale. It will be seen that the effect of the grating is to produce a finer division of the spectrum of a single slit (given by the first term of the expression for  $S(\omega)$ ) into several principal peaks with smaller ones between. The principal maxima correspond to the relation  $\sin \omega = 0$ , i.e.  $\omega\eta = n\pi$  where  $n = 1, 2, 3$ , etc., with the magnitude of the principal maxima given by  $(\frac{2}{\omega\eta})^2$ , hence the consecutive maxima are  $(S(\omega)_\theta = 0 = 1) : .4, .044, .016$ , etc.

Thus the first principal maximum is almost ten times larger than the first maximum produced by a slit. Fig. 38 can again be made to give the spectral characteristic for any other diffraction angle  $\theta$  by multiplying the scale by the factor  $\sin 10^\circ / \sin \theta$ . Since the position and magnitude

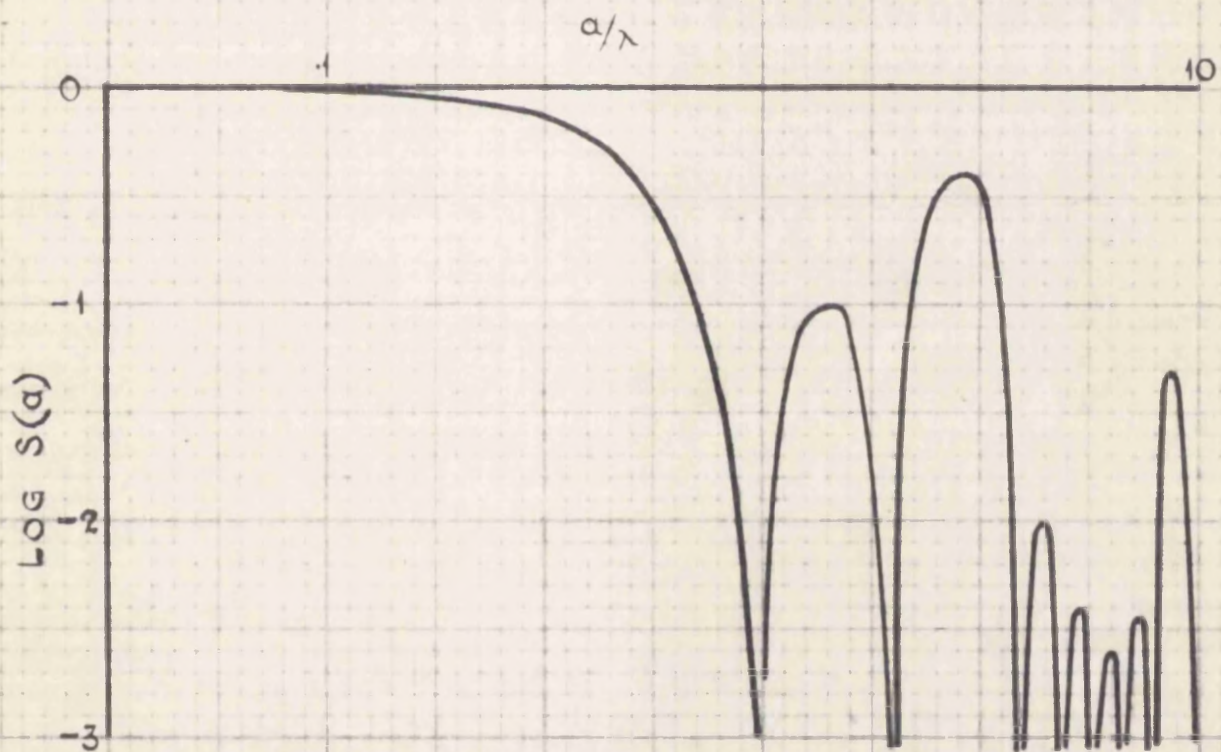


FIG. 38

THE SPECTRAL CHARACTERISTICS OF A GRATING  
CONSISTING OF 3 SLITS, AT AN ANGLE OF 10°

of the principal maxima does not depend on the number of slits ( $\omega\eta = n\pi$  and  $\frac{4}{\omega\eta}z$  respectively), the increase in the number of slits will result in the increase of the number of minor peaks and - more important - in the narrowing of the bandwidth of the principal peaks.

This method of dispersion is thus seen to be possible for the dispersion of the spectrum in conjunction with a high pass filter such as a waveguide to remove the zero order peak.

The bandwidth of the principal peaks when  $k = 3$  is seen to be comparatively large, giving  $Q$  of the spectrum of the first principal peak of about 5 which is too small for the purpose of spectrum analysis of a spark generator since it compares in magnitude with the  $Q$  of the source.  $Q$  can be increased by increasing number of slits almost in direct proportion to  $k$ , but that increase is rather limited when one considers that the total width of a grating with  $k$  slits is  $(2k + 1)a$  and if  $a = \lambda_0$ , then for  $\lambda_0 = 1$  cm the width of a 10 slit grating is 21 cm which in turn requires a very large horn to work in the Fraunhofer region. Culshaw established an empirical minimum requirement to work in the parallel beam region, namely  $\lambda_0 z > b^2$  where  $z$  is the distance from horn mouth to grating and  $b$  is horn aperture. Thus for a 20 cm horn aperture and  $\lambda_0 = 1$  cm,  $z$  must be at least 4 metres which results in considerable loss in power

output. This distance will be somewhat less for lower values of  $\lambda_0$ .

Thus, in practice, one would be limited to less than 10 slits which will result in too low a Q for measurement of the spectrum of the spark generator.

This method can be used, however, for the purpose of separating out higher frequency components from the spectrum of the source for the purpose of using it as such. Since the secondary peaks are more than 6 db below the principal ones one may be justified in following the approach described in connection with the single slit, to set the cut-off frequency of the waveguide to correspond to the first zero, which corresponds to:

$$\sin k\omega\eta = 0 \text{ or } k\omega\eta = \pi$$

hence 
$$\frac{2\pi k a \sin\theta}{\lambda_c} = \frac{2\pi k a}{\lambda_m} \cdot \frac{\lambda_m}{\lambda_c} \cdot \sin\theta = \pi$$

but  $\frac{a}{\lambda_m}$  is given by  $\frac{2\pi a}{\lambda_m} \sin\theta = \pi$  i.e.  $\frac{a}{\lambda_m} = \frac{1}{2\sin\theta}$

hence  $\frac{\lambda_m}{\lambda_c} \geq \frac{1}{k}$  or  $\lambda_c = k\lambda_m$

giving the width of the waveguide as  $< \frac{k\lambda_m}{2}$ .

Thus there is a clear advantage in using a grating with several slits in that the waveguide can be larger than that for a single slit and a change in the desired frequency band can be achieved by varying the angle of diffraction within certain limits, e.g. to extract a band around  $\lambda_m = 1 \text{ cm}$

when  $a = 2\lambda_m$  and the grating has 5 slits (i.e. guide width 2.5 cm) the standard X band guide 0.9" x 0.4" can be used and the diffraction angle  $\theta$  will have to be set to  $14^\circ 30'$  ( $\sin \theta = \frac{1}{4}$ ). Increasing this angle will cause the output to shift to longer waves right down to the guide cut-off. If the angle were reduced from  $14^\circ$  then, of course, the diffracted spectrum will contain those portions of the zero order spectrum which exceed the cut-off frequency of the waveguide so that the output will contain two wavebands of which the lower one will soon contain more energy than the higher one.

When grating is used with a spark generator and a crystal receiver one has to remember that when working above the natural frequency of the dipole as the frequency is increased the energy falls off rapidly at first and slower then, so that close to  $f_0$  the secondary maxima of the grating spectrum may produce larger output than the principal maximum which is further removed from  $f_0$ . Thus the method of bandwidth selection by varying can be used only well away from the natural frequency of the radiator. Otherwise the cut-off frequency of the waveguide has to be set close to  $\lambda_m$  and both it and  $\theta$  have to be varied to change the value of  $\lambda_m$ . On the whole this method is not very efficient in that the maximum of the desired band is still well below the maximum possible.



The reflected wave at an angle  $\theta$  is given by

$$F(t) = \int_0^a f\left(t - \frac{x \sin \theta}{c}\right) dx + \int_a^{2a} f\left(t - \frac{x \sin \theta}{c} + \frac{s(1+\cos \theta)}{c}\right) dx + \dots$$

hence,

$$\text{if } g(\omega) = \frac{1}{2\pi} \int_{-\infty}^{\infty} f(t) e^{-j\omega t} dt$$

$$\text{then } G(\omega) = \frac{1}{2\pi} \int_{-\infty}^{\infty} F(t) e^{-j\omega t} dt = \frac{1}{2\pi} \int_{-\infty}^{\infty} \int_0^a f\left(t - \frac{x \sin \theta}{c}\right) dx e^{-j\omega t} dt$$

$$+ \frac{1}{2\pi} \int_{-\infty}^{\infty} \int_a^{2a} f\left(t - \frac{x \sin \theta}{c} + \frac{s(1+\cos \theta)}{c}\right) dx e^{-j\omega t} dt$$

$$+ \dots + \frac{1}{2\pi} \int_{-\infty}^{\infty} \int_{(k-1)a}^{ka} f\left(t - \frac{x \sin \theta}{c} + \frac{s(1+\cos \theta)}{c}\right) dx e^{-j\omega t} dt$$

$$= g(\omega) \frac{a}{j\omega \eta} \left[ (1 - e^{-j\omega \eta}) + e^{j\omega \tau} (e^{-j\omega \eta} + e^{-2j\omega \eta}) + \dots \right]$$

$$= g(\omega) \frac{a}{j\omega \eta} (1 - e^{-j\omega \eta}) \left[ 1 + e^{j\omega(\tau - \eta)} + \dots + e^{j\omega(k-1)(\tau - \eta)} \right]$$

$$= g(\omega) \frac{a}{j\omega \eta} (1 - e^{-j\omega \eta}) \frac{1 - e^{j\omega k(\tau - \eta)}}{1 - e^{j\omega(\tau - \eta)}}$$

$$\text{where } \eta = \frac{a \sin \theta}{c}$$

$$\tau = \frac{s(1+\cos \theta)}{c}$$

hence

$$|G(\omega)|^2 = |g(\omega)|^2 \frac{2a^2}{\omega^2 \eta^2} (1 - \cos \omega \eta) \frac{1 - \cos \omega k(\tau - \eta)}{1 - \cos \omega(\tau - \eta)}$$

$$= |g(\omega)|^2 \frac{4a^2}{\omega^2 \eta^2} \sin^2 \frac{\omega \eta}{2} \frac{\sin^2 \frac{\omega k}{2} (\tau - \eta)}{\sin^2 \frac{\omega}{2} (\tau - \eta)}$$

thus maximum value of  $|G(\omega)|^2$  will be  $k^2 |g(\omega)|^2$  and hence

the normalised echelon spectral characteristic is given by

$$S = \frac{\sin^2 \frac{\omega y}{2}}{(\frac{\omega y}{2})^2} \cdot \frac{\sin^2 \frac{\omega k}{2} (\tau - \eta)}{k^2 \sin^2 \frac{\omega}{2} (\tau - \eta)}$$

The dispersion may be obtained by keeping  $s$  constant and varying  $\theta$  or by holding  $\theta$  constant and changing  $s$ .

The second term in the above expression

$$\frac{\sin^2 \frac{\omega k}{2} (\tau - \eta)}{k^2 \sin^2 \frac{\omega}{2} (\tau - \eta)}$$

is at a maximum when  $\sin \frac{\omega}{2} (\tau - \eta) = 0$ . Under those conditions the magnitude of this term is  $k^2$ , hence the total expression becomes  $= \frac{\sin^2 \omega y / 2}{(\omega y / 2)^2}$ . Thus it is seen that the maxima lie on the envelope of the spectral characteristic of a single element in analogy with a slit and a grating.

The first principal maximum can be obtained from

$$\frac{\omega}{2} (\tau - \eta) = \pi \quad \text{i.e.} \quad \frac{\pi a}{\lambda} \left[ \frac{s}{a} (1 + \cos \theta) - \sin \theta \right] = \pi$$

$$\therefore \frac{a}{\lambda_m} = \frac{1}{\frac{s}{a} (1 + \cos \theta) - \sin \theta}$$

thus the position of the maximum depends on both  $s$  and  $\theta$ .

The magnitude of the first principal maximum can now be found:

$$S(\theta)_m = \frac{\sin^2 \frac{\omega y}{2}}{(\frac{\omega y}{2})^2} = \frac{\sin^2 \left( \frac{\pi a}{\lambda} \sin \theta \right)}{\left( \frac{\pi a}{\lambda} \sin \theta \right)^2}$$

substituting from  $a/\lambda_m$  into the above one gets

$$S(\theta)_m = \frac{\sin^2 \frac{\pi \sin \theta}{\frac{s}{a} (1 + \cos \theta) - \sin \theta}}{\left[ \frac{\pi \sin \theta}{\frac{s}{a} (1 + \cos \theta) - \sin \theta} \right]^2}$$

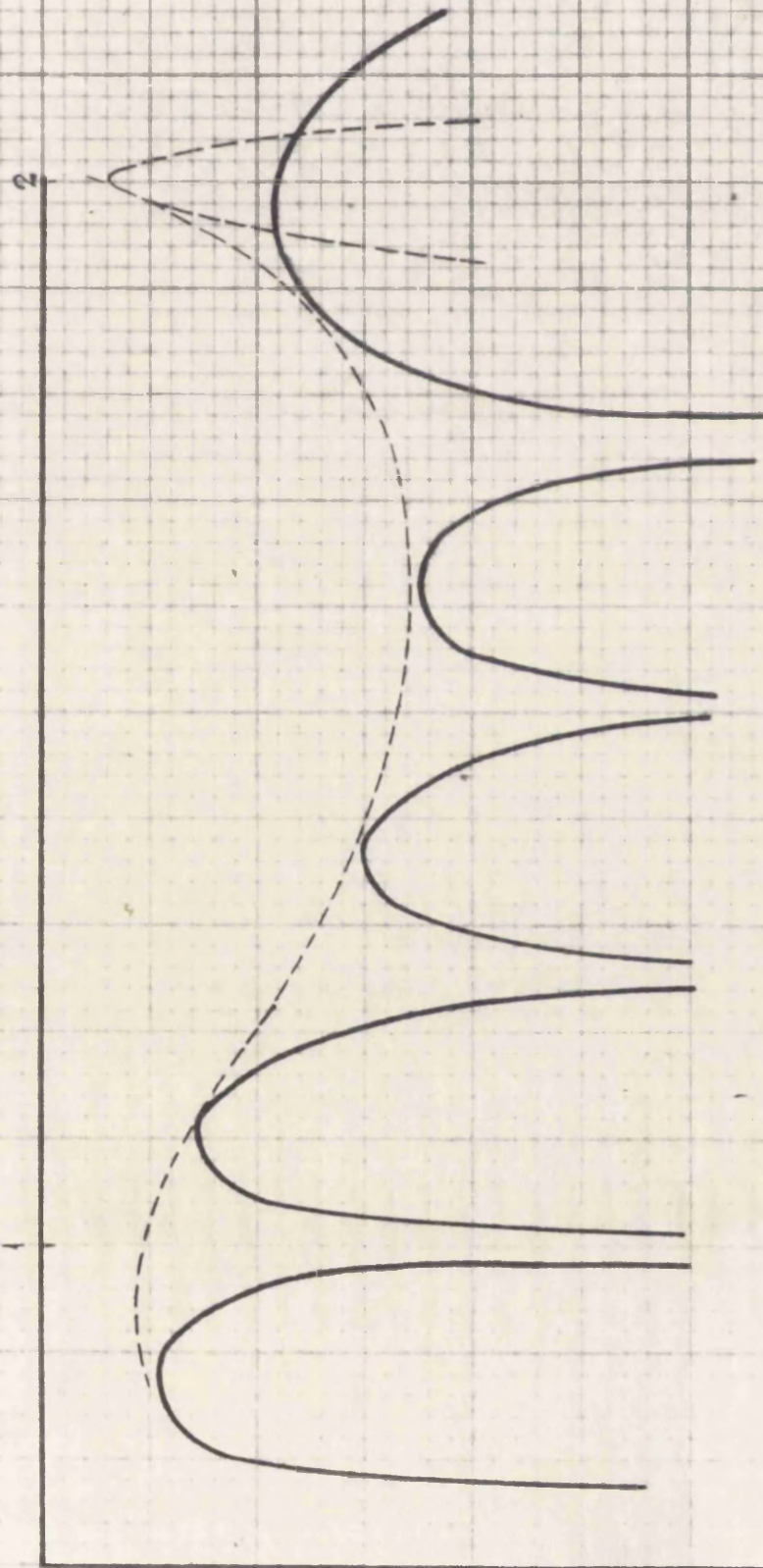
which shows that the magnitude of the maxima need not be constant as  $\theta$  is varied. The  $Q$  of the peak is the same as that of a grating having as many slits as the echelette has reflectors, but, since for a given width of a beam there are almost twice as many reflectors as slits, the echelette of equal size to a grating has almost twice larger  $Q$ .

Any desired band can be extracted by proper choice of  $s/a$  and of  $\theta$ ,  $\lambda_m$  becoming shorter as  $\theta$  increases from 0, when  $\lambda_m = 2s$ , to a value making  $s/a(1 + \cos \theta) - \sin \theta = 0$  i.e.  $\tan \theta/2 = s/a$ , when  $\lambda_m = 0$  beyond which  $\lambda_m$  begins to increase again.

The relation  $\lambda_m = 2s$  when  $\theta = 0$  leads to the best method of using the echelette, which is to keep  $\theta$  constant and small. Under those circumstances, it will be seen that the magnitude of the peaks is constant and equal to 1 and any desired frequency can be selected easily by adjusting  $s$  to  $1/2$  the desired wavelength. Fig. 40. shows part of the resultant detected power spectrum when the natural wavelength of the spark generator  $\lambda_0$  is equal to reflector width "a" and  $s = a/4$ . This shows that with 8 plates (but much more so with 20 plates) if a high pass filter with cut-off around  $1.5 \lambda_0$  were interposed a band around  $2 \lambda_0$  will be extracted from the radiation of an exponentially decaying wave whose log. dec. is 1.

It is interesting to derive the total diffracted output

$$f/f_0 = \lambda_0/\lambda$$



LOG OF OUTPUT POWER

FIG. 40.

SPECTRUM OF OUTPUT FROM AN 8-PLATE ECHELLETTE WHEN PLATE WIDTH = NATURAL WAVELENGTH OF RADIATION  $\lambda_0$  OF AN EXPONENTIALLY DECAYING WAVE WITH LOG. DEC. = 1, AND ECHELLETTE STEP =  $\lambda_0/4$ .  
DASHED LINE INDICATES THE LOCUS OF PEAKS AND ALSO ONE PEAK OF THE SPECTRUM OBTAINED WITH 20 PLATES.

of a spark generated wave  $e^{-\alpha t} \sin \omega_0 t$  as the step of the echelette is increased. This can be done by integrating the power spectrum over infinite time

$$\begin{aligned} \text{i.e. } P &= \int_0^{\infty} |G(\omega)|^2 d\omega = \int_0^{\infty} |g(\omega)|^2 \left\{ k + 2n \sum_{n=1}^{k-1} \cos(k-n)\tau\omega \right\} d\omega \\ &= \int_0^{\infty} |g(\omega)|^2 k d\omega + \sum_{n=1}^{k-1} \int_0^{\infty} |g(\omega)|^2 2n \cos(k-n)\tau\omega d\omega \\ &= \frac{\omega_0^2}{8\pi^2} \int_{-\infty}^{\infty} \frac{k d\omega}{(\omega - \omega_0 - j\alpha)(\omega - \omega_0 + j\alpha)(\omega + \omega_0 - j\alpha)(\omega + \omega_0 + j\alpha)} + \sum_{n=1}^{k-1} \frac{\omega_0^2}{8\pi^2} \int_{-\infty}^{\infty} \frac{2n e^{-j\omega\tau(k-n)} d\omega}{(\omega - \omega_0 - j\alpha)(-\omega)(-\omega)(+\omega)} \end{aligned}$$

The first term =

$$= \frac{\omega_0^2}{8\pi^2} \frac{2\pi j}{8j\omega_0(\omega_0^2 + \alpha^2)} = \frac{k}{16\pi \delta f_0 (1 + \delta^2/4\tau^2)}$$

$$\begin{aligned} \text{The } n^{\text{th}} \text{ term} &= \frac{\omega_0^2}{8\pi^2} 2n \int \frac{e^{-j\omega\tau(k-n)} d\omega}{(-)(+)(-)(+)} \\ &= \frac{2\pi j \omega_0^2 2n}{8\pi^2 8j\omega_0\alpha} \left[ \frac{e^{j(k-n)\tau(\omega_0 + j\alpha)}}{\omega_0 + j\alpha} + \frac{e^{-j(k-n)\tau(\omega_0 - j\alpha)}}{\omega_0 - j\alpha} \right] \\ &= \frac{\omega_0 n}{16\pi\alpha} e^{-(k-n)\alpha\tau} \frac{2\omega_0 \cos(k-n)\omega_0\tau + 2\alpha \sin(k-n)\omega_0\tau}{\omega_0^2 + \alpha^2} \\ &= \frac{\omega_0 n e^{-(k-n)\alpha\tau}}{8\pi\alpha \sqrt{\omega_0^2 + \alpha^2}} \cos \left[ (k-n)\omega_0\tau - \phi \right] \end{aligned}$$

where  $\tan \phi = \frac{\alpha}{\omega_0}$

$$\begin{aligned} \text{hence } P &= \frac{k}{16\pi\alpha(1 + \alpha^2/\omega_0^2)} + \sum_{n=1}^{k-1} \frac{n e^{-(k-n)\alpha\tau}}{8\pi\alpha \sqrt{1 + \alpha^2/\omega_0^2}} \cos \left[ (k-n)\omega_0\tau - \phi \right] \\ &= \frac{1}{16\pi \delta f_0 \sqrt{1 + \delta^2/4\tau^2}} \left\{ \frac{k}{\sqrt{1 + \delta^2/4\tau^2}} + \sum_{n=1}^{k-1} 2n e^{-(k-n) \frac{2\delta}{\lambda_0}} \cos \left[ (k-n) \frac{4\tau\delta}{\lambda_0} - \phi \right] \right\} \end{aligned}$$

The function  $P$  has been plotted for various values of  $\delta$  and of  $k$  in Figures 41. & 42.

If one accepted the original assumption that the radiated wave from a spark generator is given by  $e^{-\alpha t} \sin \omega_0 t$  then the interferogram of power diffracted by an echelette could be used to determine  $\alpha$  and  $\omega_0$  provided the receiver response  $R(\omega)$  could be taken as uniform over the central portion of the spectrum. That may not be easy to achieve. Nevertheless, the echelette with a large number of elements can be used to measure the natural frequency of radiations on account of the sharpness of the interference pattern.

#### 4.3.2. Radiation normal to the plane of the echelette

Consider the case shown in Fig. 43.

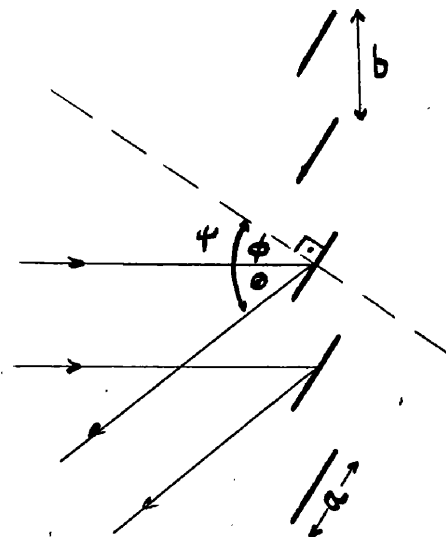


Fig. 43.

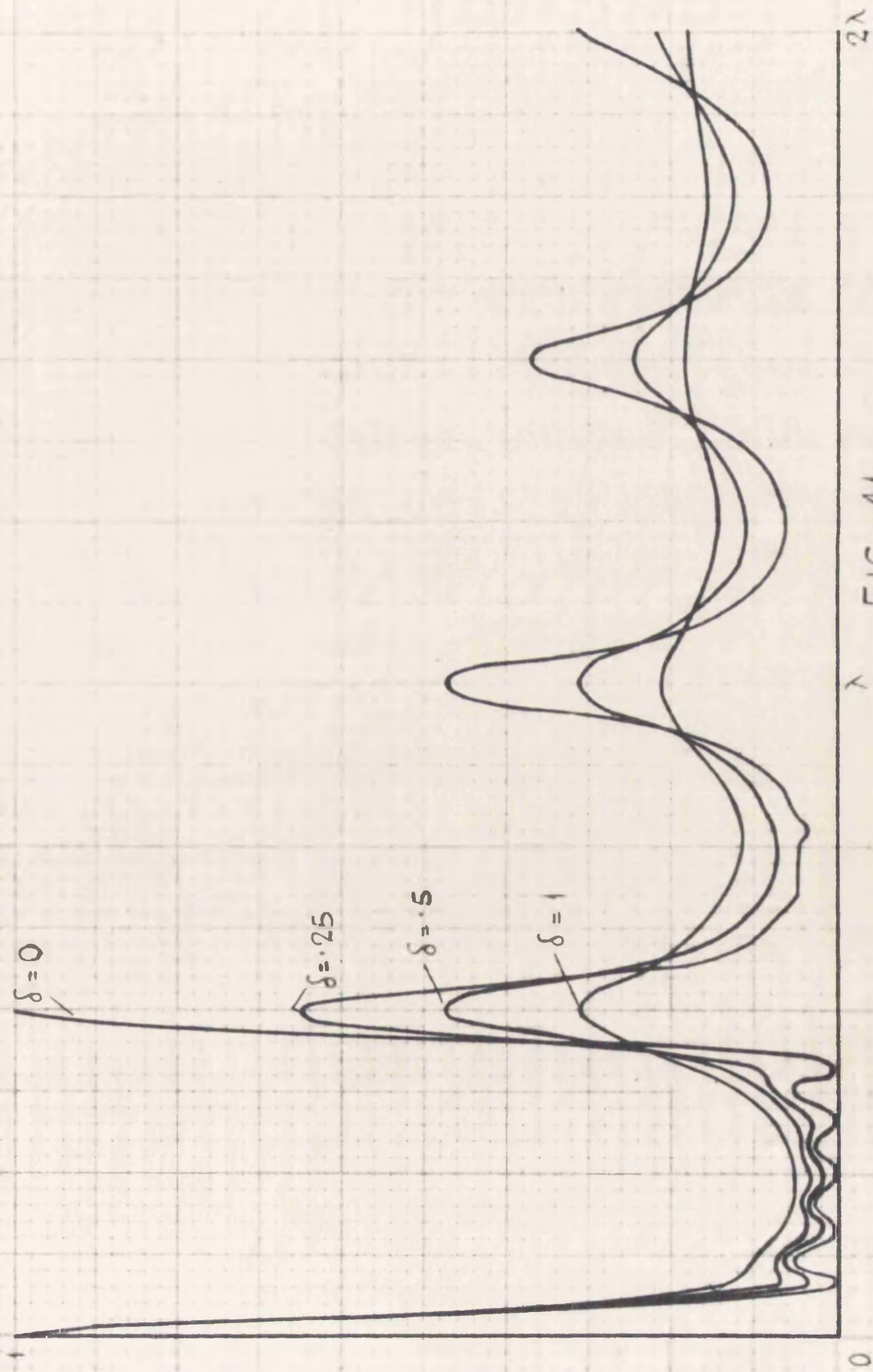
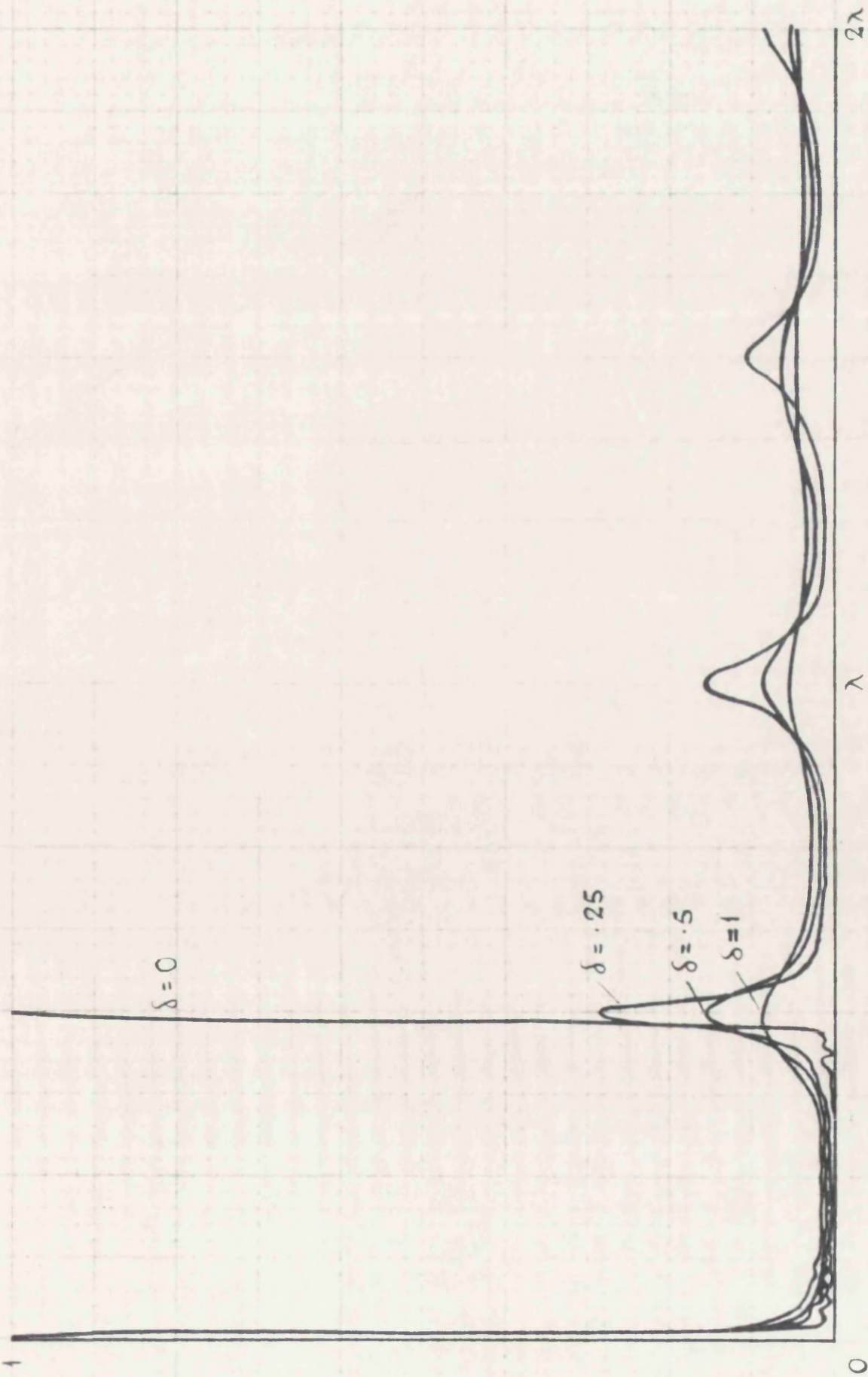


FIG. 41.

OUTPUT POWER FROM AN ECHELLETTE HAVING 6 PLATES, AS THE STEP IS INCREASED PROGRESSIVELY FROM 0 TO  $2\lambda_0$ ,  $\lambda_0$  BEING THE NATURAL WAVELENGTH OF EXPONENTIALLY DECAYING WAVE.



**FIG. 42.**

OUTPUT POWER FROM AN ECHELLETTE HAVING 24 PLATES, AS THE STEP IS INCREASED PROGRESSIVELY FROM 0 TO  $2\lambda_0$ ,  $\lambda_0$  BEING THE NATURAL WAVELENGTH OF EXPONENTIALLY DECAYING WAVE.

If the incident radiation is  $f(t)$  then it will be seen that the radiation reflected at angle  $\theta$  is

$$F(t) = \int_0^a f(t) e^{-j\frac{\omega x}{c}(\sin\phi + \sin\psi)} dx + \\ + \int_0^a f(t) e^{-j\frac{\omega x}{c}(\sin\phi + \sin\psi + \frac{b}{x}\sin\theta)} dx + \\ + \int_0^a f(t) e^{-j\frac{\omega x}{c}(\sin\phi + \sin\psi + \frac{2b}{x}\sin\theta)} dx + \dots$$

$k$  terms in all for  $k$  reflectors

$$\text{hence, if } g(\omega) = \frac{1}{2\pi} \int_{-\infty}^{\infty} f(t) e^{-j\omega t} dt$$

$$\text{then } G(\omega) = \frac{1}{2\pi} \int_{-\infty}^{\infty} F(t) e^{-j\omega t} dt$$

$$= g(\omega) \frac{c(1 - e^{-j\frac{\omega a}{c}(\sin\phi + \sin\psi)})}{j\omega(\sin\phi + \sin\psi)} \left( 1 + e^{-j\frac{\omega b}{c}\sin\theta} + e^{-2j\frac{\omega b}{c}\sin\theta} + \dots \right)$$

$$= g(\omega) \frac{c(1 - e^{-j\frac{\omega a}{c}(\sin\phi + \sin\psi)})}{j\omega(\sin\phi + \sin\psi)} \cdot \frac{1 - e^{-j\frac{\omega b k}{c}\sin\theta}}{1 - e^{-j\frac{\omega b}{c}\sin\theta}}$$

hence

$$|G(\omega)|^2 = |g(\omega)|^2 \cdot \frac{2c^2}{\omega^2} \cdot \frac{\sin^2 \left[ \frac{\omega a}{2c}(\sin\phi + \sin\psi) \right]}{(\sin\phi + \sin\psi)^2} \cdot \frac{\sin^2 \left( \frac{\omega b k}{2c} \sin\theta \right)}{\sin^2 \left( \frac{\omega b}{2c} \sin\theta \right)}$$

which, when normalised becomes

$$|G(\omega)|^2 = P(\omega)_\theta = |g(\omega)|^2 \frac{4c^2}{k^2 \omega^2 a^2} \cdot \frac{\sin^2 \left[ \frac{\omega a}{2c}(\sin\phi + \sin\psi) \right]}{(\sin\phi + \sin\psi)^2} \cdot \frac{\sin^2 \left( \frac{\omega b k}{2c} \sin\theta \right)}{\sin^2 \left( \frac{\omega b}{2c} \sin\theta \right)}$$

It will be seen by inspection that the last term of this expression has a maximum value of  $k^2$  when  $\frac{\omega b}{2c} \sin\theta = \pm n\pi$ . For  $n = 1$  (first principal maximum) this leads to

$$\frac{\pi b}{\lambda} \sin\theta = \pm \pi \quad \text{or} \quad \sin\theta = \pm \frac{\lambda}{b}$$

For positive values of  $\theta$  the maximum value of  $P(\omega)_\theta$  will

now be a function of both  $\theta$  and  $\phi$ . The more interesting, however, is the case when  $\theta$  is negative. In particular, when  $\theta = -2\phi$  or  $\psi = \theta + \phi = -\phi$  the term

$$\frac{\sin^2 \left[ \frac{wa}{2c} (\sin \phi + \sin \psi) \right]}{\left[ \frac{wa}{2c} (\sin \phi + \sin \psi) \right]^2} = 1$$

What is more, this term remains equal to 1 as long as both  $\phi$  and  $\theta$  are very small. This leads to the best method of using the echelette in this mode, namely, the distance between centres of reflectors =  $b$  must be  $\gg$  than the centre wavelength of a band which it is desired to isolate ( $\lambda_m$ ), then the corresponding  $\theta_m = -\frac{\lambda_m}{b}$  and  $\phi$  must now be set to  $\phi = -\frac{\theta_m}{2} = \frac{\lambda_m}{2b}$ . The  $Q$  of this band will depend on the number of reflectors  $k$  and by the same arguments as were used in connection with slit gratings it will be somewhat greater than  $k$ , i.e. the bandwidth will be less than  $\frac{c}{k\lambda_m}$ .

This method appears to lend itself to the examination of a spectrum of a spark generator. The apparent natural wavelength of the generator ( $\lambda_0$ ) has to be found first (say, by a Boltzmann interferometer). Then "b" has to be chosen to be  $\gg$  and  $\phi \doteq \frac{\lambda_0}{2b}$ . The receiver has now to be swung from  $\theta = 0$  to  $\theta = -\frac{2\lambda_0}{b}$  (or further, as long as  $\theta$  remains very small). If the echelette contains a large number of reflectors, say 20 or more, then the bandwidth of received radiation will be small; hence, total power received at any angle  $\theta$

$$P_{\theta} = \int_{\Delta\omega} P(\omega)_{\theta} d\omega \quad \text{where } \Delta\omega = \text{bandwidth} \doteq d\omega$$

$$= P(\omega)_{\theta} d\omega = |g(\omega)|^2 d\omega$$

and if  $\frac{\omega}{\Delta\omega} = Q = k$  i.e.  $d\omega = \frac{\omega}{k}$

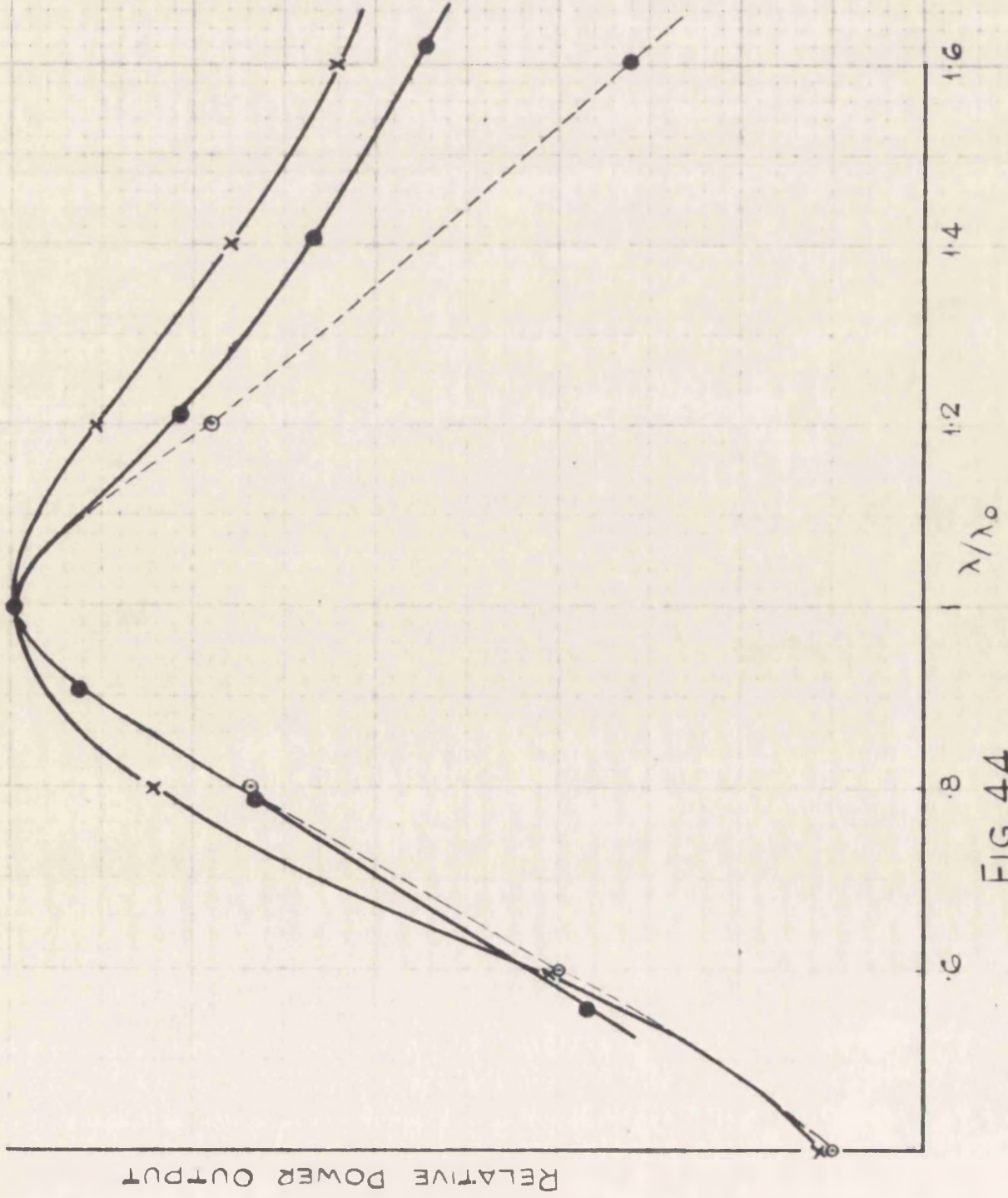
then  $P_{\theta} = \frac{|g(\omega)|^2 \omega}{k} = \frac{\omega}{k N_0^2 \left[ \left(1 - \frac{\omega}{\omega_0}\right)^2 + \frac{\delta^2}{4\pi^2} \right] \left[ \left(1 + \frac{\omega}{\omega_0}\right)^2 + \frac{\delta^2}{4\pi^2} \right]}$

When  $\omega = \omega_0$ ,  $P_{\theta_0} = \frac{1}{k N_0^2 \frac{\delta^2}{4\pi^2} \left(4 + \frac{\delta^2}{4\pi^2}\right)}$

hence the relative output power at any angle  $\theta$  compared to its maximum value corresponding to  $\omega_0$  will be

$$P_{\theta_n} = \frac{\frac{\omega}{\omega_0} \cdot \frac{\delta^2}{4\pi^2} \left(4 + \frac{\delta^2}{4\pi^2}\right)}{\left[\left(1 - \frac{\omega}{\omega_0}\right)^2 + \frac{\delta^2}{4\pi^2}\right] \left[\left(1 + \frac{\omega}{\omega_0}\right)^2 + \frac{\delta^2}{4\pi^2}\right]}$$

Daunt et al. used just such an echelette having 54 steps each  $\frac{3}{4}$ " wide spread over 40", with  $\phi = 8^{\circ}24'$ . Fig. 44. gives the results given by them as well as those calculated by the above given expression assuming  $\delta = 3.62$ , corresponding to a spherical dipole used in the experiment. Farrands, who reached the same results notes that the calculated values are appreciably larger than those obtained by Daunt but he seems to have overlooked that when the exact power spectrum is computed (shown dashed in the Fig. 44.) taking into account the fall in the principal maximum as  $\theta$  differs more and more from  $2\phi$ , the results are found to agree very much better, the small divergence being



X CALCULATED APPROX.  
 ● EMPIRICAL  
 ○ CALCULATED RIGOROUSLY

FIG. 44.

POWER SPECTRUM FROM A SPHERICAL DIPOLE AS OBTAINED EXPERIMENTALLY BY DAUNT *et al*  
 ALSO AS CALCULATED BY FARRANDS (CROSSES) AND WHEN ALLOWANCE IS MADE FOR ANGLE OF DIFFRACTION (DASHES)

possibly due to the fact that the secondary maxima becomes appreciable as one moves away from the natural wavelength, so that the resultant bandwidth of received power increases, hence total power increases.

In view of the fact that  $\theta$  is taken negative, care must be taken that the successive reflectors are not shadowed by one another, hence the reflector width "a" should be made smaller than the separation "b". This in itself will permit a wider diffraction angle  $\theta$  since the quantity  $\frac{\omega a}{c}$  will be reduced. On the other hand, there will be a fall in total reflected power due to the reduction of reflecting area.

An interesting result follows from setting  $\theta = 0$  when

$$P(\omega)_\theta = |g(\omega)|^2 \frac{\sin^2\left(\frac{\omega a}{c} \sin \phi\right)}{\left(\frac{\omega a}{c} \sin \phi\right)^2}$$

which is the same as that for a single slit of width "2a" irrespective of a number of reflectors. This result should allow one to take advantage of any useful characteristics of the spectrum of a single slot at a much higher power level if the total reflecting area is made large by the use of many steps, and also the receiver need not be moved since  $\phi$  only need be changed. Thus the echelette must be made so that all the reflectors can be tilted at any desired angle simultaneously. Such an echelette is described in part III.

#### 4.4. General comments on the diffraction methods

The above discussion shows the more important of the many methods of analysing or separating out a frequency band by the utilisation of diffraction. None of them has the characteristics expected of a good filter, i.e. low insertion loss and independence of frequency. The slit gratings which are independent of frequency within wide limits suffer from a large insertion loss, especially when the radiation beam width is limited by practical considerations. The echelette gratings, which can give nearly zero insertion loss do so within a narrow band of frequencies only and have to be recalculated and reset when an appreciable change in frequency occurs or is desired.

Also, the bandwidth considerations conflict with attenuation of frequencies well away from the desired band since the bandwidth is roughly inversely proportional to  $k$  but so is also the distance between the principal and the secondary maxima, the nearest of which may be only 6 db below the principal peak power, so that when the frequency response of the receiver and the spectrum of the radiator both favour frequencies lower than the desired, the secondary maxima may actually exceed the principal one.

Thus the diffraction method necessitates the additional use of high pass filters. The waveguide is a useful filter of that type but it limits one to standard sizes. A

similar effect could be achieved by using a number of plates parallel to the electric vector of the radiated wave. The separation between the plates will cause a cut-off at twice the wavelength. It should be observed here that the use of a waveguide as a high pass filter may lead to serious differences between calculations and observations unless only the central portion of the beam is used. That follows from the fact that the electric vector in a guide falls off to zero at the vertical walls and the same holds true for a horn, hence the "illumination" in the radiated beam is not uniform. In fact, Culshaw has shown that whereas the angular spectrum of parallel and uniform beam diffracted by a slit is of the form  $\frac{\sin^2 \phi}{\phi^2}$  when the beam intensity falls off sinusoidally towards edges, the angular spectrum becomes of the form

$$\left[ \frac{\sin(\phi + \pi/2)}{\phi + \pi/2} + \frac{\sin(\phi - \pi/2)}{\phi - \pi/2} \right]^2$$

causing the first maximum to be reduced from .0472 to .0044, the second maximum from .0165 to .0008, etc.

This means that in practice, one is limited to gratings with comparatively few elements, hence the effective  $Q$  obtainable is fairly small.

Coates has shown that in the case of an echelette grating the effect of reduction in illumination away from the beam centre causes a formation of 3 overlapping peaks

but when the intensity of the beam at the echelette edges is not more than 3 db below centre, the resultant widening of the peaks is "hardly noticeable" especially when the angles are kept  $< 35^\circ$ .

#### 4.4.1. Wire gratings used as high pass filters

Lindman made some successful attempts at removing longer waves by the use of wire gratings. The theory of wire gratings has been discussed by Ignatovsky and more recently, by Macfarlane, who obtained the following expression for the reflection coefficient of a grating consisting of infinitely long wires of radius "a", separation of centres "b", when the electric vector is parallel to the wires:

$$R_0 e^{j\phi_0} = - \frac{1}{1 + j \frac{2b}{\lambda} \cos \theta \left[ F + \log_e \frac{b}{2\pi a} \right]}$$

where  $R_0$  is the amplitude and  $\phi_0$  the phase angle of the reflection coefficient,

$\lambda$  is the wavelength of radiation

$\theta$  is the angle of incidence and reflection

$$F = \frac{1}{2} [f(\theta) + f(-\theta)]$$

$$\text{where } f(\theta) = \sum_{n=1}^{\infty} \frac{1}{n} \left\{ \frac{n\lambda}{b} \left[ (\sin \theta + \frac{n\lambda}{b})^2 - 1 \right]^{-\frac{1}{2}} - 1 \right\}$$

The plot of function F taken from the paper by Macfarlane appears in Fig. 46.

Lewis and Casey extended the above expression to take

into account the power loss in the wires

$$R_e^{j\phi} = - \frac{1}{[1 + 2b \cos \theta \sqrt{k_0/\mu_0} R_i] + j 2b \cos \theta [(F + \log_e \frac{b}{2\pi a}) \frac{1}{\lambda} + \sqrt{k_0/\mu_0} X_i]}$$

$$\text{where } R_i + X_i = \frac{1+j}{a} \sqrt{\frac{30}{\lambda \sigma}}$$

$\sigma$  being the conductivity of wires.

The power loss usually referred to in this connection as absorption loss can be shown to be given by

$$A = \frac{2R_0^2 b}{\pi a \sigma \delta} \sqrt{k_0/\mu_0} \cos \theta$$

$$\text{where } \delta = \sqrt{\frac{\lambda}{\pi \mu_0 \sigma c}}$$

Hence, the maximum possible value of A is  $A_m = \frac{2b\sqrt{k_0} f}{a\sqrt{\pi\sigma}}$

which, for copper, becomes  $2.24 \times 10^{-10} \cdot \frac{b\sqrt{f}}{a}$

For example, for  $f = 3 \times 10^{11}$  ( $\lambda = 1$  mm) and  $b/a = 10$  the maximum absorption =  $1.24 \times 10^{-3}$  which is very small indeed and since

$$R = R_0 - A \left( R_0 + \frac{\sqrt{1-R_0^2}}{2} \right)$$

it will be seen that using copper wires the error introduced by neglecting absorption loss is negligible at wavelengths longer than 1 mm. Reflection is not as important in this connection as transmission. The coefficient of power transmission is given by  $|T|^2 = 1 - |R|^2$ . Fig. 45. gives the relation between transmission (in decibels) and the ratio of wire separation to wavelength when the ratio of wire separation to wire radius is 10. It will be seen that as a filter the wire grating is not very efficient causing not

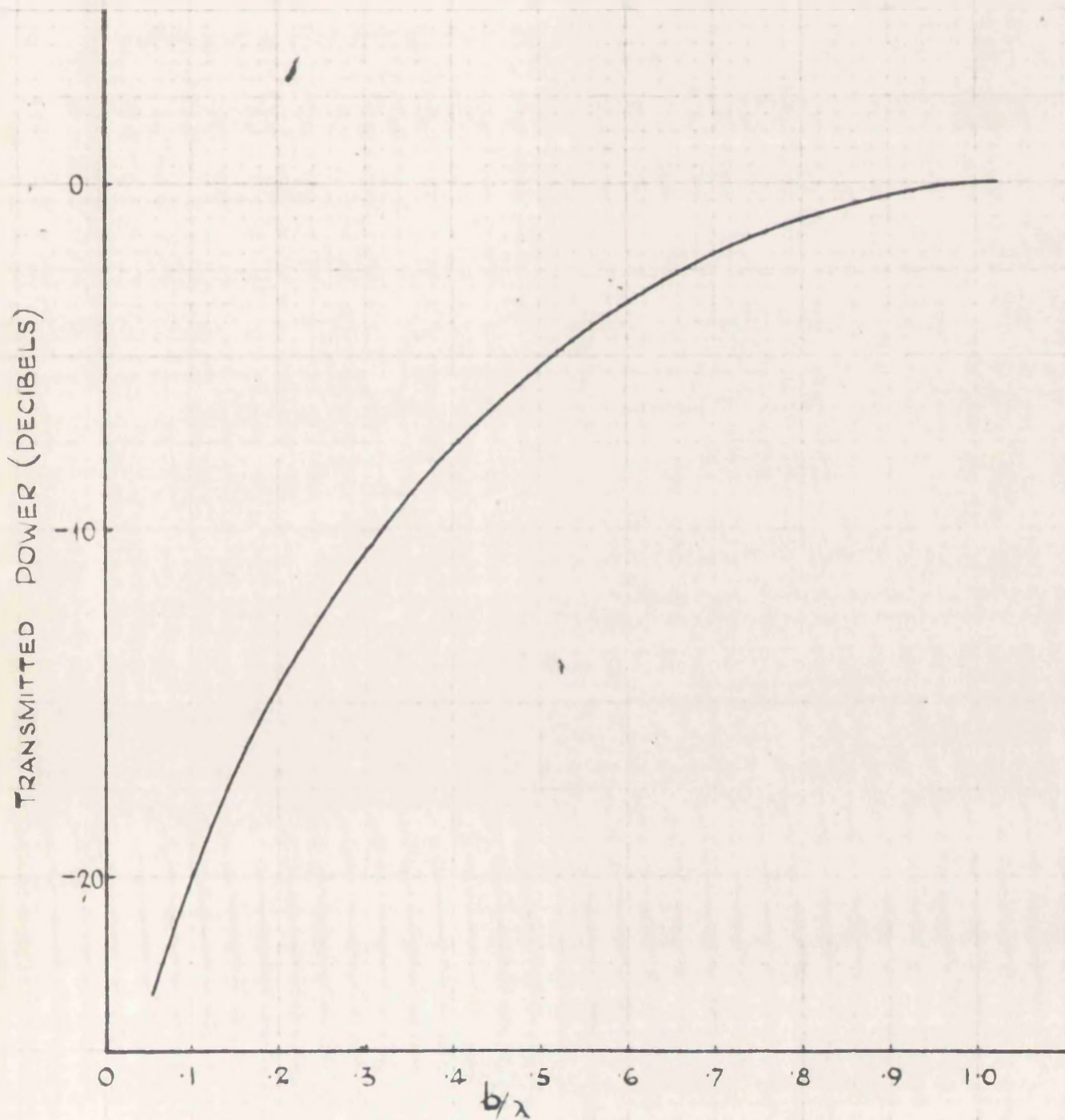


FIG. 45.

RELATION BETWEEN POWER TRANSMITTED BY A WIRE GRATING AND THE RATIO OF WIRE SEPARATION TO WAVELENGTH WHEN THE RATIO OF WIRE SEPARATION TO RADIUS OF WIRE IS 10.

more than about 6 db attenuation when the frequency is halved, nevertheless, it might be useful in reducing the amplitude of unwanted maxima when used with an echelette grating.

### 5. The Fabry Perot interferometer

(40,110)

In recent years great advances have been made in development of optical filters based on the Airy or Fabry Perot interferometer. The principle is the reflection and transmission of radiation by a dielectric or a thin metallic film.

Let the reflection coefficient of a given surface be  $R = |R| e^{j\phi}$  and its absorption be  $A$  then, if the transmission coefficient has a modulus  $|T|$ , the three are related by the expression  $|R|^2 + |T|^2 + A = 1$ .

If two such surfaces enclose a parallel slab of thickness  $d$  and dielectric constant  $k$  then the time taken by a wave to cross the slab  $\tau = \frac{d\sqrt{k}}{c}$ . Due to repeated reflections between the boundary surfaces the incident wave given by  $f(t)$  emerges on the other side in the form

$$T^2 f(t) + T^2 f(t - 2\tau) R^2 e^{j2\phi} + \dots$$

Hence, the Fourier transformer of the emergent wave in terms of the transform of the incident wave  $g(\omega)$  becomes

$$\begin{aligned} G(\omega) &= T^2 g(\omega) \left[ 1 + R^2 e^{j2(\phi - \omega\tau)} + R^4 e^{j4(\phi - \omega\tau)} + \dots \right] \\ &= g(\omega) \frac{T^2}{1 - R^2 e^{-j2(\omega\tau - \phi)}} \end{aligned}$$

$$\begin{aligned} \text{Then } |G(\omega)|^2 &= |g(\omega)|^2 \frac{\tau^4}{[1 - |R|^2 \cos(2\omega\tau - 2\phi)]^2 + [|R|^2 \sin(2\omega\tau - 2\phi)]^2} \\ &= |g(\omega)|^2 \frac{[1 - |R|^2]^2}{(1 - |R|^2)^2 + 4|R|^2 \sin^2(\omega\tau - \phi)} = P(\omega) \end{aligned}$$

This is at a maximum when  $\omega\tau - \phi = n\pi$  (assuming uniform frequency spectrum over the band)

where  $n = 0, 1, 2, \text{ etc.}$

and at a minimum when  $(\omega\tau - \phi) = (2n+1)\pi$

$$\text{Hence } \frac{P_{\max}}{P_{\min}} = \left( \frac{1 + |R|^2}{1 - |R|^2} \right)^2$$

$P(\omega)$  drops to half its maximum value when

$$\begin{aligned} (1 - |R|^2)^2 &= 4|R|^2 \sin^2(\omega\tau - \phi) \\ \text{or } |\sin(\omega\tau - \phi)| &= \frac{1 - |R|^2}{2|R|} \end{aligned}$$

this is possible only if  $\frac{1 - |R|^2}{2|R|} < 1$  i.e.  $|R| \leq \sqrt{2} - 1$

If  $\omega_m$  denotes the value making  $P(\omega)$  maximum then

$$\omega_m \tau - \phi = n\pi \quad \text{or} \quad \phi = \omega_m \tau - n\pi$$

hence  $|\sin(\omega\tau - \phi)| = |\sin(\omega\tau - \omega_m \tau + n\pi)| = |\sin(\omega - \omega_m)\tau|$

Since the aim here is to make  $\omega = \omega_m$

$$|\sin(\omega - \omega_m)\tau| = |(\omega - \omega_m)\tau| = \frac{1 - |R|^2}{2|R|}$$

$$\text{or } \omega - \omega_m = \frac{1 - |R|^2}{2|R|\tau}$$

$$\therefore Q = \frac{\omega_m}{2(\omega - \omega_m)} = \frac{\omega_m R}{1 - R^2} \times \frac{dR}{c} = \frac{2\pi d \sqrt{k}}{\lambda_m} \cdot \frac{R}{1 - R^2}$$

This shows that high  $Q$  is possible by making  $R$  approach 1.

Consider here two particular cases that of a slab of dielectric and that of two thin parallel metallic films separated by air.

### 5.1. Fabry Perot interferometer using a dielectric slab

In the case of dielectric,  $\phi = 0$ , hence  $\omega_m \tau = n\bar{\tau}$

For  $n = 1$  this leads to  $\lambda_m = 2d\sqrt{\epsilon}$

hence  $Q = \frac{\pi R}{1-R^2}$  which leads to values given in the table below:

R	.5	.6	.7	.8	.9	.95	.97	.98
Q	2	2.9	4.3	7.0	15	30	51	74

Otherwise, to obtain any value Q, R must be given by

$$\frac{\sqrt{4Q^2 + \pi^2} - \pi}{2Q}$$

This shows that if the Q is to be large enough to be useful, say of the order of 30 or more, R has to be  $\geq .95$ . A slab of polystyrene has  $R = .66$  which is not enough but Culshaw obtained very much larger effective R by making the interferometer in the form of two blocks, each consisting of a number of  $\frac{\lambda_m}{4}$  thick slabs of polystyrene separated by  $\frac{\lambda_m}{4}$  in air. The two blocks are separated by  $\frac{\lambda_m}{2}$  from one another. The effective reflection coefficient is given in

the table below for n slabs per block

n	1	2	3	4	5	6
R	.66	.86	.94	.976	.99	.996

This method will be discussed later in connection with waveguide filters. In the present form it seems a very effective method but very difficult to adjust to an appreciably different frequency and therefore basically limited to measurements at one frequency only.

### 5.2. A metal film interferometer

This type has been discussed in detail by Hadley and Dennison who derived the full theory of it. At frequencies lower than infra red the characteristic of a thin metallic layer can be described by a factor  $p = 120\pi 6h$  where  $h$  = film thickness. Then  $R = \frac{p}{2+p} e^{j\pi} = -\frac{p}{2+p}$  when air is on either side of the film, and  $A = \frac{4p}{(2+p)^2}$  hence using the expression for  $P(\omega)$  derived earlier

$$\begin{aligned}
 P(\omega)_{\max} &= \frac{T^4 |g(\omega)|^2}{(1-R^2)^2} \\
 &= \frac{(1-A-R^2)^2 |g(\omega)|^2}{(1-R^2)^2} \\
 &= \frac{|g(\omega)|^2}{(1+p)^2}
 \end{aligned}$$

$$\text{while } P(\omega)_{\min} = \frac{T^4 |g(\omega)|^2}{(1+R^2)^2}$$

$$= \frac{|g(\omega)|^2}{(1+p+\frac{p^2}{2})^2}$$

$$\frac{P(\omega)_{\max}}{P(\omega)_{\min}} = \left( \frac{1+p+\frac{p^2}{2}}{1+p} \right)^2$$

leading to the following table:

$p$	1	2	3	4	5	6	7	8	9	10
$R$	.33	.5	.6	.67	.72	.75	.78	.8	.82	.83
$P_{\max}$	.25	.111	.062	.04	.028	.021	.0156	.0123	.01	.0083
$\frac{P_{\max}}{P_{\min}}$	1.56	2.78	4.5	6.75	9.5	12.8	16.5	20.8	24.5	30.7
$Q$	-	2.0	2.9	3.8	4.7	5.35	6.25	7.0	7.9	8.4

This table shows the unsuitability of this type of interferometer to filtering millimeter waves from a spark generated spectrum. It will be seen that for a  $Q$  of only about 8 less than 1% of the incident power will be transmitted - a loss that cannot be contemplated with the already minute powers available. It will be noted that for silver films,  $p = 1$  corresponds to a film thickness of .045 mm.

### 5.3. The wire grating interferometer

The preceding paragraphs would appear to make the Fabry Perot interferometer unsuitable in all its usual optical forms. It is possible, however, to use the principle at microwave frequencies by applying the results obtained for wire gratings. This has been done successfully by Lewis and Casey.

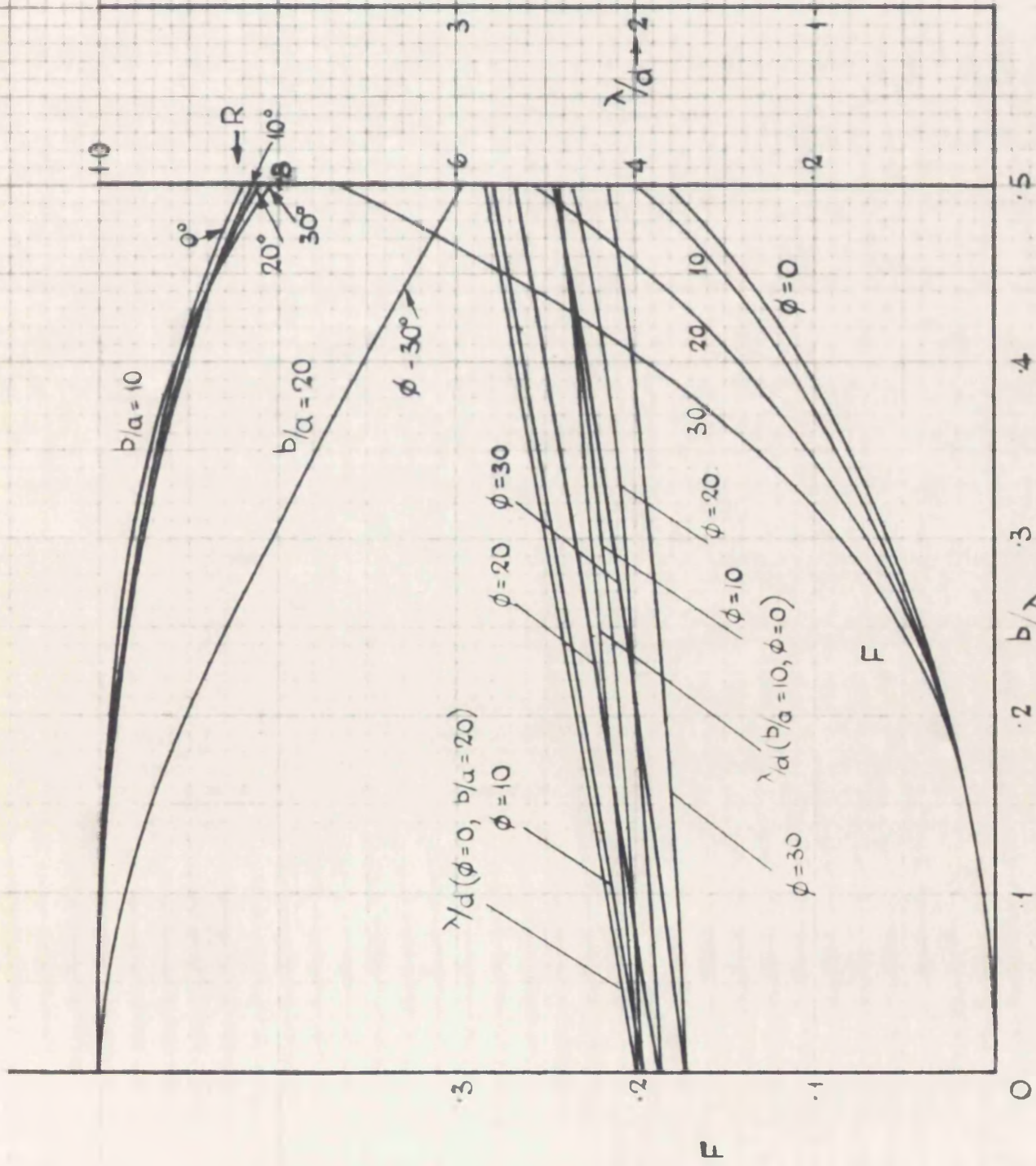
$$\text{Generally } P(\omega)_{\text{max}} = |g(\omega)|^2 \frac{1 - |R|^2 - A}{1 - |R|^2} = \left(1 - \frac{A}{1 - |R|^2}\right) |g(\omega)|^2$$

Now with certain wire gratings A was found to be very small, so small that  $\frac{A}{1 - |R|^2}$  is still small even when R is close to 1. In the case discussed in para. 4.4.1.  $A = 1.25 \times 10^{-3}$  for 1 mm waves. If  $R = .97$  (which gives Q of 50),

$$\frac{A}{1 - |R|^2} \approx 0.02 \text{ i.e. the filter insertion loss is only 2\%}$$

In practice Lewis and Casey obtained filter efficiencies of over 60% with fairly crude gratings.

When the incident radiation falls at an angle  $\theta$  to normal, the transmitted power at the corresponding angle  $-\theta$  is at a maximum when  $\frac{2\pi d \cos \theta}{\lambda} - \phi = n\pi$ .  $\theta$  can be found from the expression for  $\text{Re}^{j\phi}$  given earlier. This allows one to find  $\lambda_m/d$  for a given set of conditions. Fig. 46, gives R and  $\lambda_m/d$  when  $n = 0$  for  $b/a = 10$  and 20 and at  $\theta = 0, 10, 20$  and  $30^\circ$  (the function F is also plotted) against  $b/\lambda$  thus giving the basis for the design of a filter for any desired Q and  $\lambda_m$ . The filter will allow shorter



$R$  = REFLECTION COEFF. OF A SIMPLE GRATING.  
 $\lambda/d$  = LONGEST WAVE SELECTED.  
 $F$  = AUXILIARY FUNCTIONS FOR A WIRE GRATING.

GRATING INTERFEROMETER OF FABRY - PEROT TYPE  
 FIG. 46.

waves corresponding to  $n = 1, 2, 3$ , etc. to pass, but these will be heavily attenuated by virtue of the response characteristic of the crystal receiver.

This would appear to be a very efficient filter for the spark generated microwaves, but it presents quite a difficult technological problem at the shorter waves and on that account it is difficult to adjust if the bandwidth is to remain constant. It is not enough to vary the distance between the gratings because change  $\lambda$  affects both  $R$  and  $\phi$  hence also  $Q$ .

#### 6. Cavity and waveguide filters

All the methods described and analysed previously have their origin in the techniques common in optics. Some of them and, in particular, the various types of gratings lend themselves to accurate frequency measurement, the frequency being determined by the setting of the grating without any need for calibration against a known source.

It is now proposed to discuss briefly the filters based on waveguide technique. They are as a rule much less adaptable to changes in frequency and able to be operated in much narrower ranges and usually have to be calibrated by external means.

The most common type is the cavity filter which behaves like a high  $Q$  tuned circuit. There is extensive literature

dealing with these and it will suffice to say here that attempts have been made to operate a sparked dipole inside a cavity. These have met with a reasonable success. In particular Ludenia obtained a fifteenfold reduction in bandwidth by placing the dipole in a circular cavity while Anders by varying cavity dimensions could shift the wavelength between 1 and 3 cm. The radiated wave as measured by him had log. dec. of .013 at 2 cm corresponding to a bandwidth of 60 Mc/s. This method would appear to be very well suited to produce cm waves of any desired length, but it offers a great many difficulties below 1 cm on account of the small cavity required and consequent problems arising from the mounting of the dipoles and their insulation at the high voltages used. Thus it would appear that filters would be more suitable for the mm waves.

Another point should also be borne in mind and that is: it may sometimes be advantageous to have a wide band source and to do the filtering on the receiver side. This could be accomplished either by the use of cavities or filters.

The working of waveguide filters is almost universally based on the two stub matching principle. One stub placed in a matched guide introduces a susceptance which is cancelled out by another susceptance further along.<sup>(74)</sup> If the two stubs are identical and their normalised susceptance is  $B$  then it can be shown easily that the cancellation is

complete when they are at a distance  $\ell$  apart such that

$$\ell = \frac{\lambda_g}{2\pi} \left( n\pi + \tan^{-1} \frac{2}{B} \right)$$

and in that case it has been shown that the equivalent Q of the filter (defined as the ratio of centre frequency to half power bandwidth) is <sup>(94)</sup>

$$Q = \frac{1}{4} \left( \frac{\lambda_g}{\lambda_0} \right)^2 \left[ -B \sqrt{B^2 + 4} + \tan^{-1} \frac{2}{B} + \frac{2B^2}{\sqrt{B^2 + 4}} \right]$$

which for reasonable large, negative, values of B tends to  $\frac{\pi}{4} B^2 \left( \frac{\lambda_g}{\lambda_0} \right)^2$  (which in itself is nearly  $= B^2$ ).

### 6.1. The iris-type filters

A suitably shaped iris in a transverse metallic screen across a waveguide is known to have resonant properties but the resultant Q is seldom greater than 10 which is not <sup>(16,44)</sup> enough for our purpose. Higher Q's can be obtained by using capacitive or inductive slits in place of the stubs mentioned earlier. Thus for inductive slits (which is negative therefore  $\ell < \frac{n\lambda_g}{2}$ ) can be made greater than 300 if the slit is not much less than  $\frac{1}{10}$  of guide width. With capacitive slits it is difficult to make B greater than 20 unless the slits become infinitesimally narrow, what more, when B is positive (capacitive),  $\tan^{-1} \frac{2}{B} \doteq \frac{2}{B}$  and  $Q \doteq \frac{B}{2} \left( \frac{\lambda_g}{\lambda_0} \right)^2$  which is small. On the other hand it has been shown that whereas tuning the inductive slit filters results in considerable change in bandwidth, capacitive slit filters give a constant bandwidth over a considerable tuning range.

Full data are available for the design of filters with vertical or horizontal slits and also with circular irises resulting in any desired Q up to 1000 or even more. The data have usually been collected at 3 cm range but they should hold at shorter wavelengths.

### 6.2. The inductive-post type filters

The stub effect can also be obtained with posts across the guide. Such posts can be made to have a susceptance of the order of 10 or more when used singly but Reed has shown that a pair of posts disposed along the centre line of the waveguide and separated by a distance  $d$  has a combined susceptance of  $B = -\frac{\lambda_g}{a} \cot^2 \frac{\pi d}{2a}$  where  $a$  = guide width. If  $d$  is small,  $B$  can be made of the order of 15 or more leading to Q's of about 300.

### 6.3. The quarter wave transformer type filter

This filter does not appear to have been described elsewhere, although it is closely related to the Fabry Perot interferometer described by Culshaw (see paragraph 5.1.). The theory of this filter is dealt with in the Appendix II. It is shown there that by choice of a suitable number of quarter wave sections Q's of any desired range can be obtained. At 3 cm wavelength when polystyrene is used for one type of the quarter wave transformers  $Q = \pi \cdot 2^n$  where  $n$  is the number of quarter wave transformers in one half of the filter.

Since for ease of assembly  $n$  must be odd,  $Q$  of 380 results from 7 sections, giving an overall length of the filter of four wavelengths. This method is, however, only suitable for working with comparatively narrow frequency bands, because frequencies far removed from the filter band centre are not attenuated very much the sections not behaving as quarter wave transformers. For example, if the .4" x .9" guide were used to filter 1 cm waves, the response of the filter to other frequencies would be as shown in Fig. 53. below

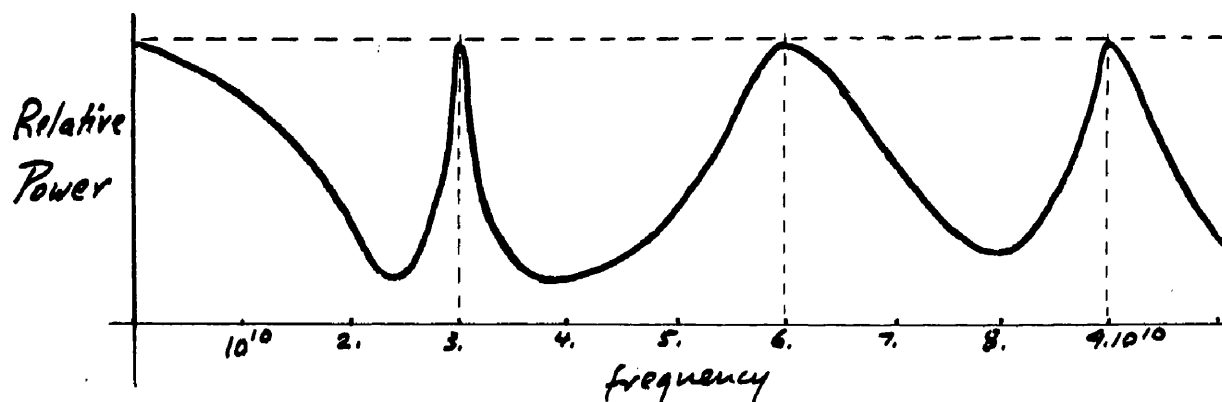


Fig. 53.

The higher frequencies are not of importance since the crystal will attenuate those effectively as compared with the longer waves but it will be seen that waves longer than 1.5 cm are very little attenuated and since more power is available at the longer waves they will swamp the waves in the pass band of the filter. This behaviour is, of course, identical with the Fabry Perot interferometer. Thus for effective use the filter will have to be mounted in a waveguide whose cutoff wavelength is not greater than 1.5 times

the desired pass band centre, a requirement quite common in waveguide technique.

#### 6.4. Conclusions on filters for spark generated waves

An analysis of the various types of filters and cavities available shows that they form a suitable means of narrowing down the radiated band around any desired frequency. In particular, the inductive post or slit type of transmission filter is the most promising as it allows for simple adjustment of wavelengths by varying the physical distance between the two susceptances.

Where a predetermined centre frequency is aimed at, the quarter wave transformer type filter has the advantage of very low insertion loss which is important at these small powers.

The use of filters rather than mounting of the dipole in a cavity has several important advantages in applications apart from simplifying the mounting and high voltage feeding to the dipoles.

These advantages are:-

1. The same source can be used to work through a number of filters tuned to different frequencies so that one can work simultaneously at several wavelengths. These can, if

necessary, be modulated separately.

2. Filtering can be done at the receiver end which can be useful when measuring characteristics of dielectrics, etc.

3. Since the output from the dipoles tends to fluctuate from spark to spark, it is possible to monitor these fluctuations by a wideband receiver, the output being then compared to that of the individual filters or receivers, to correct for power level changes.

The waveguide filters do not appear to be as suitable as the semi-optical methods for measurement of radiation characteristics, hence the two methods are complementary. By avoiding the use of horn and mirrors and containing the radiated power within a waveguide much larger power densities result hence signal to noise ratio of receivers is improved and one can go to shorter waves.

#### 7. Power output from a simple radiator

The accuracy of an estimate of radiated power depends largely on the knowledge of the mechanism which takes place in the system during the breakdown and radiation. It has not been possible as yet to explain the mechanism fully, but

all evidence, especially the experiments by Lindman which led to results very close to those theoretically expected on the assumption of a sudden collapse of field, indicates that it is, in fact, a case of a build up of a charge across the gap, due to the high voltages induced, followed by a rapid breakdown of the gap.

Stratton has proved that the field of the fundamental mode of oscillation of a conducting sphere is that of an electric dipole whose moment is given by  $p = 4\pi k_2 \frac{N^2 - 1}{N^2 + 2} a_1^3 E$

where  $k_2$  is dielectric constant of the medium

$a_1$  is the radius of the sphere

$E$  is the electric force

$$\text{and } N = \frac{\sqrt{2}}{1-j} \frac{61\mu_1}{\omega k_2 \mu_2}$$

where suffix (1) refers to the sphere and suffix (2) to the medium.  $N$  is seen to be very large for the frequency range discussed, hence  $p = 4\pi k_2 a_1^3 E$  and the potential energy of the sphere becomes  $pE = 4\pi k_2 a_1^3 E^2$ .  $E$  is the potential gradient at which the gap will break down.

Thus, for  $n$  breakdowns per second, assuming that each spark leads to a complete discharge of the sphere, the total power radiated - neglecting absorption - will be  $P = 4\pi n k_2 a_1^3 E^2$ . Taking for  $E$  the figure given in paragraph 1, say 500 kV/cm,  $a_1 = 0.5$  mm,  $k_2$  for paraffin =  $2.5 \times .885 \times 10^{-11}$ ,

$P \doteq 85 \mu\text{W/spark}$  distributed over the whole frequency

spectrum with a peak at around  $\lambda = 5.5$  mm.

No similar estimate has been arrived at for the cylindrical dipoles because of the mathematical difficulties, but it is interesting to note that a sphere in an electrostatic field E has the same moment as the oscillating sphere. Now King has shown that the self-capacity of a radiating cylindrical dipole aerial of overall length h is within a few per cent of the static capacitance of two cylindrical end-on conductors, which has been shown to be

$$C = \frac{h}{60c(\Omega - 2.485)}$$

where c is velocity of light

$$\Omega = 2 \log_e \frac{2a}{b}$$

2a being the length = h

b being the radius

Taking  $\lambda = 5$  mm and  $\lambda/h = 4$ , Hallen's solution leads to

$\Omega \doteq 5.2$  hence

$$C = \frac{125 \times 10^{-3}}{60 \times 2 \times 10^8 \times 2.7} = 0.385 \times 10^{-12}$$

hence potential energy at breakdown assuming a voltage of 20 kV will be  $\frac{1}{2} CV^2$  giving power of 7.7  $\mu$ W per spark but since the corresponding log dec is 1.5 against 3.62 for sphere, the power will be concentrated much more around the natural wavelength. The proportion of power within the bandwidth defined by the "half peak power" points for various values of log dec  $\delta$  has been computed. Computation

has also been carried out of power contained in a band equal to  $\frac{1}{100}$  of the centre frequency at natural frequency and also at twice and three times natural frequency neglecting the radiation at harmonics of natural frequency the power levels of which it has not been possible as yet to estimate. The results appear in the table below:

TABLE

Proportion of power radiated in:

- (a) " $1/2$  power band" of total radiated power  
 (b) a band =  $\frac{1}{100}$  of natural frequency  $f_0$  centred at  $f_0$   
 (c) - " - - " - - " - - " - - " -  $2f_0$   
 (d) - " - - " - - " - - " - - " -  $3f_0$

for various values of log. dec.  $\delta$ .

$\delta$	a	b	c	d
.25	48%	.64	$4.4 \times 10^{-4}$	$.62 \times 10^{-4}$
.5	48%	.32	$8.8 \times 10^{-4}$	$1.2 \times 10^{-4}$
1	48%	.16	$17 \times 10^{-4}$	$2.5 \times 10^{-4}$
2	48%	.08	$33 \times 10^{-4}$	$5.1 \times 10^{-4}$
3.62	60%	.055	$60 \times 10^{-4}$	$10 \times 10^{-4}$

By using the arguments of para. 3.2. it can be shown that the total radiated power over the whole spectrum is

given in terms of natural wavelength and log dec by the relation  $P = \frac{1}{2\delta f_0}$  and since within narrow limits both  $\delta$  and  $f_0$  vary more or less linearly with dimensions one can expect power to vary proportionally to square wavelength. This is, in fact, what has been found by Webb and Woodman over a wide range of dimensions using both cylinders and spheres. They also found that for any given  $\lambda$  the power radiated by a sphere is almost twice larger than that from a cylinder, which is in reasonable agreement with the discussion above when one considers that the bandwidth of the receiver was constant. The only disagreement appears to be with the expression derived by Stratton according to which power should be proportional to cube of wavelength, but it is very likely that - as follows from the discussion in para. 1.2. - the required electric gradient is reduced as wavelength is increased, thus reducing radiated power.

In conclusion, it is seen that power radiated by the spark generator is very small and decreases rapidly as frequency increases. If one attempts to use a part of the spectrum away from natural frequency, the available power is very small indeed and for that reason, it is inadvisable to use filters with effective  $Q$  in excess of 100.

PART III. EXPERIMENTAL1. Introduction

The review of microwave generators undertaken in part I tends to the conclusion that with the exception of backward travelling wave tubes (which were in the very early development stage when this work was undertaken) the spark generator offers an important source of microwaves in the centimetric and millimetric region.

Having analysed the theoretical background of the radiating cylinder and sphere and the not inconsiderable evidence collected by earlier workers on the lines of the first sections of part II, a plan of work emerged in which the following points became apparent:

- (a) The evidence on the whole supports the Abraham-Hallen theories. In particular the experiments of Lindman make this point fairly convincingly.
- (b) The reduction in dimensions and the consequent increase in the effects of mounting, of irregular thickness and outlines, impossible in practice to control, introduce into the theory factors which cannot be at present allowed for fully enough to make an accurate prediction of results possible.

- (c) In view of points (a) and (b) it appeared that the theoretical aspects of the matter should not be pursued any further but taken as established. Instead, new methods of studying the radiated spectrum - in particular the Boltzmann interferometer - should be examined.
- (d) An attempt should be made to utilise the wide band spectrum of radiation by filtering out any desired band of frequencies and thus evolving a variable frequency and a multiband source. In this connection little can be expected from slits and gratings after the analysis of these given earlier. Instead waveguide filters should be employed.
- (e) Waveguide techniques should be utilised to the fullest extent. In view of the minute powers expected in the mm region and the well developed technique and component design in the 3 cm region most of the experimental work should, in fact, be carried out between 1 and 3 cm.
- (f) Modern pulse methods should be employed, a single spark source being used for simplicity. No attempt will be made to study multi-spark

sources such as arrays or mass radiators.

## 2. Measurement technique

In all experiments, crystal diodes obtained commercially were used as detectors. No power was measured beyond estimates based on the characteristics of these crystals.

In view of the considerable fluctuations of output from the spark radiators, some thought had to be given to developing a method that would enable one to differentiate between changes in output and fluctuations. Previous workers used a galvanometer of long time constant, hence insensitive to rapid fluctuations. An ordinary moving coil meter in the output of a balanced amplifier will have a similar effect.

Both of these methods have been used at various stages of the work but they were found not accurate enough to determine wavelengths, etc., being too insensitive to small changes in output. A pen recorder would allow one to observe the changes in output level against the fluctuations but the considerable damping of the pen may make this method insensitive. Hence, instead of using a pen it was decided to use a cathode ray oscilloscope trace and a camera. Instead of averaging out the fluctuations by damping, use is made here of the integrating property of a film exposed to a moving point of light. The signal is applied to the Y plates with a time base on the X plates. The trace will

consist of a line of height proportional to individual pulse strength in output, hence the line length will fluctuate with the output. If at any setting of the gear the film is exposed to the trace for a fixed time, the record will appear on developing as a line of light tapering off at the ends more or less depending on the fluctuation of power.

If for each new setting of the gear the beam is shifted to a new position in the X direction, then on completing the set of measurements the film will reproduce the power changes to an accuracy which depends on one's ability to follow the envelope of the picture keeping at a constant intensity of light - a skill which is quickly acquired in practice although it is realised that much more reliable results could be obtained by using a suitable photometer which could either be made to follow the contour at any desired light intensity or else the interferogram could be scanned by a light beam and the light intensity converted to an electric signal. Instead of traversing the beam one could move the film with identical effect, but moving the beam can be done automatically in many cases where a movement of the measuring gear can be directly translated, via a potentiometer coupled to it, to the X plates in the form of an increasing voltage which shifts the beam across.

This technique, which, in spite of its simplicity, appears to be quite novel, has proved very helpful and should

find application in other fields such as radiation pattern plotting etc. Long persistence cathode ray tube should be very useful here.

## 5. Equipment

### 5.1. Pulse generator

Having examined several possible high voltage pulse generators it was decided to concentrate on a hard valve type in order to have the maximum freedom of pulse length and frequency. The final design is given in Fig. 47. and the complete equipment is shown in Fig. 48. The maximum voltage obtainable was limited by the availability of a suitable hard valve. The 715 B was found the best valve obtainable for the job. Its maximum safe voltage on the anode is 20,000V - which was thus fixed as the maximum pulse voltage. The valve is driven by a "bootstrap" type amplifier from a Dawe pulse generator capable of giving 1, 10 and 100  $\mu$  sec pulses up to 5200 per second.

The 20 kV dc supply is obtained by a Cockroft-Walton type rectifier multiplier from an 3000V secondary, 180V primary 2000 c/s transformer, the supply being obtained from a suitable dc/ac converter. The 2000 c/s frequency permits the use of smoothing capacitors of reasonable size.

In order to cause the breakdown at as high a voltage as possible the pulse must have a steep front. The actual pulse obtained reaches 15,000 volts within just over 0.1  $\mu$  sec.

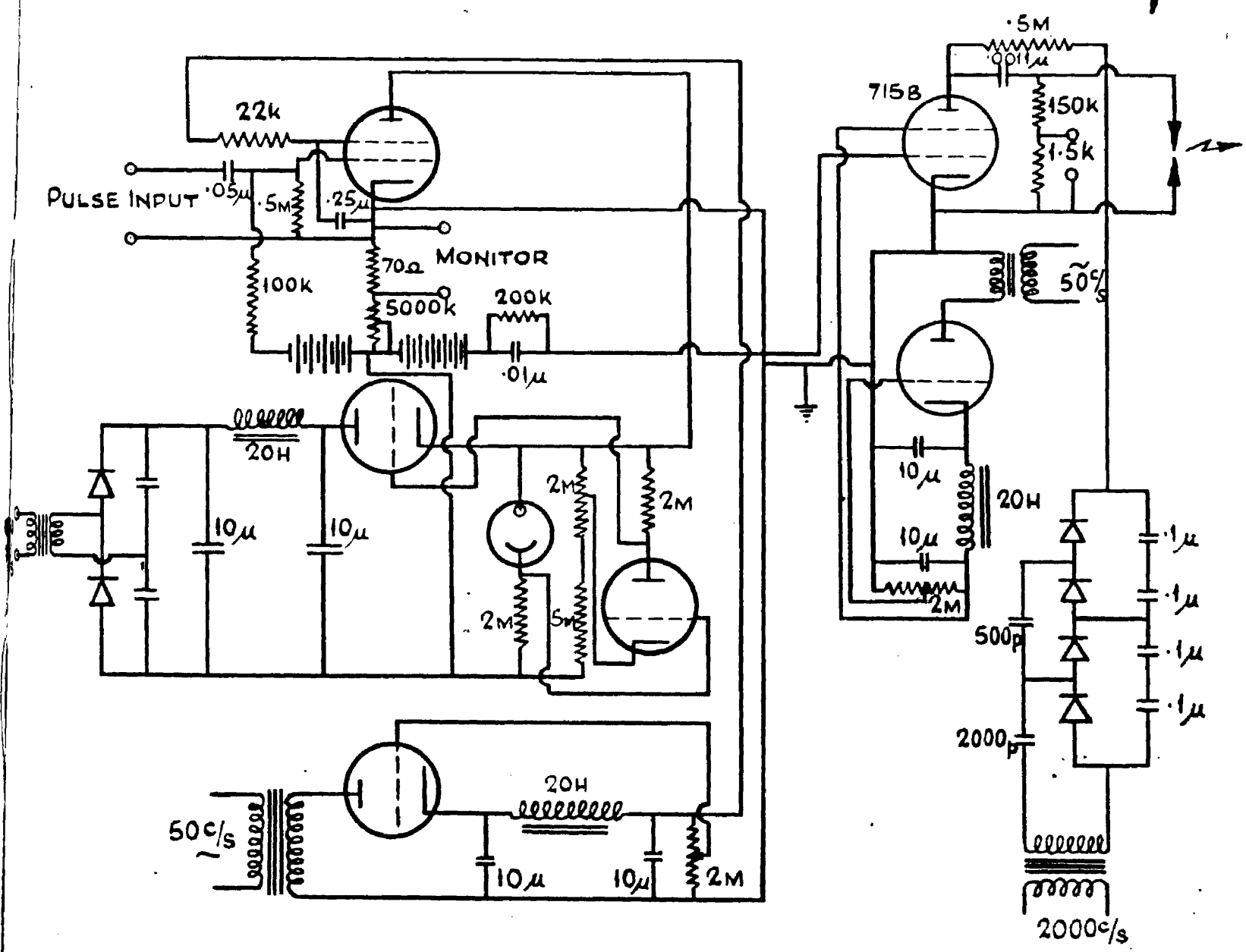


FIG. 47.

PULSE GENERATOR CIRCUIT.

B.V. High Voltage Equipment

The design of the cylinder arrangement was modified with...

radiat  
in gl  
a bras  
be co  
axial  
oil.  
elect  
prev  
osail  
This  
paraf  
and t  
Each  
other  
parab  
fit a  
compl

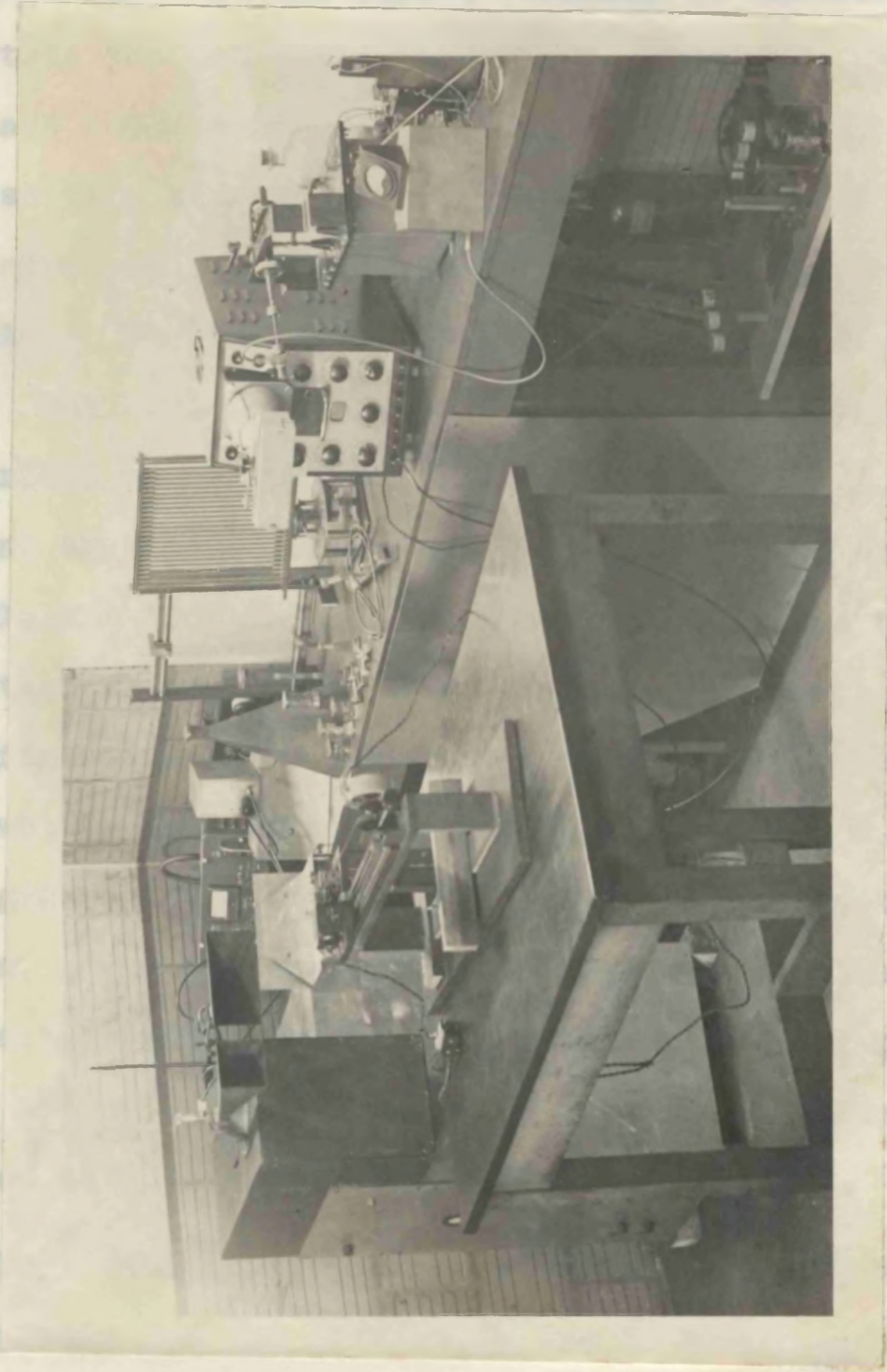


Fig 48.  
The complete equipment.

in the tubes. At first it was thought that tungsten has  
to be used to slow down erosion due to sparking. Then  
platinum and even copper was found satisfactory but even so

### 3.2. Radiating elements

Two designs of the radiator arrangement were experimented with. In the first, referred to hereafter as mark 1 radiator, the two elements forming the dipole were mounted in glass tubes 5 mm in diameter. The tubes were held in a brass tank as shown in Fig. 49A. One of the tubes could be centred with respect to the other which could be moved axially. The tank was filled with paraffin or transformer oil. The h.v. pulses were brought to the dipole via electrodes running inside the tubes in air. In order to prevent these electrodes and the whole h.v. system from oscillating 1000- $\Omega$  resistors were incorporated in them. Thus the system consisted of three gaps: central one in paraffin between the two elements constituting the dipole and two air gaps between each element and the h.v. supply. Each gap could be adjusted in length independently of all others. The bottom of the tank was fitted with a movable parabolic reflector, while the top was reduced gradually to fit a standard X-band waveguide coupler. A horn could be coupled at this end if desired.

This radiator proved very efficient and trouble free to operate, but the difficulty was in mounting the dipole in the tubes. At first it was thought that tungsten has to be used to slow down erosion due to sparking. Then platinum and even copper was found satisfactory but even so

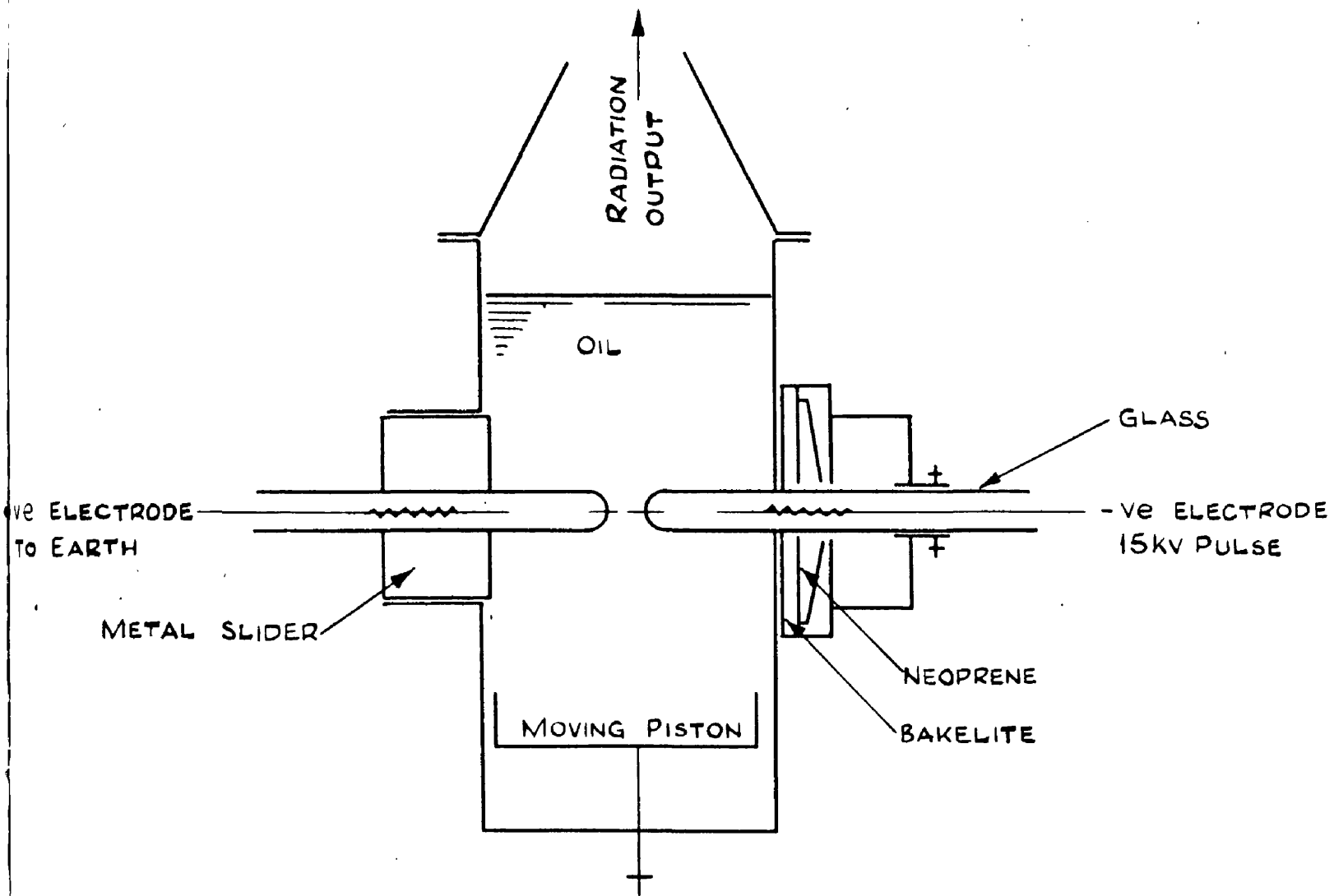


FIG. 49 A.

SCHEMATIC DIAGRAM OF RADIATOR MARK I.

in spite of a great deal of effort and expert help, the technological difficulty of a paraffin-tight mounting of elements shorter than 5 mm was found too great. Nor could any suitable technique be developed to mount suitably in the tube ball bearings of 1, 2 or 3 mm in diameter.

While this set up was examined, it was found that under suitable conditions one electrode could be dispensed with, and even the earth return could be omitted. Thus, a mark 2 radiator was developed consisting of an h.v. electrode sealed into a 10 mm dia glass tube filled with paraffin or other suitable liquid. Into this tube is inserted a dielectric rod carrying on its end the radiating element sealed or glued on. The dielectric rod could be adjusted axially and centred with respect to the h.v. electrode so that the gap could be adjusted, a fine screw providing the final adjustment. Fig. 49B. shows the arrangement. The larger glass tube is fixed across a waveguide so that the radiating element is centrally situated. A plunger in one end of the guide can be moved to any desired distance from the radiator.

This system simplifies the mounting of the radiator, reduces the amount of paraffin or other liquid that has to be used and could be developed into a straightforward plug-in unit.

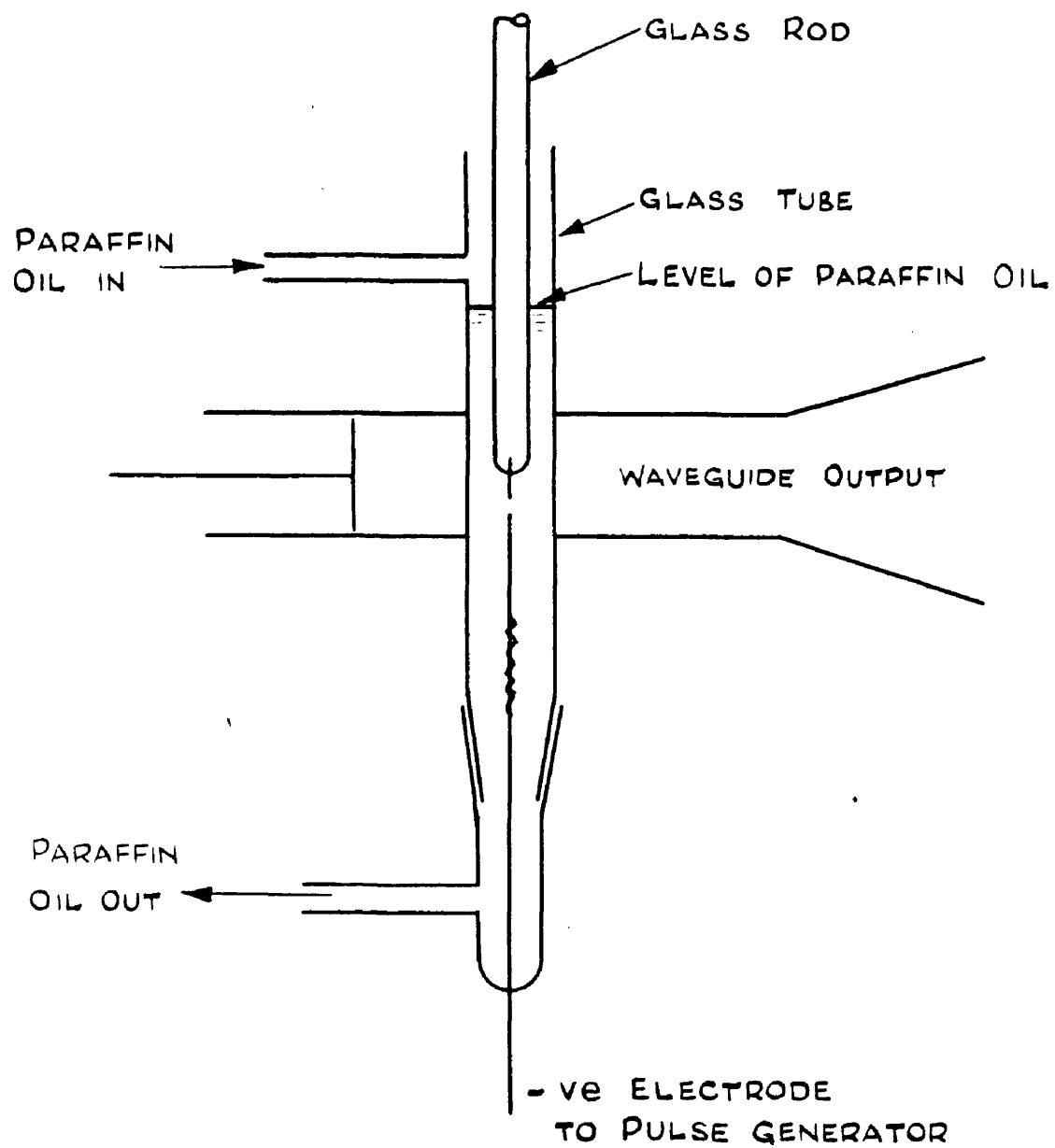


FIG. 49B.

SCHEMATIC DIAGRAM OF RADIATOR MARK II.

### 3.3. Detected signal amplifiers

Since the received signals consist of short pulses, ac amplifiers can be used with the crystal detector, simplifying the design.

Three types of amplifiers were used. The first (for circuit diagram see Fig. 50.) was used primarily as a visual monitor of output level since it operates a micro-ammeter, the moving coil of which acts as an integrator. The second, two of which were used at times, is a straight-forward R<sub>6</sub> coupled two stage amplifier with a gain of 50,000 and a bandwidth of 1,000 to 50,000 c/s. This "wide band" amplifier was used for general purpose work. Its circuit is given in Fig. 51.

The third type of amplifier built was a tuned amplifier with a gain of 30,000 and a bandwidth of 50 c/s centred on 2000 c/s. The circuit diagram is given in Fig. 52. This amplifier by virtue of its narrow band gave a sinusoidal output which was very good for photographing purposes since the resultant trace was clear and uniform both below and above the zero axis, whereas the wide band amplifiers gave very sharp and therefore faint positive swing followed by a much smaller negative one.

### 3.4. Wavelength measuring equipment

A Boltzmann interferometer was used as a general piece

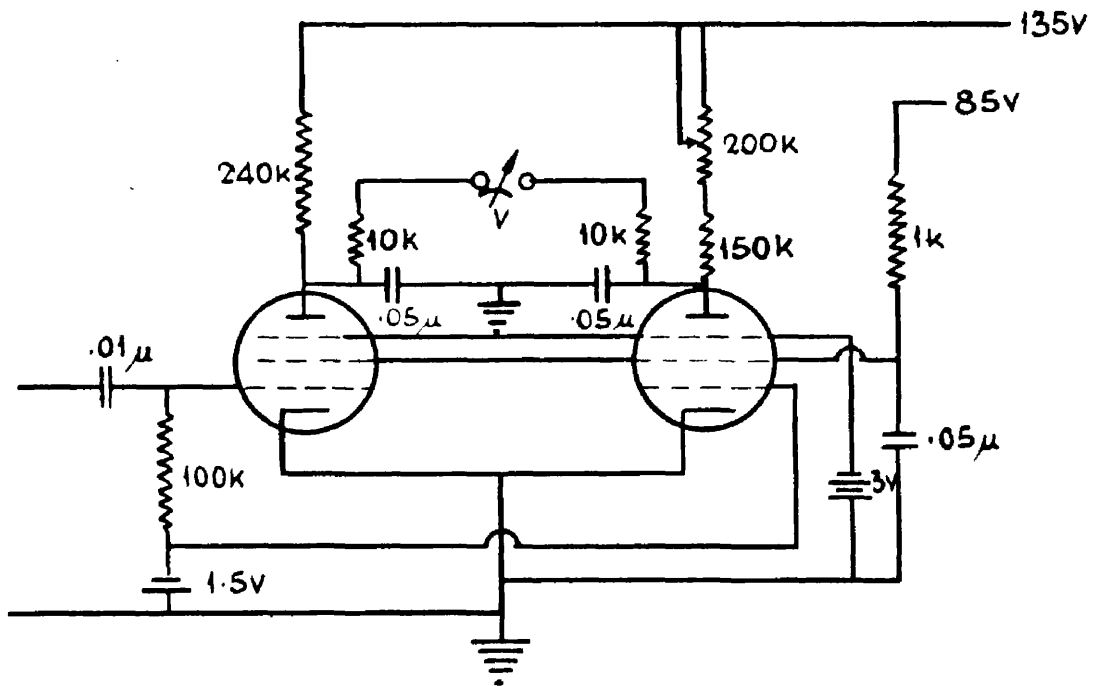


FIG. 50.

CIRCUIT OF MONITOR.

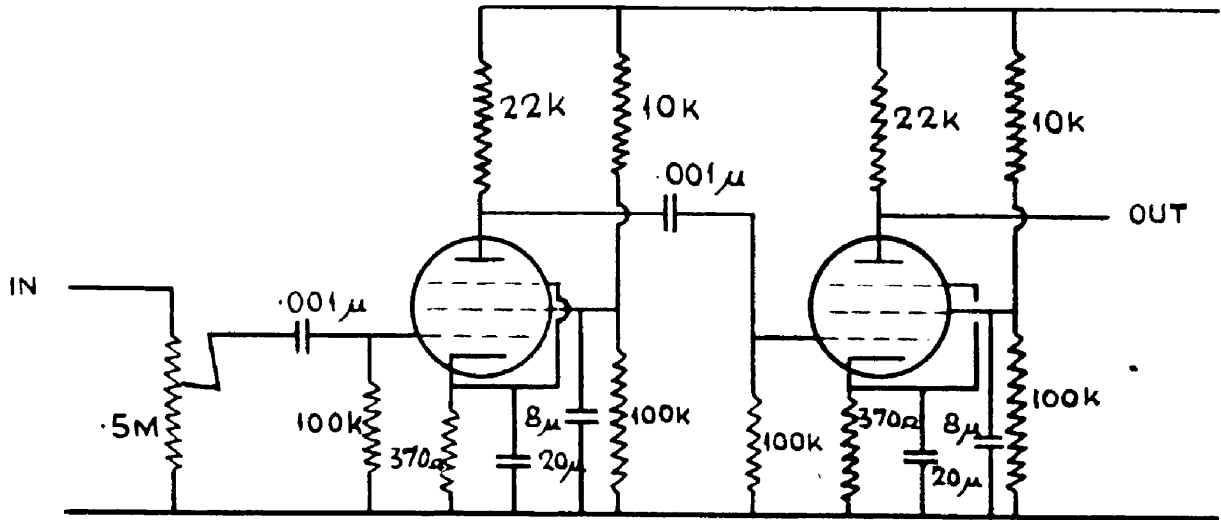


FIG. 51.

CIRCUIT OF VIDEO-AMPLIFIER.

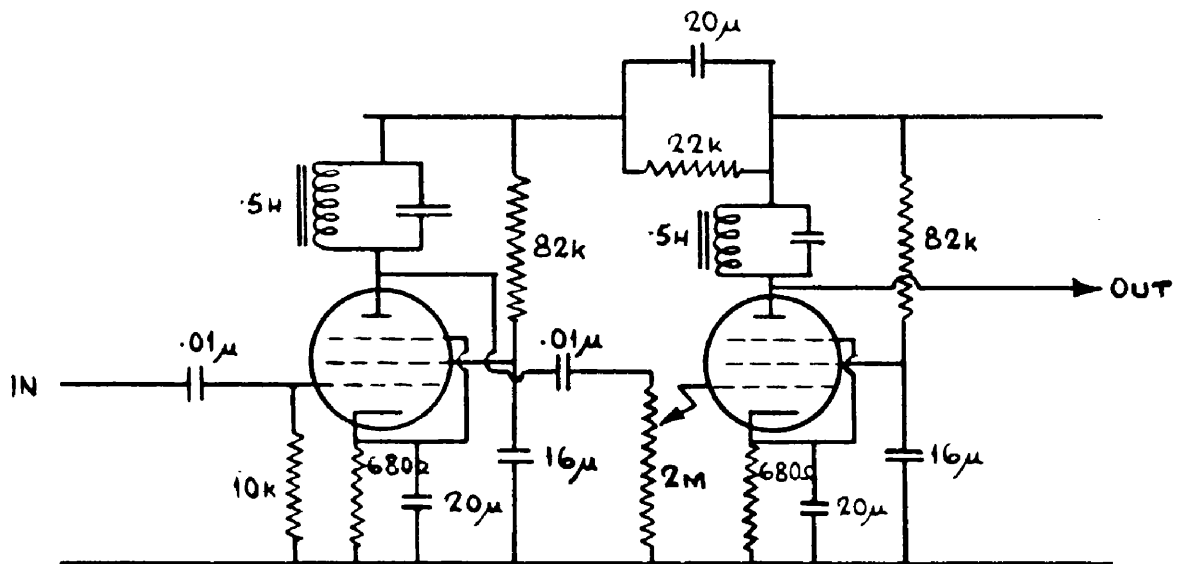


FIG. 52.

CIRCUIT OF NARROW BAND AMPLIFIER.

$$f_0 = 2000 \text{ c/s}$$

$$Q = 50$$

130

of measuring equipment, especially at wavelengths greater than 8 mm because of its simplicity, independence of the wavelength of measured signal (at least within the range of interest here) and the facility it offers to apply the photographic technique developed. The resultant interferograms can be used to determine the whole received spectrum by a method described in part II. The other method of measuring wavelength and spectrum by producing standing wave in front of a reflector and then measuring it by means of a probe is considered to be less suitable and especially where a short aerial is used as a probe, this is likely to give false readings due to re-radiation. This method is, however, very useful when the radiated energy is confined to a waveguide. An ordinary S W R meter can then be employed to measure the standing waves. If the resultant standing wave is to be interpreted for the purposes of estimating  $\delta$ , the probe must not be tuned or tunable, otherwise the reading will correspond to the probe frequency and not to the source.

At lower wavelengths it is found that the Boltzmann interferometer is not accurate enough to determine  $\lambda_0$ . Instead an echelette grating has been used. Slits and slit gratings have also been tried with some success but the output level of the first order spectrum is low and on account of the low Q (see part II) it is difficult to

estimate the wavelength accurately. Fabry Perot interferometers have also been built and tested.

### 3.4.1. The Boltzmann interferometer

A photograph of the apparatus built is given in Fig. 53. It consists of a fixed aluminium plate 4" x 8". Immediately above is carried another identical plate. This can be moved by a motor driven gearing up to 2 inches in the direction normal to the reflecting surface while the whole cradle carrying the motor and reflector can be moved along rails by an 18" long OBA screw (1 turn = 1 mm forward movement). Thus the moving reflector can be made to traverse from 1" in front of the fixed one to several inches behind it by turning the screw, while any two inches of this traverse can be examined at a uniform rate by a motor drive. A non-elastic belt connects the two mirrors, passing over a roller geared to a potentiometer, so that any relative movement of the mirrors can be translated accurately to the X plates of an oscilloscope as a deflecting voltage proportional to distance between mirrors. If, at the same time, the Y plates are fed with the amplified output signal, the resultant picture will be a direct graph of output level versus mirror displacement, i.e. the interferogram.

The interferometer was examined for possible errors due to lateral displacement of mirrors (since the radiating and

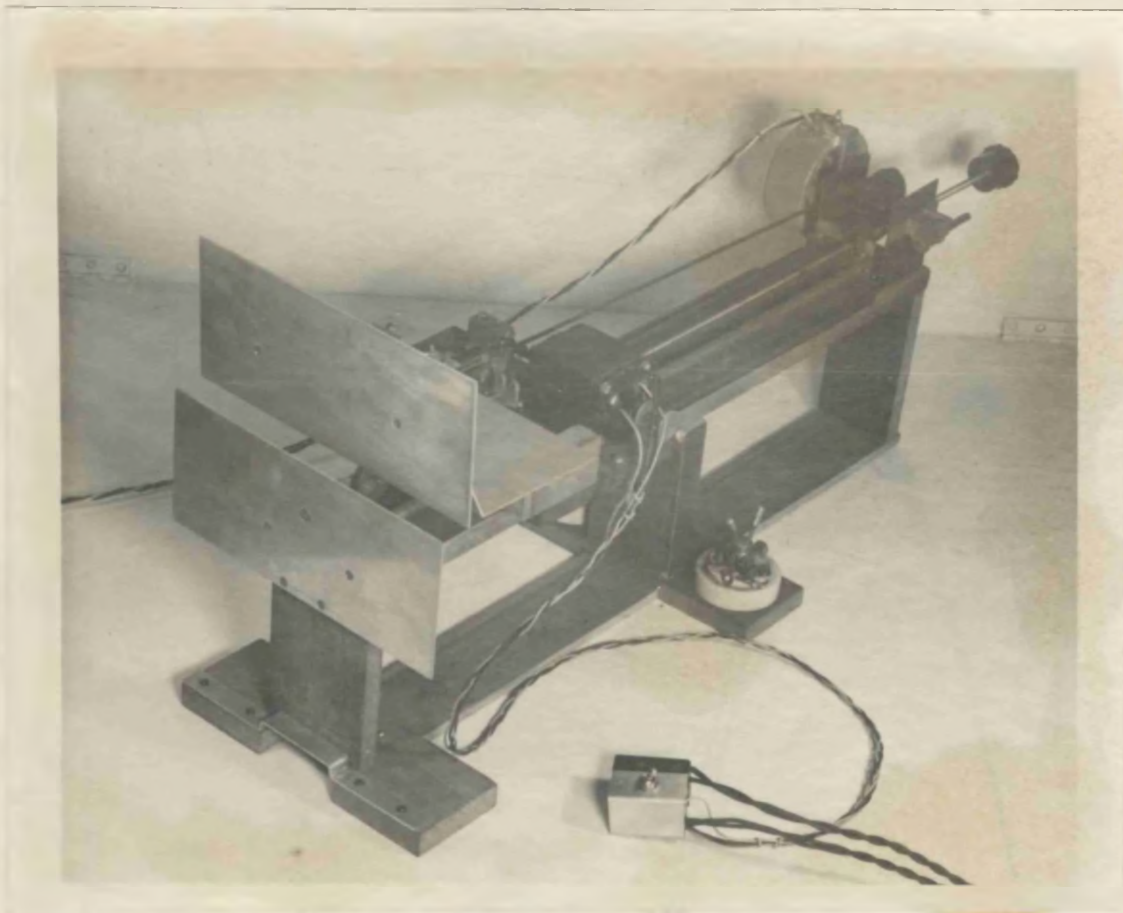
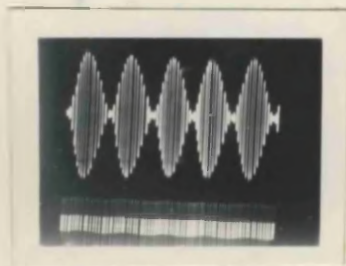
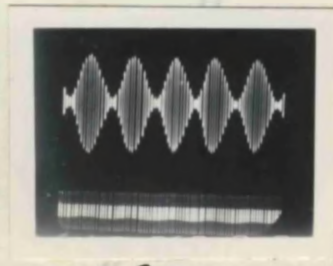


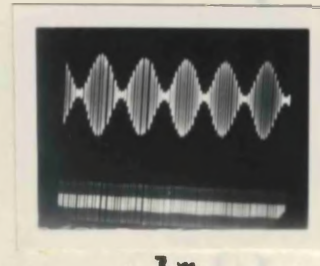
Fig 53  
Boltzmann Interferometer



1m.



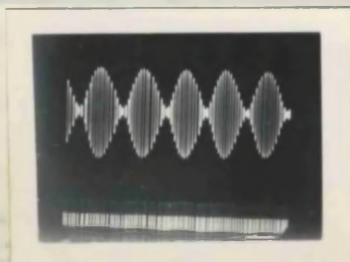
2m.



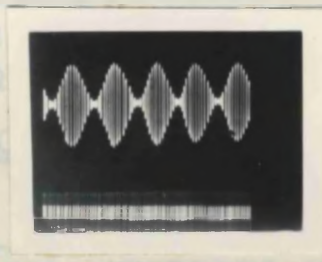
3m.

Fig 54.

Interferometer at increasing distance



Facing radiator



Facing receiver

Fig 55

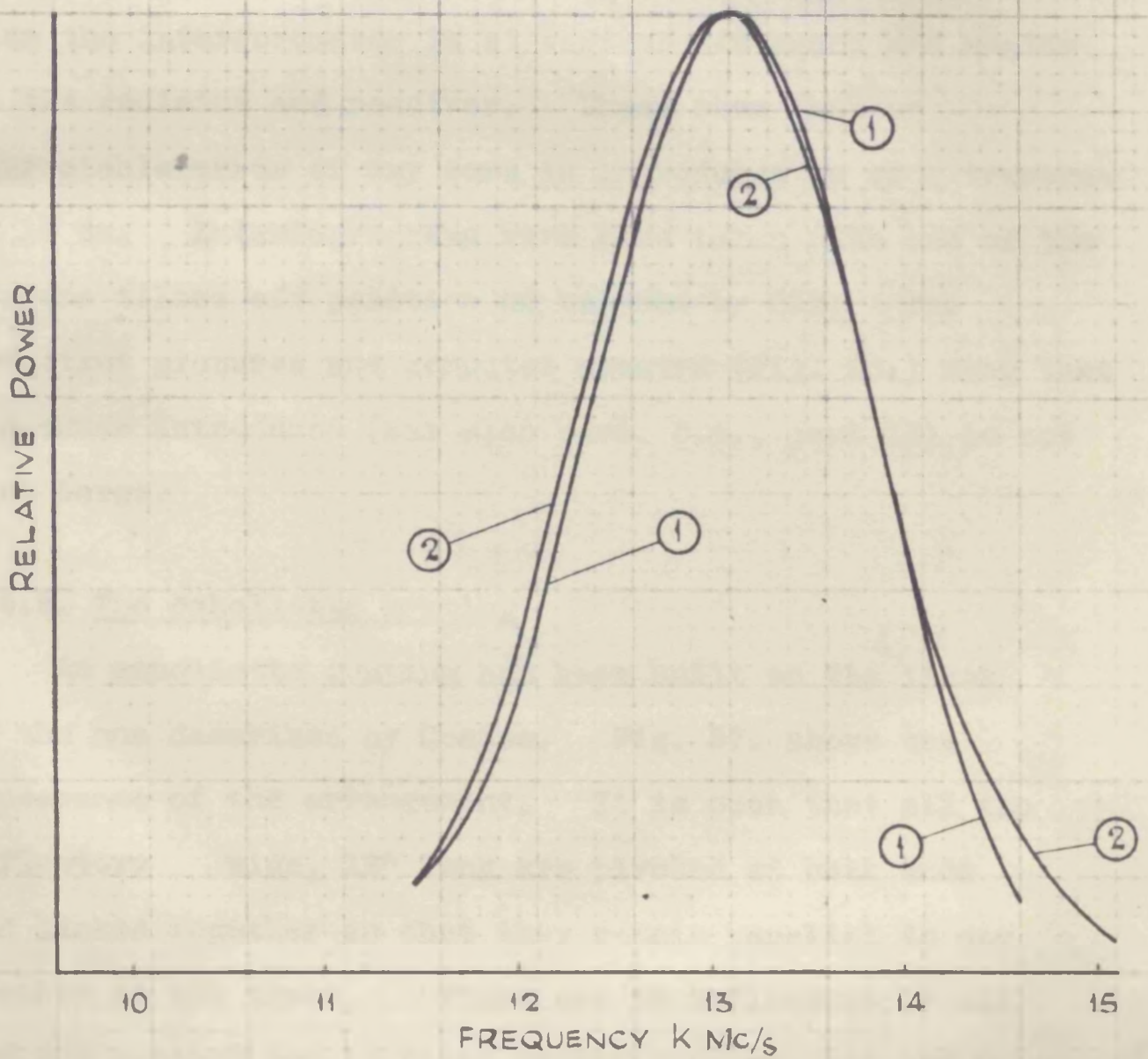


FIG. 56.

EFFECT OF UNBALANCE IN REFLECTION FROM THE TWO MIRRORS OF THE BOLTZMANN INTERFEROMETER.

① BALANCED ② TOP MIRROR REFLECTING 25% MORE THAN BOTTOM MIRROR.

receiving horns are separate and side by side the interferometer is not set at right angles to the radiated beam but with its normal bisecting the angle between the two horns), and the effects of variation in crystal law as the power level varies from 0 to maximum. Figures 54. & 55. show the interferograms obtained with a klystron oscillating at 3.2 cm when the output power is varied and also when the interferometer is at various distances and angles to the radiator and receiver. These show that no appreciable error of any sort is introduced up to a traverse of 10 cm. Interferograms were also taken with one of the mirrors tilted off position of balance by 25%. The resultant pictures and computed spectra (Fig. 56.) show that the error introduced (see also para. 3.4., part II) is not very large.

### 3.4.2. The echellette grating

An echellette grating has been built on the lines of the one described by Coates. Fig. 57. shows the appearance of the arrangement. It is seen that all the reflectors wide, 12" long are pivoted at both ends and linked together so that they remain parallel to one another at all times. There are 23 reflectors in all and the central one is fixed to the base so that the frame carrying all the other ones can rotate round it. Thus by turning the frame, the steps between the reflectors are

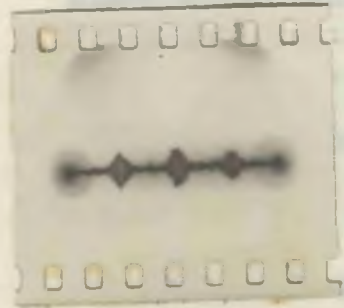


Fig 58.



Fig 57.  
Echelette.



Fig 54  
Output variations.

varied while they remain parallel to the original plane. The table itself can be turned also around the axis of the frame. The turning of the frame can be done by a gear drive and a potentiometer is also geared to it so that the angle of rotation can be translated to an oscilloscope as an excursion of the beam in the X axis. The total rotation is limited to  $\pm 40^\circ$  (i.e.  $80^\circ$  in all) so that the orders can be repeated on both sides of the normal. Fig. 58. shows the interferogram obtained with a 9 mm klystron. These show a certain irregularity in the shape of the zero and first orders. It was found that utmost care must be taken to centre the echellette on to the beam to reduce this irregularity to a minimum. Some of the irregularity is due to reflections from the frame which of necessity had to be made large and heavy to avoid distortion of the plane of reflectors. A second frame suitably ridged can be fixed on to the main one to reduce its effect on the reflected pattern. It is found, however, that for the purposes of measurement the distance between the two peaks of first order spectra gives a good measure of wavelength irrespective of the distortion. In addition the accuracy of this device is reduced by a backlash of  $1^\circ$  caused by the friction in the many pivots. The reflectors themselves are made of  $1/2''$  ground stock chromium plated. The wavelength corresponding to the first order peaks is given by

$$\lambda = 25.4 \sin \theta$$

where  $\lambda$  is measured in millimeters and  $\theta$  is the angle between normal to reflector and normal to frame at the peak.

Thus the longest wave that can be measured by this echellette is  $= 25.4 \sin 40 = 16.3$  mm.

It will be noted that also the intensity of the first order should be equal to the zero order for a monochromatic source, the total power received - which is what was measured here - is, in fact, reduced because a smaller portion of the beam is reflected as the frame of the echellette is rotated (even assuming a perfectly uniform beam which is not likely to be the case here), according to the cosine law of reflection. This can be observed in Fig. 58.

### 3.5. Other equipment

A large quantity of other devices was designed and used but as they are of a particular rather than general character they will be described when being dealt with in the experiments quoted.

## 4. Experiments with mark 1 dipole radiator

### 4.1. Output fluctuation

after initial difficulties due to pickup of low frequency pulses, this radiating system was found to work very satisfactorily for prolonged periods, requiring adjustment of central gap at half hour intervals or so.

The output fluctuated a great deal and steps were taken to examine the possibility of reducing this. Fig. 59. shows a typical output variation, each pulse of radiation being detected by a crystal. Observation of the liquid during sparking shows the formation of tiny vapour bubbles which slowly diffuse away from the spark. It was thought that these bubbles cause a random change in the medium between the radiating electrodes so that the breakdown strength varies continuously. Thus not only may there be a change in capacity due to dielectric change but also the gap may break down at different voltages each time. This change of breakdown voltage was, in fact, observed on the CRO. No improvement in regularity was, however, observed when the liquid was stirred, put under pressure or played on the gap in the form of a jet. Nor was the situation affected by irradiating the gap with a radium source or by shaping the ends. It has, however, been observed that as the gap is reduced, the peak output drops but becomes more regular. It is probable that since the reduction in gap causes breakdown at a lower voltage, since this voltage is reached very much quicker than the actual peak, the gap breaks down under a condition of considerable over voltage which leads to more uniform results

On the basis of all experiments it can be concluded that for most uniform output the gap must be reduced to the

very minimum at which it will still radiate. This calls for regular adjustment of the gap and since at each adjustment power level changes, it is absolutely essential for any measurements to work with a power level monitor so that corrections can be applied between individual measurements should these be taken before and after an adjustment has taken place.

As to the effect of voltage applied to the electrodes, once the sparking commences further increase in voltage makes it more violent, but as soon as radiation has become more or less regular no further increase in power output is observed, supporting the argument that the gap now breaks down at a fairly constant value of overvoltage. The actual voltages used varied between 10 and 18 kv and it was found that below 12 kv it was difficult to stabilise the sparking. That applies to electrodes less than 6 mm long. Longer electrodes require lower voltage. That figure is not borne out by all other published information. It seems that at least some of the earlier workers used sinusoidal supply and voltages of the order of 5000 V; it is possible, however, that they accepted a much greater fluctuation of power than was allowed here.

#### 4.2. Auxiliary gaps

With the auxiliary gaps about 1 cm long, the sparking was violent and loud and specially careful screening had to

be adopted to reduce direct pickup. It was found, however, that the gap between dipole and earth return electrode (positive) could be increased and when this reached some 2 or 3 cm the noise dropped off suddenly to a barely audible hiss. The sparking in the central gap was less violent but still plainly visible. All pickup vanished but no appreciable reduction in output power was observed. This is a most interesting observation because under these circumstances very little power is taken from the source and no noticeable wear or corrosion of electrodes takes place. Thus there is no need to use tungsten or platinum electrodes. Also bubbling is reduced.

Further experiments have shown that both the earth return and one of the radiating electrodes can be removed altogether provided the one remaining gap is flooded with paraffin oil or similar high strength liquid. This observation led to the development of a novel form of radiator (mark 2) described later.

#### 4.3. Spectrum analysis by Boltzmann interferometer

A long series of tests was carried out using various lengths of dipoles and varying the size of the waveguide at the receiving end, steps being taken to avoid any filtering by the metal box in which the radiators are mounted.

Since it is often difficult to decide what is the value of  $P_{\infty}$  which has to be subtracted from the instantaneous

values obtained from the interferogram before performing the computation leading to power spectrum ( $|g(\omega)|^2$ ), a computation has been carried out on an interferogram for two fixed but different values of  $P_{\infty}$  and also for two values of  $P_{\infty}$  slowly varying with distance (in case the interferogram is tilted). The results given in Fig. 60. show that the error in spectrum near the peak is negligible. Fig. 61. shows the spectrum of power (corrected for assumed crystal characteristics) for a dipole 0.5 mm dia, 8 mm overall length and another 0.5 mm dia, 12 mm overall length. From these one can deduce the following information:

$l$	$d$	$\lambda_0$	$\lambda_0/2l$		log. dec. $\delta$	
			observed	calculated	observed	calculated
8 mm	.5 mm	26.6 mm	1.67	1.51	1.0	.95
12 mm	.5 mm	40 mm	1.67	1.56	.6	.82

The calculated values of  $\lambda_0/2l$  were derived by assuming that half the dipole length is in air, 2 mm of its length is embedded in glass ( $k = 6$ ) and the rest is in paraffin oil ( $k = 2.25$ ).

It is seen that the calculated ratio of  $\lambda_0/2l$  agrees fairly well with observation when one considers the difficulty of estimating the depth of glass seal (the large

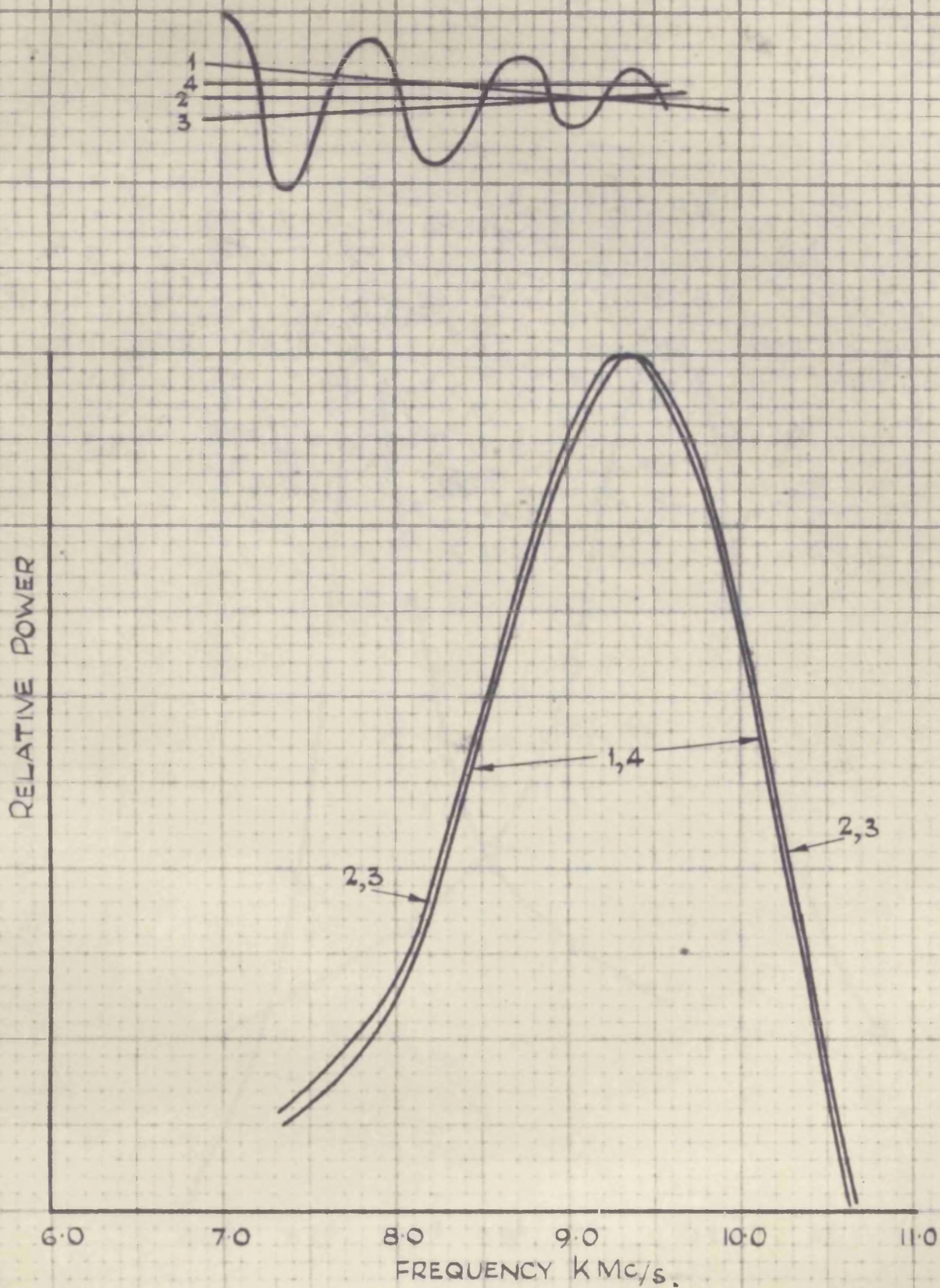


FIG. 60.

THE EFFECT OF SHIFTING THE ZERO AXIS OF THE INTERFERROGRAM ON THE COMPUTED SPECTRUM.

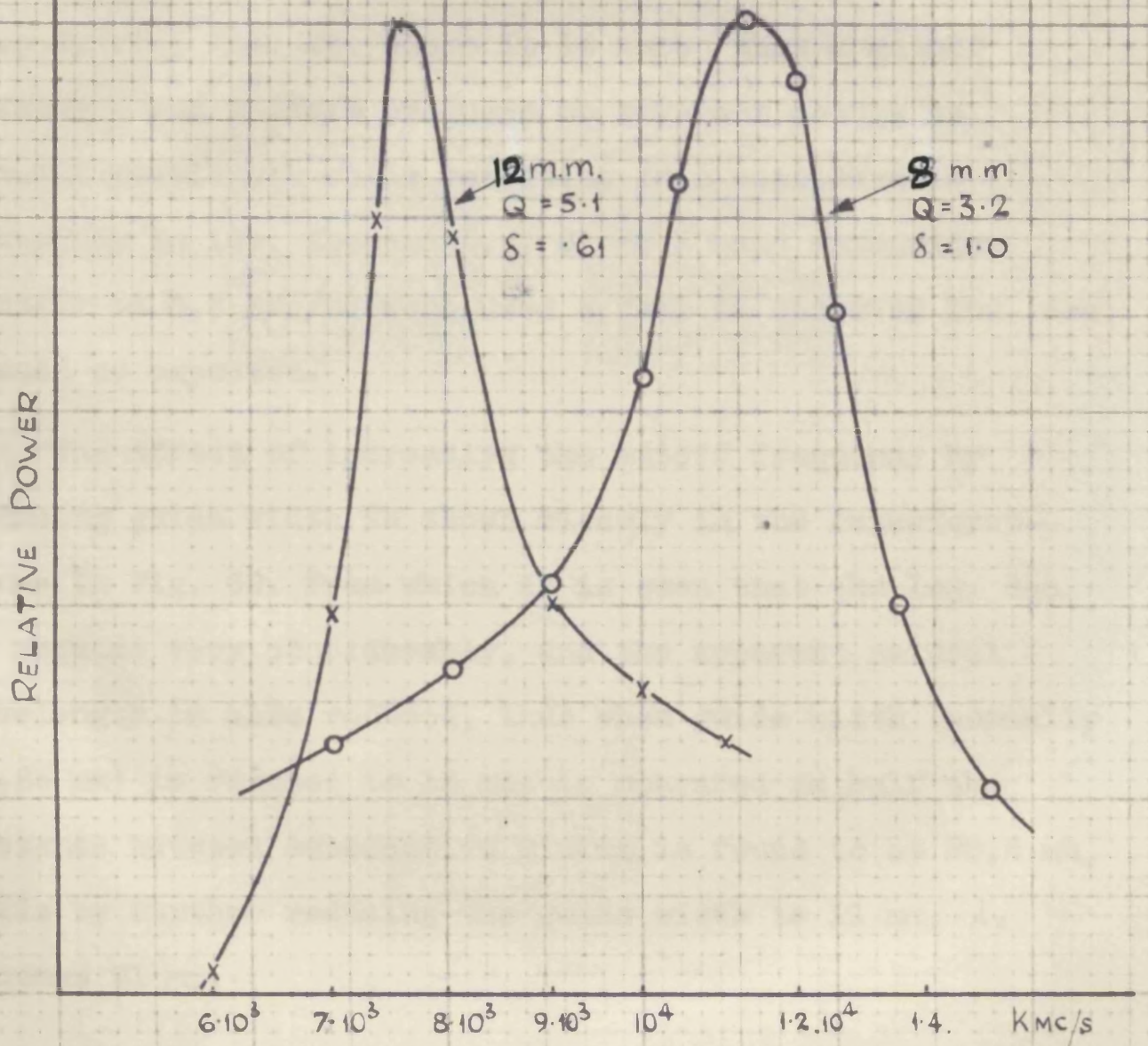


FIG. 61.

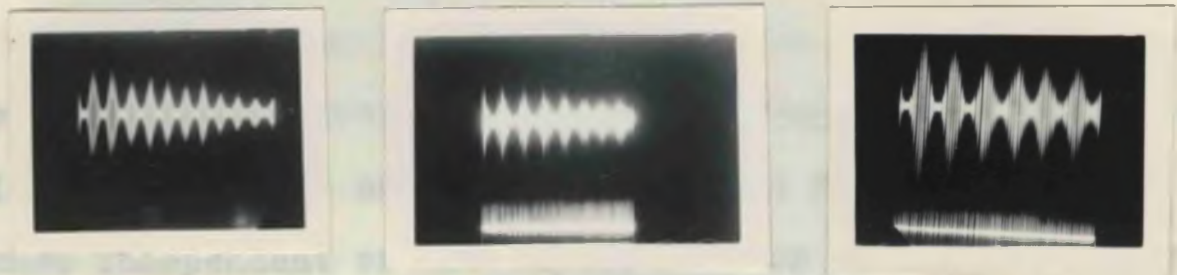
SPECTRA OF 8 m.m. AND 12 m.m. RADIATORS.

dielectric constant of glass makes an error here very pronounced on final results thus by assuming the depth of seal 1.5 mm instead 1 mm per each element, the ratio would increase to 1.84 for the 8 mm dipole). The divergence is much greater when one examines the log dec of the wave, which is especially pronounced at the longer wave. This, however, can be explained by reference to the discussion in part II, para.3.5.1., Fig. 28. where it is shown that a cutoff between 6 and 8 kMc/s produces no apparent change in natural wavelength while resulting in a considerable reduction in log. decrement. Since X band waveguides (cutoff at 6.6 kMc/s) were used a fall in observed log. dec. should be expected.

The effect of increasing the cutoff frequency by reducing guide width is shown clearly in the interferograms in Fig. 62. from which it is seen that the log. dec. is reduced very considerably, and the apparent natural wavelength is also reduced, thus when guide width (normally 22.85 mm) is reduced to 15 mm,  $\lambda_0$  measured as half the distance between consecutive minima is found to be 28.6 mm, while by further reducing the guide width to 11 mm,  $\lambda_0$  becomes 21 mm.

A certain irregularity can be observed in the interferograms when due to the frequency selective nature of the waveguide system and the resonant nature of dipoles, the

frequency spectrum... the single peak form to a double peak form... by Anderson

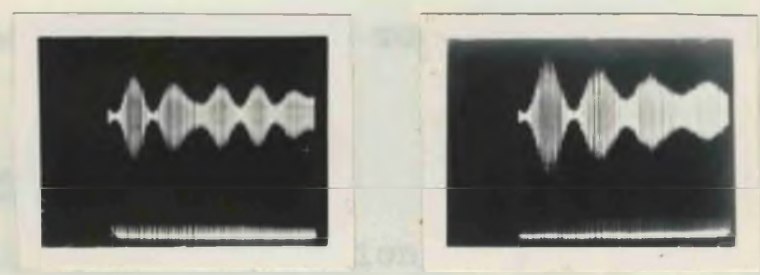


$\lambda_c = 20 \text{ mm}$

$\lambda_c = 22 \text{ mm}$

$\lambda_c = 30 \text{ mm}$

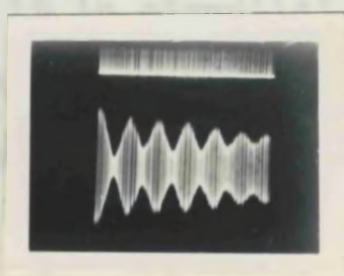
approach of frequency selection and control by filters appears the preferable one, and has been followed



$\lambda_c = 40 \text{ mm}$

$\lambda_c = 45 \text{ mm}$

The... Is initially the same as the... dipole... is again based on the... field changes caused by the electron



Effect of a post filter

Attempts were made by... Fig 62.

Interferograms obtained when out-of frequency is reduced also with a post filter

frequency spectrum deviates from the single peak form to a double peaked one. This has been observed also by Lindman and by Kawano. The effect is removed by increasing the  $Q$  of either the receiver or the sender waveguides system by a cavity or a filter, so that the received power spectrum becomes independent of the dipole form or shape. In view of the great technological difficulties in making and mounting minute dipoles the approach of frequency selection and control by filters appears the preferable one, and has been followed in all further work.

5. The mark II radiator

The principle of operation of this radiator is basically the same as that of mark I dipole. The mechanism is again based on the sudden field changes caused by the electron avalanche crossing the gap between the main and the radiating electrode under the stress of a very high field existing between them. That it is essential to have a high and non uniform field has been proved by a series of experiments in which the main electrode end was variously shaped. Only when this was fairly sharp was the sparking uniform and continuous enough to compare with that obtainable with mark I radiator.

Attempts were made to establish wherein lies the source of microwave radiation. To this end a very small metallic reflector was placed behind the radiator, where moving the

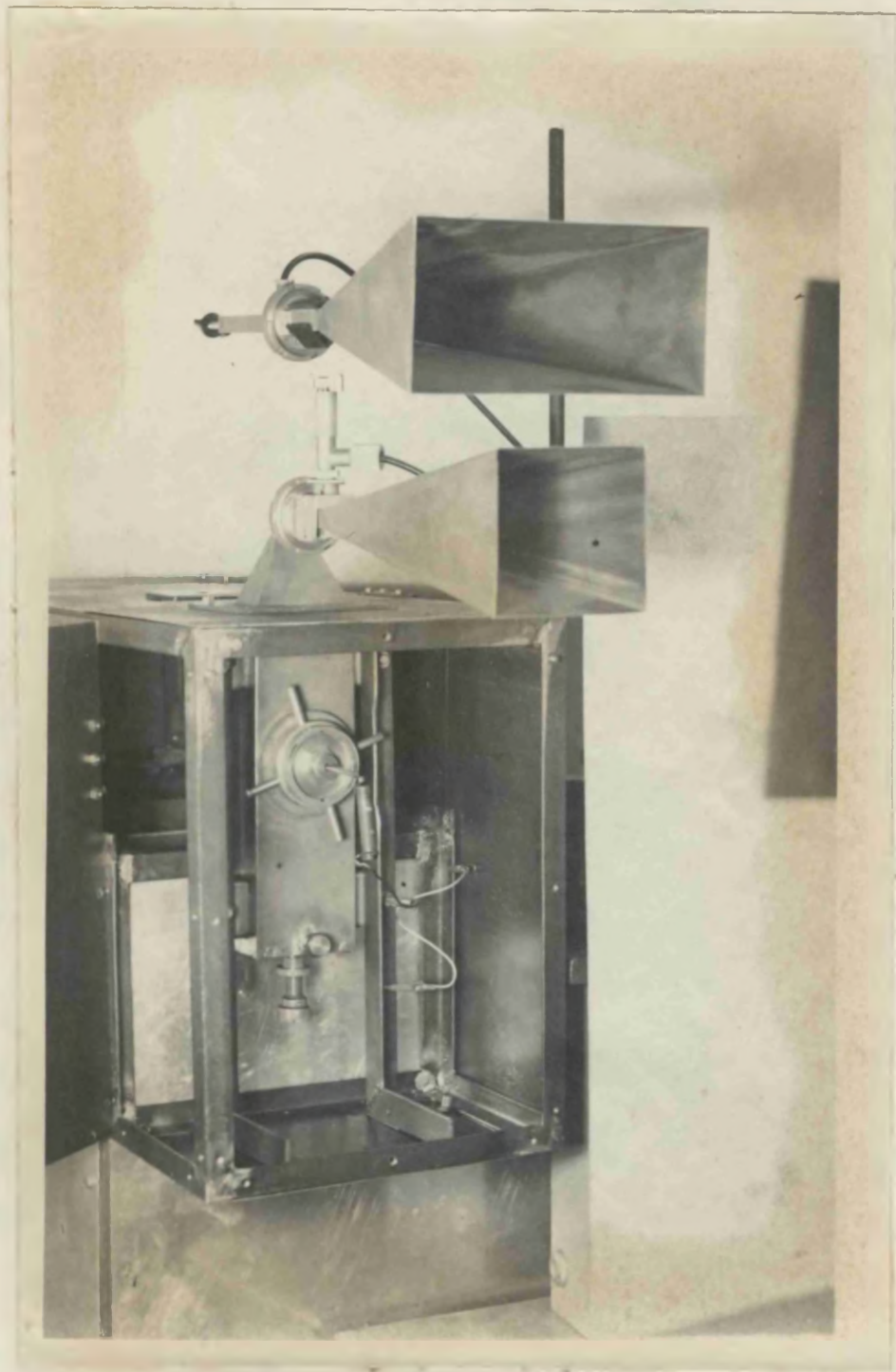


Fig 63.

Mark I radiator

with pulse generator

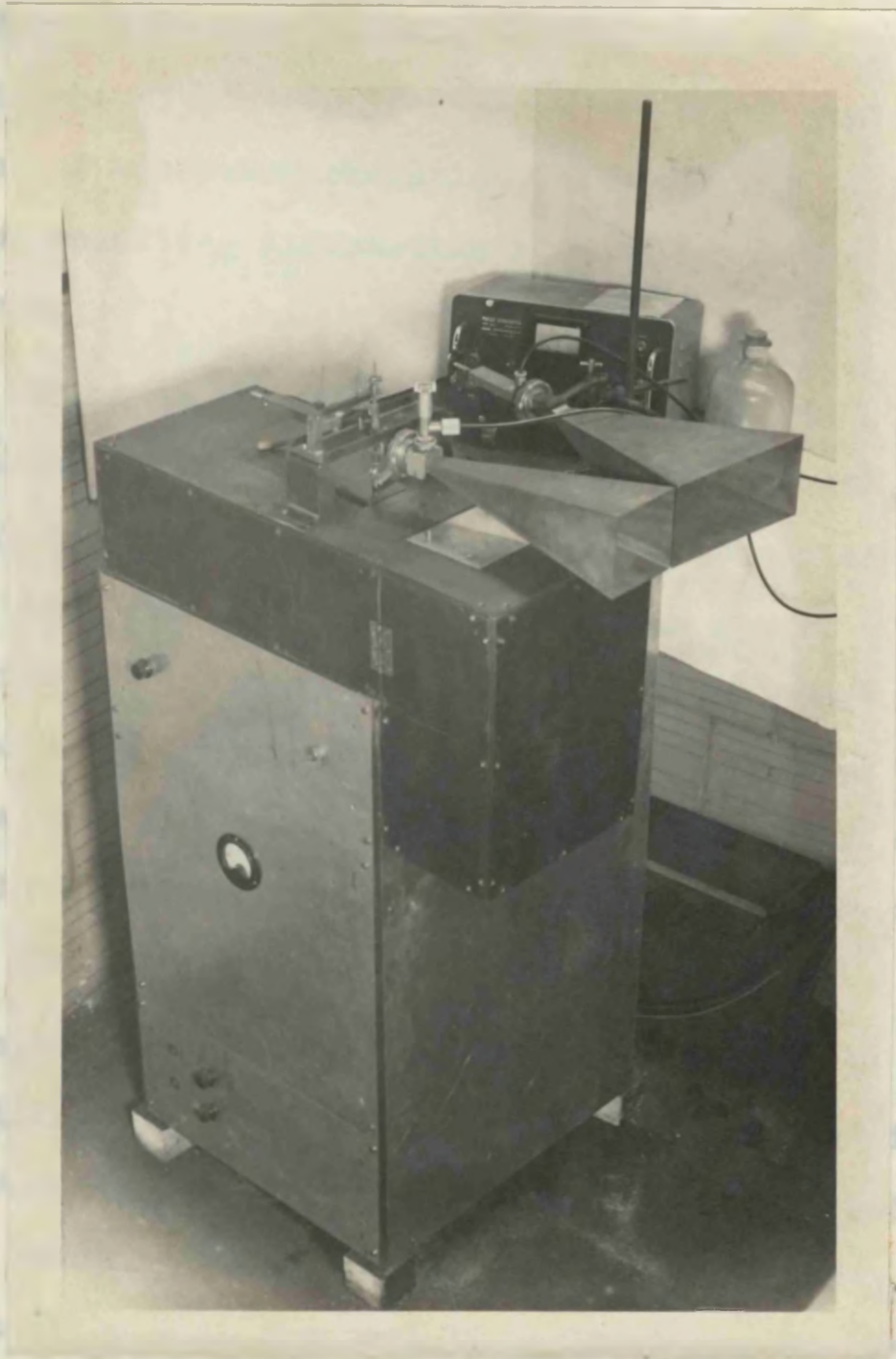


Fig 64.

Mark II. radiator  
with pulse generator

mirror up and down parallel with the electrodes it was found that invariably greatest output was obtained when the mirror was exactly behind the isolated element, supporting the view that it is the dipole itself and not the spark gap that is the source of microwave radiation, although the size of the mirror and resulting diffraction effects may introduce a large error.

The structure of this radiator permits it to be mounted easily across a waveguide, which may be fitted with a plunger at one end for tuning purposes. Otherwise output could be taken from both ends. A certain amount of energy escapes from the guide via the top and bottom apertures which need be fairly large to avoid discharges from the electrodes to guide walls. By circulating the oil or paraffin in the glass tube surrounding the electrodes prolonged operation results with few adjustments.

The operation of this type of radiator might be thought as not unlike the simple buzzer which, when mounted in a cavity, produces, by virtue of sudden discharges, wide band radiation extending into microwave region. However, experiments have shown that the mark II radiator has an advantage over the buzzer in power and stability because, first of all, the paraffin oil permits higher voltages across the gap before breakdown and, secondly, the short element radiator acts as a tuned circuit concentrating the radiation in the

region of its natural frequency.

The experiments have shown that, in fact, both the natural frequency and the log dec of the wave is identical with that obtained when two such elements forming a dipole are used in mark I radiator. Thus the single element acts as a quarter wave aerial.

Prolonged attempts were made to obtain millimetre waves by making the element very short since mounting is simpler as only one end of the element has to be accessible. This work was unsuccessful because as the element length is reduced below some 3 mm, the sparking becomes most irregular making measurements impossible. Thus once again one is forced to work with longer elements and to use filters for band selection.

On the author's advice, Professor Kawano has also experimented with a radiator mark II and in a private communication reported a trebling of the power he used to obtain with the conventional radiator.

## 6. Experiments with filters in the 1 to 3 cm region

Two types of filters were examined: the post and the iris type.

### 6.1. The post type filter

#### 6.1.1. Measurements at 3.1 cm

All the available solutions of impedance of a post in

guide are limited to wavelengths which are longer than guide width, which together with the complexity of the formulae make them of little use here. Instead one has to rely on experimental results.

The simple idea is to make a two-post filter as described in part II for the shortest possible wavelength and then to lengthen the filtered wave by increasing the effective separation between the posts by a capacitive screw placed between them. The shortest wave that can be filtered by this simple method is limited by relative magnitude of the insertion loss which the filter presents to the natural frequency of dipole and the amplitude of the power spectrum of the filtered band in the dipole spectrum. This is seen in Fig. 65, where solid line represents the transmitted power of a 3.12 cm wave against separation of two 6 BA screws right across the X band guide parallel to E vector (narrow side) while the dashed line represents the power spectrum of a decaying wave whose natural wavelength is 3.12 cm and log. dec. is 1. This figure shows that when the distance between the screws ( $d$ ) is less than 7.5 mm the transmitted wave will have in its spectrum a larger component around the 3.12 cm band than around the frequency for which it is tuned. The position is actually even worse than that shown because the decaying wave by virtue of its wide spectrum will suffer a smaller total insertion loss than a

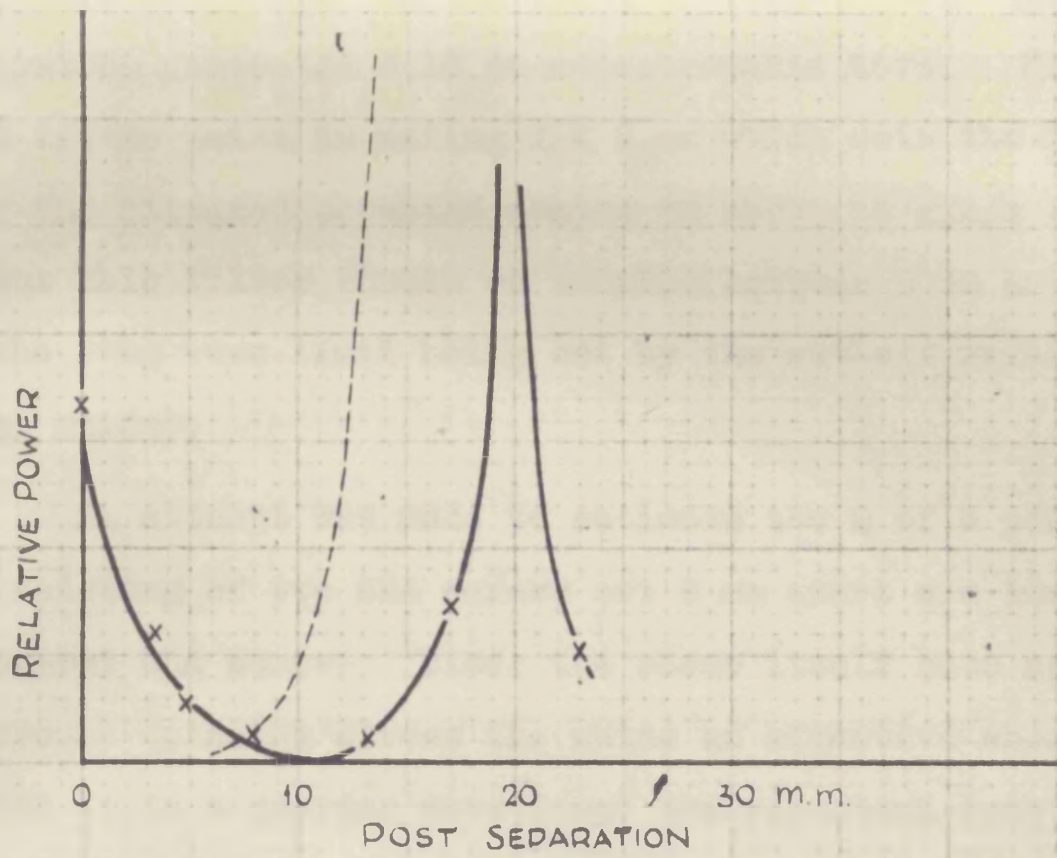


FIG. 65.

ATTENUATION OF A 3.14 CM. WAVE BY TWO  $\frac{1}{16}$  POSTS  
DASHED LINE REPRESENTS THE CORRESPONDING POWER  
SPECTRUM OF A DECAYING OSCILLATION WHOSE NATURAL  
WAVELENGTH IS 3.14 C.M. AND LOG. DEC. IS 1.

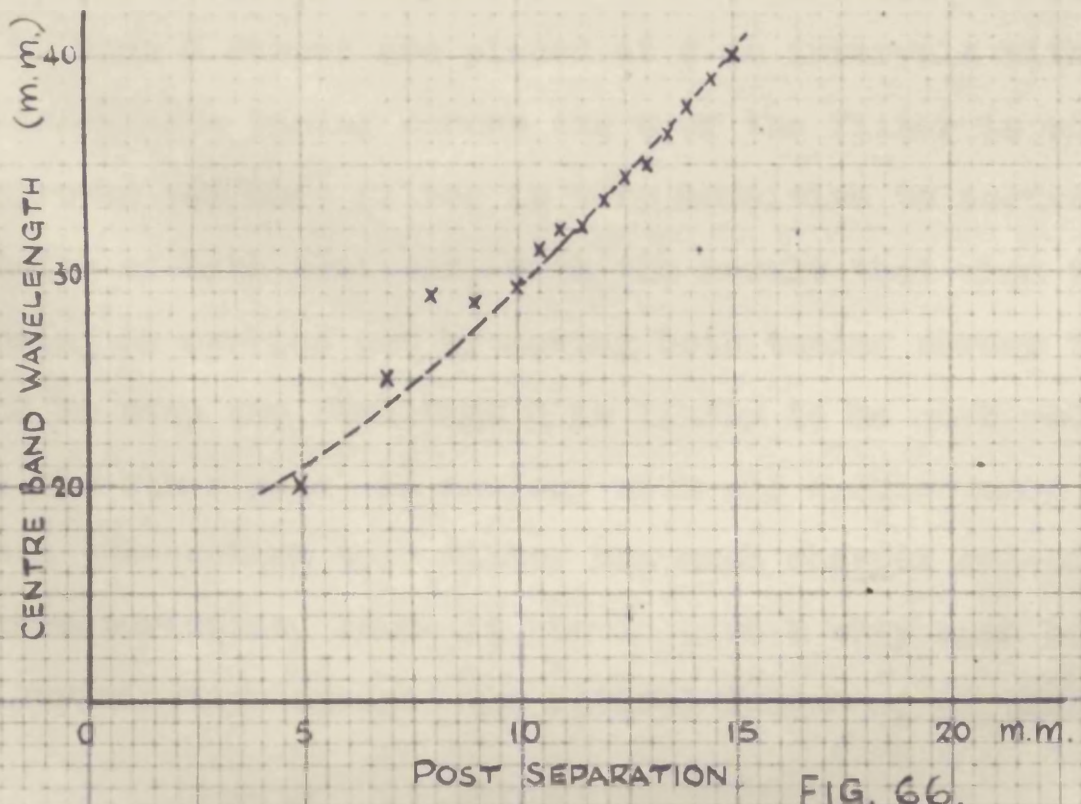


FIG. 66.

WAVELENGTH AT CENTRE OF FILTERED BAND VERSUS  
SEPARATION OF  $\frac{1}{16}$  POSTS IN X BAND GUIDE.

klystron generated 3.12 cm monochromatic wave. Hence, there is little point in making  $d < 8$  mm which sets the lower limit of the filtered waveband centre to about 15 Mc/s (2 cm). Thus this filter should be tunable between 2 cm and 4.5 cm (the long wave limit being set by the cut-off wavelength of the guide).

An attempt was made to estimate the Q of a post filter consisting of two 6BA screws set 8 mm apart and tuned by a central 6BA screw. Since the screw itself acts as a tuned circuit (placing across the guide an effective short circuit when it is a quarter wave long) the resultant spectral characteristics of the filter are double peaked. The actual "half-power" width of the spectrum could not be measured because of the klystron frequency limits, but Q was estimated as less than 20.

When 3 screws are placed at 8 mm intervals with 2 intermediate tuning screws the Q of the filter is somewhat improved but this filter is very sensitive to accurate tuning of both sections, with the result that when the tuning is carried out by moving both tuning screws together and in step the resultant Q is likely to be much reduced. On the other hand, in analogy with all double-tuned circuits this two-section type filter has much sharper cut-off characteristics, hence it should give a very much better discrimination against the natural frequency of the radiator

than the single section (two posts with one tune).

### 6.1.2. Measurements with spark generated wave

Boltzmann interferograms were taken with various arrangements. From these the spectra were computed using the Beavers Lipson 3° strips.

The expression for the length of a post filter is  $\frac{\lambda_g}{2\pi} (\pi + \tan^{-1} \frac{2}{B})$ . Since B of the post is negative (inductive) the filter is shorter than half guide wavelength. For  $\frac{1}{16}$ " posts which were used in the experiments Marcuvitz gives  $\frac{B}{\lambda_0} = 0.36$  at 3.2 cm. Since for a given guide width  $\lambda_g$  approaches  $\lambda_0$  as it is reduced well below cut-off, it would appear that by bringing the posts closer together ever shorter waves would be filtered out. In fact, this is not the case. Measurements on a variable post separation filter show that the wavelength to which the filter tunes decrease fairly linearly down to about 2 cm for a separation of 6 mm beyond which, however, no reduction in wavelength is obtained (Fig. 66.). This is in accordance with theoretical analysis and experimental measurement of the reactance of inductive posts according to which the inductance of the post increases as the ratio of post length to wavelength increases, i.e. B decreases causing  $\tan^{-1} \frac{2}{B}$  to increase rapidly. As B decreases, so does Q of the filter

$$\left[ Q \doteq \frac{1}{4} \left( \frac{\lambda_g}{\lambda_0} \right)^2 \left( -B \sqrt{B^2 + 4} \tan^{-1} \frac{2}{B} \right) \right]$$

so that according to the discussion of paragraph 3.4.2.,

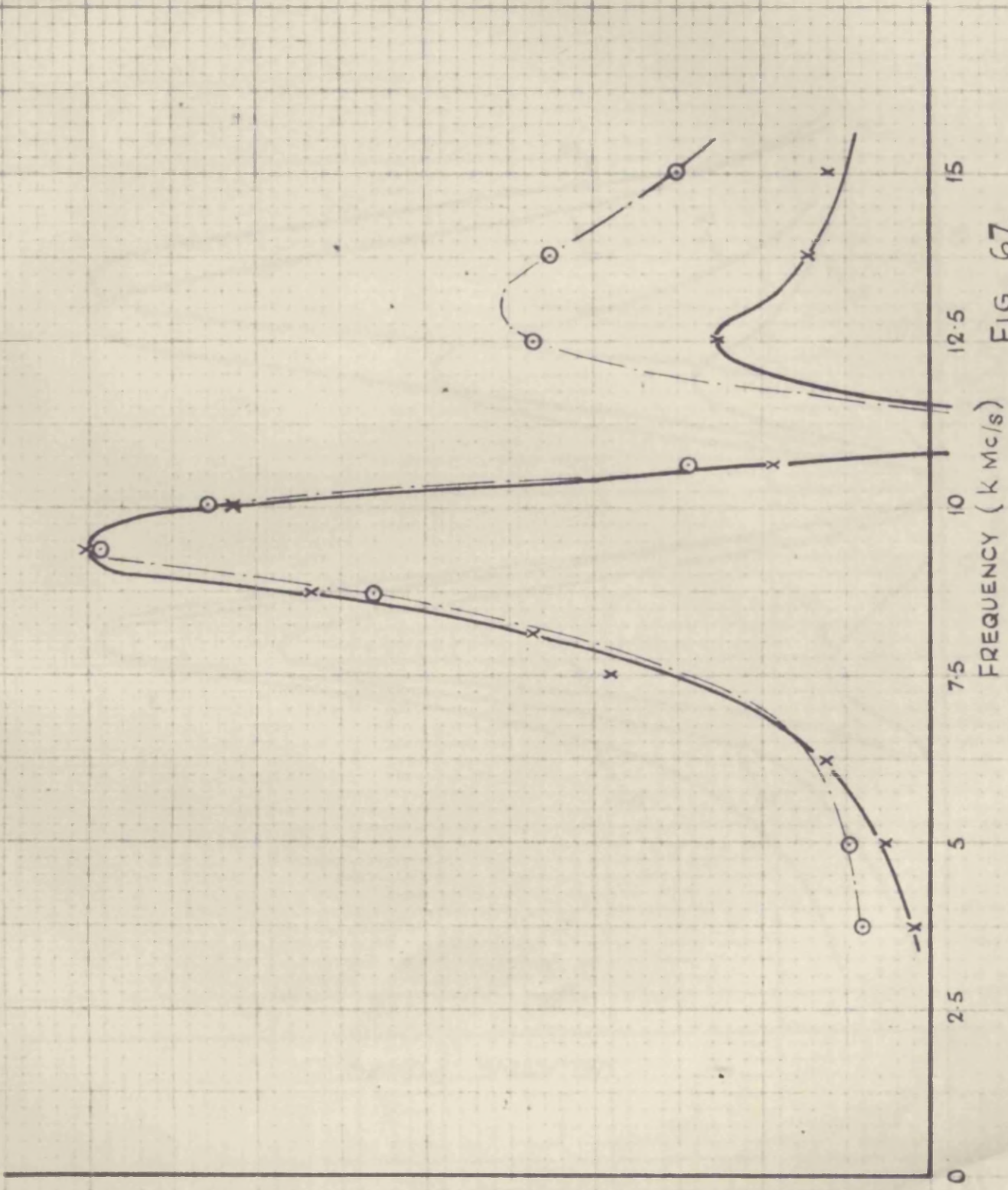


FIG. 67.

SPECTRA OF AN EXPONENTIALLY DECAYING WAVE FILTERED BY A TWO POST FILTER WHEN THE POST SEPARATION IS 4 m.m. (SOLID LINE) AND 8 m.m. (DASHED LINE). THE POST WERE 6 BASCREWS IN A X BAND GUIDE.

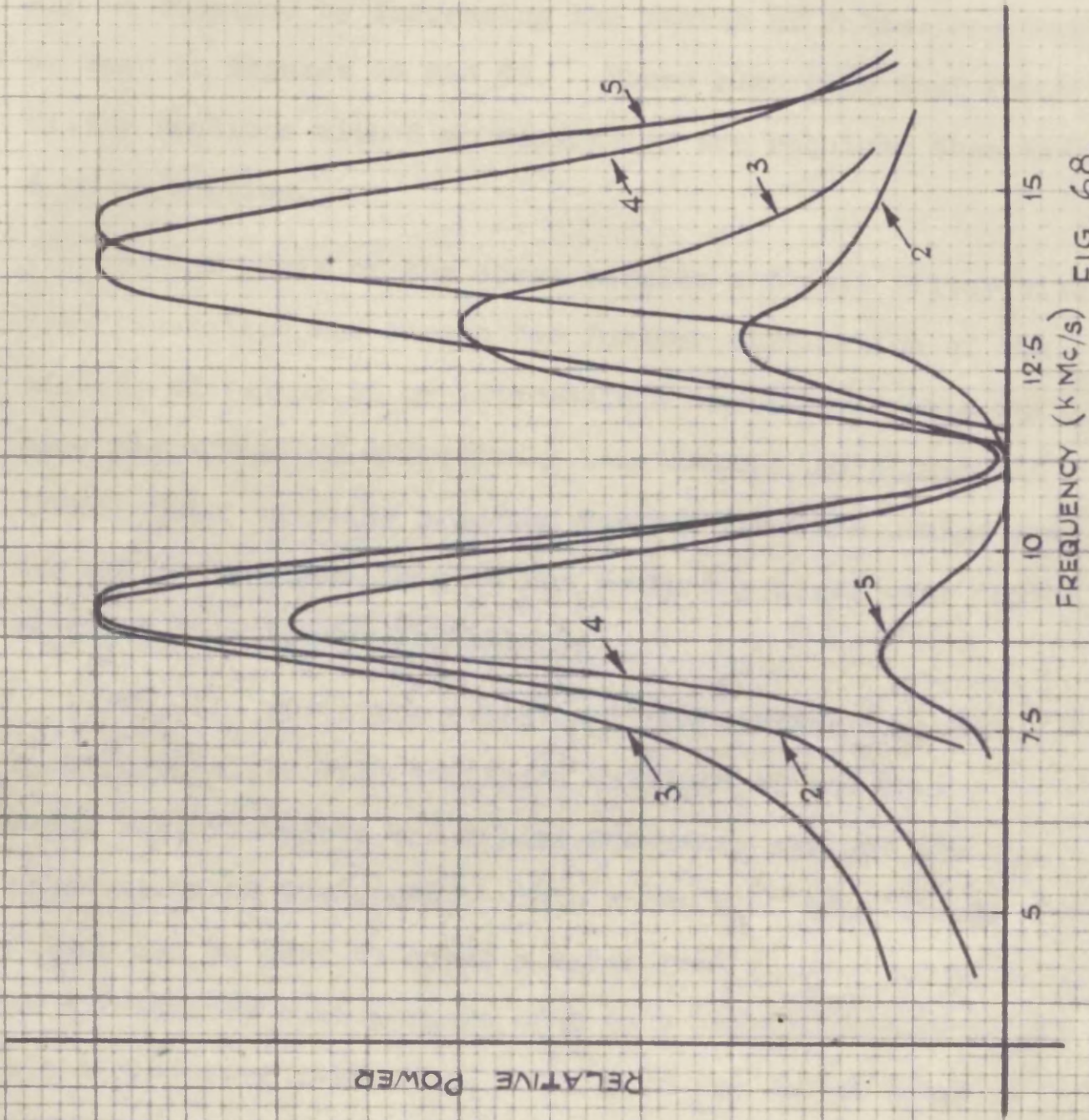
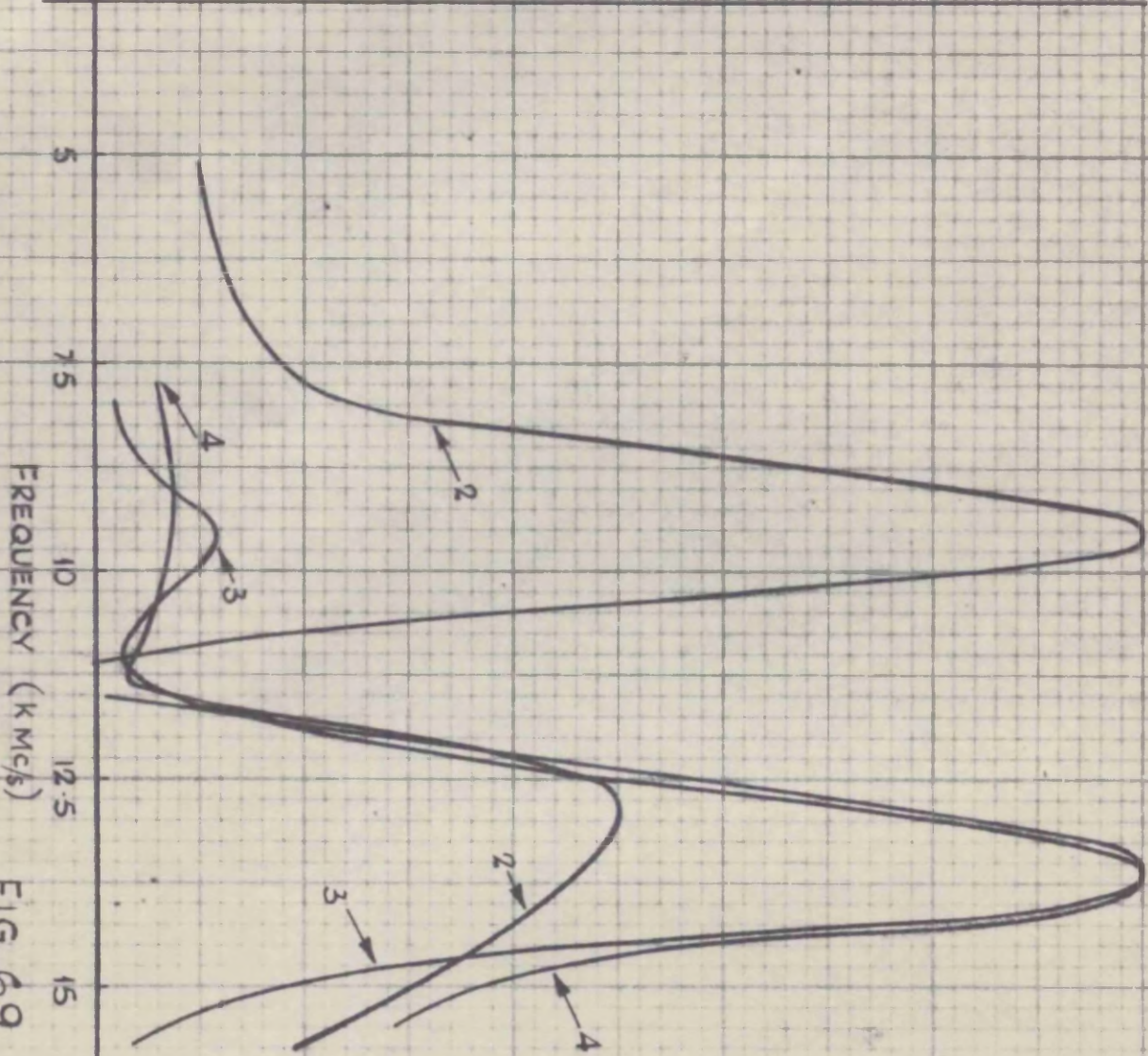


FIG. 68.

POWER SPECTRUM OF EXPONENTIALLY DECAYING WAVE PASSED THROUGH A POST FILTER CONSISTING OF 2, 3, 4 AND 5 POSTS SEPARATED 4 M.M. FROM ONE ANOTHER. POSTS ARE 6 BA SCREWS.

RELATIVE POWER



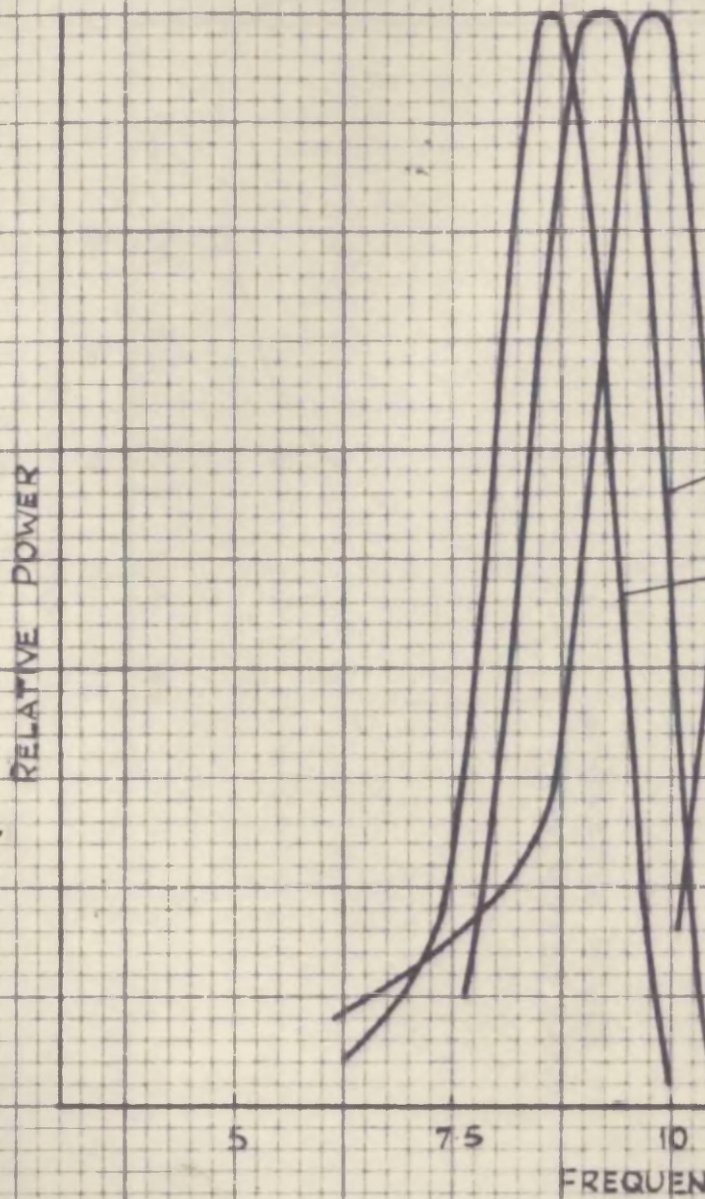
POWER SPECTRUM OF EXPONENTIALLY DECAYING WAVE PASSED THROUGH A POST FILTER CONSISTING OF 2, 3 AND 4, 6 BA POSTS, 8 M.M. APART FROM ONE ANOTHER.

FIG. 69.

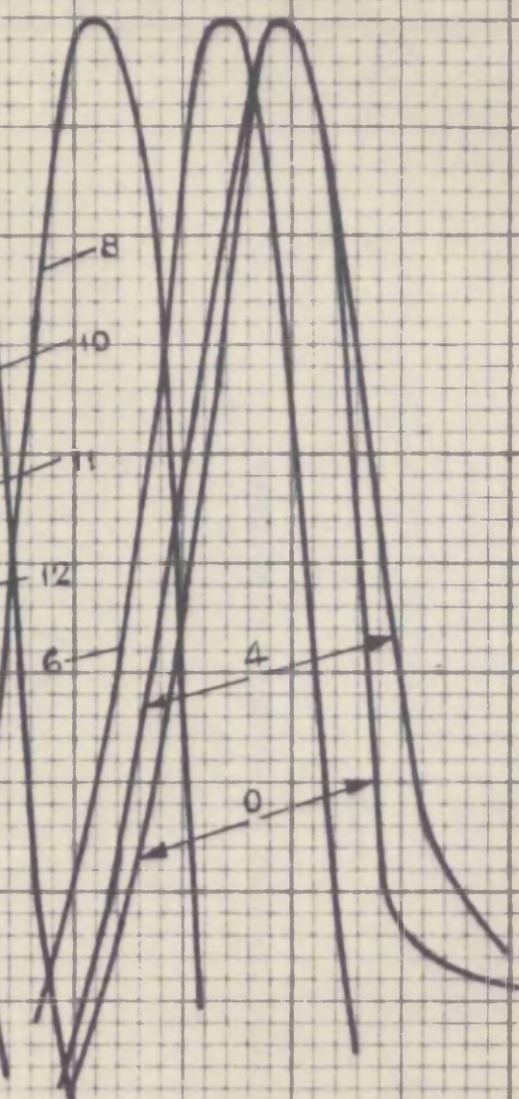
part II, the resultant spectrum has an ever increasing proportion of the longer waves characteristic of the spark generated wave. This is seen by examining figures which give spectra obtained with a post separation of 4 and 8 millimetres (Fig. 67.). An improvement in the spectrum can be obtained by increasing the number of filter sections as seen in Figures 68 and 69. These also show that fewer filter sections with 8 mm separation are required than with 4 mm separation.

On the basis of the above results a 3 post filter with 8 mm separation was chosen for further examination of the effects of tuning it by intermediate capacitive posts which have the effect of effectively lengthening the filter the larger their capacity i.e. the further they are pushed into the guide (provided they do not reach the cross over depth at which they become inductive).

Fig. 70. gives the results of computation of power spectra obtained with different settings of the tuning posts while Fig. 71. plots the centre frequency against depth of penetration of the posts. This shows that this simple filter can be made to cover a range from 7 kMc/s to 14 kMc/s or a frequency tuning range of 2 to 1 not achievable by any other microwave generator. The Q of the filter when corrected according to Fig. 33. part II (interferograms only 2 to 3 wavelength long could be recorded) is of the



SPECTRA OF FILTERED WAVE FOR  
REFER TO N° OF TURNS OF A 6 B A



12.5  
15  
CY KMc/s

FIG. 70.

FOR VARIOUS DEPTHS OF THE TUNING SCREW. THE NUMERALS  
A SCREW (PITCH = 133 mm) USED FOR TUNING.

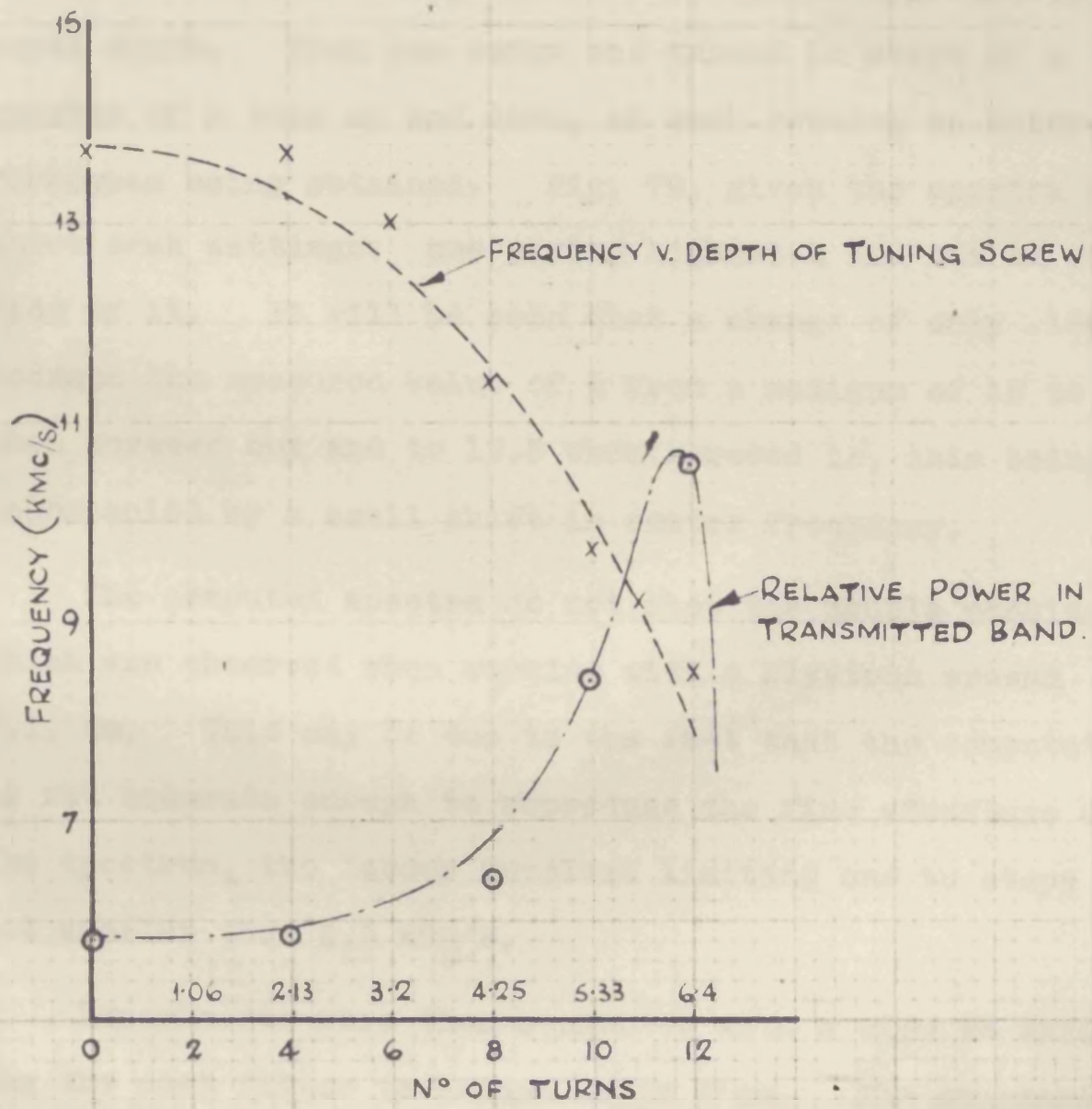


FIG. 71.

FREQUENCY AT CENTRE OF BAND AND RELATIVE POWER IN THE BAND AT VARIOUS DEPTHS OF TUNING SCREW.

order of 10. This figure is lower than that obtained for the filter when tested around 3.1. cm because of the fact that it is unlikely that the two filter sections were identical hence an equal depth of tuning post is not likely to mean that both are tuned to the same frequency. To check this point a series of measurements was carried out in which both the tuning screws were set at approximately equal depth. Then one screw was turned in steps of a quarter of a turn up and down, at each setting an interferogram being obtained. Fig. 72. gives the spectra at three such settings: one giving highest Q and one on either side of it. It will be seen that a change of only .133 mm reduced the measured value of Q from a maximum of 19 to 14 when screwed out and to 12.5 when screwed in, this being accompanied by a small shift in centre frequency.

The computed spectra do not show the double peaking which was observed when working with a klystron around 3.1. cm. This may be due to the fact that the computation is not accurate enough to reproduce the fine structure of the spectrum, the labour involved limiting one to steps not smaller than 0.5 kMc/s.

Experiments were then conducted with a view to extending the post filter technique below 2 cm. . The standard X band guide WG16 (0.4" x 0.9") was reduced gradually to fit size WG20 (0.2" x 0.5"), and the smaller guide was fitted

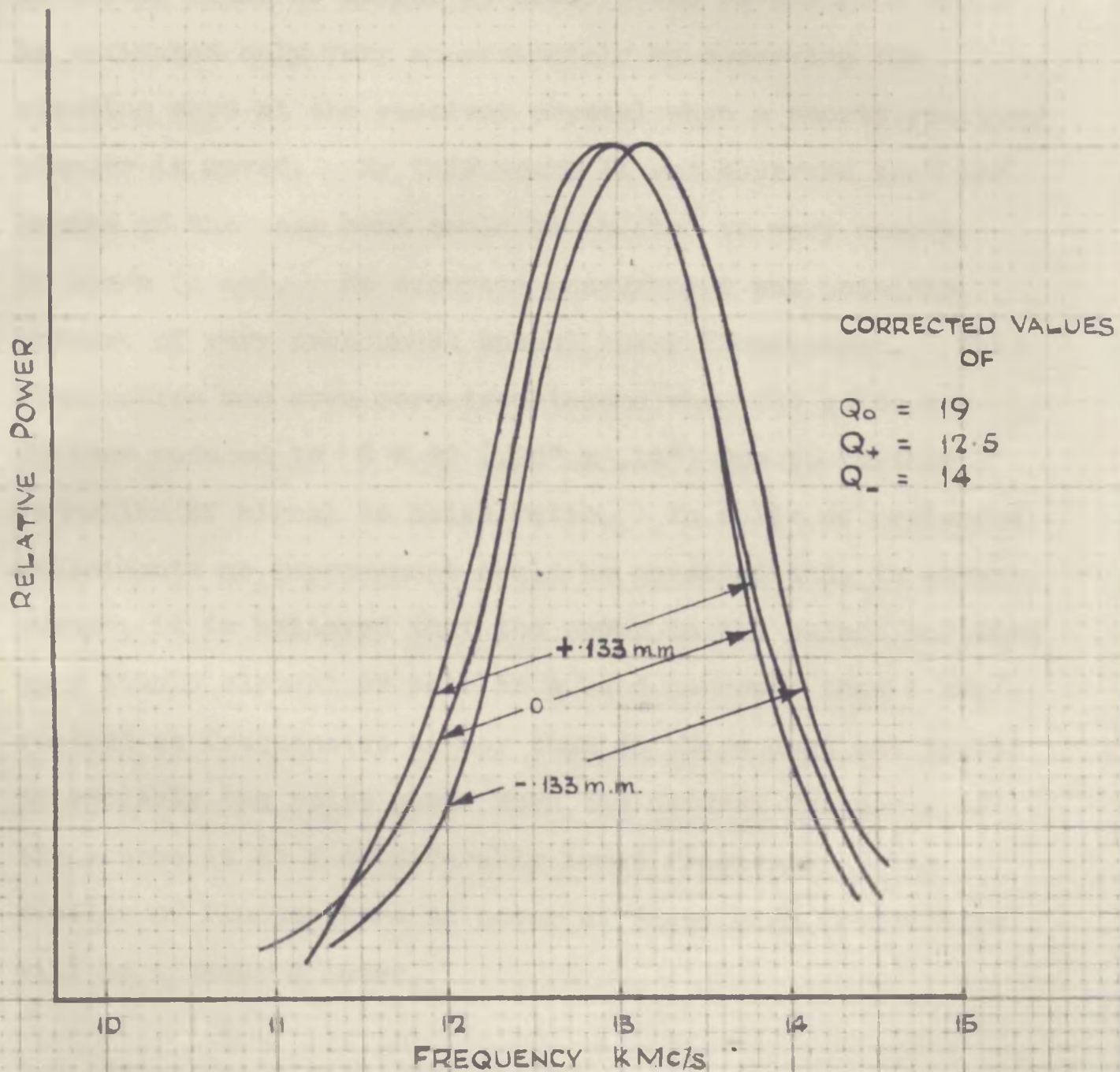


FIG. 72.

EFFECT OF DISPLACING THE SECOND TUNING SCREW FROM  
THE POSITION OF OPTIMUM TUNING (0) UP AND DOWN BY  
¼ TURN OF 6 BA SCREW. (.532 m.m. PITCH).

with adjustable posts. While the immediate effect of reducing the guide dimensions was to reduce the band centre frequency from 4 to 2 cm the introduction of the filter reduced the power level to so low a value that the interferometer could no longer be used. The wavelengths could be estimated only very approximately by observing the standing wave at the receiver crystal when a shortcircuiting plunger is moved. By this means it was observed that the centre of the pass band could be shifted to very nearly 30 kMc/s (1 cm). No accurate measurement was possible because of very pronounced output power fluctuation. This fluctuation was even more troublesome when the guide was further reduced to S W 22 (.28" x .14") due to further reduction of signal to noise ratio. In spite of prolonged experiments no improvement could be obtained and, in consequence, it is believed that the power in the pulses radiated by a simple element or pair in a band narrower than 1 kMc/s centred at frequencies higher than 30 kMc/s does not exceed appreciably the noise power when the natural frequency of the source is at a considerably lower frequency. The problem of fluctuations of power at these high frequencies will be discussed later.

## 6.2. Experiments with iris filter

Various iris filters were designed and tested in an attempt to develop one giving the maximum range of tuning.

After lengthy experiments an iris filter was built having the following dimensions: Iris width 0.2", filter length  $\frac{13}{32}$  ; diaphragm thickness  $\frac{1}{16}$  in a standard X band guide (.9" x .4"). This filter should tune in theory to 2 cm with a Q of 90.

A central 6BA screw was provided to tune the filter. The resultant spectra for various depths of the tuning screw are given in Figures 73 and 74. It will be seen that for a small insertion of the screw two peaks are present one due to the natural frequency of the generator, the other due to the filter. As the filter frequency is reduced, the filter response begins to predominate (see discussion in para. 3.4.2. part II). The frequency range over which this filter can be usefully employed extends from 7.1 kMc/s (4.2 cm) to 12.0 kMc/s (2.5 cm) with Q well above 20 and possibly as high as 100 (the correction factor at this range is so large as to make the accurate estimate of Q impossible unless a much longer interferogram can be obtained). Thus this filter gives a bandwidth considerably narrower than 1 kMc/s. The output power falls off so rapidly at the upper frequency end that it is unlikely that useful amounts of energy could be obtained in such a narrow band at wavelengths shorter than 2 cm (see also table of Fig. 54., part II). Some improvement can be obtained by reducing the radiator length, but that again leads to technological difficulties incommensurate with the improvement in power output.

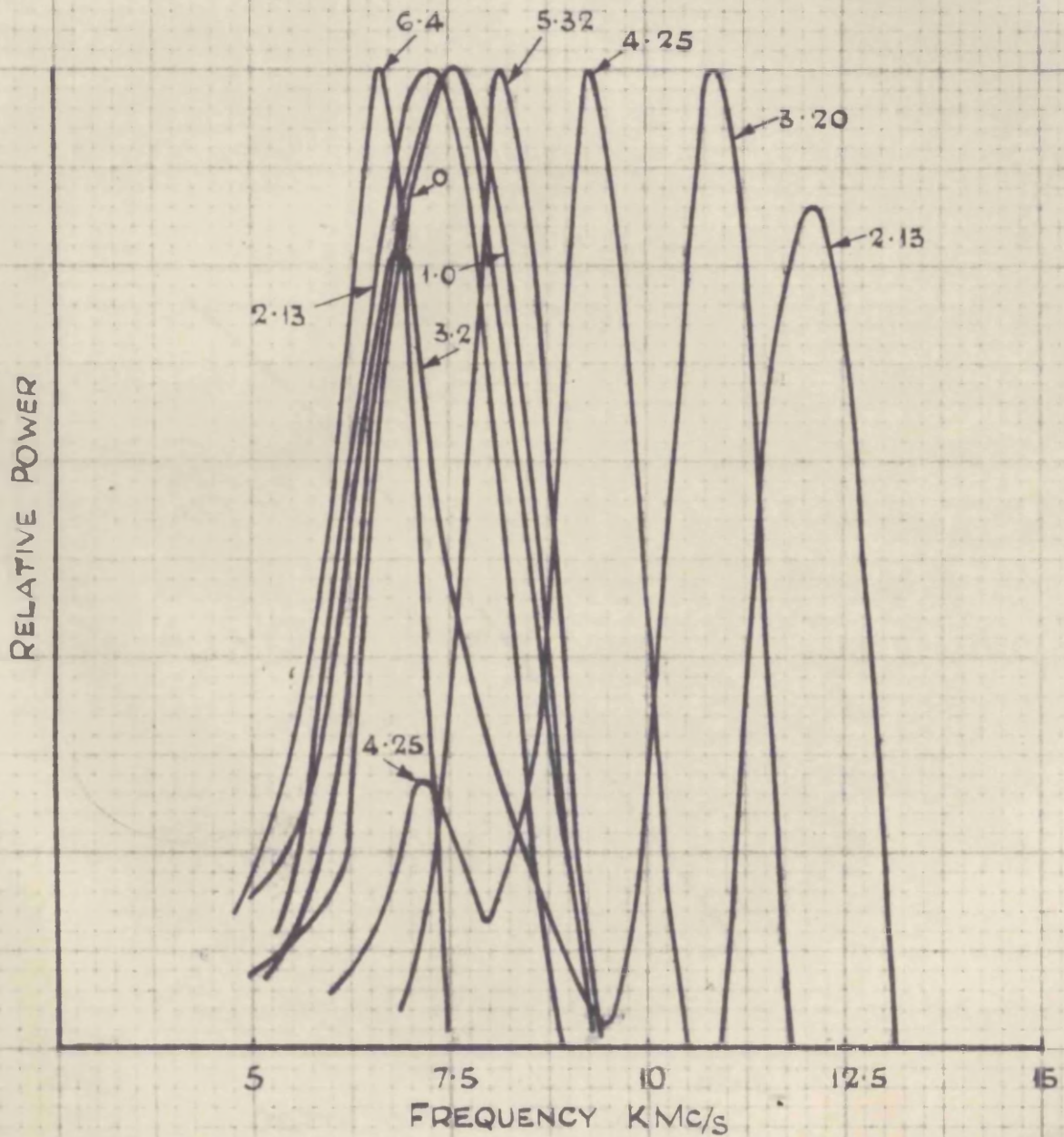


FIG 73.

SPECTRUM OF WAVE PASSED THROUGH AN IRIS  
FILTER FOR VARIOUS DEPTHS OF TUNING SCREW  
(DEPTH INDICATED BY NUMERALS DENOTING MM)  
CORRECTED  $Q > 30$ .

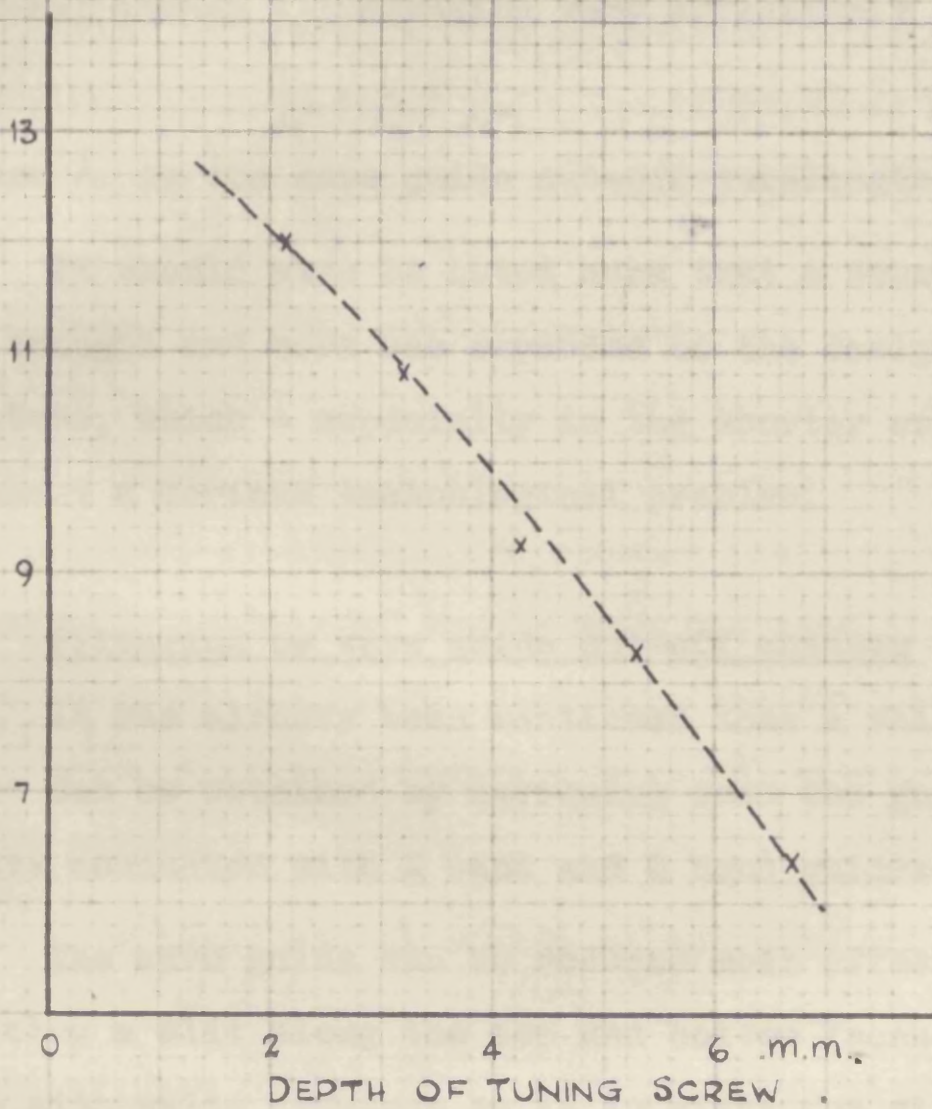


FIG 74.

CENTRE BAND FREQUENCY VERSUS DEPTH OF TUNING SCREW FOR THE IRIS FILTER.

When this filter was used in conjunction with a standing wave meter, very clear and distinct standing waves could be observed and measured. Without the tuning screw this standing wave had a separation between minima of just over 1 cm showing that the filtered wave band centre lies close to  $\lambda_0 = 2$  cm, the SWR meter itself being used to remove the longer wave peak. As the tuning screw was inserted, the measured  $\lambda_g$  increased until it eventually extended over several inches illustrating very effectively the relation

$$\frac{1}{\lambda_g^2} = \frac{1}{\lambda_0^2} - \frac{1}{\lambda_c^2}$$

where  $\lambda_c$  is the wave guide cut-off wavelength.

It should also be noted here that a considerable amount of thought and work was expended on the design of iris filters, which - especially in the shorter wavelength range - present a serious technological problem.

#### 7. Filtering by wave guide cut-off changes

It has already been mentioned that a shift in output band can be obtained by narrowing down the guide. Experiments conducted with X band and Q band guides confirm this.

The wave guide can be reduced most effectively by cutting a slit along the top and bottom faces and pressing the side walls together so as to close the slit. This method is familiar in phase shifting techniques. It gives excellent results with spark generators. A simple Q band

squeeze section has resulted in a shift of output band from 12 mm down to 8 mm with a bandwidth of the order of 3 to 5 kMc/s.

One can also go in the opposite direction by introducing into the guide a dielectric of constant  $k$ , which lowers the cut-off frequency by  $\sqrt{k}$ . Experiments with polystyrene, perspex and glass filling again confirmed these results. The difficulty here is in that the changes can only be obtained in steps depending on the available dielectrics, although the development of polystyrene foam of different density provides a suitable range of filters.

### 8. Experiments with wire netting

It has been mentioned in part II (para. 4.4.1.) that wire gratings could be used to attenuate longer waves in the radiator spectrum. To examine their effectiveness, brass wire netting of square mesh was used in place of the wire grating. Fig. 75. gives the spectra resulting from netting of different mesh and Fig. 76. gives the relative power output.

An attempt was also made to use wire grating Fabry Perot interferometers. For this purpose two identical wire nettings were placed at a distance apart at which the output was at a maximum. The resultant spectrum for mesh 4" is given in Fig. 77. It will be observed that while the wire mesh does tend to reduce the bandwidth of the radiation

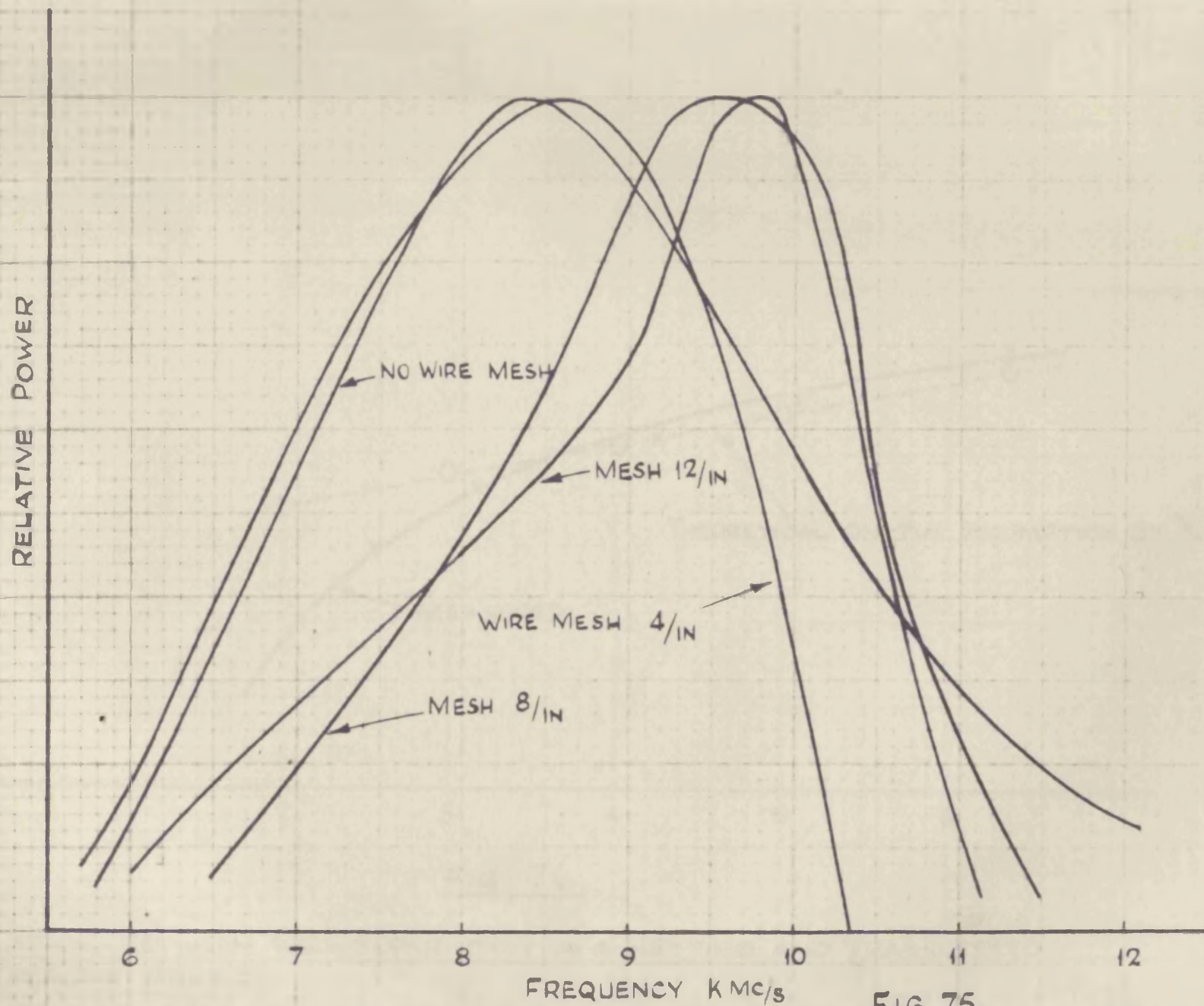


**FIG 75.**

SPECTRA OF RADIATION FROM A DIPOLE WHEN A WIRE NETTING OF DIFFERENT MESH IS INTERPOSED BETWEEN SOURCE AND RECEIVER.

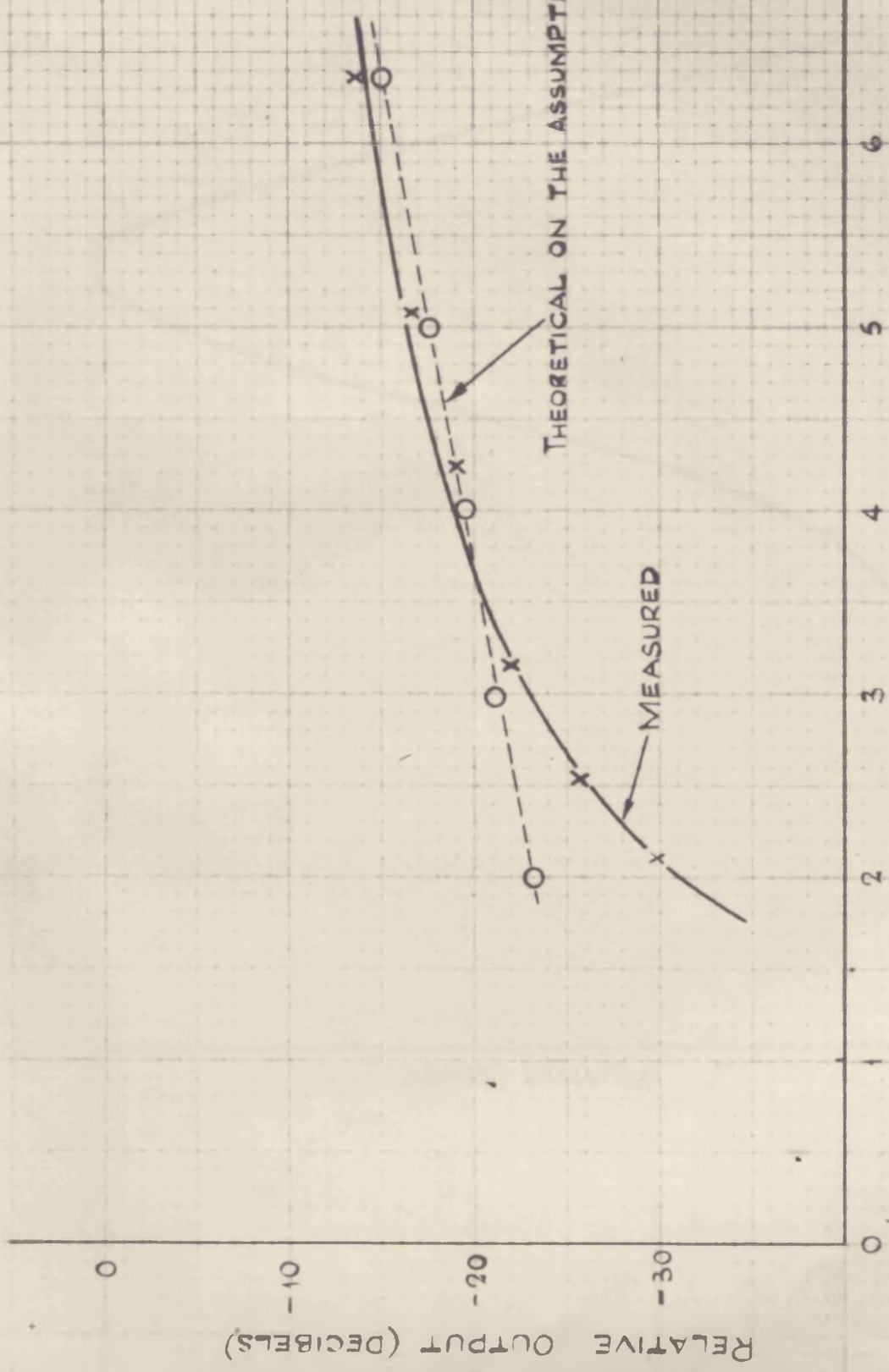
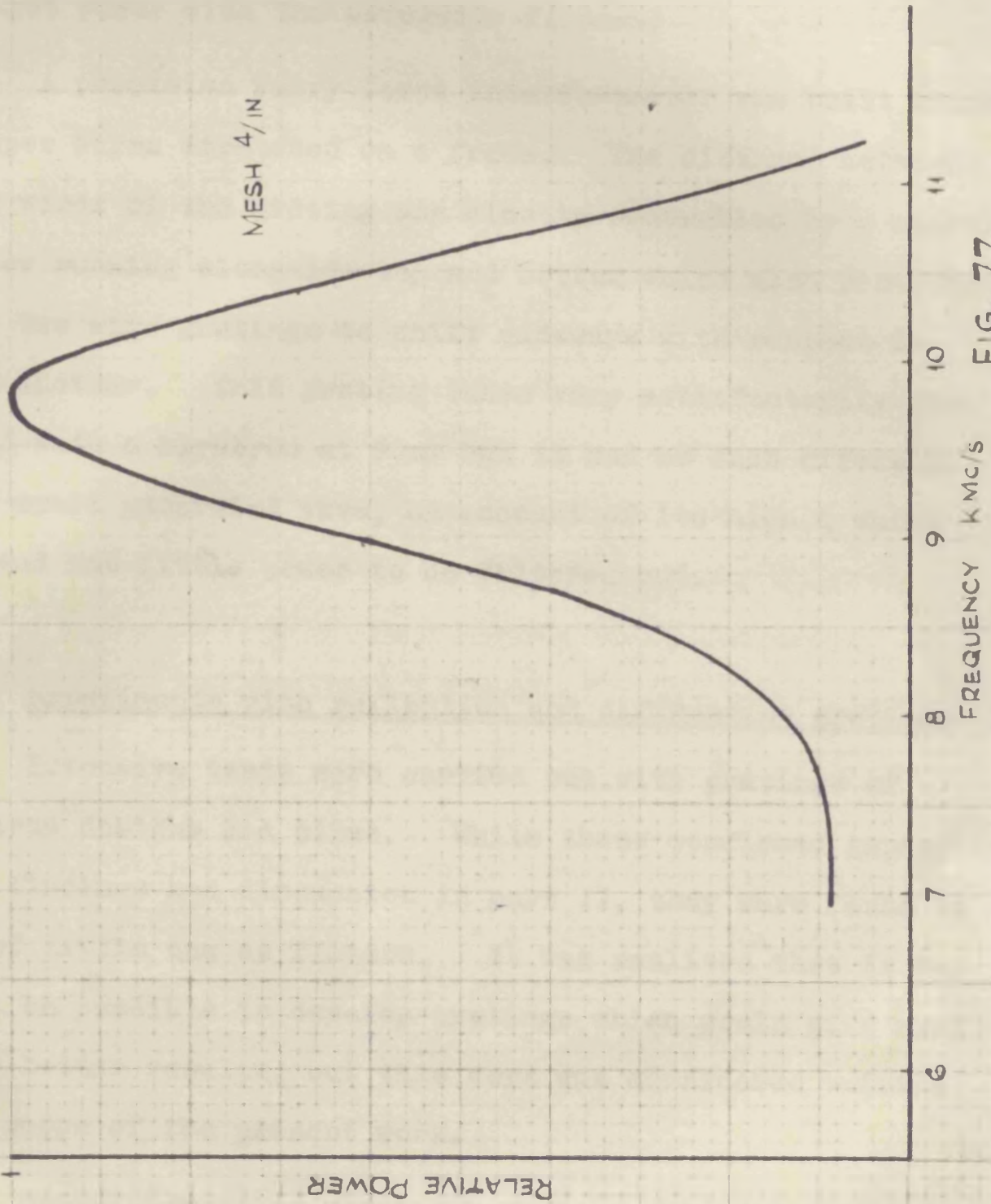


FIG. 76.

RELATION BETWEEN WIRE SEPARATION IN A NETTING AND TRANSMITTED MICROWAVE POWER.  
DASHED LINE IS OBTAINED BY ASSUMING A MONOCHROMATIC SOURCE AT WAVELENGTH EQUAL TO THE NATURAL WAVELENGTH OF RADIATION FROM THE DIPOLES.



FREQUENCY SPECTRUM OF RADIATION FROM A DIPOLE WHEN TWO WIRE NETTINGS SEPARATED BY 15 MM ARE INTERPOSED BETWEEN SOURCE & RECEIVER. FIG. 77.

and a further improvement is possible by using a Fabry Perot arrangement, the method does not compare in usefulness and output power with the waveguide filters.

A precision Fabry Perot interferometer was built using copper wires stretched on a frame. The distance between the wires of the grating was closely controlled by a spiral screw running alongside top and bottom which also permitted the two wire gratings to shift sideways with respect to one another. This grating tuned very satisfactorily when used with a klystron at 9 mm but it had no such effect on the spark generated wave, on account of its high  $Q$  which caused too little power to be filtered out.

#### 9. Experiments with reflection and diffraction gratings

Extensive tests were carried out with gratings of various designs and sizes. While these confirmed generally the findings and discussion in part II, they were found to be of little use as filters. It was realised that it may well be possible to develop gratings which would give very much better results, but this work was considered outside the scope of the present work.

Some interesting results have been obtained using slits and slit gratings in confirming the applicability of Kirchhoff's solution when the source is non-monochromatic.

These results together with the underlying theory are given in Appendix III. published by the author. The arrangement of screen and slits which are fully adjustable has been developed for this purpose. The patterns were obtained by a photographic technique described earlier.

The most disappointing were experiments with the previously described echellette grating. Due to the small errors in the alignment of the individual mirrors and to the difficulty of obtaining a parallel beam and to the nature of radiation the resultant patterns were so irregular as to be meaningless and work on this had to be suspended at this stage. Much greater degree of accuracy than was possible with the existing workshop facilities seems necessary to achieve useful results.

#### 10. Output power

No absolute measurements of power were carried out because the wide band of the radiation involves in the concept of power the received bandwidth. Thus the results of power measurement are only applicable to this particular set up.

However, some measurements were carried out to gauge the order magnitudes involved. These have shown that in the case of radiator mark I the output voltage from the crystal (matched) in a guide directly connected to the

chamber in which the radiators are mounted was of the order of 10 mV peak with 6 mm dipoles. When an iris filter (iris width .2") was used reducing the bandwidth to about  $\frac{1}{100}$  of centre frequency, the peak output corresponding to various centre frequencies was as given below (agreeing well with the results of analysis given in

$f_0$	$\lambda_0$	$\hat{V}_{out}$	Power output relative to total
7.5 kMc/s	4.0 cm	500 $\mu$ V	.25%
9.4 "	3.2 cm	200 $\mu$ V	.04%
11.1 "	2.7 cm	20 $\mu$ V	.0004%
15 "	2.0 cm	10 $\mu$ V	.0001%

While this shows that the available signal is not only very low but also falls off very rapidly at higher frequencies it should be realised that the output is in the form of pulses at a pre-determined repetition frequency, hence not only can high gain A.C. amplifiers be used but these can be gated (coherent detectors) to reduce their noise very considerably.

The total power output from a 6 mm dipole was estimated by direct measurement of crystal current to be of the order of 20  $\mu$ W at the maximum pulse repetition frequency of 5200 c/s,

100

falling off linearly with frequency. This linear relation indicates that it should be possible to raise the frequency still higher before the sparking would become irregular and power cease to increase in proportion. This would require a corresponding increase of input power which was not available. In fact the existing pulse generator when run at 5200 c/s could only produce a 12 kV pulse without a serious overload. It will be noted that previous workers who operated with pulses of long time rise have reported that pulse frequency had to be kept low (between 80 and 400 per sec), showing that sharp pulses with short time rise and long gaps resulting in less violent sparking used here offers greater powers than obtainable hitherto.

Measurements of power against pulse peak voltage have shown that although power output increases with pulse voltage the increase is small especially above 12 kV, and is due primarily to greater regularity of output caused by the increased overvoltage across the paraffin oil gap.

#### 10.1 Output power fluctuations at the upper frequency range

The cause of the increased fluctuation of power observed as one appreciably increases the cut-off frequency has been examined critically and appears to lie in the random character of the spark discharge mechanism. It is clear that the radiated spectrum has its "source" in the sudden

voltage change which occurs while the electron avalanche builds up and crosses the gap as explained in para. 1 of part II. Since the  $Q$  of the radiator (acting as a tuned circuit) is very low a considerable latitude is allowed in the avalanche current  $I = \frac{eu}{d} \alpha \cdot ut$  which, in fact, has a large random variation. The resultant oscillation, however, has a somewhat different spectrum at each pulse: the steeper the pulse, the larger the high frequency components in the spectrum. Thus, within an octave or two of the natural frequency the spectrum is fairly uniform and power fluctuations can be kept low by a proper degree of overvoltage but for even higher frequencies the individual spectra diverge more and more resulting in pronounced power fluctuation as between one pulse and another. This situation is made worse by the fact that the radiators oscillate at harmonics of natural frequency if these are excited, but the overvoltage required to excite frequencies in excess of  $3 \cdot 10^{10}$  c/s has been shown to be difficult to attain even with paraffin oil in the gap, hence only some pulses will contain these harmonics. The problem is thus seen not to be limited to the cases of filtered band but is also present when the natural wavelength is reduced to the millimetre region. On this account alone the spark generated millimetre waves require special techniques of detecting and recording to minimize the effects of power fluctuation. Further work on these techniques is required.

11. Conclusions

It is necessary at this stage to analyse the results of the experiments in the light of the review of microwave generators given in part I and with reference to the analysis of spark generation and spectrum dispersion given in part II.

11.1 Performance

This work was primarily concerned with generation of waves in the shorter centimetric and millimetric range (X, K and Q band) and the results of prolonged tests indicate that in the X band region very satisfactory results can be obtained by the spark generators, although absolute power was not measured, the estimated power in this region is of the order of 20  $\mu$ W distributed, of course, over a very wide spectrum. More power could be obtained by raising the pulse repetition frequency.

The technological difficulty of making and mounting dipoles resonating and producing regular output in the Q band and the comparatively simple solution of the same problem in the X band lead one to the conclusion that for reliable generation of K and Q band spectra by spark generators, it is preferable to work with longer radiators and so shift the spectrum to the desired range by high pass filters - the simplest being the waveguide. The resultant power in particular in the Q band is much reduced (estimated 60 db drop in power level) this being accentuated by the loss in

crystal sensitivity at those frequencies as compared with the X band region. Further development in millimetre wave detectors may lead to improved performance of spark generators.

The power fluctuations which are inherent in the spark generator are also less pronounced in the X band than in the Q band. The fluctuation in the 2 to 4 cm region can be reduced to a very small fraction by a careful adjustment of the gap and by using high voltage pulses of steep front giving a large overvoltage.

The position is less satisfactory as the frequency is increased and the evidence of experiments is that no further improvement can be expected. Any further work should concentrate rather on improving the detector amplifier design to increase the signal to noise ratio possibly by the use of coherent detectors or by some form of automatic gain control.

The mark II radiator offers a simple and effective device for spark generation covering the examined frequency range.

### 11.2 Filtering

When used with a suitable filter the spark generator offers a source of variable frequency. The most suitable filters are of the waveguide post or iris type. The various

grating and echellette types of filters have their uses, but are limited by a greater difficulty of shifting the filtered band and errors arising from non parallel beams, dispersion and attenuation and the comparatively unwieldy structures. The experiments have established the feasibility of having a source with an almost 2:1 frequency ratio. The resultant wave is non-monochromatic, but the bandwidth can also be varied at will.

This should have several important applications such as possibility of examining properties of materials anywhere in the spectrum; testing of wide band matching devices, which is becoming particularly important with the development of backward travelling wave tubes tunable over a wide frequency range provided a good match holds; testing microwave filters. This last technique offers a new approach to the problem, because by analysing the interferogram without and then with the filter structure, one can arrive at the complete filter characteristic including higher mode transmission, etc.

### 11.3. Measurement technique

Most of the quantitative part of this work was done with the help of a Boltzmann interferometer. A full analysis of this piece of equipment given in part II and confirmed by experiments shows that it is simple, versatile and reliable and should find extensive use in the field of

microwave measurements in particular in connection with the photographic technique described in chapter 2 of part III.

#### 11.4. Further developments

Apart from the points already made such as the detector amplifier improvements more work should be done now on artificial lense structures and their application to wide band sources.

Also with the help of the spark generator an extensive study should be made leading to the tabulation of impedance of various types of waveguide obstacles and irises over the whole microwave spectrum.

Some technological development in making the radiator unit self-adjusting, possibly by a servo system, is also called for.

The essential simplicity and reliability of the microwave spark generator establishes it as a useful piece of laboratory equipment, not the least of its uses lying in the value it can have in demonstrating waveguide and optical phenomena and in teaching microwave techniques.

12. REFERENCES

1. M. Abraham. "Electrical oscillations around a conducting rod".  
Ann. Phys. Lpz. 66. 1898. p.435.
2. H. Anders. "A spark generator of lightly damped cm waves of continuously variable frequency".  
Z. Phys. 45. 1951. p.129.
3. C.A. Beevers. "Fourier Strips at  $3^{\circ}$  interval".  
Acta. Cryst. 5. 1952. p.670.
4. L. Boltzmann. "Investigation into Hertzian Phenomenae".  
Ann. Phys. Lpz. 40. 1890. p.399.
5. C.J. Bouvkamp. "Diffraction theory".  
Rep. Prog. Phys. 17. 1945. p.35.
6. T.J. Bridges. "A gas discharge noise source for 8 mm waves".  
Proc. I.R.E. 42. 1954. p.818.
7. L. Brillouin. "Antennae for u.h.f. - wide band antennae".  
Elect. Comm. 21. 1944. p.257.  
22. 1944. p.11.
8. M Brillouin. "Propagation of electricity". Vol. I.  
Herman. Paris 1904.
9. C.A. Burns  
and W. Gordy. "Submillimetre wave spectroscopy".  
Phys. Rev. 93. 1954. p.897.
10. P.A. Cerenkov. "Emission of light from pure liquids under influence of fast  $\beta$  rays".  
C.R. Acad. Sci. URSS. 14.  
No. 3. 1937. p.101.

11. H. Christensen. "Harmonic generation and detection as a means of establishing useful signal power in mm waves".  
Tekn. Skriften No. 7N. 1953.
12. W.V. Christensen and D.A. Watkins. "Helix mm wave tube".  
Proc.I.R.E. 43. 1955. p.93.
13. L.J.Chu and J.A. Stratton. "Forced oscillations of a prolate spheroid".  
J. App. Phys. 12. 1942. p.241.
14. R.J. Coates. "A grating spectrometer for mm waves".  
Rev.Sci.Inst. 19. 1948. p.587.
15. J.D. Cobine. "Gaseous conductors".  
McGraw Hill. New York & London, 1941.
16. S.B. Cohn. "Analysis of wide band wave guide filters".  
Proc.I.R.E. 37. 1949. p.651.
17. P.D. Coleman. "Generation of mm waves".  
Ph.D. thesis. M.I.T. 1951.
18. P.D. Coleman et al. "Progress report on research leading to methods of generating and detecting radiation in 100 to 1000 micron range".  
El.Eng.Res.Rep. Univ. of Illinois.
19. J.P. Codey and J.H. Rohrbaugh. "The production of extremely short waves".  
Phys. Rev. 67. 1944. p.114.
20. W. Culshaw. "The Michaelson interferometer at mm waves".  
Proc. Phys. Soc. 63B. 1950.p.939.
21. W. Culshaw. "The Fabry Perot Interferometer at mm wavelength".  
Proc. Phys. Soc. 66B. 1953.p.597.

22. W. Culshaw. "A spectrometer for millimetre wavelengths".  
Proc. I.E.E. IIA. 100. No. 3. 1953. p.5.
23. M. Danos and H. Lashinsky. "Mm wave generation by Cerenkov radiation".  
Trans I.R.E. MTT. 2. No. 3. 1954. p.21.
24. J.G. Daunt, D.A. Jackson, R.A. Hull and C. Hurst. "Experiments on the production, detection and measurement of millimetric radiation and its absorption by atmosphere".  
C.V.D. Report C.L. Misc. 44.
25. G.L. Davies, C.B. Pear and P.E.P. White. "Kilomegacyde buzzer test oscillator".  
Electronics. 23. July 1950. p.96.
26. F.R. Dickey. "The production of mm waves by spark discharges".  
Cruft Lab. Rep. No. 123. July 1951.
27. F.R. Elder, R.V. Langmuir and H.C. Pollock. "Radiation from electrons accelerated in a synchrotron".  
Phys. Rev. 74. 1948. p.52.
28. J.L. Farrands. "The generation of mm waves".  
I.E.E. Monograph No. 112. 1954.
29. J.L. Farrands and J. Brown. "Boltzmann interferometer".  
Wireless Eng. 31. 1954. p.81.
30. I. Frank and I Tamm. "Coherent visible radiation from fast electrons passing through matter".  
C.R. Acad. Sci. URSS. 14. No. 3. 1937. p.109.
31. I.A. Getting. "Proposed detector for high energy electrons and mesons".  
Phys. Rev. 71. 1947. p.123.

32. V.L. Ginsburg. "Radiation of microwaves and their absorption".  
Bull.Acad.Sci. URSS. Phys.11.  
No. 2. 1947.
33. A. Glagoleva  
Arcadieva. "A new source of ultra short waves".  
Z. Phys. 24. 1924. p.153.
34. A. Glagoleva  
Arcadieva. "On the theory of mass radiator".  
C.R.Acad.Sci. URSS. 132.  
1941.p.540.
35. A.Glagoleva  
Arcadieva and  
H. Sokolov. "On the method of resonance thermo-  
couples used for the investigation  
of complete radiation in the ultra  
short band".  
C.R.Acad.Sci. URSS. 32.  
1941. p.543.
36. M.J.E. Golay. "A pneumatic detector".  
Rev. Sci. Inst. 18. 1947. p.357.
37. M.J.E. Golay. "The theoretical and practical  
sensitivity of pneumatic infra red  
detector".  
Rev.Sci. Inst. 20. 1949. p.816.
38. M.J.E. Golay. "Bridges across the infra red radio  
gap".  
Proc.I.R.E. 40. 1952. p.1161.
39. W. Gordy,  
W.V. Smith and  
R.F.Trambarulo. "Microwave spectroscopy".  
John Wiley, New York, 1953.
40. L.N. Hadley and  
D.M. Dennison. "Reflection and Transmission  
Interference Filters".  
J.Opt.Soc.Amer. 37. 1947. p.451.
41. E. Hallen. "Theoretical investigation into the  
transmitting and receiving qualities  
of antennae".  
Nova Acta Upsala 11. No.4. 1938.

42. A.F. Harvey. "Instruments for use in the microwave band".  
Proc.I.E.E. 98 II. 1951. p.781.
43. H. Hertz. "Electric waves".  
London 1893.
44. J. Hessel,  
G. Couben and  
L.R. Battersby. "Microwave filter theory and design".  
Proc.I.R.E. 37. 1949. p.990.
45. W.V. Ignatovsky. "On the theory of gratings"  
Ann.Phys.Lpz. 44. 1914. p.339.
46. Z. Jelonek. "Noise problems in pulse communication".  
J.I.E.E. Vol.94. pt.IIIA.  
1947. p.533.
47. C.M. Johnson,  
R. Trambarulo  
and W. Cordy. "Microwave spectra from 2 to 3 mc".  
Phys. Rev. 84. 1951. p.1170.
48. L.M. Johnson,  
D.M. Slager and  
D.D. King. "Mm waves from harmonic generators".  
Rev.Sci,Inst. 25. 1954. p.213.
49. H. Johnson and  
H.R. Decker. "Gaseous discharge super h.f. noise source".  
Proc.I.R.E. 39. 1951. p.908.
50. A. Kapp. "Travelling wave tube - experiments at cm wavelengths".  
Proc.I.R.E. 43. 1955. p.41.
51. Tadasu Kawano. "Propagation of heavily damped microwaves through a waveguide and microwave spectrum analysis by means of standing waves".  
J.Inst.El,Comm.Jap. 33.  
1953. p.531.
52. Tadasu Kawano. "Weakly damped microwave oscillators excited by spark discharge in oil".  
Jap.J.Inst.E.E. 74. 1954. p.11.

53. R. King and C.W. Harrison, Jr. "The impedance of long, short and capacitively loaded antennas".  
J. App. Phys. 1944. p.170.
54. R. King. "Theory of electrically short transmitting and receiving antenna".  
J. App. Phys. 23. 1952. p.1174.
55. W. Kleen. "History, systematics and physics of u.h.f. valves".  
Elect. Z. A76. 1955. p.53.
56. C.A. Klein. "On the production of radio waves by Cerenkov effect".  
Ann. Telecomm. 8. 1953. p.38.
57. J.R. Klein, J.H.N. Loubser, A.H. Nethercot & C.H. Townes. "Magnetron harmonics at mm wavelengths".  
Rev. Sci. Inst. 23. 1952. p.78.
58. R. Kompfner. "Travelling wave tubes".  
Proc. Phys. Soc. Prog. Rep. 15. 1952. p.275.
59. R. Kompfner and T. Williams. "Backward wave tubes".  
Proc. I.R.E. 41. 1953. p.1602.
60. E.A. Lewis and J.P. Casey. "Metal grid interference filters".  
J. Opt. Soc. Amer. 41. 1951. p.360.
61. E.A. Lewis and J.P. Casey. "Electromagnetic reflection and transmission by gratings and resistive wires".  
J. App. Phys. 23. 1952. p.605.
62. E.A. Lewis and J.P. Casey. "Filter action of parallel wire grids".  
Nuovo Cimento Suppl. 9. Serie 9. No. 3. 1952. p.336.
63. P. Lebedev. "The double refraction of electric waves".  
Ann. Phys. Lpz. 56. 1895. p.1.

64. M.A. Levitzky. "Study of resonances at shortest Hertzian waves".  
Phys. Zeit. 28. 1927. p.821.
65. K.F. Lindman. "Standing waves in air".  
Ann. Phys. Lpz. 38. 1912. p.523.
66. K.F. Lindman. "Secondary electric oscillations".  
Ann. Phys. Lpz. 40. 1914. p.992.
67. K.F. Lindman. "On electrical and optical resonance".  
Ann. Phys. Lpz. 45. 1914. p.580.
68. K.F. Lindman. "On natural oscillations of cylindrical rods".  
Ann. Phys. Lpz. 13. 1932. p.358.
69. K.F. Lindman. Letter.  
Ann. Phys. Lpz. 15. 1932. p.127.
70. K.F. Lindman. Research reports 1929-1947.  
Acta Academiae Aboensis.
71. J.H.N. Leubser and C.H. Townes. "Spectroscopy between 1.5 and 2 mm".  
Phys. rev. 76. 1949. p.178.
72. W. Ludemia. "The excitation of cavities by decaying oscillation".  
Elect. Nachr. Tech. 19. 1942. p.7.
73. G.G. Macfarlane. "Surface impedance of an infinite parallel wire grid at oblique angles of incidence".  
J.I.E.E. 93 IIIA. 1946. p.1523.
74. N. Marcuvitz. "Waveguide handbook".  
McGraw Hill, New York, 1951.
75. A.C. Menzies. "Radiation measuring instruments in the infra-red to ultra-violet waveband".  
Proc.I.E.E. 98 II. 1951. p.771.

76. D. Middleton and R. King. "The thin cylindrical antenna".  
J. App. Phys. 17. 1946. p.273.
77. W. Möbius. "The dispersion of waves between 7 and 35 mm long by water and alcohol".  
Ann. Phys. Lpz. 62. 1920. p.293.
78. A. Montani. "A generator of damped microwaves".  
Electronics 17. Sept. 1944.  
p.114.
79. P.M. Morse and P.J. Rubenstein. "Diffraction of waves by ribbons and slits".  
Phys. Rev. 54. 1938. p.895.
80. H. Motz. "Applications of the radiation from fast electron beams".  
J. App. Phys. 22. 1951. p.527.
81. H. Motz, W. Thon, R.N. Whitehurst. "Experiments in mm wave and light generation".  
Convention record 1953 I.R.E.  
Part 6. p.124.
82. R. Müller. "A vigorous treatment of the diffraction of e.m. waves by plane grating".  
Z. Naturforsch. 8a. 1953. p.56.
83. W.W. Mumford. "A broad band microwave noise source".  
B.S.T.J. 28. 1949. p.608.
84. A.H. Nethercot. "Molecular spectroscopy with a Hertzian oscillator source of mm waves".  
Univ. Microfilm Publ. No.2629.  
1951.
85. A.H. Nethercot. "Harmonics at mm wavelengths".  
Trans. I.R.E. MTT.2. No.3.  
1954. p.17.
86. E.F. Nichols and J. Tear. "Short electric waves".  
Phys. Rev. 21. 1925. p.588.

87. H.Q. North. "Properties of welded contact germanium rectifiers".  
J. App. Phys. 17. 1946. p.912.
88. L. Page and N.I. Adams. "The electrical oscillations of a prolate spheroid".  
Phys. Rev. 53, 1933. p.819.
89. J.R. Pierce. "Generation of mm waves".  
Physics to-day. Nov. 1950.
90. J.R. Pierce. "Millimetre waves".  
Electronics 24. 1951. p.66.
91. J.R. Pierce. "Some recent advances in microwave tubes".  
Proc.I.R.E. 42. 1954. p.1735.
92. M.H.N. Potok. "A critical review of researches into millimetric wave spark generators".  
J. Brit. I.R.E. 13. 1953. p.490.
93. M.H.N. Potok. "Diffraction of non-monochromatic electromagnetic waves by slits and gratings".  
Proc. Phys. Soc. 68B. 1955. p.171.
94. J. Reed. "Low Q microwave filters".  
Proc.I.R.E. 38. 1950. p.793.
95. A. Righi. "Treatise on electric oscillations".  
Bologna. 1897.
96. S. Robin. "On focussing in vacuum monochromators with concave systems at normal incidence for ultraviolet".  
J. Phys. et Rad. 11. No.5. 1950.
97. R.M. Ryder. "The electrical oscillations of a perfectly conducting prolate spheroid".  
J. App. Phys. 13. 1942. p.327.

98. H. Sanfferer. "The measurement of radiation from mercury arc for wavelength in tenths mm region".  
Z. Phys. 131. 1952. p.376.
99. S.A. Schelkunoff. "Advanced Antenna Theory".  
John Wiley and Sons.  
New York 1952.
100. K. Schwarzschild. "Diffraction and polarisation of light by a slit".  
Math. Ann. 55. 1902. p.177.
101. B. Sieger.. "The diffraction of plane e.m. waves by an elliptical obstacle".  
Ann. Phys. Lpz. 27. 1903. p.626.
102. W.M. Sinton. "Detection of mm waves solar radiation".  
Phys. Rev. 86. 1952. p.424.
103. A.G. Smith,  
W. Gordy,  
J.W. Simmons &  
W.V. Smith. "Microwave spectroscopy in 3 to 5 mm region".  
Phys. Rev. 75. 1949. p.260.
104. K.R. Spangenberg. "Vacuum Tubes".  
McGraw Hill, New York 1948.
105. J.A. Stratton and L.J. Chu. "Diffraction theory of e.m. waves".  
Phys. Rev. 56. 1939. p.99.
106. J.A. Stratton and L.J. Chu. "Steady state solution of electromagnetic problems".  
J. App. Phys. 12. 1941. p.230.
107. J.A. Stratton. "Electromagnetic theory".  
McGraw Hill, New York 1941.
108. J.W. Sullivan. "A wideband voltage tunable oscillator".  
Proc.I.R.E. 43. 1955. p.1658.

109. J.J. Thomson. "Recent researches".  
Oxford, 1893.
110. S. Tolanski. "Multiple beam interferometry".  
Oxford, 1948.
111. H.C. Torrey and C.H. Whitmer. "Crystal rectifiers".  
McGraw Hill, New York 1948.
112. R.W. Twiss. "On the generation of mm radiation".  
SERL Tech. J. 2. No.1.  
May 1952. p.10.
113. J.R.M. Vaughan. "A millimetre wave magnetron".  
Monograph I.E.E. No.142R. 1955.
114. R. Warnecke and P. Guenard. "Some recent work in France on new types of valves for the highest radio frequencies".  
Proc.I.E.E. 100. III. 1953. p.351.
115. H.W. Webb and L.E. Woodman. "Systematic study of vibrators and receivers for short waves".  
Phys. Rev. 30. 1909. p.199.
116. Wei Guan Lin. "Microwave filters with simple cavity excited in more than one mode".  
J. App. Phys. 22. 1951. p.989.
117. J.U. White. "Gratings as broad band filters for infra-red".  
J. Opt. Soc. Amer. 37.  
1947. p.713.
118. W.E. Wilshaw, H.R.L. Lamont & E.M. Hickin. "Experimental techniques for a study of mm wave propagation".  
Proc.I.E.E. 102B, 1955. p.99.
119. D.J. Wooton. "A reflex klystron oscillator for the 8 - 9 mm band".  
Monograph I.E.E. No.143R. 1955.